Machine Learning and Statistical Analysis of Complex Mathematical Models

An Application to Epilepsy

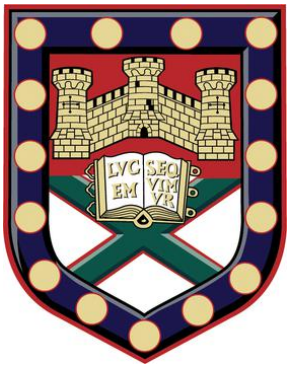

Submitted by Lauric Ferrat to the University of Exeter
as a thesis for the degree of
Doctor of Philosophy
In June 2018.

Signature: .....

To my grandfathers, Charles Armand Ferrat and Ruben Otge

Acknowledgements

It would be nearly impossible to acknowledge everyone who has contributed or guided me along my path to obtaining a PhD. I would like to mention some of them here.

First and foremost I would like to express my gratitude to my two supervisors John and Marc. Working with Professor John Terry with his great expertise and leadership has been an insightful experience. His commitment to research has impressed and inspired me. I thank Doctor Marc Goodfellow for his time, his passion and his friendly guidance. His expertise, patience and understanding have greatly enhanced my research experience.

I have had the pleasure of working with some incredible people throughout my time here and I would like to thanks my colleagues as well. Particularly Harry, Leandro and Marinho for our deep discussions about epilepsy and many other things around the pool table. I would also like to thank Chris, Diane, Eder, George, Harun, Hossein, Jen, Jordan, Kevin, Khulood, Luke, Petroula, Piotr, Sarah, Wessel and Zoe for their help which has made a huge difference.

Doing a PhD does not just consist of just 3 years of research. I would particularly like to thank Mr Comps, Professor Ian Sims, Professor Daniel Lehmann and Dominique Verrier for their help along the way.

Attending the Pennsylvania Road home group has always been a joy and I would like to thank its members for their fraternity.

I would like to thank Lauris, Sebastien, Vincent and Yoan for being part of my life.

Finalement merci à toute ma famille. Tout particulièrement, je n'aurais jamais assez de mots pour décrire combien vous êtes extraordinaires alors permettez moi de vous dire: merci maman, merci papa, merci Gaël.

Merci Lucy :)

Abstract

The electroencephalogram (EEG) is a commonly used tool for studying the emergent electrical rhythms of the brain. It has wide utility in psychology, as well as bringing a useful diagnostic aid for neurological conditions such as epilepsy. It is of growing importance to better understand the emergence of these electrical rhythms and, in the case of diagnosis of neurological conditions, to find mechanistic differences between healthy individuals and those with a disease. Mathematical models are an important tool that offer the potential to reveal these otherwise hidden mechanisms. In particular Neural Mass Models (NMMs), which describe the macroscopic activity of large populations of neurons, are increasingly used to uncover large-scale mechanisms of brain rhythms in both health and disease.

The dynamics of these models is dependent upon the choice of parameters, and therefore it is crucial to be able to understand how dynamics change when parameters are varied. Despite they are considered low-dimensional in comparison to micro-scale neural network models, with regards to understanding the relationship between parameters and dynamics NMMs are still prohibitively high dimensional for classical approaches such as numerical continuation. We need alternative methods to characterise the dynamics of NMMs in high dimensional parameter spaces.

The primary aim of this thesis is to develop a method to explore and analyse the high dimensional parameter space of these mathematical models. We develop an approach based on statistics and machine learning methods called decision tree mapping (DTM). This method is used to analyse the parameter space of a mathematical model by studying all the parameters simultaneously. With this approach, the parameter space can efficiently be mapped in high dimension. We have used measures linked with this method to determine which parameters play a key role in the output of the model.

This approach recursively splits the parameter space into smaller subspaces with an increasing homogeneity of dynamics. The concepts of decision tree learning, random forest, measures of importance, statistical tests and visual tools are introduced to explore and analyse the parameter space. We introduce formally the

theoretical background and the methods with examples.

The DTM approach is used in three distinct studies to:

- Identify the role of parameters on the dynamic model. For example, which parameters have a role in the emergence of seizure dynamics?
- Constrain the parameter space, such that regions of the parameter space which give implausible dynamic are removed.
- Compare the parameter sets to fit different groups. How does the thalamocortical connectivity of people with and without epilepsy differ?

We demonstrate that classical studies have not taken into account the complexity of the parameter space. DTM can easily be extended to other fields using mathematical models. We advocate the use of this method in the future to constrain high dimensional parameter spaces in order to enable more efficient, person-specific model calibration.

Table of contents

List of figures

List of tables

Declaration

I declare that the work in this dissertation was carried out in accordance with the requirements of the University's Regulations and Code of Practice for Research Degree Programmes and that it has not been submitted for any other academic award. Except where indicated by specific reference in the text, the work is the candidates own work. Work done in collaboration with, or with the assistance of, others, is indicated as such. Any views expressed in the dissertation are those of the author.

Lauric FERRAT
February 2019

List of abbreviations

AED	Anti Epileptic Drugs
ANOVA	Analyse of variance
BOA	Bayesian optimization algorithm
CAT	Computed Axial Tomography
CNS	Central Nervous System
DTM	Decision Tree Mapping
EDA	Estimation of distribution algorithms
EEG	Electroencephalogram
EMG	Electromyogram
EPSP	Excitatory Post-Synaptic Potential
fMRI	Functional magnetic resonance imaging
GABA	Gamma-Aminobutyric Acid
GP	Gaussian Process
NMM	Neural Mass Model
iEEG	Intra-Cranial EEG
i.i.d	Independent and identically distributed
IPSP	inhibitory Post-Synaptic Potential
IGE	Idiopathic Generalised Epilepsy
MEG	Magnetic Resonance Spectroscopy
MRI	Magnetic Resonance Imaging
MSE	Mean Square error
ODE	Ordinary Differential Equations
PET	Positron Emission Tomography
PSP	Post-Synaptic Potential
SPECT	Single-Photon Emission Computed Tomography
SWD	Spike-Wave Discharge
TLE	Temporal Lobes Epilepsy

Mathematical notation

$\mathbb{1}$	indicator function
$\|A\|$	cardinality of the set A
$\dot{y}(t)$	first derivative of $y(t)$
$\ddot{y}(t)$	second derivative of $y(t)$
$\mathbb{E}_j(.)$	conditional expectation knowing the value of the jth parameter
$G(R, j, s)$	gain function in region R for parameter j at value s
GI_j	Gini importance of the j^{th} parameters
$\int$	integral
I_{R_m}	impurity of region R_m
μ	mean
$\mathcal{N}$	normal distribution
n	size of sample
p	dimension of the parameter space $\mathbb{X}$
$P(A)$	probability of event A
$\hat{P}(A)$	estimated probability of event A
$\phi_j(x_j)$	partial dependence function of the j^{th} parameter
$\phi_{\mathbf{z}}(\mathbf{x}_{\mathbf{z}})$	partial dependence function of the $\mathbf{z}^{\text{th}}$ parameters
PI_j	permutation importance of the j^{th} parameter
$\psi_{ij}(x_i, x_j)$	partial interaction function of the i and j^{th} parameters
R	region of the parameter space $\mathbb{X}$
$r_{a/b}$	ratio of the parameter a over b
σ	standard deviation
$\sum$	sum
$\mathbb{R}$	set of real numbers
$\mathbf{x}$	parameter vector
$\mathbf{X}$	random variable vector of p dimensions contained in $\mathbb{X}$
$\mathbb{X}$	parameter space - an Euclidian space
χ	sample in $\mathbb{X}$
$\mathbb{Y}$	output space

Preamble

In this thesis, we present new tools to aid mathematical modelling of the brain. Modelling requires selecting and identifying relevant aspects of a system of interest and a rigorous evaluation of the model. As pointed out by George Box,"*all models are wrong*" and "*the practical question is how wrong do they have to be to not be useful*" [36]. In this thesis, we are particularly interested to develop a method to know how wrong they are and what they can teach us. We particularly focus on better understanding epilepsy. Epilepsy is a serious neurological condition affecting around 50 million people in the world. It is characterised by an increased predisposition to seizures. A seizure is a succession of hypersynchronous discharges of neuronal activity. Mathematical models are commonly used to simulate and study brain dynamics. In this thesis, we focus on one of the major class of mathematical models, the neural mass model (NMM). These complex models are composed of many components which interact with each other. We present a new approach, decision tree mapping (DTM), to analyse the parameter space of neural mass models and identify the role of the values of parameters on the dynamics of the models.

Chapter 1 gives the necessary background to understand our work. Firstly, we focus on the brain and present an overview of its multi-scale highly complex but structured organisation. Secondly, we define epilepsy, its consequences, its main treatments and their limitations. Thirdly, we present an overview of mathematical and computational approaches that have been used to describe and understand the mechanisms underlying epilepsy and seizures. We highlight the role of neural mass modelling as an efficient tool to study epilepsy. We also show that neural mass models need to be used with caution to avoid unfounded and misleading interpretations.

In **chapter 2**, we present our method to explore and analyse the parameter space of a mathematical model. Firstly, we introduce an overview of the DTM approach previously presented in [83]. We detail its key aspects; optimal design, simulations, decision tree learning, random forest and measure importance. Secondly, to overcome the main limitation of decision tree learning approach, we focus on the identification of potential interactions between parameters. We present two approaches which complement each other to understand and cope with non-linear interactions between parameters. The first one consists of the visualisation of

interactions between parameters. The second one consists of a statistical test to detect potential interactions. To demonstrate the interest of our approach, we introduce examples along this chapter.

In **chapter 3**, we apply this method to a commonly used NMM in the context of transitions to seizure dynamics. This chapter is based on the work published in [83]. We find that the inhibitory sub-system is most crucial for the generation of seizure dynamics, confirm and expand previous findings regarding the ratio of excitation and inhibition, and demonstrate that previously overlooked parameters can have a significant impact on model dynamics.

In **chapter 4**, we apply the DTM method to clinical data. We define the plausible parameter space of another neural mass model. Previous analyses have been done on this model but we show that DTM extends these previous results. We show that the plausible parameter space is much wider than the previous results and that many combinations of parameter sets can lead to similar simulations.

In **chapter 5**, we apply the DTM method to clinical data. We compare the plausible parameter space of different groups of people, control, idiopathic generalised epilepsy (IGE) and their relatives. We demonstrate the controls and relatives share a similar plausible parameter space. However, patients with IGE have a plausible parameter space slightly different from the two other groups.

In **chapter 6**, we summarise and discuss our results and conclude the thesis.

Chapter 1

Introduction

> Epilepsy is not just a seizure. It's the lack of control, the worried family, forgetting medication, the crippling anxiety, the depression, the body jerks, the ache after a seizure which feels like your bones are wearing away. It's the 2 AM phone calls because you forgot to let them know you're ok. It is the fear you won't wake up next time, it's the medication side effects, it's the isolation, it's waking up in an ambulance, it's being grateful for waking up at all, it's eating hospital food time and time again, it's the scars of wounds and forgotten memories. Epilepsy is not just a seizure.
>
> Anonymous

In this chapter, we present the necessary background to understand the importance of the problem and the significance of the research. Firstly, we give a brief overview of the brain and the current tools to study it; we introduce some notions such as neuronal network and Electroencephalography (EEG) and discuss the spatial and temporal scales of the brain. Secondly, we give a brief overview of epilepsy from clinical, historical, patient and research perspectives. Finally, we introduce the notions of mathematical models and dynamical systems, particularly the neural mass models (NMMs) which have been used to better understand the brain and epilepsy.

1.1 The brain, the problem

The difficulties in understanding epilepsy flow from the difficulties in understanding the brain. In this section, we describe the brain and some approaches used to understand neural activity.

1.1.1 A complex system

"*I am a brain, Watson. The rest of me is a mere appendix*" [75]. One can argue that Sherlock Holmes is a bit presumptuous[1] but no one can dispute the central and pervasive role that the brain plays in our life. The brain is one of the most complex organs with only slightly fewer than one hundred billion neurons connected by more than one hundred trillion connections [10]. The relationship between the activity of neurons and the activity of the whole brain is complex. The brain is composed of an impenetrable network of neurons [2], which interact both within and across multiple spatial and temporal scales [202]. According to [24], the brain can be studied with different scales, spatial, temporal and topological:

1. a network's spatial scale refers to the granularity at which its nodes and edges are defined. A node can represent a neuron or a larger part of the brain;

2. networks can be characterised over temporal scales with precision ranging from a sub-millisecond to the entire lifespan of the brain; and

3. networks can also be analysed at different topological scales ranging from individual nodes to the network as a whole.

In terms of spatial scale, as in [245], one can consider that there are three principal levels of analysis for the brain: micro, meso and macro-scales. In this section, we present the principal components of the brain at different spatial scales. This overview gives the necessary knowledge to understand the macro-scale, level of our study.

1.1.2 Micro scale

This scale is defined at a neuron level. The spatial scale is measured in micrometres. In the following subsection, we briefly describe neurons and their inter-connections. We only present the most important characteristics of neurons. There is a wide diversity of neurons and other cells in the brain [7] and it needs to

[1] Empirical evidence shows that brain activity not only influences but is in turn influenced by, physical activity taking place in other parts of the organism (such as the endocrine and immune systems) [60].

[2] A network is a collection of connected objects and their connections [220] (here, neurons or groups of neurons).

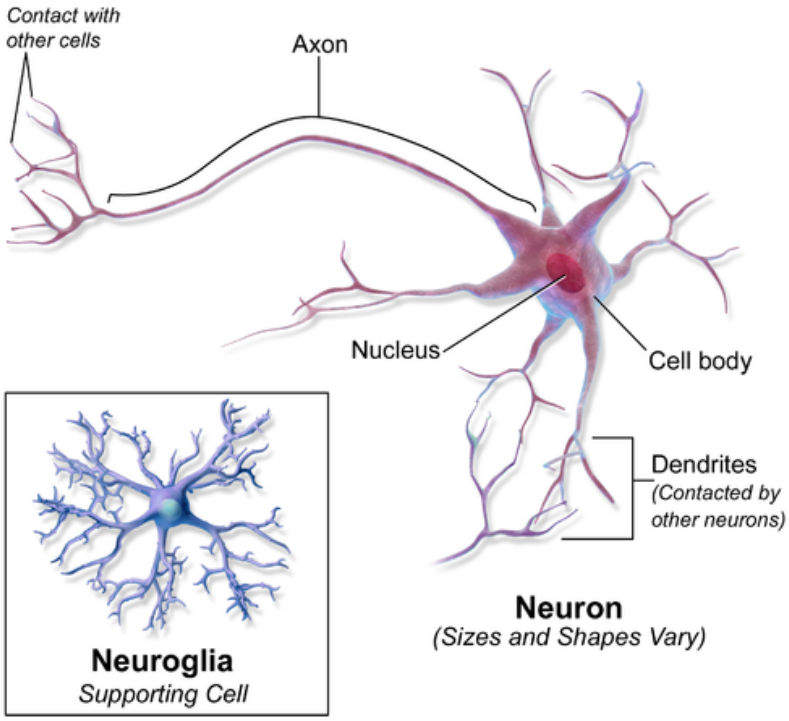

Fig. 1.1 Anatomy of a neuron and glia cells.
Modified and reproduced with permission from Bruce Blausunder under CC BY 3.0 licence term.
Source :https://commons.wikimedia.org/wiki/File:Blausen_0672_MultipolarNeuron.png.

be noted there are many exceptions which are not presented here[3]. One can read [16] for a more complete overview of the brain at a micro scale.

Neurons

A neuron is an electrically excitable cell that processes and transmits information through electrical and chemical signals, see Figure 1.1. The cell body of a neuron is called the soma. The soma contains a nucleus separated from the extra-cellular fluid by a semi-permeable membrane containing a bi-lipid phosphate layer. The intra-cellular fluid (cytoplasm) contains the mitochondria which provide the cell with energy and the chromosomes which contain the subject's genetic information as well as various proteins which serve several functions [16]. A typical neuron consists of a cell body (soma), dendrites, and an axon. A neuron has up to 100,000 dendritic branches attached to its soma [3]. They extend for hundreds of micrometres and branch multiple times, giving rise to a complex "dendritic tree". Neurons have a single axon which arises from the soma and travels for a long distance.

[3]For example, neurons are surrounded by glia which play important roles in ensuring a healthy balance in the brain. They have multiple roles; they hold neurons in place, supply nutrients and oxygen to them, insulate one neuron from another and finally destroy pathogens and remove dead neurons [143]. A limitation of the models that we use in this thesis is that the roles of glia are not introduced.

Connectivity between neurons

Electrical signals known as action potentials are issued from a single neuron (called the presynaptic neuron) and transit by its axon. The axon is not directly in contact with the dendrites of other neurons (postsynaptic neurons). The small space in between is either a gap junction or (most of the time) a chemical synapse. At a chemical synapse, the plasma membrane of the presynaptic neuron comes into close apposition with the membrane of the target postsynaptic neuron. The space between the two membranes is called the synaptic cleft and typically varies from about 20-50 nm [255]. Both the presynaptic and postsynaptic sites contain extensive arrays of molecular machinery that link the two membranes together and carry out the signalling process, see Figure 1.2. Electrical activity in the presynaptic neuron is converted (via the activation of voltage-gated calcium channels) into the release of a chemical called a neurotransmitter that binds to receptors located in the plasma membrane of the postsynaptic cell [16]. The neurotransmitter will cause changes in the membrane potential, called post-synaptic potential (PSP). It initiates an electrical response or a secondary messenger pathway that may either excite or inhibit the postsynaptic neuron. Chemical synapses can be classified according to the neurotransmitter released. There are two main neurotransmitters which can be found in 90% of neurons, Glutamate and Gamma-Aminobutyric Acid (GABA). Often glutamate neurotransmitters are excitatory and GABA are inhibitory. There are however some exceptions [101]. Neurons will often release the same neurotransmitters at their synapses with few exceptions [240]. Multiple axons from different pre-synaptic neurons are connected to synapses and many PSPs are conveyed to the recipient post-synaptic neuron. At the neuron's soma, all of the PSPs are integrated and contribute to the net value of the membrane potential [15]. If their sum is greater than the threshold value of the membrane potential, the deporalised cell releases an action potential. After firing, the neuron has a refractory period during which it repolarises and cannot produce another action potential. The duration of the refractory period is dependent on the type of neuron.

1.1.3 Macro scale

Here, the Macro scale corresponds to a few millimetres to the whole brain. Many experimental techniques, including EEG (see section 1.1.4), measure the activity of large populations of neurons across multiple brain regions.

Regions of the brain

For scientists, an advantage of studying the brain at a micro scale is that neurons are relatively easily demarcated and well defined. In contrast, brain areas and neuronal populations are more difficult to delineate. No single universally accepted parcellation scheme currently exists for human brain regions (e.g., areas of the

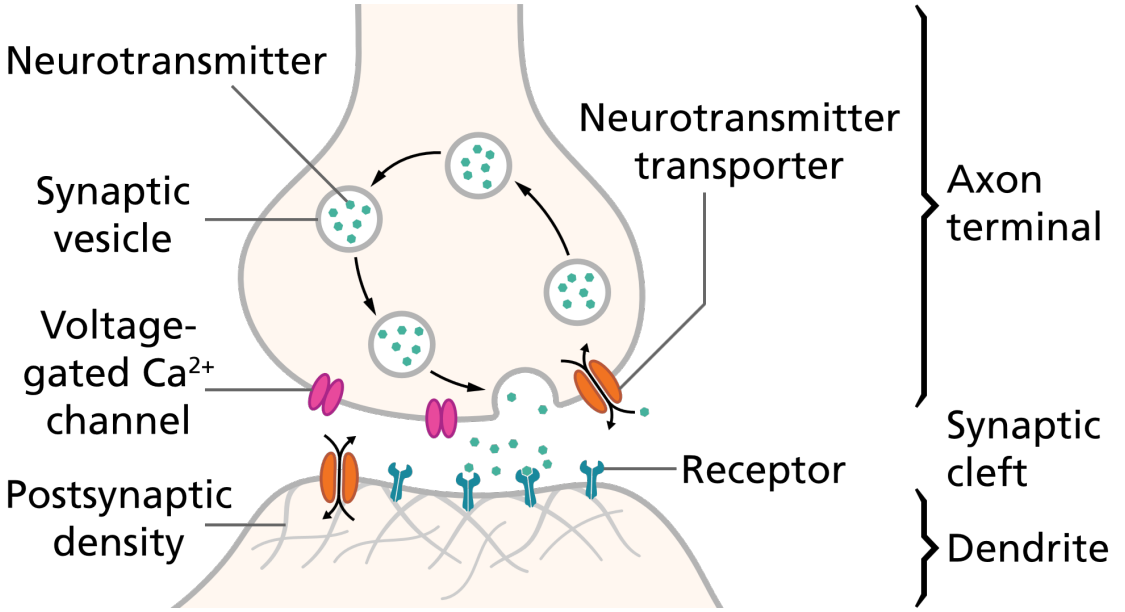

Fig. 1.2 Synapse schematic. When an action potential arrives at the end of the pre-synaptic axon, it causes the release of neurotransmitter molecules that open ion channels in the post-synaptic neuron. The sum of multiple excitatory potentials from several synapses may depolarise the membrane enough to provoke a new action potential.
By Thomas Splettstoesser, reproduced with permission under CC BY-SA 4.0 licence term.
Source:https://commons.wikimedia.org/wiki/File:SynapseSchematic_en.svg.

cerebral cortex), posing a significant obstacle to study the brain at this scale [245]. Nevertheless, some notions are commonly accepted [15]. The brain can be partitioned into different regions, some regions play an important role in epilepsy, such as the cortex. Figure 1.3 shows the main lobes of the cortex. In the cortex, the temporal lobes are the most common site of localized epileptic seizures [284]. This type of epilepsy is called temporal lobe epilepsy (TLE) and is one of the most frequent [58]. TLE that arises from the Hippocampus is the most common subtype, which is typically associated with hippocampal sclerosis [4] [261]. Other lobes may also play a role in the emergence of seizures such as the occipital lobes [57] or frontal lobes [19]. Outside the cortex, the thalamus is known to have an important role in epilepsy [33]. Indeed these different sections of the brain are all connected and influence each other.

Neurons in the cortex are organised into distinct layers [70]. Each layer contains particular populations of neurons that input and output to specific areas of the cortex and subcortical areas. The layers in the cortex are histologically and functionally defined [73]. Within cortical regions, neurons are aggregated into six horizontal layers: three supra-granular layers (L1-L3), a granular layer (L4) and two

[4] Hippocampal sclerosis is a neuropathological condition with severe neuronal cell loss and gliosis.

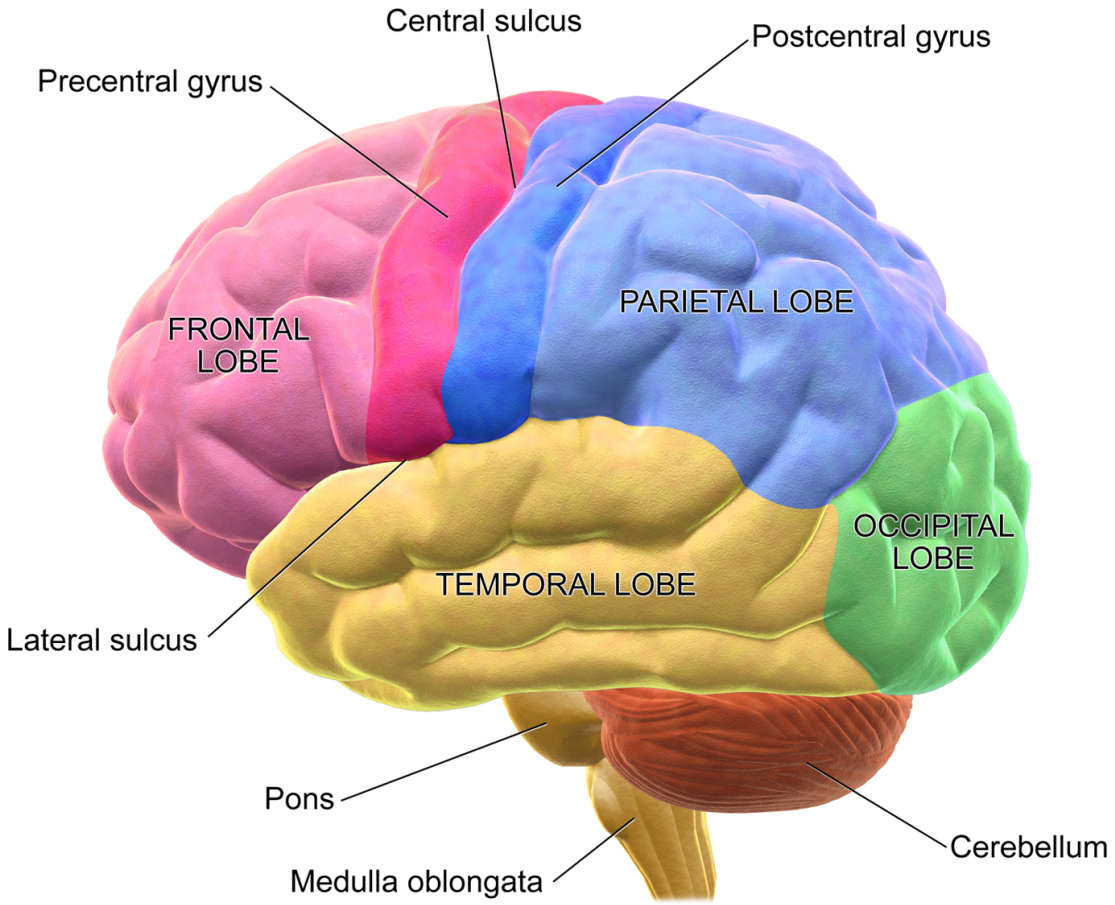

Fig. 1.3 Lateral View of the Brain. An illustration showing the main lobes of the cortex. From [70], Under CC-BY, version 4.0. terms.

infra-granular layers (L5/L6). Figure 1.4 presents the principal types of neurons found in each layer and how they are connected.

1.1.4 Recording the activity of the brain

Knowing the activity of the brain remains a complex task. Many methods do exist each with their advantages and disadvantages. Important methods are computed axial tomography (CAT),functional magnetic resonance (fMRI), electroencephalogram (EEG), magnetoencephalogram (MEG), magnetic resonance imaging (MRI), magnetic resonance spectroscopy (MRS), positron emission tomography (PET) and single-photon emission computerized tomography (SPECT) (see [235] for an overview of the methods and references therein). These multiple approaches are complementary and take into account specific features of the brain. However, in the scope of this thesis, we will focus mainly on EEG recording as this method is particularly useful for epilepsy as seen below.

Electroencephalography

The predominant approach to record neuronal activity in epilepsy is the EEG due to its favourable time resolution, low cost and non-invasiveness [228]. An EEG is a recording of electrical signals from the brain made by putting in contact electrodes to the subject's scalp, see Figure 1.5. The principal generators of EEG fields measured on the surface of the brain or at the scalp are synaptic potentials; i.e., Excitatory Post-Synaptic Potentials (EPSPs) and Inhibitory Post-Synaptic Potentiala (IPSPs) of the pyramidal neurons located in cortical layers III, V, and VI [195, 228]. It gives a 2-dimensional activity map of the cerebral cortex. The spatial resolution is quite low since only superpositions of brain signals originating from the mass of neurons can be recorded. However, EEG provides a high temporal resolution and can detect seizures (see section 1.2.4), thus making EEG an attractive technique for studying epilepsy. Indeed, EEG can detect changes within a millisecond timeframe, this is excellent, considering an action potential takes approximately 0.5-130 milliseconds to propagate across a single neuron, depending on the type of neuron. Other methods of looking at brain activity, such as PET and fMRI have a time resolution between seconds and minutes. EEG measures the brain's electrical activity directly, while other methods record changes in blood flow (e.g., SPECT, fMRI) or metabolic activity (e.g., PET), which are indirect markers of brain electrical activity.

The interpretation of EEG data can require a reconstruction of the sources from the recorded data. This, however, requires a solution of an 'ill-posed' inverse problem, for which infinitely many solutions exist. To select a unique solution, prior knowledge of the source characteristics is needed. The choice of an inverse method is a factor that heavily influences the reconstructed brain activity [111, 173].

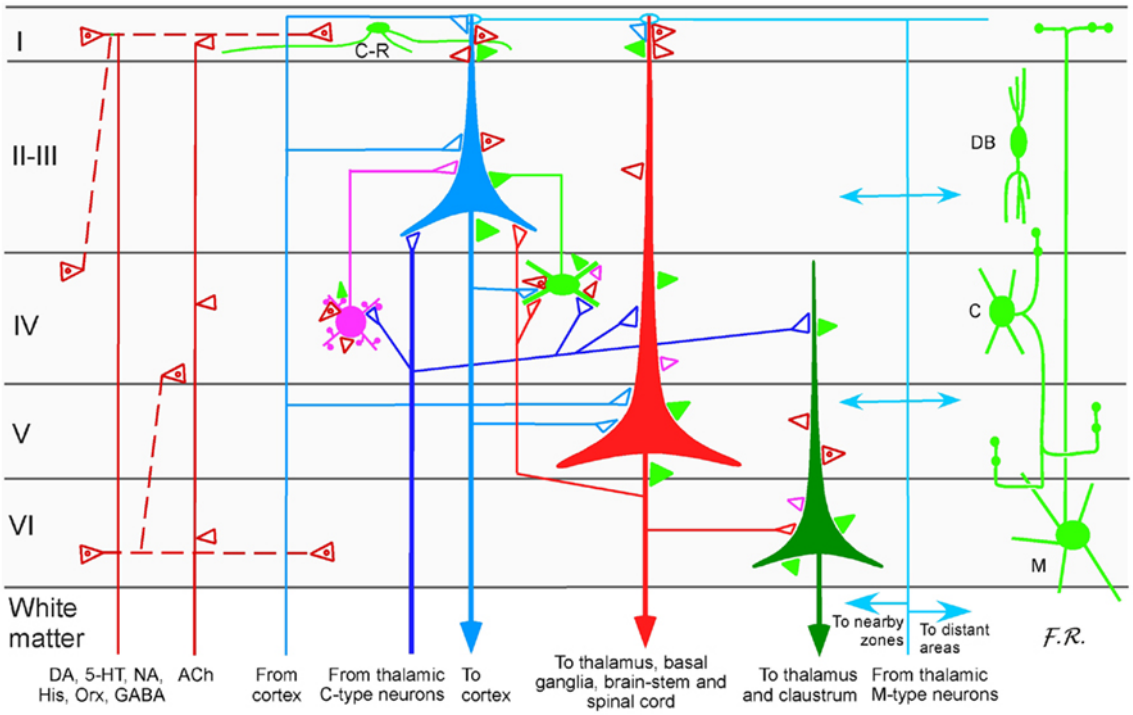

Fig. 1.4 Schematic representation of the fibre and neuronal organization of the cerebral cortex. The projection neurons (pyramidal neurons in layers II, III, V and VI) are represented in different colours according to their origin and targets. The two types of interneurons are represented in different colours: (1) the excitatory interneuron, a spiny stellate cell, is in pink; and (2) the inhibitory interneurons are in light green. There are four specific examples of inhibitory interneuron: two dendrite-and tuft-targeting cells [Cajal-Retzius (C-R) and Martinotti (M) neurons], one dendrite targeting cell [double bouquet (DB) neuron], and one axon targeting cell [chandelier (C) neuron]. Afferent fibres from cortical and subcortical origins are represented in different colours and specific distributions. The wide distributions of dopaminergic (DA), serotonergic (5-HT), noradrenergic (NA), histaminergic (His), orexinergic (Orx), and GABAergic (GABA) fibers originating in brainstem, diencephalic, and basal prosencephalic structures are represented by their terminals, as is the topographically organized terminals of the basal forebrain cholinergic (Ach) fibres. Thalamocortical fibers targeting cortical layers I (M-type) and IV (C-type) are also shown. I to VI, cortical layers one to six. Open triangles, excitatory terminals; solid triangles, inhibitory terminals. From [70], under CC-BY, version 4.0. terms.

Fig. 1.5 EEG brain scan. The recording is obtained by placing electrodes on the scalp with a conductive gel.

EEG recordings are also subject to artefacts, for example, a small movement of the eyes can drastically change the recording [65]. Intensive research has been done in this area (see [56, 267] and references therein) but it is still mainly an unresolved problem. To record a specific region of the brain, it is possible to practice invasive EEG [231]. Particularly, in the case of Intra-cranial EEG (iEEG) [155], the electrodes are directly put into the brain. The data produced are much cleaner and have less of the distortions and attenuations produced by the inhomogeneous layers of the cerebrospinal fluid, skull and scalp. Nevertheless, the process of implementation can be followed by complications including intracranial haemorrhage, superficial infection, elevated intracranial pressure and cerebral infections [231].

1.2 Epilepsy

1.2.1 Definition

Defining epilepsy is a complex problem in itself. Epilepsy cannot be described as a single disorder but rather as a collection of conditions manifesting from underlying brain abnormalities, affecting sensory, motor, and cognitive behaviour. According to the International League Against Epilepsy and the International Bureau for Epilepsy, epilepsy is "*a disorder of the brain characterized by an enduring predisposition to generate seizures and by the neurobiological, cognitive, psychological, and social consequences of this condition. The definition of epilepsy requires the occurrence of at least one epileptic seizure*". Formally, a seizure is defined as "*a transient occurrence of signs and/or symptoms due to abnormal excessive or synchronous neuronal activity in the brain*" [85]. A seizure is the clinical manifestation

of a hyperexcitable neuronal network, in which the electrical balance underlying normal activity is pathologically altered.
The International League Against Epilepsy commissioned a task force to formulate an operational definition of epilepsy for purposes of clinical diagnosis [84]. According to this definition, epilepsy is a disease of the brain defined by any of the following conditions:

- at least two unprovoked seizures occurring more than 24 hours apart;
- one unprovoked seizure and a probability of further seizures similar to the general recurrence risk (at least 60%) after two unprovoked seizures, occurring over the next 10 years; and
- diagnosis of an epilepsy syndrome as detailed in [22].

1.2.2 A historical perspective

As describe by Rajendra Kale, "*the history of epilepsy can be summarised as 4,000 years of ignorance, superstition and stigma, followed by 100 years of knowledge, superstition and stigma*", [207]. The history of epilepsy is indeed long and sorrowful. The disease has been experienced by humanity for at least 3000 years; some tablets even described precisely some kind of epileptic seizures which are still being studied [292]. Historically, epileptic seizures were seen as a symptom of possession by good or bad spirits [207]. It is only 500 hundred years later that Hippocrates considered that epilepsy may be a brain disorder [207]. Unfortunately, his point of view was not accepted until centuries after his death. People with epilepsy have been persecuted, treatments were rudimentary and potentially deadly, see for example in Figure 1.6 a case of trepanation and cauterisation [156]. It is only in the last three centuries that opinions have started to change. In 1849, R.B. Tood was the first person to revolutionize the concept of the disease by advocating the idea that epileptic seizures were the result of electrical discharges in the brain. In 1857, the potassium bromide, the first effective antiepileptic agent, was discovered [199]. The discovery of phenobarbital in 1912 marked the beginning of the modern pharmacotherapy of epilepsy [296]. The apparition of the first prototype of the EEG for humans in 1929 led to a new area of discovery [23]. It is really only with the destigmatisation of epilepsy and the realisation that it is neither a mental disorder nor a spiritual possession that the treatment of people with epilepsy could evolve. However, despite the progress made by scientists to understand epilepsy, people with epilepsy were still stigmatised. The shift has been really slow and for the United Kingdom, it was only in 1971 that the Nullity of Marriage Act removed epilepsy as a reason upon which a marriage could be voidable [47].

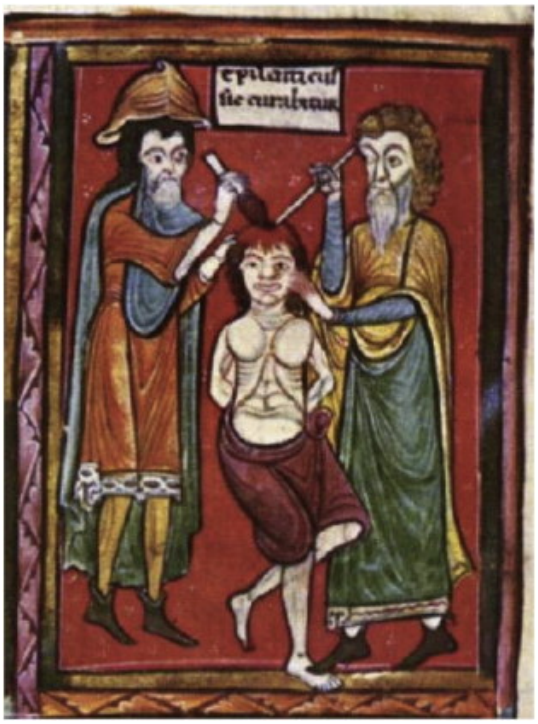

Fig. 1.6 Epilepticus Sic Curabitur ("the way to cure an epilepticus"). In this picture, the person with epilepsy is undergoing trepanation and cauterisation at the same time.
From Sloane manuscript, a collection of medical manuscripts. Miniature painted at the end of the 12th century. Collection: British Museum, London. Artist: unknown, source: http://www.epilepsiemuseum.org/english/kunst/sicepilepticus.html.

1.2.3 Burden of epilepsy

There are between 50 to 70 million people currently living with epilepsy [1, 191]. There is an increase in the prevalence among people living in low and middle-income countries [232]. Approximately 5 - 10% of all people will suffer a single seizure before the age of 80, with a 40% to 50% probability of experiencing a second seizure if the first encounter remains untreated [21]. In 40% of cases, epilepsy can be directly linked to an infection, a trauma, mental illness or the abuse of alcohol or drugs. In Europe in 2010, the total cost of epilepsy was estimated at €13.8 billion per year [196]. The consequences of epilepsy include shortened lifespan, physical injury, neuropsychological and psychiatric sequels, and social and financial disadvantage [66, 242]. It is the sheer unpredictability of seizures that impedes the most on lifestyle and mobility. "When will be the next one?" is a question which haunts people with epilepsy [13]. Because of this patients require constant monitoring and care. The stigma linked to this disease is still a burden for patients and their close relations. Fear, misunderstanding and the resulting social stigma and discrimination surrounding epilepsy often force people with this disorder "*into the shadows*" [13]. The social effects vary from country to country but in general, living with epilepsy remains a struggle. The stigma can be really important for example in both China and India, epilepsy is commonly viewed

as a reason for prohibiting or annulling marriage [1]. An epileptic seizure is still seen as a demoniac possession in some regions of the world [144, 194], even in specific cases in the United Kingdom [52]. Furthermore, as noted in [181], some people still use archaic and potentially dangerous treatments such as trepanation, a surgical intervention in which a hole is drilled or scraped into the human skull. It is easy to understand that even in countries where there is no such stigma, this disorder is responsible for isolation and increases the risk of depression and suicide, [154]. Overall, however, huge progress has been made to treat or help people living with epilepsy. 70% of patients with epilepsy can be treated with drugs. Some treatments can be expensive but there are other effective treatments based on more affordable generic medicine (around $250 a year). Unfortunately, between 80 and 90% of the people with epilepsy are in developing countries [1, 191] where they cannot be adequately treated [236].

1.2.4 Signs and symptoms

There is a multitude of different types of epilepsy which are all linked to the fact of seizure recurrence. The symptoms can be very different from one type of seizure to another. For some, like the absence seizure [198], the person has a brief loss and return of consciousness. For others, the symptoms are more dramatic. For tonic-clonic seizure [198], the skeletal muscles suddenly tense, either causing the extremities to be pulled towards the body or rigidly pushed away from it, which will cause the patient to fall. The patient's muscles start to contract and relax rapidly, causing convulsions. The eyes can roll back and the tongue can be strongly bitten. Seizures can lead to death; sudden unexpected death in epilepsy [147] occurs in about 1 in 1,000 adults and 1 in 4,500 children with epilepsy a year [121].
Different types of seizure may have different causes, outcomes and treatments. Seizure types are divided into two broad categories: generalised or focal [86]. Generalised seizures distort the electrical activity of the whole brain while focal seizures impact only a specific part. As specified in section 1.1.4, EEG is frequently used to diagnose and advance research in epilepsy [150]. A seizure recording via EEG is presented in Figure 1.7 where the transition to seizure can be directly observed. EEG rhythms associated with epileptic processes (epileptiform rhythms) can be revealed, in most cases, by visual inspection. Some of the key temporal features distinguishing epileptiform rhythms from background EEG are wave form, frequency and amplitude. The rich diversity in the EEG manifestation of seizures can be associated with a range of physical symptoms [132]. The most frequent dynamics are spike and wave discharges (SWD) or polyspikes and wave. The term “spike-wave" gives an intuitive description of the multi-modal nature of this rhythm in that there is a fast component (the spike) followed by a slow component (the wave). Patients with certain epilepsies can also present transient inter-ictal abnormal activity, such as inter-ictal spikes or slow waves [247]. Understanding

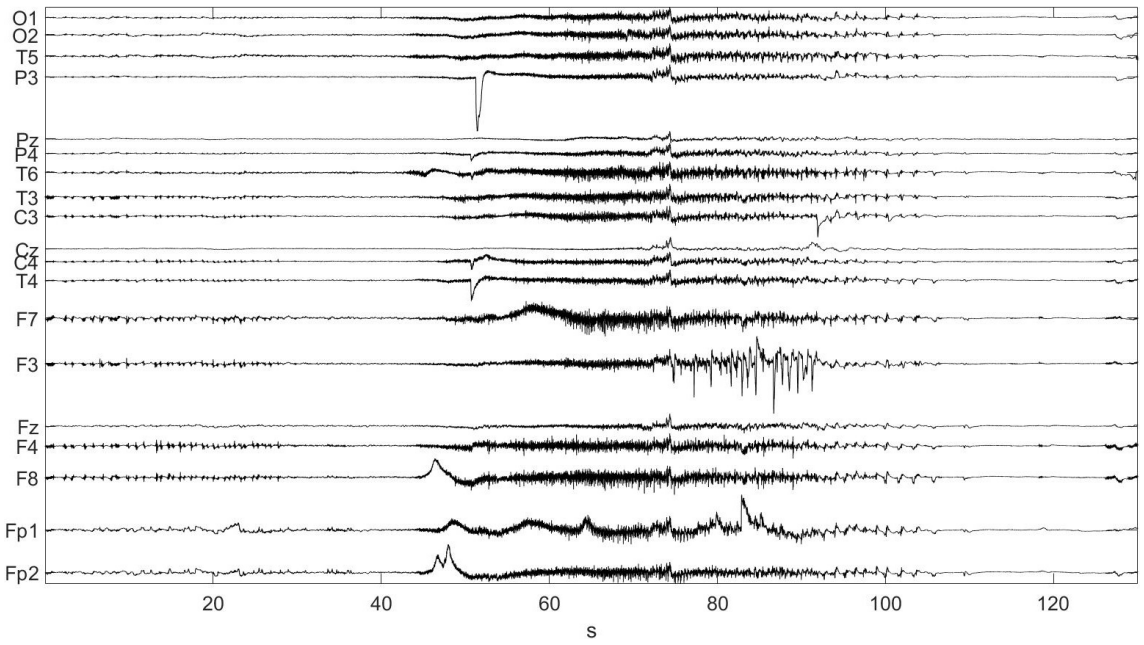

Fig. 1.7 Epilepsy seizure recorded by EEG of a patient with Left TLE. Adapted from Marinho Lopes' research with authorisation.

these dynamics is one of the purposes of mathematical modelling as we will see in section 1.3.

1.2.5 Treatments

In terms of treatment response, people with epilepsy can be classified into three groups [293]: those who enter remission spontaneously, those whose seizures are effectively controlled through the use of anti-epileptic drugs (AEDs), and those whose seizures cannot be controlled using standard therapeutic interventions. The recent progress in the treatment of people with epilepsy has been tremendous. According to the respected Global Burden of Disease Study 2015 [277], out of the 30 most important disorders, epilepsy is the disorder where the world amount of years lived with disability has decreased the most (in percentage). Furthermore, even if recurrent, the stigmatisation of epilepsy is decreasing. Nevertheless, epilepsy remains one of the most important neurological disorders and an active community of researchers are trying to understand and treat epilepsy. Computational neuroscientists and clinical epileptologists research together in interdisciplinary teams to overcome this burden [180].

Drugs

During the past century, many new antiepileptic drugs (AEDs) have been created. Effective seizure treatment generally augments or decreases the activity of specific neurons. Their mechanisms of action fall into a number of general categories: the main groups include sodium channel blockers, calcium current inhibitors, γ-

aminobutyric acid (GABA) enhancers, and glutamate blockers. However, the mode of action of some AEDs falls outside of these broad categories. Many AEDs also possess multiple mechanisms of action. However, even with the proliferation of drugs (more than 10 new drugs in the last 20 year [226]), more than 30% of people with epilepsy remain unresponsive to existing AEDs [4], these people are pharmacoresistant: they continue to experience seizures despite treatment with maximal doses of multiple AEDs with different molecular targets and mechanisms of actions. Furthermore taking drugs is often followed by side effects [188, 226] such as cognitive problems, kidney stones, speech problems and weight loss. It is thus important to develop tools other than AEDs.

Surgery

For pharmacoresistant people, surgical treatment options may be considered [145], including surgical resection of the epileptogenic zone, i.e. an area of the cortex that is indispensable for the generation of epileptic seizures [79, 171, 182, 238]. In some cases, the person is seizure-free after an operation but these procedures are not entirely efficient. For example, complete seizure freedom, twelve months post-surgery, is only achieved in approximately half of the people and can be as low as 15% in extra-temporal cases (see [71, 189, 285], and references therein).

Electrical stimulations

Vagal nerve stimulation and brain stimulation are other approaches which can be considered when the person is pharmacoresistant. Vagal nerve stimulation is the equivalent of a pacemaker for the brain [131]: intermittent pulses arising from a generator implanted subcutaneously in the chest travel along a lead to electrodes wrapped around the vagus nerve in the neck. These signals then travel in an efferent manner via the vagus nerve to exert widespread brain effects [205]. It appears to be a safe therapy, even among children [115]. There are different type of simulations including deep brain stimulations [118] (stimulations through depth electrodes), transcranial direct current stimulations [223] and transcranial magnetic simulations [218, 279]. Nevertheless, these approaches are still at an experimental stage and further, larger and well-designed trials on intracranial electrical stimulation treatments are needed to validate and optimize the efficacy and safety of the electrical stimulation and to compare this treatment to currently available treatments [246].

Promising treatments

Evolving technologies coupled with new areas of research are promising. New types of drugs such as the anti-inflammatory drugs [273] are being explored. Specific person pharmacogenetic markers could help to target the most efficient drugs

and minimize the side effect of drugs, an example can be found in [55]; patients who carried the HLA-B*1502 allele were advised to avoid the carbamazepine as a drug and a significant decrease of incidence of Stevens-Johnson syndrome was observed. In term of surgical operation, recent discoveries have also been made. Firstly some reasons for the failures of certain existing operations have been identified. For example, primary temporal lobe epileptogenic zone extending to neighbouring regions were a marker of failed surgery [14]. Secondly, new approaches are being considered in order to find the optimal zone of brain resection [106]. Surgery is also improving, with, for example, laser interstitial thermal therapy [289]. Intracranial neurostimulation has the potential to become a new method to prevent or interrupt a seizure [262]. This method could be a potential game-changer for people who do not want or cannot have a resection and are pharmacoresistant.

1.2.6 Seizure causes

To develop new treatments, it is necessary to improve our understanding of the brain and epilepsy. The exact nature of the dynamic transitions from a normal background EEG to seizure type dynamic is unknown at present. Why and how ictal episodes occur is difficult to comprehend based only on current knowledge of pathophysiology, due to the complexity of the factors that jointly are responsible for their occurrence. In order to understand seizures, it is useful to apply concepts derived from the mathematics of nonlinear complex systems for the analysis of the workings of neuronal networks [12, 163, 164]. Four main mechanisms could underly the emergence of seizures [12, 164], see figure 1.8:

1. bifurcation: a biological change of a component in the neuronal system leads to a seizure.;

2. bistability: an external input (visual for example) which causes a sudden change in the neuronal system resulting in a seizure. Another external input will cease the seizure;

3. excitability: an external input (visual for example) which causes a sudden change in the neuronal system resulting in seizure but the system comes back to its initial state without any external input; and

4. intermittency: due to the neural network composition, spontaneous transitions lead into and out of the seizure rhythms.

An important aspect of research in epilepsy consists of understanding and predict these possible mechanisms. Part of the scope of this thesis consists of building tools to do so robustly.

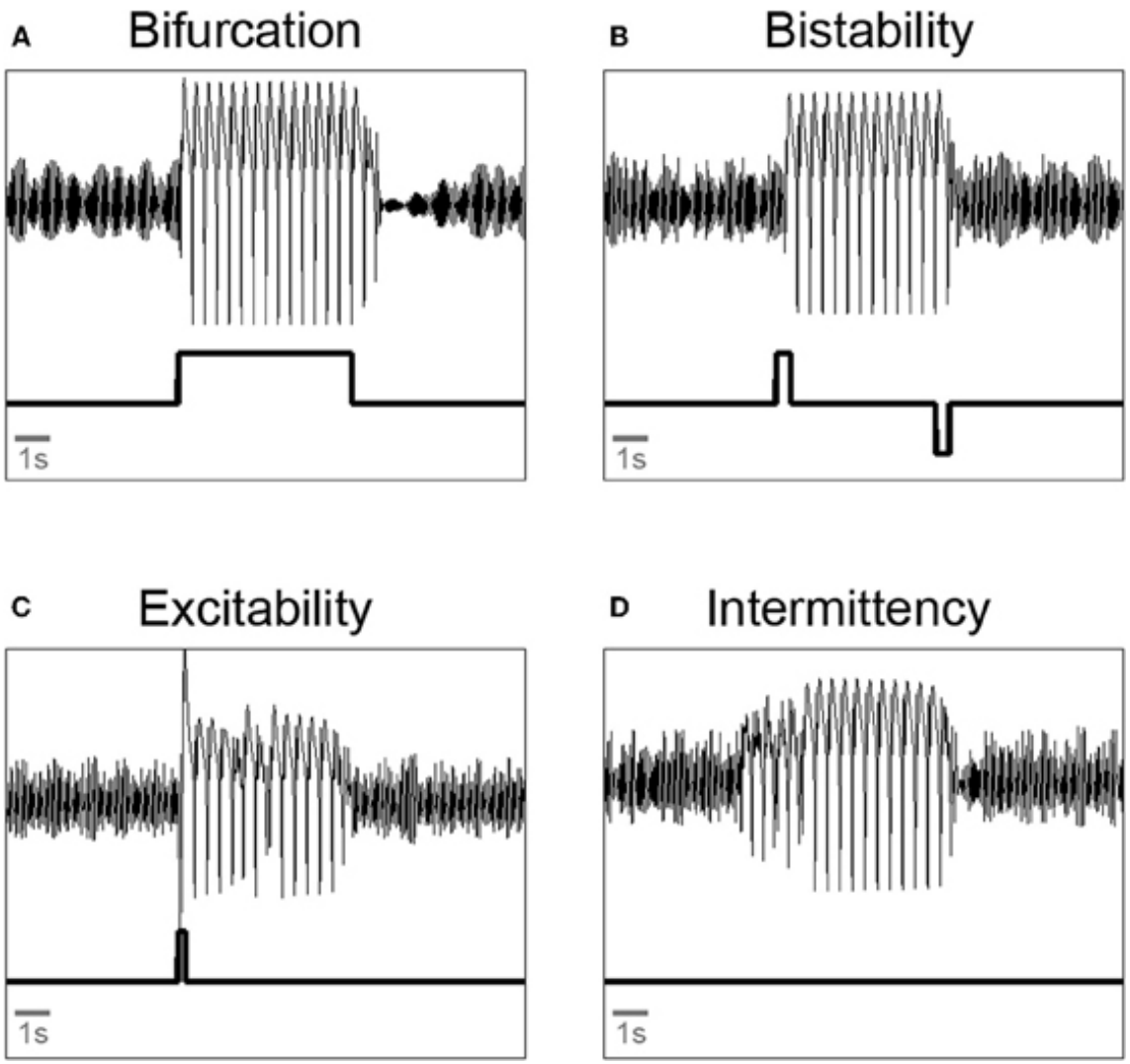

Fig. 1.8 Illustration of qualitatively different transitions from background oscillations to pathological spike-wave and back again in a mathematical framework. In each subfigure the above oscillating time series reproduce the EEG activity, the below time series reproduce the value of one biological parameter. (A) Bifurcation: a parameter is changed such that it crosses a bifurcation point. (B) Bistability: two pulse perturbation are applied to start and terminate a seizure. (C) Excitability: a single pulse perturbation is applied to induce a seizure. (D) Intermittency: parameter setting allows spontaneous transitions into and out of the seizure rhythms. From [12].

1.3 Mathematical models

1.3.1 Understanding epilepsy using mathematical models

In the field of epilepsy research, the modelling approach has become an extensively used tool [37, 172, 254, 283, 293]. The development of models representing the core of human knowledge and the development of mathematics have always gone hand in hand with each other [177]. Mathematics is a universal language that allows us to see the hidden structures underneath the incomprehensible seeming surface of our world. Algorithms and models have always been central in the development of mathematical sciences but their potential was limited by the lack of computer power. In the last century, high power computation capacity has changed the role of mathematical modelling.

A mathematical model is an abstract model that uses mathematical language to describe the behaviour of a system [20]. A mathematical model is useful to analyse a system; mathematicians can build a descriptive model of the system as a hypothesis of how the system could work and try to estimate how an unforeseeable event could affect the system. They can also explain which part of the system is responsible for abnormal activity in the system. A mathematical model usually describes a system by a set of variables and a set of equations that establish relationships between the variables. Variables may be of many types; real or integer numbers, boolean values or strings. Models can be used in two main different ways, forward and inverse [300]:

- the forward approach projects the final state of a system given its initial condition; and
- the inverse approach takes a solution and attempt to determine the initial and boundary conditions that gave rise to it.

Whatever the problem studied and the chosen approach, the same logic stands: going from a complex biological system which is beyond human understanding to a complex mathematical system which can be extensively and easily studied using mathematical tools [237]. Experiments that one can do in a mathematical model are ideal in comparison to real experiments which are always performed under non-ideal conditions. Further one can change parameters in mathematical models easily, something that is difficult or even impossible in real experiments.

A mathematical model needs to be “a representation of the essential aspects of an existing system (or a system to be constructed) which presents knowledge of that system in usable form” [80]. The challenge faced by any modelling approach is to capture the main features of the system under study in a simple but efficient way. The model has to be able to reproduce similar activity given the same input as the original system itself. A crucial part of the modelling process is to determine whether or not a given mathematical model describes a system accurately.

Mathematical models can take many forms, including dynamical systems [168], statistical models [31] or game theoretic models [276]. Dynamical systems are mathematical objects used to model physical phenomena whose state (or instantaneous description) changes over time. Mathematical models to study epilepsy are often dynamical system due to the temporal characteristics of seizures. As there are different scales on which to study the brain, there are several categories of models of epilepsy.

Micro scale models

First, there are detailed models of individual neurons. These model are designed to answer questions related to the dynamical behaviour of individual neurons including the neural ion channels, neural morphology (dendritic tree, axonal arborisation) and interactions between neurons and their local environment (see [248] for an overview). The most famous in this category of models was designed by Hodgkin and Huxley in the early 1950s [127]. Many models inspired by their approach exist [104, 139] and are still used to simulate and study large networks of individual neurons.

Macro scale models

Neural mass models (NMMs) describe the interaction of different populations of neurons at the mesoscopic and macroscopic levels [140, 290]. By coupling neurons together into larger ensembles or (sub)populations, networks of variable size are constructed as sets of coupled differential equations. Simulating these networks then gives the evolution of the state-variables of every population of neurons and reveals the emerging spatiotemporal patterns at a network level. NMMs consider the average behaviour of different types of neurons. The key advantage of NMMs is that some of their variables represent the measured electrical field potentials and thus the model simulations and data recording can be easily compared. Another advantage is that due to the relative simplicity of the equations, it is an efficient class to simulate data and to perform some analyses with a limited computation power. Furthermore, the dimension of the NMM model is slightly less important than the other classes of models and facilitate the use of many mathematical tools such as bifurcation analyses. This thesis focuses primarily on NMMs as these models are useful in understanding the meso scale and can be used at a macro scale with relatively little computing power. There is a distinction between networks of NMM and neural field models to model the whole or at least large part of the brain [37]. A network of NMMs can be viewed as an extension of NMMs, [64] where different NMMs are connected together. Each NMM represents a part of the brain. The other approach consists of considering the cortex as a smooth sheet composed of dense short-range connection [5, 291]. Neural fields models model the large-scale dynamics of spatially structured biological neural networks.

They use differential equations whose associated integral kernels represent the spatial distribution of neuronal synaptic connections [44]. In this thesis, we use both approaches to study different aspects of epilepsy.

1.3.2 The development of neural mass models

History of neural mass models

In 1938, the neural mass concept was introduced by Lorente de Nó [167]. But it was only 20 years later that the notion of NMMs (called mass of cells at the times) was formally established [25]. This notion was consolidated by the work of Mountcastle [186] who presented physiological evidence for the existence of spatially localised neural populations. This notion was further developed on a theoretical level by Ventriglia [272] and by Wilson and Cowan [290] who studied the interaction of excitatory and inhibitory cells. From a practical approach, two main schools appeared: da Silva was interested in the emergence of alpha rhythm in the brain [165, 166] while Freeman wrote a series of articles focusing on the olfactory system [88–91]. The models were extended in the following years [92, 271] with the introduction of networks of NMMs.

In the 1990s, Jansen and Rit explored this approach further and published a new NMM [140, 141]. This model includes three populations of neurons, the pyramidal neurons, the inhibitory neurons and the excitatory neurons. Within this model, excitatory neurons can be regarded as spiny stellate cells found predominantly in layer IV (see Figure 1.4) and in receipt of forward connections [179], the inhibitory neurons occupy both supra- and intra-granular layers (layers I-III in Figure 1.4). They showed that the model was able to produce a large variety of EEG-like waveforms and rhythms. The end of the 1990s and the early 2000s saw the creation of many models with specific features of interests and applications: Wendling et al. [281, 282] added a fourth population to model the hippocampal activity following the work of Pearce et al. [200]. They distinguished two classes of inhibitory neurons: slow and fast neurons. They used this model to explain epileptic brain dynamics. The model of Robinson et al. [214] focused on the link between the cortex and the thalamus. The model of Liley et al. [160] paid particular attention to the role of synaptic reversal potential. Other NMMs include the interaction between the neurons of the thalamus and the cortex [215, 251, 252], the interaction between the neurons, the glial cells and blood vessels [8]. Some models try to explain multiple dynamics of interest and contain up to 8 different populations of neurons [241]. Even if not recent, NMMs are an increasingly active area of research. As indicated by the Figure 1.9, the number of articles with a title containing the term “neural mass model(s)” has increased during the last years. In 2017, 24 article titles mention this term. The number of articles mentioning the term neural mass model(s) in their corpus has also increased. This increasing

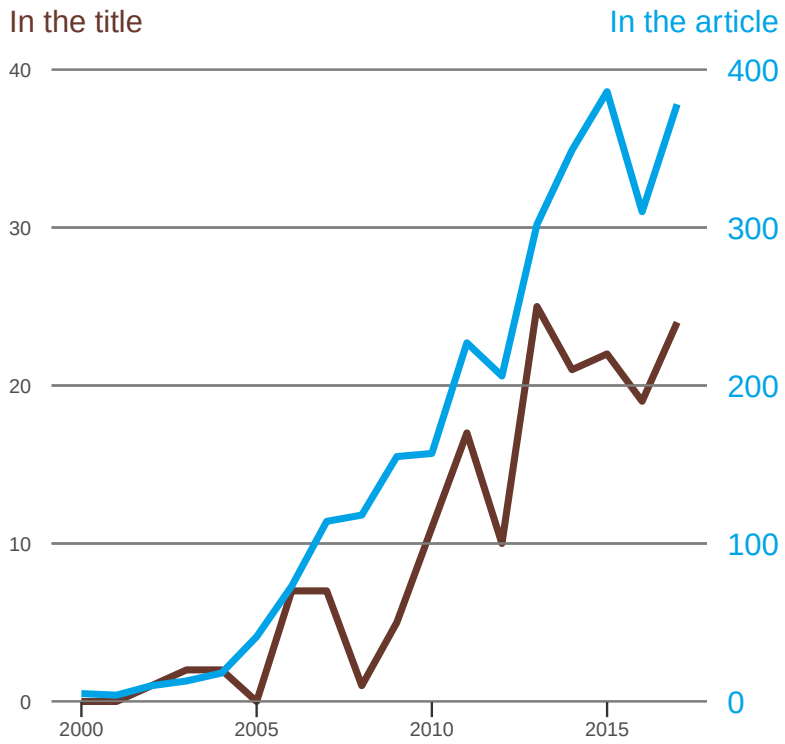

Fig. 1.9 Neural mass model, an active area of research. Representation since 2000 of the articles published containing in their titles or their corpus the term "neural mass model(s)". The number of publications has drastically increased in the past ten years. The data have been extracted from Google Scholar.

popularity shows the necessity to develop tools to study and assess the quality of NMMs. We only present studied the increase of the presence of NMMs but we note that the term "lumped model" is also present in the literature to mean NMM.

Component of neural mass models

As described in section 1.1.2, the inputs one neuron receives at the synapses from other neurons cause transient changes in its resting membrane potential, called postsynaptic potentials (PSP). When the PSP reaches a certain threshold, the neuron produces an impulse. It is possible to model this process at a single neuron level [127] but another approach is possible. In NMMs, similar neurons can be treated as an averaged bulk entity [88]. Instead of modelling neurons individually, NMMs treat a population of neurons as an ensemble and describe their behaviour in terms of distributions. [72, 203] describe thoroughly the link between individual neurons and the macro scale models. NMMs are based on the assumptions of the existence of different populations of neurons and that each neuron in a population can be well represented by the average of its population, the mass. In the simplest case, there are two populations: excitatory and inhibitory neurons. The activity of each population is governed by the interactions between them and potential

extrinsic input from other parts of the brain. Each of the neuron populations is modelled by two blocks [140]:

1. The first block transforms the average presynaptic pulse density of afferent action potentials of other populations of neurons (the input) into an average postsynaptic membrane potential (the output) via a kernel:

$$k(t) = Ggte^{-gt}\mathbb{1}(t > 0). \tag{1.1}$$

G is the gain in the population of neurons and $1/g$ is the average dendritic time constant. Depending of the intrinsical characteristics of the neurons in the population, this kernel can have different properties. See for example, Figure 1.10, where two different populations of neurons are presented, excitatory neurons and inhibitory neurons. This block introduces two differential

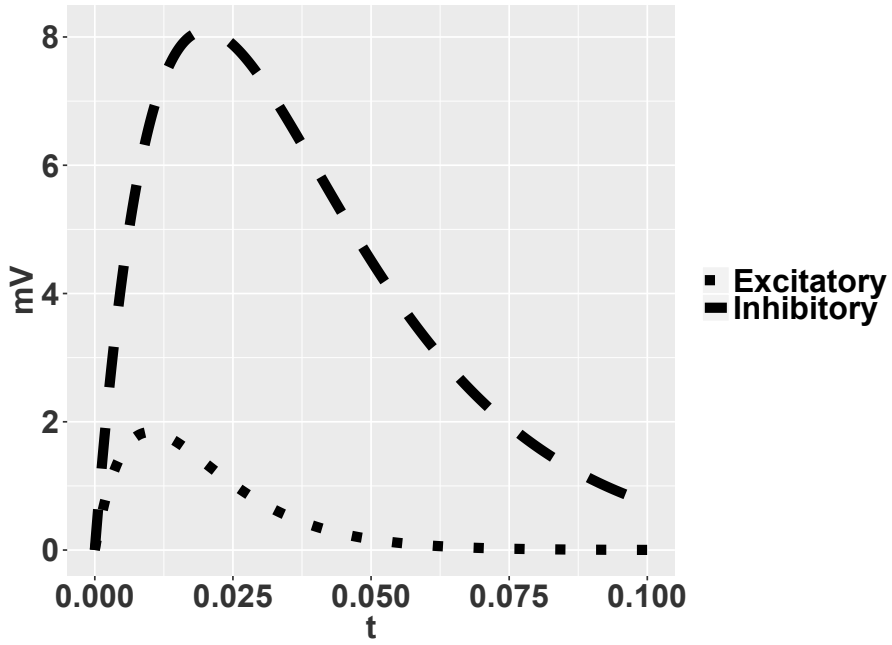

Fig. 1.10 Average postsynaptic membrane potentials: excitatory and inhibitory, obtained from impulse responses given by $h_e(t) = Aate^{-at}$, $h_i(t) = Bbte^{-bt}$ (see Table 3.2 for parameter values).

equations of the form:

$$\ddot{y}(t) = Ggx(t) - 2g\dot{y}(t) - g^2y(t), \tag{1.2}$$

which can be rewritten as:

$$\dot{y}(t) = z(t), \tag{1.3}$$
$$\dot{z}(t) = Ggx(t) - 2az(t) - a^2y(t), \tag{1.4}$$

where $x(t)$ is the action potentials of other population of neurons and $y(t)$ is the average postsynaptic membrane potential.

2. A second block which transforms the average post synaptic membrane potential into average pre-synaptic pulse density. This is typically a static nonlinear function (a nonlinear function is a function in which the change of the output is not proportional to the change of the input). A common nonlinear function used is the sigmoidal function:

$$S(v) = \frac{2e_0}{1 + e^{(r(v_0 - v))}}. \tag{1.5}$$

It relates the average postsynaptic potential of a given population to an average pulse density of action potentials outgoing from the population. See an example Figure 1.11. For further information on its derivation, see the paper by [91] which was one of the first papers to try and rigorously derive the sigmoid function from experimental data.

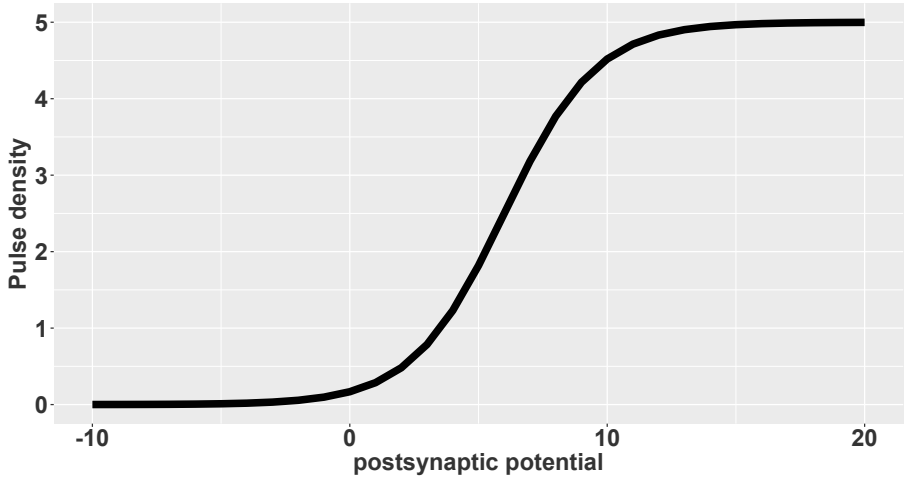

Fig. 1.11 From postsynaptic potential to average pulse density. The sigmoid function models the transformation of postsynaptic potential into average pulse density. The function is nonlinear and is bounded.

1.3.3 Common approaches for studying neural mass models

One of the reasons for the increasing presence of NMMs in academic publications is their success in improving our understanding of the brain. NMMs have been proposed to understand the effect of stimulations including from an external input such as transcranial magnetic simulation [62], auditory simulation [225] and anaesthetic drugs [152]. Equally, the power spectrum of the brain in different states and their transitions can be well-replicated [61, 219, 268, 298]. The applications of NMMs to epilepsy are particularly prolific. Detailed reviews of the insights gained by NMM can be found in [37, 67, 248, 283, 293]. To answer questions, two main approaches have been used: the forward problem and the inverse problem approaches. The forward problem can be described as the simulation of the model given a set of input parameters [300]. The inverse problem can be described as

the identification of the parameters which would have simulated an output similar to our data [300]. Both approaches are useful and complementary in the context of studying epilepsy. In this thesis, we focus mainly on the forward approach.

As specified in section 1.2.4 there are four possible mechanisms which can explain the seizure onset. NMMs give us the possibility of exploring these four options in a mathematical framework and of comparing the context in which they could arise. Three main approaches have been used in the past and are described in detail in the following section:

- activity map: the model is simulated a large number of time to identify by a visual approach the relationship between dynamics and parameters;
- sensitivity analysis [204]: Sensitivity analysis tries to determine how the change of input parameters would affect the change of the output by using a statistical approach.
- numerical continuation and bifurcation techniques [151]: a bifurcation occurs when a small change made to the parameter values (the bifurcation parameters) of a system causes a sudden 'qualitative' or topological change in its behaviour [28]; and

Activity map

NMMs can be directly simulated to reproduce the activity of populations of neurons. The solution of NMMs ODE can generally not be solved analytically so temporal discretisation methods are used to approximate solutions. Runge–Kutta methods are often used [46]. This helps to understand how the interactions between populations of neurons can lead to seizures. Parameters are modified to identify for which values particular dynamic appears. This approach has been intensively used to understand the potential of NMMs for simulating specific rhythms of the brain. Activity maps have given the insight to explain the role of the different populations of neurons to explain epilepsy [68, 140, 281]. However, due to the large number of parameters, only a certain number of parameters are studied, the rest are fixed at predefined values.

Bifurcation analysis

A bifurcation occurs when a small change made to the parameter values (the bifurcation parameters) of a system causes a sudden 'qualitative' or topological change in its behaviour [151]. Numerical continuation tools exist to track these bifurcations[5] and have been intensively used to study seizure onset [29, 38, 107,

[5] such as AUTO, MATCONT, or DDEBIFTOO.

124, 135, 183, 244, 253, 265]. These studies typically only examine two parameters simultaneously. Clearly, in high dimensional systems such as NMM, we expect that changing a third parameter could affect the distribution of dynamics obtained. NMMs such as the Jansen model [140] have been studied comprehensively by simultaneously altering 3 parameters [265]. A potential downside to such analyses is that results can be cumbersome and difficult to summarise, thus moving beyond 3 parameters with these techniques would prohibit a succinct evaluation of the role of each of parameter. Another approach is to extend multiple bifurcation analyses in a single parameter across 5 further dimensions, whilst classifying different bifurcations and their prevalences [244]. Although this is a valid approach to understanding some elements of the complexity over large dimensional parameter spaces, it does not give a comprehensive overview of the role that each parameter plays. Even if very enlighting about the role and co-dependence of few parameters numerical continuation cannot be used to approach simultaneously all parameters. In high dimensions (e.g. ≥ 3) this approach soon becomes computationally intractable. On the other hand, studying a restricted number of parameters is unsatisfactory.

Sensitivity analysis

Sensitivity analysis investigates how the variation in the output of a numerical model can be attributed to variations of its input parameters [34, 204]. If one is interested in performing the analysis around a point of interest in the model parameter space, then one is performing a local sensitivity analysis.

The simplest way to interrogate a model is to study the model output when we vary one model parameter at a time [34]. The procedure is straightforward:

1. moving one parameter value, keeping others at their baseline (nominal) values; then,

2. returning the parameter to its nominal value and repeating for each of the parameters in the same way.

This method is used in the NMM field [61, 184, 219, 251, 268]. However, this approach suffers the same limitation of the two approaches presented above. One needs to select an initial parameter set to do a local analysis. It is possible to use more advanced approaches such as global sensitivity analyses (variance-based methods [128, 222, 239], variogram analysis of response surfaces [210, 211], screening [50] or generalised models [113]) which have previously been used to identify the existence of relationships between dynamics and parameters (in fields other than NMMs). However, these methods would only assess the importance of one parameter and would not indicate for which values the parameter is important, or its relationship with other parameters.

1.3.4 An important limitation of the current approaches: high dimensionality of the parameter space

One of the inconveniences of NMMs is their relatively large dimensional parameter space. Thus it is difficult to apprehend the role of each parameter for the dynamics of the NMMs in more than few dimensions. A classical approach chosen by most of the studies in this section consists of fixing all parameters but a few and explore this new sub-parameter space. This leads to a much easier analysis but there is no guarantee that a fixed parameter could have influenced the role of the parameters which were not fixed. To show the effect of a third parameter which has been fixed let us consider by example the model f:

$$\begin{cases} f : \mathbb{R}^2 & \to \mathbb{R} \\ (x, y) & \mapsto xy. \end{cases} \tag{1.6}$$

If one would fix $y < 0$ and analyse the role of x, x would appear to be negatively correlated to the output. However, if $y > 0$ the analysis would provide other results; x would be positively correlated to the output. Thus studying only x with y fixed can lead to misleading analyses. Fixing default values a priori in order to study the generation of particular dynamics does not allow to understand the behaviour of the system at unexplored, potentially plausible parameter values. Thus we cannot discover whether other regions of parameter space permit the same or different conclusions. When specifying prior distributions for model inversion, we usually, therefore, do not know to what extent any resulting inference is dependent upon the particular choice of priors or whether unexplored regions of parameter space could also provide reasonable solutions.

If fixed parameter values and a priori distributions reflected our knowledge and experimental data, this would not be a problem. However experimental data show that this is not the case. The parameter values extracted from experimental data are uncertain: a large variability has been shown to exist in parameters measured directly from neurons and neural masses [88, 266] (see chapter 3 for more details). Thus chosen prior distributions of fixed parameter values are assumptions which are likely to be false.

We saw that fixing parameters or working with strong a priori distributions is not well founded. It is necessary to study the repertoire of NMM dynamics over all parameters that cannot be sufficiently constrained. It would facilitate a deeper understanding of complex, high dimensional models. It would also facilitate choosing appropriate priors and initial parameter settings in model inversion algorithms (by identifying for example parameters which do not influence the dynamics and by fixing them). The methods presented above do not allow to quantify the impact that changes in multiple (e.g. all) parameters have on dynamics

and to identify specific regions of parameter space in which changes in dynamics occur.

To overcome current limitations of the use of NMMs and the potential of studies to mislead (e.g. where only a set of parameters were studied at the same time) a new approach is needed. The approach needs to be able to explore and analyse the parameter space of a mathematical model in a relatively short amount of time, to visualise this high dimensional parameter space by identifying the role of the parameters in different subspaces of the parameter space. This approach needs to be able to address multiple questions to lead to a better understanding of the NMMs:

1. Which parameters influence the dynamics?
    - Which parameters globally influence the dynamics, i.e. regardless of the values of the others parameters, a global parameter would influence the dynamics when its value changes.
    - Which parameters only influence the dynamics locally, and in this case to which others parameters are they linked?
    - Are there some parameters that never influence the dynamics and thus can be fixed without detriment to the study?
2. Are some parameters interacting together?
3. For which parameter values do dynamical transitions appear?
4. Does the model give meaningful output in the biologically constrained parameter space?

In this thesis, we propose a new method to analyse the parameter space of a NMM, the decision tree mapping (DTM) method. DTM consists of mapping the parameter space of a given NMM over features of interest in an interpretable and succinct manner. To do so, the NMM is successively simulated a large number of times with different combinations of parameters and then a machine learning method called decision tree learning algorithms [43] and random forest [122] are used to map and analyse the parameter space.

1.4 Conclusion

We have seen in this chapter that epilepsy is a complex disorder with a huge burden at different levels of society. Due to the complexity of this disorder, until recently treatments could be potentially more dangerous than epilepsy itself. Recently, progress has been made to treat and reduce the burden of epilepsy. However, the path to a world without epilepsy is long.

The causes of epilepsy are difficult to apprehend due to the complexity of the brain. The brain is a multi-scale system and its dynamics are relatively difficult to observe. To study the brain, mathematical models have been developed. These mathematical models have given insights to explain the dynamics observed in EEG recordings and how neuronal populations interact.

Nevertheless, as explained above, the parameter space of NMMs can be highly nonlinear and need to be studied in its entirety. The history of epilepsy reminds us of the danger of “playing” with the brain without a deep understanding of its mechanisms.

Current methods are useful to explore parameter spaces but do not provide a rigorous and robust method to analyse the parameter space. It is thus critical to develop a new approach which gives the possibility to better understand the models that scientists use on a daily basis.

Therefore, we introduce DTM for the characterisation of NMM dynamics simultaneously over all parameters. This approach is useful to identify the parameters which impact most the dynamics of NMMs and for which values changes are more likely to occur. In the next chapter we describe DTM and in the following chapters, we apply DTM to different problems.

Chapter 2

Methodology

> The fertile field of discovery lies for the most part on those borderlands where one science meets another.
>
> D'Arcy Thompson. *The College*

This chapter is based on the work published in [83] in collaboration with Dr. Marc Goodfellow and Prof. John Terry.

In this chapter, we introduce the necessary background to understand the DTM approach and analyse the parameter space of a NMM. This approach is based on a new combination and adaptation of different previous methods available in the literature. We briefly present an overview of DTM in section 2.1.1. Then we detail its different components, from section 2.1.5 to section 2.1.6. We then focus on the interaction between parameters which is not directly taken into account by the DTM approach, see section 2.3, and which are helpful to better analyse a parameter space, as in chapters 3 and 4. To help the reader to understand the different concepts and show the efficiency of the approach, diverse examples are presented in the chapter.

2.1 Tree decision mapping approach

2.1.1 Overwiew of the tree decision mapping approach

In this section, we give a brief descriptive overview of DTM and provide further mathematical details of each component in subsequent sections, see Figure 2.1 for a general overview.

The first step consists of choosing a NMM, see section 2.1.2. The parameter space is also defined, i.e. some constraints on the extreme values that each parameter can take and an approach to classify or order the output.

The second step in the methodology consists of transforming the mathematical model into a database, see section 2.1.2. To do this the NMM is simulated a

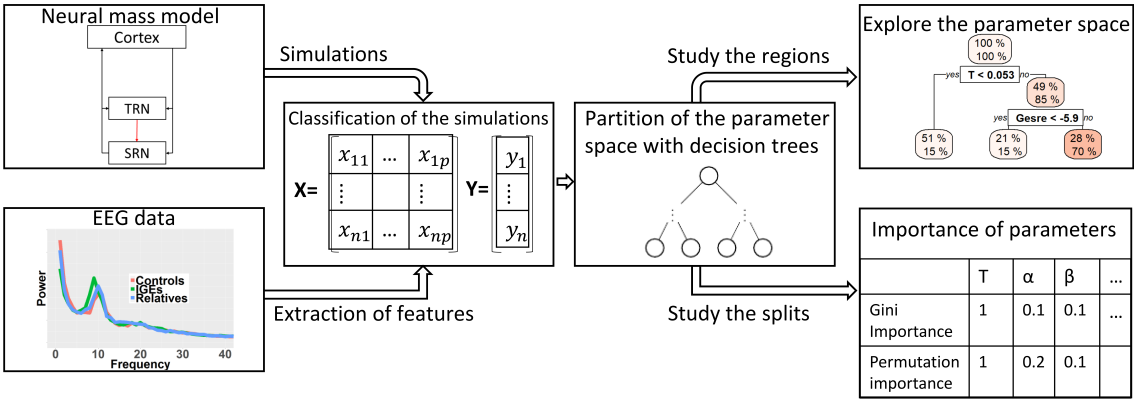

Fig. 2.1 Schematic of the methodology of decision tree mapping. The dynamic features of interest are identified and characterised and a model able to reproduce the dynamic of interest is selected. The NMM is simulated a large number of times over its parameter space and each simulation is classified. Then the simulations are partitioned using decision tree learning. Finally the final partitions are used to characterise the parameter space of the NMM.

large number of times using different parameters, which are chosen using a latin hypercube design [176]. This is a space filling design which allows to efficiently explore the whole parameter space given a fixed number of simulations.

The final step is to fit the data with a statistical model, see section 2.1.3. We use decision tree learning and random forests, see sections 2.1.5 and 2.1.6. These models cut the parameter space into rectangular regions of different sizes and is amenable to high dimensional analyses. These regions are created with the aim that each one contains a high proportion of the presence of a dynamic of interest or a high proportion without the presence dynamic of interest. Of course, we do not expect that the parameter space can be completely mapped to a set of rectangular regions, but it will reveal important trends and for example identify some regions of parameter space without a dynamic of interest. The statistical model captures parameter space trends of the mathematical model and summarises them in an efficient way, therefore facilitating the estimation of the effect of the variations in a particular parameter. In this way, critical or important parameters for a given output can be found.

2.1.2 From neural mass model to database

The first step of DTM consists of choosing a NMM, defining its parameter space and an approach to classify or order the output.

Choice of model

To recall Eykhoff's words a mathematical model needs to be "a representation of the essential aspects of an existing system (or a system to be constructed) which presents knowledge of that system in usable form" [80]. The choice of the neural

mass model is study-dependent. We define in the scope of this thesis “simulation” as the approximations of the NMM by computational approaches. As we have seen in the introduction (section 1.3), specific NMMs have been made to take into account specific knowledge of the brain. For example, one would not use a NMM modelling the full brain with a large number of parameters to study only the olfactory system. Here, a NMM is defined by its function F which maps the parameter space $\mathbb{X}$ of p dimensions to the output space $\mathbb{Y}$. The parameter space $\mathbb{X}$ can be defined upon experimental knowledge. We remarked in some cases (see chapter 3) that the parameter space was defined by mathematical studies and not on experimental data[1]. We derive F by first simulating the model using ODE solvers such as Runge–Kutta methods [46] and by mapping the output onto some feature of interest (for example the presence of oscillations). Let $\mathbf{x} = (x_1, x_2, \ldots, x_p)$ be a parameter vector belonging to the parameter space $\mathbb{X}$. Then $\mathbf{y} = F(\mathbf{x}) \in \mathbb{Y}$ is the image of $\mathbf{x}$. the choice of F needs to be relevant to the purpose of the study. If the purpose was to study seizure dynamics, as in chapter 3, one could focus on the classification of the dynamics as being seizure-like or not. In this case, the output would be binary and we would have F defined as:

$$F(\mathbf{x}) = \begin{cases} 0, & \text{seizure dynamics;} \\ 1, & \text{non seizure dynamics.} \end{cases} \tag{2.1}$$

In the context of fitting a NMMs to some data, $\mathbf{z}_{data}$, the output could be expressed as the values of some specific loss function $L(\mathbf{z}_{data}, S(\mathbf{x}))$ where $S(\mathbf{x})$ could be a time series simulated using the model. In this case, the output would be a positive number. F would be defined as

$$F(\mathbf{x}) = L(\mathbf{z}_{data}, S(\mathbf{x})).$$

Space filling design to simulate the neural mass models

To simulate the model over the whole parameter space we use a space-filling design. A space filling design allows to efficiently explore the whole parameter space given a fixed number of simulations [274, 275, 297]. A Latin hypercube design is constructed in such a way that each of the dimensions is divided into equal levels (sometimes called bins) and that there is only one point (or sample) at each level. As originally proposed [176], a random procedure is used to determine the points' locations. Figure 2.2 shows three examples of designs with 2 dimensions and 20 points. The extreme case illustrated in Figure 2.2 (a) is a design with very poor space filling qualities. Randomisation alone could improve the experimental design to the point exemplified by Figure 2.2 (b). On the other hand, optimisation of point placement would lead to the better choice shown in

[1] By doing so, one risks to oversimplify an analyse and miss important results (see chapter 3 and 4).

Figure 2.2 (c), where points are more uniformly distributed over the domain with respect to Euclidian distance. There exist many latin hypercube algorithms, for

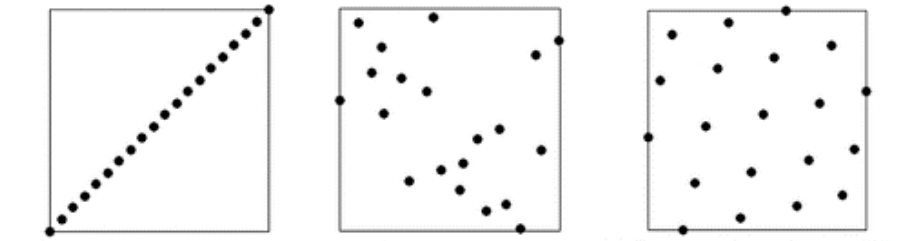

(a) Design with very poor space filling properties. (b) Randomized design. (c) Design with good space filling properties.

Fig. 2.2 Examples of Latin hypercube designs with 2 dimensions and 20 points. Reproduced with authorisation from [275] under licence 4358761312382.

a review see [275]. For the rest of this thesis, let us consider the set of all the N parameter vectors, $\chi = \left(\mathbf{x}_{i\in[1:N]}\right)$, which have been selected in the latin hypercube design and its image $(y_i = F(\mathbf{x}_i),\ i \in [1:N])$.

2.1.3 Quantifying dynamic transitions in high dimensions

We are interested in understanding the relationship between the variable $\mathbf{X}$ and its image Y. The function F is complex and it is difficult to apprehend which parameters play an important role and for which values of parameters certain output of interest can be simulated. As an example let us consider the case where the codomain is binary $\mathbb{Y} = \{0,1\}$. We denote $P(Y = 1|\mathbf{X} \in R)$ as the probability of the event $Y = 1$ (for example, the dynamic observed has seizure characteristics) given that the parameter vector $\mathbf{X}$ belongs to region R, which is a hypercube subset of the full parameter space. We have for example:

$$Y = \begin{cases} 0, & \text{no event;} \\ 1 & \text{event.} \end{cases}$$

and a region defined, for example, by

$$\{\mathbf{X} \in R\} = \Big\{\mathbf{X} \mid (X_1 < U_1) \cap (L_1 < X_3 < U_2)\Big\}. \tag{2.2}$$

In this case $P(Y = 1|\mathbf{X} \in R)$ represents the likelihood of event when the parameter X_1 is inferior to U_1, X_3 is between L_1 and U_2 and the other parameters are not constrained. The value of $P(Y = 1|\mathbf{X} \in R)$ is given by

$$P(Y = 1|\mathbf{X} \in R)) = \int_{x\in R} P(Y = 1|\mathbf{x})\ d\mathbf{x}. \tag{2.3}$$

Since the function mapping $\mathbf{X}$ onto Y is unknown, we take a sampling approach and use the database created by simulations. Assuming that χ is sampled independent and identically distributed from $\mathbb{X}$. We can therefore estimate the term $P(Y = 1|\mathbf{X} \in$

R) for the given region R by computing

$$\hat{P}(Y = 1|X \in R)) = \frac{1}{|\chi \in R|} \sum_{\chi \in R} y, \tag{2.4}$$

where $|A|$ denotes the cardinality of the set A. The quantity $P(Y = 1|\mathbf{X} \in R)$ can be further used to determine which parameters are important to find regions of interest.

Confidence in the likelihood estimated in a subregion

To analyse the parameter space it is necessarily to know the confidence that we can give in the likelihood estimated in each region. Given our sampling it is possible to estimate a confidence interval for each feature in each region. All these estimations are based on the central limit theorem:

Lindeberg–Lévy central limit theorem [27]. Suppose $(Y_1, Y_2, \dots)$ is a sequence of independent and identically distributed random variables with $E[Y_i] = \mu$ and Var$[Y_i] = \sigma^2 < \infty$. Then

$$\sqrt{n}\left(\left(\frac{1}{n}\sum_{i=1}^{n} Y_i\right) - \mu\right) \xrightarrow{d} N\left(0, \sigma^2\right). \tag{2.5}$$

If the number of simulations in the regions is too small, the estimation of $P(Y|\mathbf{X}_i \in m_n))$ could be biased. In certain contexts, it is possible to find an upper bound on the variance σ^2. Suppose a distribution has minimum m, maximum M, and expected value μ. The Bhatia–Davis inequality says:

$$\sigma^2 \leq (M - \mu)(\mu - m). \tag{2.6}$$

Equality holds precisely if all the probability is concentrated at the endpoints m and M. For $m = 0$ and $M = 1$:

$$\sigma^2 \leq 1/4, \tag{2.7}$$

and so the confidence of interval of a feature can be bounded by the maximum bound of its variance (1/4):

$$\Pr\left(\bar{Y} - \frac{1.96}{4\sqrt{n}} \leq \mu \leq \bar{Y} + \frac{1.96}{4\sqrt{n}}\right) \geq 0.95. \tag{2.8}$$

For $n \geq 400$ the confidence interval of μ will be inferior to 0.05. This means that as long as the size of a region is larger than 400, they should be meaningful and indicate with a good accuracy the proportion of the event.

2.1.4 Partition of the parameter space

An obvious question that arises is how to choose a partition of the parameter space such that each region is meaningful. A first approach consists of fixing the regions $R_{i\in[1:m]}$ such that each region is the same size, i.e. the parameter space is cut into pre-defined disjoint regions and that the union of the regions is equal to $\mathbb{X}$. This approach can be a useful tool to display the parameter space by the projection of the parameter space to two parameters at the time as we will see later (see section 2.3).

Another approach consists of partitioning the parameter space by selecting M "optimal" regions, $R_1, \ldots, R_M$. By optimal, we mean the number of regions M is as small as possible such that in each region the discrepancy of the event Y is low. By discrepancy we mean the output in a region is similar (same class when the output is categorical or close to the mean of the region for continuous output). In principle, this results in a more efficient mapping of the dynamics of the model onto its parameter space. The boundaries between regions are useful, as they indicate which parameters have an important role in a rapid change of output like the emergence of dynamics of interest. Effectively they describe the transitions as parameters are varied between different dynamic types that can correspond to bifurcations or other types of phase transition in the underlying dynamic model.

To define optimal regions, we use an approach called decision tree learning algorithms [43]. Here, the parameter space is partitioned recursively into rectangular disjoint subspaces by axis parallel splits. The size of each region is determined by ensuring that it consists, insofar as possible, of only a single type of dynamics. An example of a parameter space containing 3 classes and a tree splitting the parameter space is given in Figure 2.3.

Tree-based methods are a conceptually simple, yet very powerful tool to study highly nonlinear functions for the purpose of regression or classification. These methods are inherently non-parametric; no assumptions are made regarding the underlying distribution of parameter values. They can be trained quickly, provide a vehicle to efficiently predict the output of new simulations and scale well to large datasets. Introduced by [43], we focus on classification and regression tree (CART) algorithms. These produce binary splits recursively from the root (the complete parameter space) to its leaves (the regions corresponding to dynamics of a single type or as close as possible). CART models are easy to interpret as they offer a visual representation of the parameter space [208].

We have tested other statistical methods to partition the parameter space. Particularly we focused on the use of Gaussian processes (GPs) [78, 287]. This method has been applied with success in the past to explore parameter space of complex mathematical models which are slow to run [48, 264]. However, in our studies, if good results were achieved for a parameter space with a small number of dimensions (<4), poor results were achieved with more parameters. By

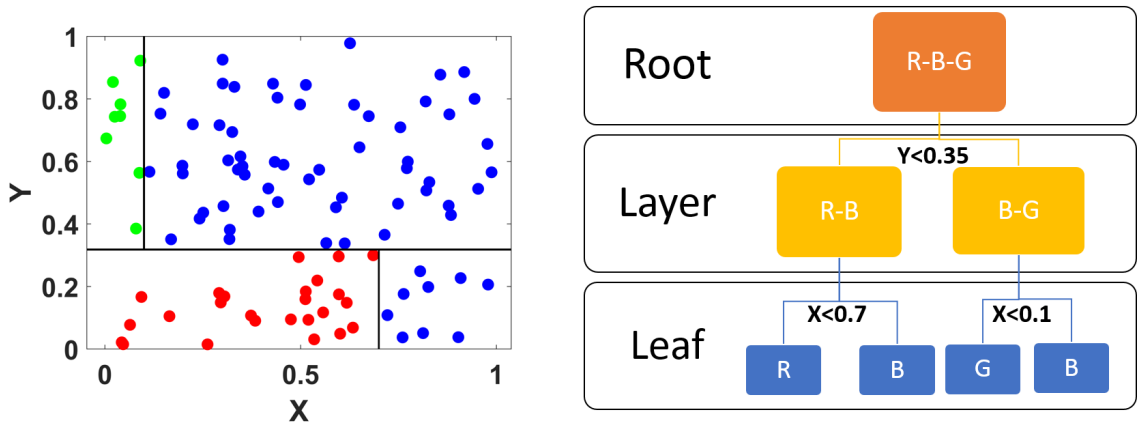

Fig. 2.3 The parameter space consists of two parameters X and Y ranging from 0 to 1. There are 3 classes of dynamics. The full parameter space is represented in the tree by its root. In this region, all classes are represented. In the intermediate layer, two subregions are identified, one containing the classes red and blue and the other containing the classes blue and green. Finally, in the leaf of the tree, there is now only one class per region.

increasing the number of simulation we were able to achieve better results (up to 5 dimensions), however as Gaussian process necessitates to inverse a matrix of the size of the sample of the dataset, this approach could not be scaled. We tried more advanced machine learning tools such as Bayesian Treed Gaussian Process [18, 109, 110] and developed an algorithm using local GPs in different regions of space without success.

Other approaches could be used for modelling the relationships in a design space using machine learning techniques. For example, the field of Estimation of distribution Algorithm (EDA) [6] build explicit probabilistic models to identify the regions of parameter space where a dynamic of interest is the most likely to be found. Two examples of algorithms are the Bayesian optimization algorithm (BOA) [201] and Linkage-tree Genetic Algorithm (LTGA) [260]. These algorithms are initially stochastic optimization methods. Their purpose is to build explicit probabilistic models of the optimal solution. The algorithms consists of a series of incremental updates of a probabilistic model, starting with the model encoding the uniform distribution over admissible solutions and ending with a set of parameters which generates only the global optima [120]. By slightly changing the algorithms it should be possible to generate all the parameter vectors which can simulate the dynamics of interest. It would require some transformations of the current algorithms but it is a promising approach. One of the key advantage of the EDA approach would be to sample in the regions of space of interest and thus avoid to sample in the regions of space where it is unlikely to simulate the dynamic of interest, furthermore they could be used to fit specific data while the DTM is limited to the exploration of parameter space. However one of the key constraints of the EDA approach is to interpret and visualise the complex probabilistic models.

At the opposite, trees and their extensions, the random forests, are directly able to explore and analyse the parameter space in an efficient way. Trees have several advantages:

- they perform well with large datasets. Due to the relative simplicity of the algorithm (describe below) large amounts of data ($\mathcal{O}$(1,000,000 observations)) can be analysed using standard computing resources. This is particularly useful for models with complex parameter space where a large number of simulations is needed to explore well the parameter space;
- they do not necessitate normalisation of the variables and can handle qualitative and quantitative parameters and output simultaneously; and
- they are easy to understand and to be visualised. This is particularly important to understand and visualise the parameter space.

However as there is no free lunch[2], tree approaches have constraints:

- tree approaches are based on a axis parallel separability approach and thus has a decrease in performance when this assumption is not respected.
- the non respect of this assumption increases the number of regions and increases the difficulty to visualise the parameter space.

2.1.5 Building a tree

In general, finding the optimal partitioning of parameter space is a NP-complete problem [136]. Therefore, decision tree learning algorithms are based on heuristics whereby locally optimal decisions are made within each region of the tree. Whilst such an approach is not guaranteed to give the globally-optimal decision tree, CART methods have been shown to give good results in practice [43]. Here, we summarise the approach, which is described in detail in [123]. We also provided an example in Figure 2.4 which describes how the tree presented in Figure 2.3 is achieved.

[2] If an algorithm performs well on a certain class of problems then it necessarily pays for that with degraded performance on the set of other problems [294].

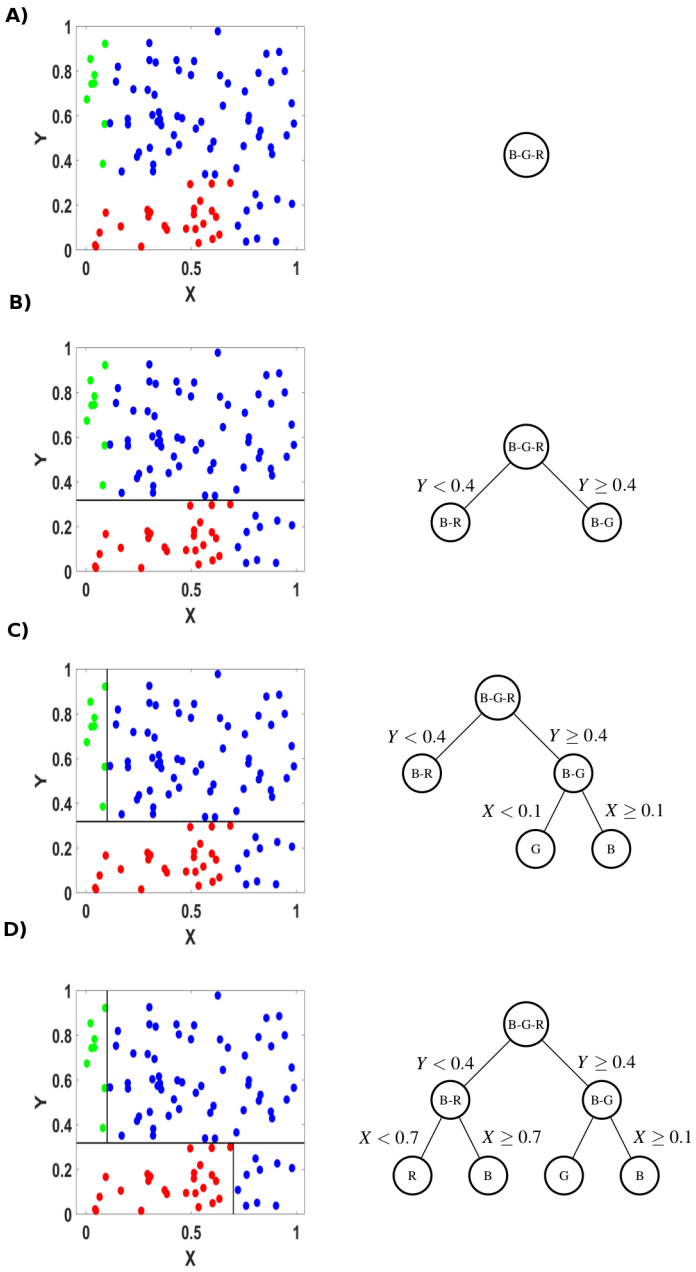

Fig. 2.4 The different steps to construct a tree. In this example, the parameter space consists of two parameters X and Y ranging from 0 to 1. There are 3 classes of dynamics indicated by green, blue and red which are assumed to be the results of the simulations. A) This full parameter space is represented in the tree by its root. In this region, all classes are represented. The impurity (see equation 2.9) in this region is equal to 0.48. B) The split (see equation 2.11) at $Y = 0.4$ drastically decreases the impurity in its two subregions which are now 0.13 and 0.14. Nevertheless, the regions themselves are not pure. C) The region with the larger impurity is then targeted by the CART algorithm. The split at $X = 0.1$ totally removes the impurity in its two sub-regions which are now equal to 0. There is only one type of observation per region in this parameter subspace. D) The last region with some impurity is again targeted by the CART algorithm. The split at $X = 0.7$ totally removes the impurity in its two sub-regions. There is now only one type of dynamic feature within each region of the tree defined by a leaf.

The algorithm can be summarised as such
Pseudocode for tree construction by exhaustive search

1. Start at the root node. Initialise the temporary tree T_{temp}.
2. For each parameter in each region, find the split that minimises the sum of the node impurities in the two child nodes and choose the split that gives the minimum overall. Update T_{temp}.
3. If a stopping criterion is reached, exit. Otherwise, apply step 2 to each child node in turn.

Formally we have a data set consisting of n points in $\mathbb{R}^p$. The set of outputs consists of the class of observed dynamics y_i for each simulation. Suppose that we have a partition into M regions, $R_1, \ldots, R_M$. For a given region R_m the splitting stage is chosen by finding an optimal split point in terms of the impurity criterion described equation 2.9.
The measure I_{R_m} of region impurity represents the quality of classification in a region. By this, we mean how well a region of parameter space maps onto model dynamics of a single type. When the output is categorical, it is defined by the Gini index:

$$I_{R_m} = \frac{1}{N_m} \sum_{k=1}^{K} \hat{p}_{mk}(1 - \hat{p}_{mk}), \tag{2.9}$$

where $\hat{p}_{mk}$ is the estimation of $\hat{P}(y \in k | x \in R_m)$, the probability of the event k in the region R_m.

$$\hat{p}_{mk} = \frac{1}{N_m} \sum_{\chi \in R_m} I(F(\mathbf{x}) = k), \tag{2.10}$$

is the proportion of class k observations in a given region R_m. When $I_R = 0$, the region is pure and it contains only a single class of dynamics. By contrast, a large Gini index indicates a region with large impurity, and thus contains parameters that map onto different types of dynamics in the model. For the temporary tree T_{temp}, we seek the j^{th} split parameter and split point, s, and the region R such that the gain function $G(R,s,t)$:

$$G(R, j, s) = I_R - (I_{R_L(m,j,s)} + I_{R_R(m,j,s)}), \tag{2.11}$$

is maximised. Here $R_L(m, j, s) = \{\mathbf{x} | \mathbf{x} \in R_m, x_{.j} \leq s\}$ and
$R_R(m, j, s) = \{\mathbf{x} | \mathbf{x} \in R_m, x_{.j} > s\}$ are respectively the potential left and right split of the region of interest. For each region, the determination of the split points can be done very quickly ($\mathcal{O}(p \times n)$ operations) and hence by scanning through all of the inputs, determination of the best pair (j, s) is feasible in finite time. An example of a tree and its construction can be found in Figure 2.4. To estimate a new set of parameters $\mathbf{x}$, the class with the largest frequency $k(m) = \underset{k}{\operatorname{argmax}}\ \hat{p}_{mk}$ is attributed to $\mathbf{x}$. Figure 2.4 presents an example of construction of a tree.

Loss function

As we will see in example f_1 (see equation 2.20) and chapter 5, sometimes one particular class is of interest. It is possible to focus specifically on a certain class by adding a weighted loss function, $\mathbf{L}$ [43]. The value of the loss function is interpreted as the cost incurred by predicting $\hat{y}$ when the true output is y. It is based on the idea of regret, i.e., the loss associated with a bad decision to predict a class. For example, one can consider that correctly finding all seizure dynamics (see equation 2.1) is more important than wrongly identifying non seizure dynamics as seizure dynamics. In the classical framework, the loss weight is equal for each class:

$$\mathbf{L} = \begin{bmatrix} 0 & 1 & 1 & \dots \\ 1 & 0 & 1 & \dots \\ \vdots & \dots & 0 & \vdots \\ 1 & \dots & 1 & 0 \end{bmatrix}. \tag{2.12}$$

The impurity index $I(R)$ of the region R has its maximum at $p_1 = p_2 = ... = p_K = 1/K$. However, if a problem had a misclassification loss for class 1 which was twice the loss for a class 2 or 3 observation, ie, we would have

$$\mathbf{L} = \begin{bmatrix} 0 & 1 & 1 \\ 2 & 0 & 1 \\ 2 & 1 & 0 \end{bmatrix}. \tag{2.13}$$

One would wish to have its maximum at $p_1 = 1/5$, $p_2 = p_3 = 2/5$, since this is the worst possible set of proportions on which to decide a node's class. To account for the loss, we present the method of "altered priors" [43] implemented in R via the package rpart [259]. The new $p_{mk \text{ corrected}}$ is estimated via

$$\hat{p}_{mk \text{ corrected}} = \frac{\pi_i \, L_i}{\sum_j \pi_j \, L_j} \frac{1}{N_m} \sum_{x_{i.} \in R_m} I(y_i = k), \tag{2.14}$$

where π_i is the prior probability for group i and $L_i = \sum_j L_{ik}$. When altered priors are used, they only affect the choice of split. The ordinary losses (i.e same weight for any error) and priors are used to compute the prediction. The altered priors simply help the impurity rule choose splits that are likely to be "good" given the loss function.

Regression tree analysis

When the predicted outcome is continuous we use regression tree analysis. The Gini Index is replaced by the variance reduction function,

$$I_{R_m} = \frac{1}{N_m} \sum_{i \in R_m} \sum_{j \in R_m} \frac{1}{2} (y_i - y_j)^2. \tag{2.15}$$

This is equivalent to choosing the split to maximize the between-groups sum-of-squares in a simple analysis of variance.

2.1.6 Random forests

Problems faced when focussing on a single tree, as in the previous section, include overfitting and the inability of the heuristic to find the optimal partition. To overcome these problems, the aggregation of a large number of trees is often used and provides much greater insight. In a series of papers and technical reports, [40–42] demonstrated that substantial gains in classification and regression accuracy can be achieved by using ensembles of B trees, where each tree in the ensemble is grown in accordance with a random set of rules. This method is called random decision forests. This method remains one of the most accurate machine learning algorithms [51, 82] and its consistency have been demonstrated [230].

In this study, the use of multiple trees is equivalent to mapping the parameter space using different rules of segmentation. If a segmentation appears consistently, this implies it is important. The training algorithm for random forests applies the general technique of bootstrap aggregating [39], i.e. for each tree, a random sample with replacement of the simulations set is selected. This random sample is called the in-of-bag data. The set of simulations not selected is called out-of-bag data. Furthermore, for each region, a random subset of parameters is selected, and the split is optimised on the basis of the chosen parameters. For each bootstrap sample Z_b, $\{b = 1,\ 2, \ldots,\ B\}$, we fit a tree according to a succession of random rules (for each split select $\sqrt{p}$ parameters to find the optimal split), giving the tree t_b. Then the random forest f is given by:

$$f = \frac{1}{B}\sum_{b=1}^{B} t_b. \tag{2.16}$$

The estimation of the probability for a parameter set x to belong to class k is given by:

$$\hat{P}(y \in k) = \frac{1}{B}\sum_{b=1}^{B} \hat{P}_b(y \in k). \tag{2.17}$$

In the case of an imbalanced dataset, i.e. the classes are not represented by the same ratio in the dataset. In the case of an imbalanced dataset, it is advised to use under-sampling to correct imbalanced classes and misclassification costs [35, 53].

2.1.7 Determining the importance of parameters

Knowing which parameters have a high impact on the probability of an event is crucial to improve our understanding of the system so that we may focus on these parameters. There are many ways to compute the importance of a parameter in

a tree. In the following part, some of the most classic measures are presented. These measures are complementary and capture different aspects of the influence of parameters for the probability of an event.

The Gini importance $GI_j,\ j \in [1:p]$ [103] is defined as the sum of all decreases in impurity in the tree due to the given parameter divided by the number of splits, N_s, i.e.

$$GI_j = \frac{1}{N_s} \sum_{R_m \in T} I_{R(m)} - I_{R_L(m)} - I_{R_R(m)}. \tag{2.18}$$

A parameter with a large GI indicates that a change in the values of the parameter is more likely to influence the dynamics than a parameter with small GI.

Note: for an easy interpretation, the variable importance GI_i of the parameter i is expressed in terms of a normalised quantity relative to the variable having the largest measure of importance:

$$GI_i = \frac{GI_i}{\max(GI)}. \tag{2.19}$$

A parameter, therefore, has an important influence on the dynamics of interest in the model if its GI is close to 1 and a small importance if it close to 0. These values are only indicative and small differences in GI between two parameters would not necessarily indicate that a parameter is more important than another. Furthermore, it quantifies *global* parameter importance; it is possible that in some parts of the parameter space a parameter described as important does not affect dynamics.

The variable importance by permutation PI_j is calculated by noising up a parameter by randomly changing its values [138, 170]. They estimate the mean decrease or increase of prediction accuracy after X_j is permuted. A given x_j is randomly permuted in the out-of-bag data and permuted out-of-bag data is dropped down the tree grown from the in-bag data. This is done for each tree in the forest and an out-of-bag estimate of the prediction error is computed from the resulting parameter. The difference between this value and the out-of-bag error without random permutation is the PI_j. Large positive values indicate j is predictive, whereas zero or negative importance values identify parameters not predictive.

The presence of a parameter in a split at an early stage of a tree shows that this parameter is often preferable to cut the parameter space and so it is an important parameter at a global level. We denote by R_j total number of trees in which X_j is used for splitting the root node (i.e., the whole set of simulations is divided into two based on the value of X_j).

We implemented random forests using *R* [209] with the packages *RandomForest* [257]. The figures were built with some adaption of the package *rpart* [258] and *rpart.plot* [178].

2.2 Examples

In this section, we present different examples. The purpose is to show the advantages and the limitations of the tree mapping approach.

2.2.1 Nominal examples

Nominal variables have two or more categories, but which do not have an intrinsic order. The examples present different manifolds which could be potentially found in mathematical models. For each example, artificial parameters are added to the model. These parameters do not influence the output of the functions. To encompass for the relatively simple function created, the parameter space is only simulated a thousand times while in a real study the model is simulated in the order of million to be certain that the parameter space has been efficiently explored and that its complexity can be well represented. The first example f_1 is extracted from the *R* package *mlbench* [159]. The function is defined as:

$$f_1(x_1,\ldots,x_{30}) = \begin{cases} 0, & \text{if } x_1^2 + x_2^2 < \frac{4}{\pi^2}; \\ 1, & \text{otherwise.} \end{cases} \tag{2.20}$$

The parameter space $\mathbb{X}$ is defined as $[0,1]^{30}$. A projection of the first four parameters of a set of 1000 simulations can be found in Figure 2.5. This function as a binary output. The first class is in a 2-dimensional ball in the middle of the hypercube, the remainder forms the second class. The size of the ball is chosen such that both classes have an equal prior probability (0.5). We added 28 false parameters which do not influence the classes. In this example, the manifold of interest is non-rectangular and a priori non-suitable for a method like DTM. There are different approaches to capture the manifold of interest, one can be interested to find specifically all the regions where a specific event happens. It is possible to increase or decrease the weight of the loss for a specific event, see equation 2.14. Tree mapping with different losses are shown in Figures 2.6 and 2.7. One can see that the ball is approximated with more or less accuracy. In Figure 2.6, the loss is chosen such that the loss for class 0 is larger than the loss for class 1. The tree presents regions such that there are regions of pure class 0 and a large region with the presence of class 1 and 0 but where class 0 is prevalent. Figure 2.7 shows a tree where the weights of the loss are equal. In each region there is a class in majority, however, there is a small probability to simulate the other class.

x_1 and x_2 are the only parameters which are used to partition the parameter space in the Figures 2.6 and 2.7. Given these trees, it appears that only these two parameters have an impact on the simulations. Figure 2.8 confirms the importance of these two parameters and the non-effect of the others by averaging the importance measures over 500 trees.

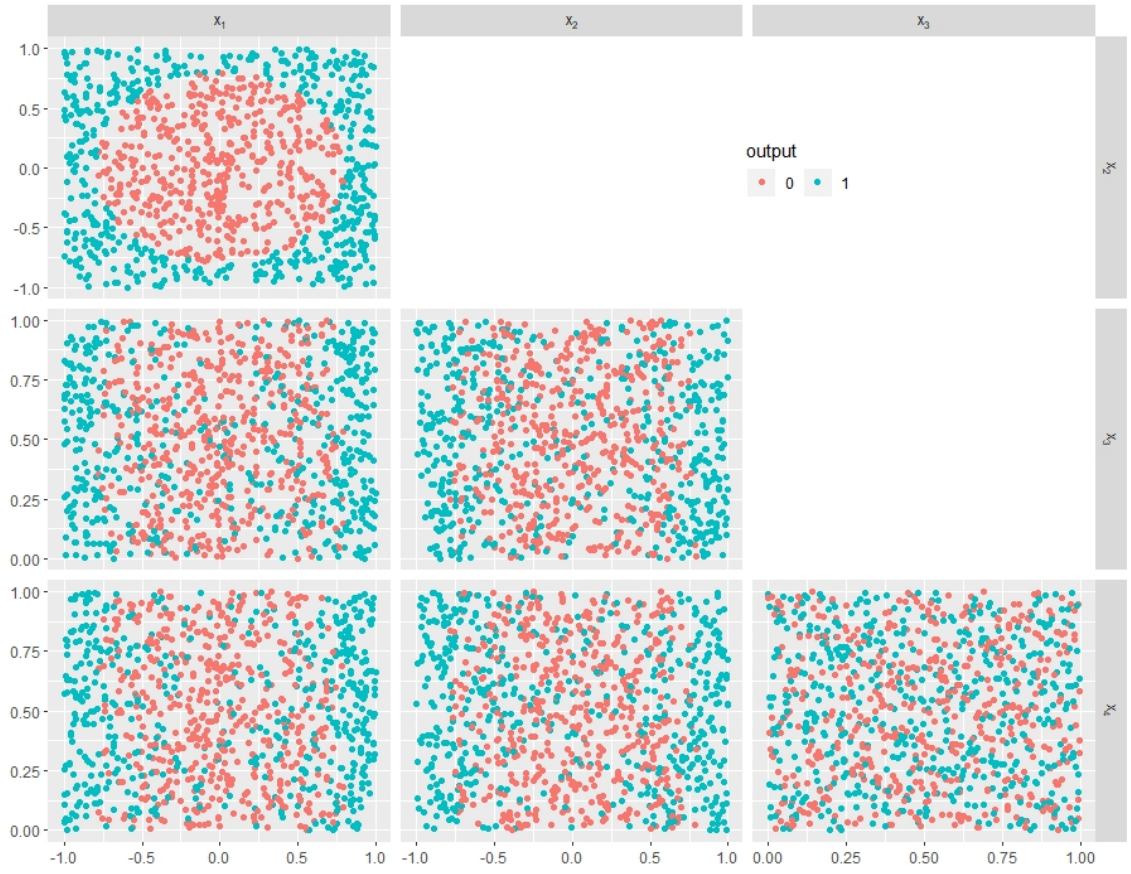

Fig. 2.5 Pairwise plot between the first parameters of the function f_1. The axis are indicated by the banners on the top and on the right. The 2-dimensional disc in the middle cube can be visualised in the first-row, first column. At the opposite, the parameters X_3 and X_4 do not affect the output.

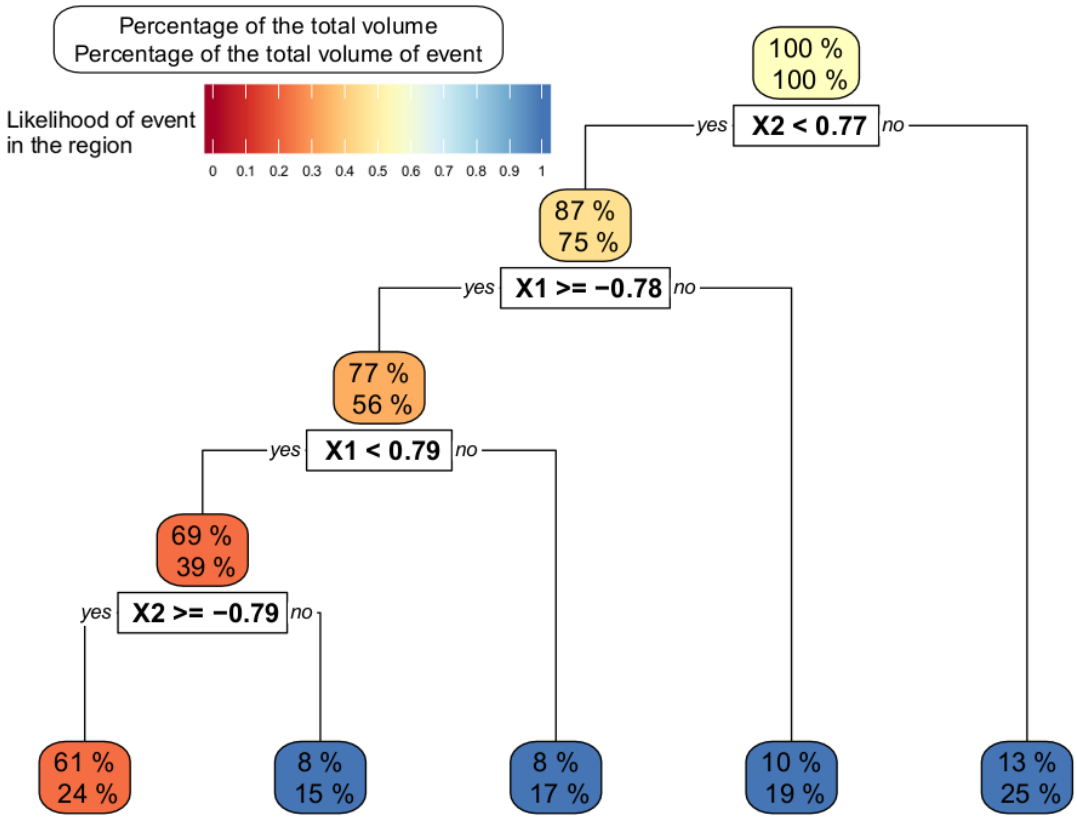

Fig. 2.6 Tree mapping of the function f_1 with a strong preference for the event 1. The loss of a badly predicted event 1 has been increased. As a result, the tree splits the parameter space with the aim to identify the regions without the event 0.

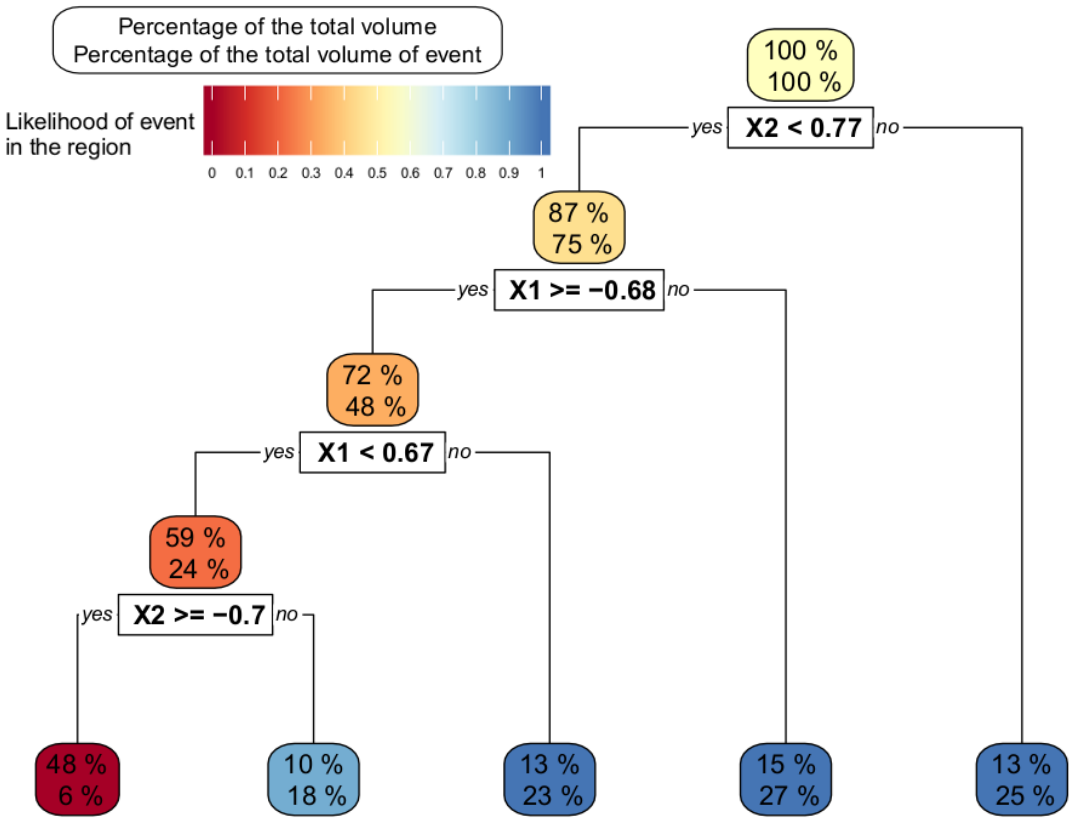

Fig. 2.7 Tree mapping of the function f_1 with an equal preference for the events 0 and 1. The loss of a badly predicted event 0 and 1 are equal. As a result the tree splits the parameter space with the aim to identify the regions by giving a same weigh for false estimations.

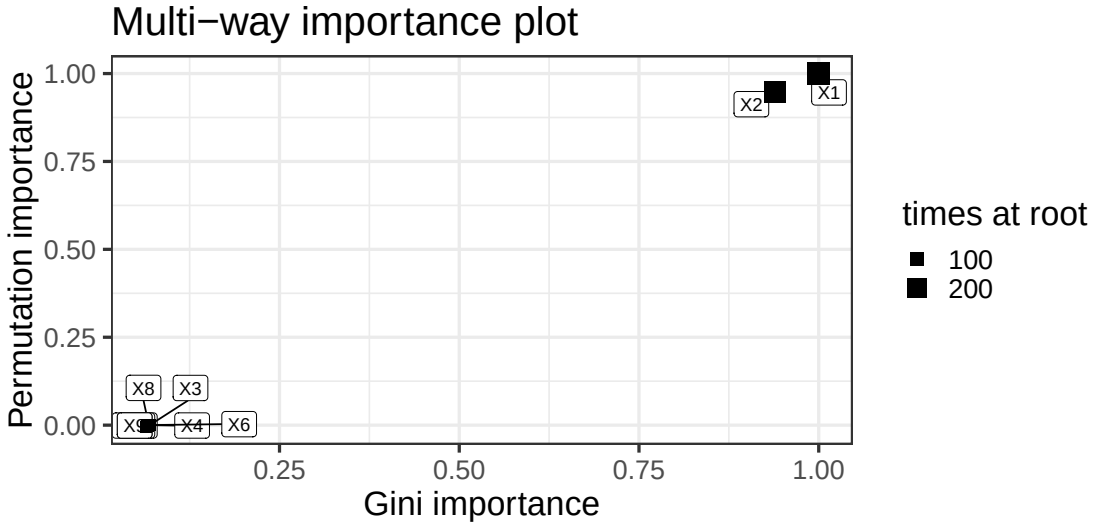

Fig. 2.8 Multi-way parameter importance for the function f_1. The importance of parameters as determined by variable importance measures (see section 2.1.7) averaged over a random forest of 500 trees. The parameters X_1 and X_2 are correctly identified as the only parameters which influence the output.

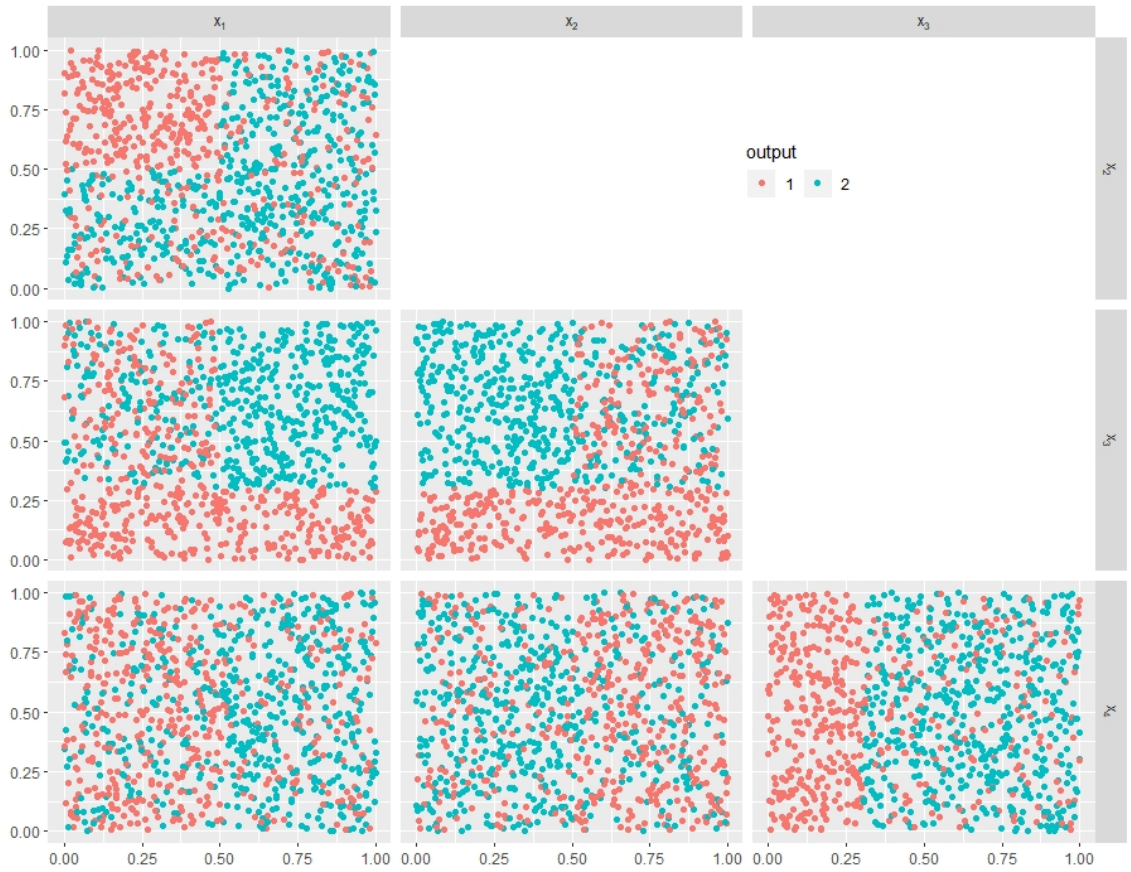

Fig. 2.9 Pairwise plot between the first parameters of the function f_2. The axis are indicated by the banners on the top and on the right. The parameter space is more complex to visualise than the example of function f_1. The parameters x_1, x_2 and x_3 influence the output of the function f_2.

The second function f_2 is a function with non-linear complex manifolds.

$$f_2(x_1,\ldots,x_{30}) = \begin{cases} 0, & \text{if } (e^{x_1} < 1.65 \ \& \ x_2 > 0.5) \text{ or } x_3 < 0.3; \\ 1 & \text{otherwise.} \end{cases} \tag{2.21}$$

The parameter space $\mathbb{X}$ is defined as $[0,1]^{30}$. The tree mapping is efficient and presents a map corresponding exactly to the function, see Figure 2.10. The importance of the parameters is well estimated, see Figure 2.11. Indeed, the values of x_3 directly influence the output while a combination of x_1 and x_2 is necessary. The measures of importance of x_3 are the highest followed by the x_1 and x_2 measures of importance while for the other parameters, the importance measures are close to 0, see Figure 2.11.

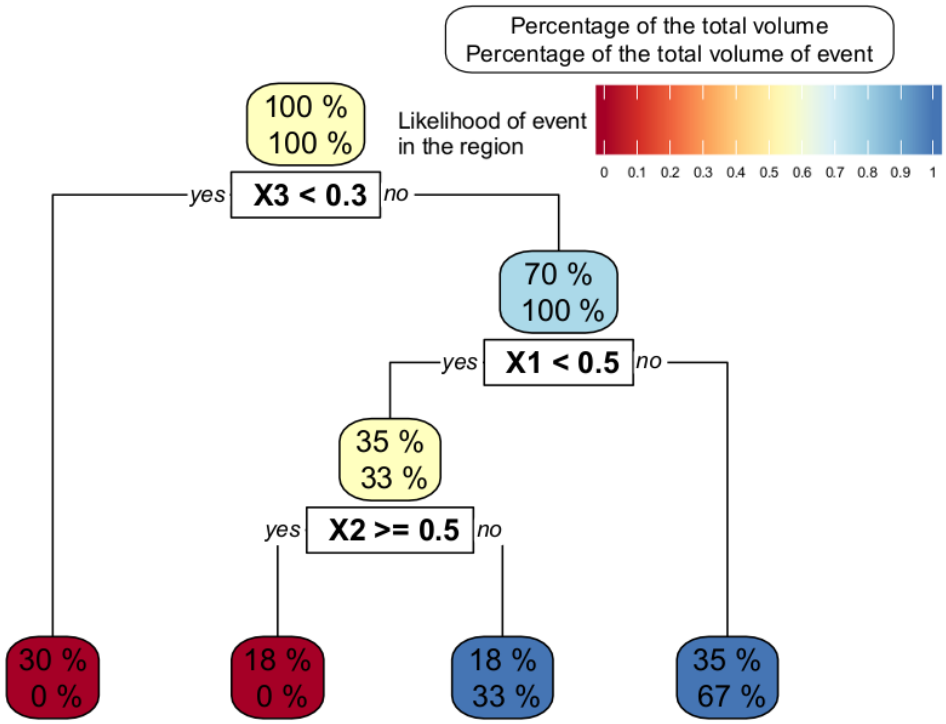

Fig. 2.10 Tree mapping of the function f_2. The algorithm identifies correctly the parameters of interest and the parameter space is efficiently mapped.

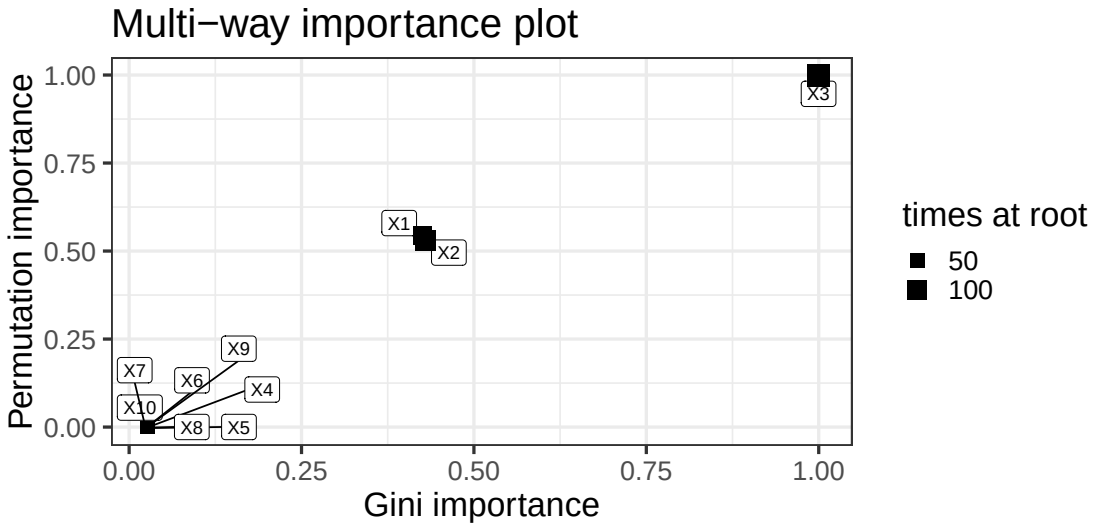

Fig. 2.11 Multi-way parameter importance for the function f_2. The importance of parameters as determined by variable importance measures (see section 2.1.7) averaged over a random forest of 500 trees. The parameters x_1 and x_2 are correctly identified as having the same influence on the output while x_3 has the highest importance measure.

The third example f_3 is another function with a non-linear complex manifold.

$$f_3(x_1,\ldots,x_{30}) = \begin{cases} 0, & \text{if } sin(3\pi x_1 x_2) < 0 \text{ or } x_3 < 0.4; \\ 1 & \text{otherwise.} \end{cases} \tag{2.22}$$

The parameter space $\mathbb{X}$ is defined as $[0,1]^{30}$. In this example there is linear interaction between x_1 and x_2 coupled to a sinusoidal function. A projection of the first four parameters of a set of 1000 simulations can be found in Figure 2.12. As

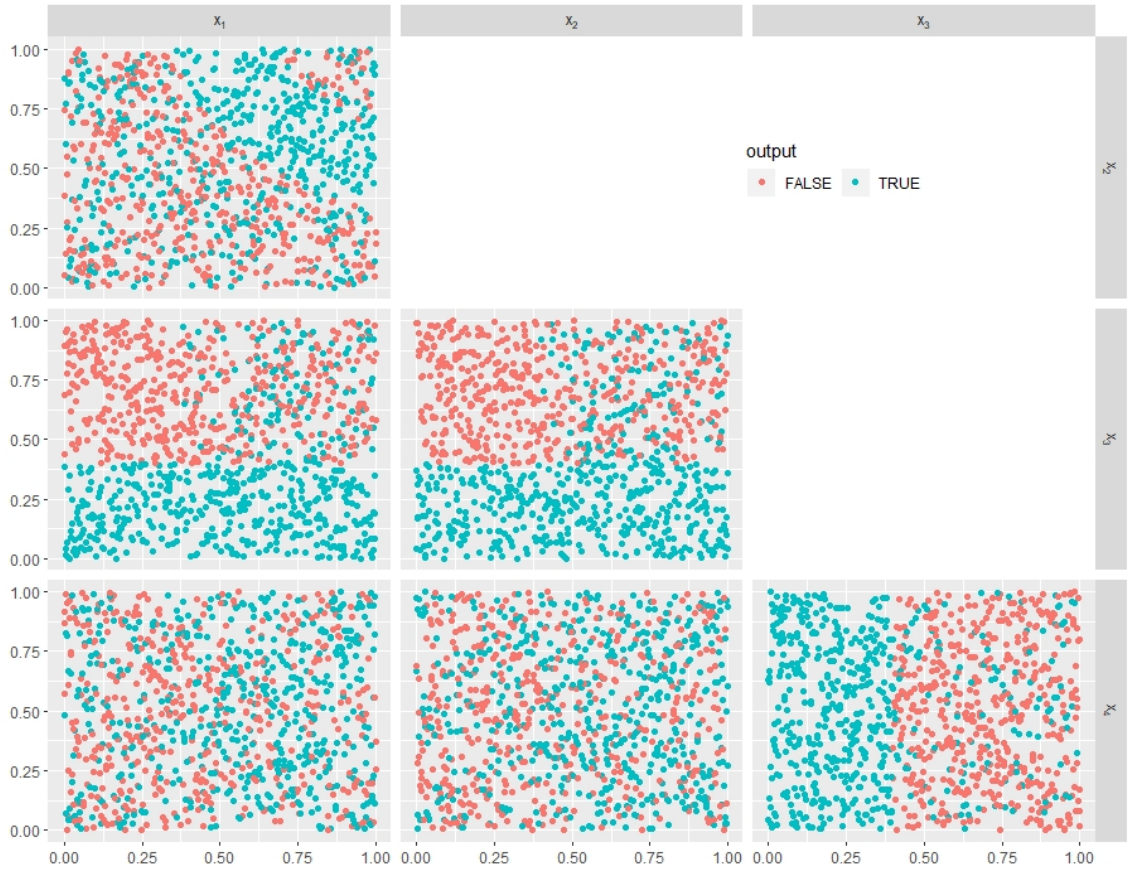

Fig. 2.12 Pairwise plot between the first parameters of the function f_3. The axis are indicated by the banners on the top and on the right. There is a nonlinear interaction between the parameters x_1 and x_2.

opposed to the previous example, the tree mapping is not optimal and does not capture all aspects of the different manifolds. The reason is that we try to split a parameter space in rectangular areas whereas there is a complex relationship between two parameters and the input. We will discuss later, see section 2.3 how the parameter interactions can be found and used to map the parameter space more efficiently. Once again, the measures of importance are able to identify correctly the parameters which influence the most the outputs, see Figure 2.14.

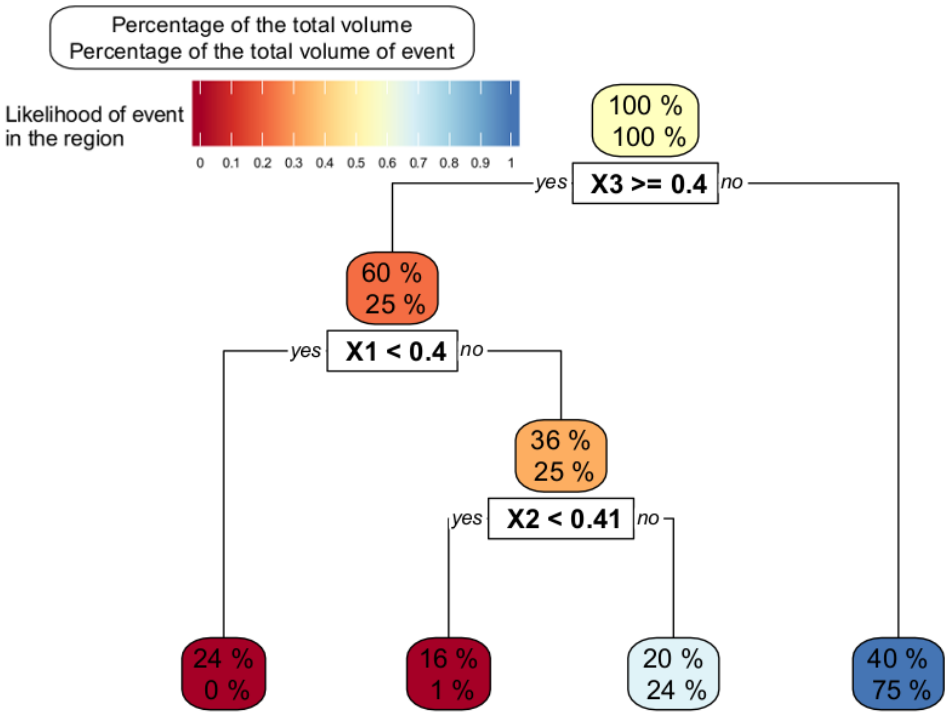

Fig. 2.13 Tree mapping of the function f_3. The algorithms identify correctly the parameters of interest but the parameter space is not perfectly mapped.

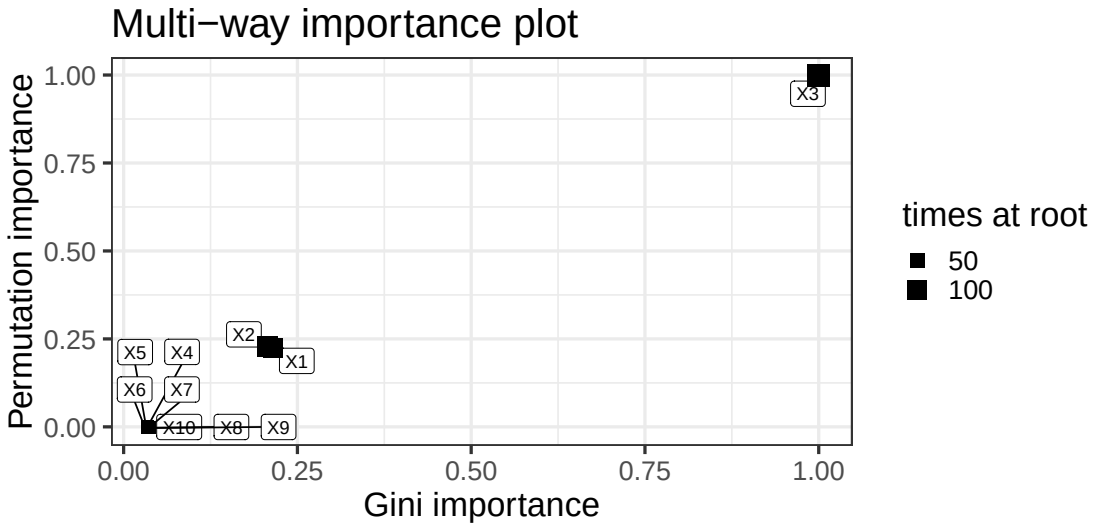

Fig. 2.14 Multi-way parameter importance for the function f_3. The importance of parameters as determined by variable importance measures (see section 2.1.7) averaged over a random forest of 500 trees. The parameters x_1 and x_2 are correctly identified as having the same influence on the output while x_3 has the highest importance measure.

2.2.2 Continuous examples

We use two further examples, f_4 and f_5 to show how DTM can be applied to model with a continuous output. The function f_4 is the Matyas function [3]:

$$f_4(x_1,\ldots,x_{30}) = 0.26 * (x_1^2 + x_2^2) - 0.48 x_1 x_2. \tag{2.23}$$

The parameter space $\mathbb{X}$ is defined as $[0,1]^{30}$. The function f_4 takes is extremum values when

- x_1 value is large and x_2 value is small; and
- x_1 value is small and x_2 value is large.

The tree in Figure 2.15 correctly identifies the regions with the maximum values. The multi-way importance analyses in Figure 2.16 correctly indicates that x_1 and x_2 are the only important parameters.

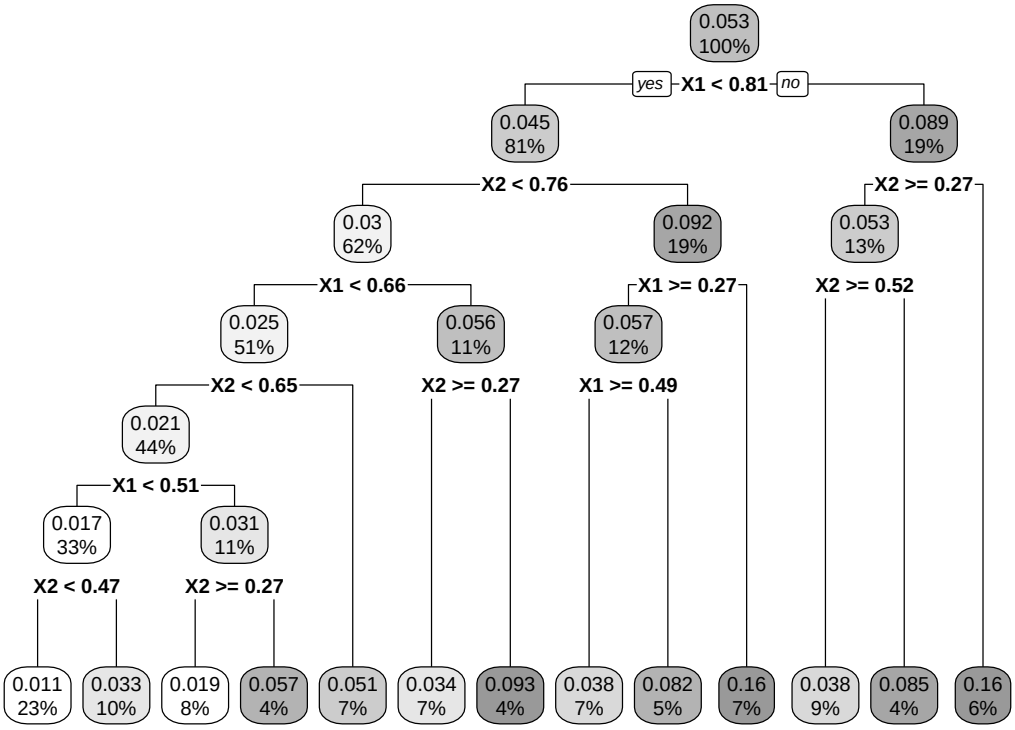

Fig. 2.15 Tree mapping of the function f_4. Small values are displayed in clear grey while large fitted values are display in a darker grey. The algorithm correctly identifies the parameters of interest by only using them to partition the parameter space and the parameter space is efficiently mapped.

[3] http://www.sfu.ca/ ssurjano/

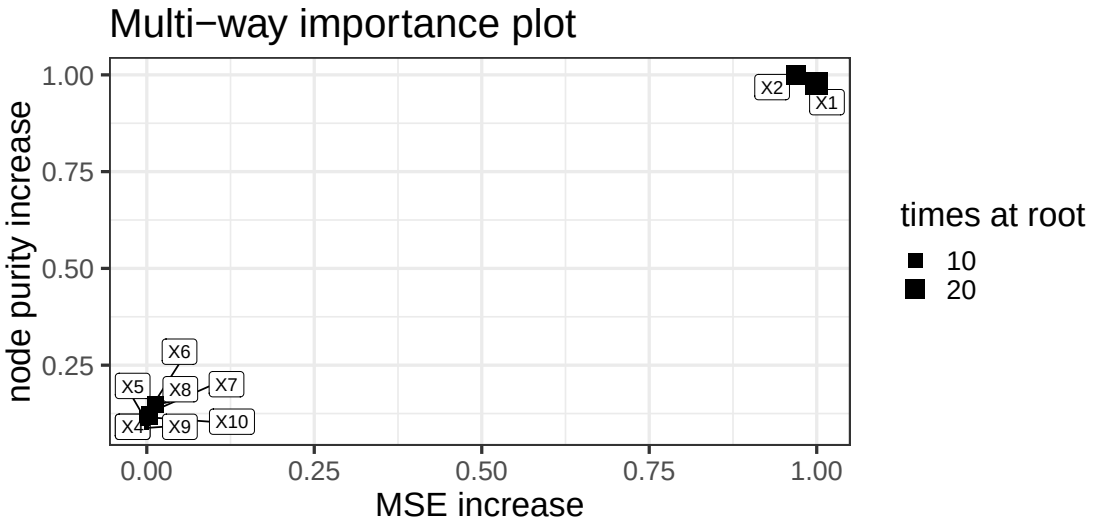

Fig. 2.16 Multi-way parameter importance for the function f_4The parameters X_1 and X_2 are correctly identified as having the same influence on the output. The other parameters have a measure of importance close to 0.

Finally, we consider f_5, the sum of f_4 and some nonlinear terms (including a nonlinear interaction between three parameters):

$$f_5(x_1,\ldots,x_{30}) = 0.26 * (x_1^2 + x_2^2) - 0.48 x_1 x_2 + 0.5 e^{(-x_3)} + 0.5 e^{(-\frac{x_4}{x_5})} + 0.5 e^{(1-e^{(\frac{x_1}{x_5 x_6})})}. \quad (2.24)$$

This function is complex and it is difficult to apprehend which parameters have a key role on its output. DTM efficiently summarises the key aspect of this function.

The tree in Figure 2.17 indicates for which combinations of values of parameters the output is large and small while the multi-way parameter importance in Figure 2.18 indicates the order of importance of the parameters. Different combinations of parameters can increase the output. Large values of x_5 and x_6 always increase the output. For the parameters x_3, x_4 and x_1, their values need to be close to 0 to increase the output. This is coherent with the function f_5. The importance measure indicates which parameters influence the most the variability of the output, see Figure 2.18. The parameter x_5 appears in two exponential terms ($0.5e^{(-\frac{x_4}{x_5})}$ and $0.5e^{(1-e^{(\frac{x_1}{x_5 x_6})})}$) in the function f_5 and is identify as the most important parameter. The parameter x_1 and x_4 appears to be similarly important. The high values for importance measures of x_1 are not surprising as this parameter is present in many terms of f_5. x_4 is important even if it is presents in only one term of the function f_5 with the term $0.5e^{(-\frac{x_4}{x_5})}$ because this term as a large amplitude compared to the other terms of the function f_5. The importance of x_4 is maybe a bit over estimated due to its interaction term with f_5. However, the parameter x_3 which appears in a similar term $0.5e^{(-x_3)}$ has close estimation of importance measure. We remark

that the parameter x_2 does not appear in this small tree, however, importance measures identify correctly that this parameter influences the output. The fake parameters are correctly identified as being unimportant for the output values.

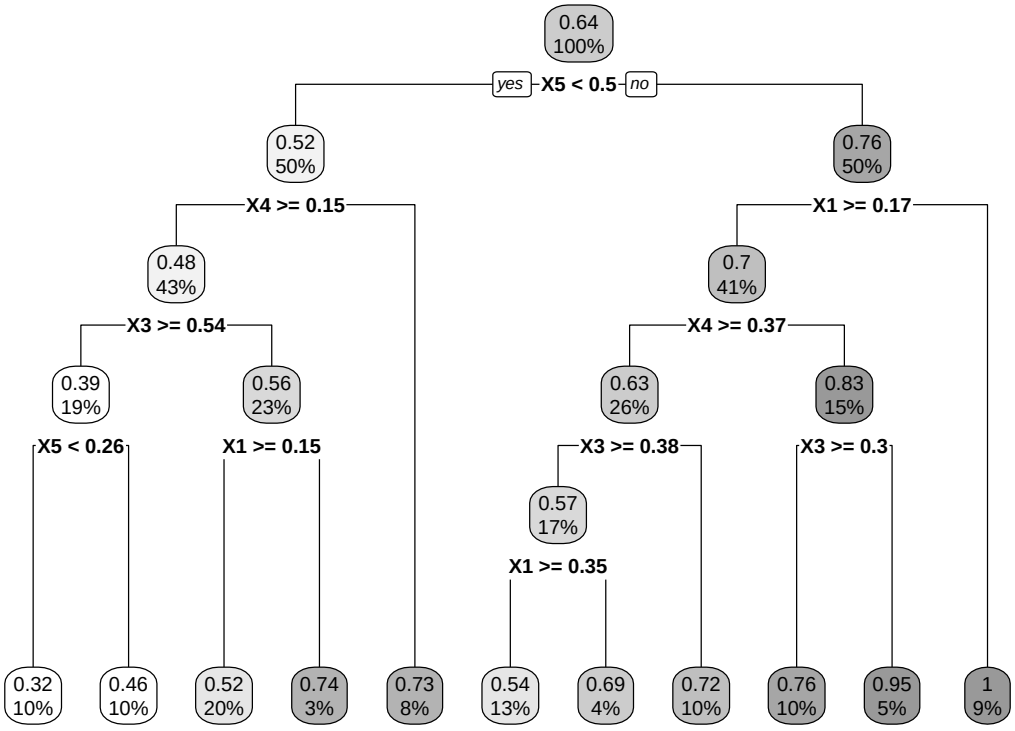

Fig. 2.17 Tree mapping of the function f_5. Small values are displayed in clear grey while large fitted values are display in a darker grey. The algorithm identifies correctly the parameters of interest and the parameter space is efficiently mapped.

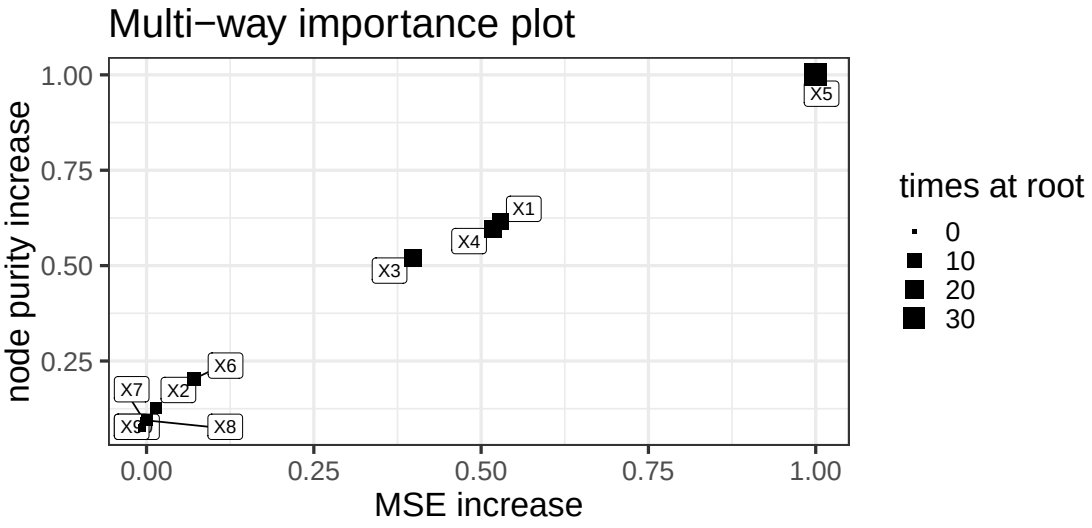

Fig. 2.18 Multi-way parameter importance for the function f_5. The parameters influencing the outputs are correctly identified. The parameters x_5 appears as having a large influence on the output. The other parameters have a measure of importance close to 0 while the parameter x_6 influence marginally the output.

2.2.3 Summary of the examples

We used different examples to emphasise the different scenarios which can be met in mathematical models. Overall, mapping of the different parameter spaces and their related functions gave good results. Non-rectangular manifolds (f_1) or multiple manifolds (f_2) were well approximated. Even complex manifolds as in function f_3 were relatively well mapped. The continuous examples, f_4 and f_5, were well mapped and indicated for which combination of values of parameters low or high outputs could be found.

Crucially the importance can still be correctly determined and indicates which parameters are mainly influencing the output of the functions. As one can observe the results of multi-way importance are robust and show efficiently which parameters influence the most the output. However, it is important to remark that rank order by the measure “times at first root” can give inconsistent results.

2.3 Interactions

"Interaction between parameters" describes a situation in which the simultaneous influence of two or more parameters on the output is not additive. Interactions between parameters can play a potentially crucial role in the dynamics of a mathematical model, see chapter 3 and 5, thus it is necessary to develop tools to identify and understand these interactions occurring in mathematical models. The study of a mathematical model often starts with previous knowledge of the model, see chapter 3 for an application. Knowledge can be extracted from biological experiments or previous studies of the model and an artificial parameter representing the interaction can be added to split the parameter space. For example, in the case of the parameter space of f_3 (see equation 2.22) by adding an artificial parameter P_{x_1,x_2}, the product of the parameter x_1 and x_2, it is possible to perfectly map the parameter space, see Figure 2.19. A brute force approach, inspired by [97], consists

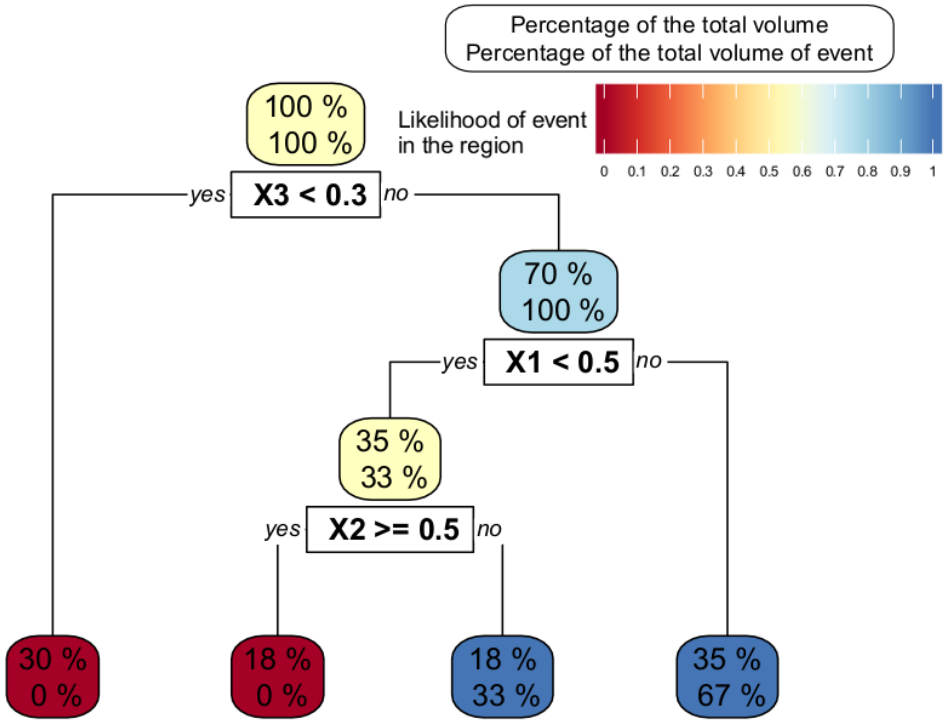

Fig. 2.19 Tree mapping of the function f_4 with artificial interaction parameters. The algorithms correctly identify the parameters of interest and the parameter space is efficiently mapped.

of testing all possible interaction effects and focussing on the parameters with a possible interaction. This approach, however, is cumbersome and slow when there is a large number of parameters. Indeed the number of combinations of artificial parameters is proportional to $p(p-1)$ and the computation time when building trees is proportional to the number of parameters. A priori knowledge can help to take into account known interactions. When a relationship between two param-

eters is supposed, an artificial parameter is created to represent the supposed relationship between the two (or more) parameters. When the knowledge of the model is limited we propose two complementary methods:

- *Visualisation*. With this approach, artificial parameters are created after a visual inspection of the relationship between parameters, using some appropriate visualisation.
- *Statistical test*. With this approach, a systematic test of plausible interactions is performed to automatically detect potential interactions. All possible combinations of interactions are tested and the ones with the higher measures of importance are investigated.

In the next sections, we describe the two approaches.

2.3.1 Visual inspection to identify interaction between parameters

Visualisation is one of the most powerful interpretation tools and can give strong insight into the interaction between parameters. To address the issues of interaction, an efficient approach can consist of projecting the parameters space over a selection of parameters. If a particular shape appears, interactions between these two parameters should be investigated. This visualisation tool is limited to pairs of parameters.

Partial dependence plots

To estimate the effect of a parameter, Friedman introduced the concept of partial dependence plots [96]. In the case of a single covariate x_j, the idea is that the partial dependence function $\phi_j(x_j)$ tells us how the value of the variable x_j influences the model predictions after we have "averaged out" the influence of all other variables. Friedman's partial dependence plots are obtained by computing the following average and plotting it over a useful range of x_j values:

$$\begin{aligned}\phi_j(x_j) &= \mathbb{E}_j\left(F(\mathbf{X}|X_j = x_j)\right) \\ &= \int_{\mathbb{X}} F(X_1,\cdots,X_{j-1},x_j,X_{j+1},\cdots X_n)\; dX_1,\ldots,dX_{j-1},dX_{j+1},\ldots dX_n.\end{aligned} \tag{2.25}$$

$\mathbb{E}_j\left(F(\mathbf{X}|X_j = x_j)\right)$ is the conditional expectation of F, knowing the value of the j^{th} parameter. For example, for linear models, the resulting plots are simply straight lines whose slopes are equal to the model parameters. Indeed, let us define a linear model:

$$f: \begin{cases} [-1 \quad 1]^1 0 \to \mathbb{R}, \\ \mathbf{x} \mapsto \sum_{k=1}^{10} a_k x_k, \end{cases} \tag{2.26}$$

then we have:

$$\begin{aligned}\phi_j(x_j) &= \mathbb{E}_j\left(f(\mathbf{X}|X_j = x_j)\right)\\ &= \mathbb{E}_j\left(\sum_{k=1}^{10} a_k X_k | X_j = x_j)\right)\\ &= \sum_{k\neq j} \mathbb{E}_j\left(a_k X_k | X_j = x_j)\right)\\ &= a_j x_j + \sum_{k\neq j} C_k.\end{aligned} \tag{2.27}$$

This definition can be extended for any number of parameters, particularly, we have for two parameters i and j:

$$\phi_{ij}(x_i, x_j) = \mathbb{E}_{(i,j)}\left(F(\mathbf{X}|X_i = x_i, X_j = x_j)\right). \tag{2.28}$$

Let us recall that the vector $\mathbf{x} = (x_1, x_2, ..., x_p) \in \mathbb{X}$ represents the parameters in a model whose model function is $F(\mathbf{x})$. If we partition the index of the vector $\mathbf{x}$ into two vectors of index $\mathbf{z} \in [1, 2, \ldots, p-1, p]$ and its compliment, $\mathbf{z}^c = [1, 2, \ldots, p-1, p] \backslash \mathbf{z}$. Let say p = 5, an example of decomposition could be $\mathbf{z} = [1, 3]$ and $\mathbf{z}^c = [2, 4, 5]$. Another indexing could be $\mathbf{z} = [2, 3]$ and $\mathbf{z}^c = [1, 4, 5]$. We can define then define $\mathbf{x_z}$ has a subset of the vector $\mathbf{x}$ where only the element with an index in $\mathbf{z}$ are kept. For example with $\mathbf{z} = [1, 3]$ and $\mathbf{z}^c = [2, 4, 5]$ we would have $\mathbf{x_z} = (x_1, x_3)$.

$$\phi_z(\mathbf{x_z}) = \mathbb{E}_\mathbf{z}\left[F(\mathbf{X})|\mathbf{X_z} = \mathbf{x_z}\right]. \tag{2.29}$$

In some cases $\phi_s(x_s)$ can be directly calculated (such as a linear function), however, for complex models such as NMMs, this is not the case; $\phi_s(x_s)$ needs to be estimated. In the next section, two approaches are considerated to estimate: $\mathbb{E}_\mathbf{z}\left[F(\mathbf{X})|\mathbf{X_z} = \mathbf{x_z}\right]$.

Estimation of marginal expectation by binning

If the number of simulations is large, the preferable approach is to bin the j$^{\text{th}}$ parameter into different smaller intervals. Then based on the assumption that

$$\mathbb{E}_j\left(F(\mathbf{X}|x_j)\right) = \mathbb{E}_j\left(F(\mathbf{X}|x_j \in m_n)\right), \tag{2.30}$$

i.e. at a bin level a change of value of the parameter i^{th} can be represented by the expectation in the binnage. The bins need to be small enough to capture and represent changes of output due to the i^{th} parameter. The original simulated parameter spaces which fall in a given small interval, a bin, can be replaced by a value representative of that interval, the likelihood of the event 1 in the bin. For a partition $\mathbf{x}$ into an interest set $\mathbf{z}$ and its compliment, $\mathbf{z}^c = [1, 2, \ldots, p-1, p] \backslash \mathbf{z}$ we wish to determine the average values of the function F given $\mathbf{X_z} \in R$. Then we

have

$$\mathbb{E}_{\mathbf{z}}[F(\mathbf{X})|\mathbf{X}_{\mathbf{z}} \in R] = \int_{\mathbb{X}} F(\mathbf{X}|\mathbf{X}_{\mathbf{z}} \in R)d\mathbf{x}, \tag{2.31}$$

Equation 2.31 can be estimated from a set of training data by:

$$\frac{1}{|(\mathbf{x}, \mathbf{x}_{\mathbf{z}} \in R)|} \sum_{(\mathbf{x}, \mathbf{x}_{\mathbf{z}} \in R)} F(\mathbf{x}). \tag{2.32}$$

This approach is relatively fast but needs large data set training as seen in section 2.1.3.

Estimation of marginal expectation by using the random forest

If there are not enough simulations to estimate the values of F with accuracy in some regions of interest because the computation of the function F becomes too expensive, it is possible to use the approximation by the random forest, $\hat{F}$.

$$\mathbb{E}_{\mathbf{z}}[F(X)|\mathbf{X}_{\mathbf{z}} = \mathbf{x}_{\mathbf{z}}] = \frac{1}{N} \sum_{\mathbf{x}} \hat{F}(\mathbf{x}|\mathbf{x}_{\mathbf{z}}), \tag{2.33}$$

for the case in one dimension, we have:

$$\hat{\phi}_j(x_j) = \mathbb{E}_j\left(\hat{F}(\mathbf{X}|X_j = x_j)\right) = \frac{1}{N} \sum_{\mathbf{x}} \hat{F}(x_1, \ldots, x_{j-1}, x_j, x_{j+1}, \ldots, x_p). \tag{2.34}$$

The advantage is that an accurate estimation of $\hat{\phi}_j(x_j)$ can be estimated, the inconvenience being that if the random forest does not fit F properly some errors will appear.

An example using the function f_3 is given in Figure 2.20. The approximately linear interaction between x_1 and x_2 appears clearly. In contrast, the visual approach shows that the parameters x_4 and x_5 have small impact on the outputs.

However, for more complex models, the effect of interaction between parameters can be hidden because of other terms in the function. This is the case for the function f_5, see Figure 2.21. Due to the large number of parameters interacting and having a strong effect on the output it is difficult to determine which parameters interact with other parameters.

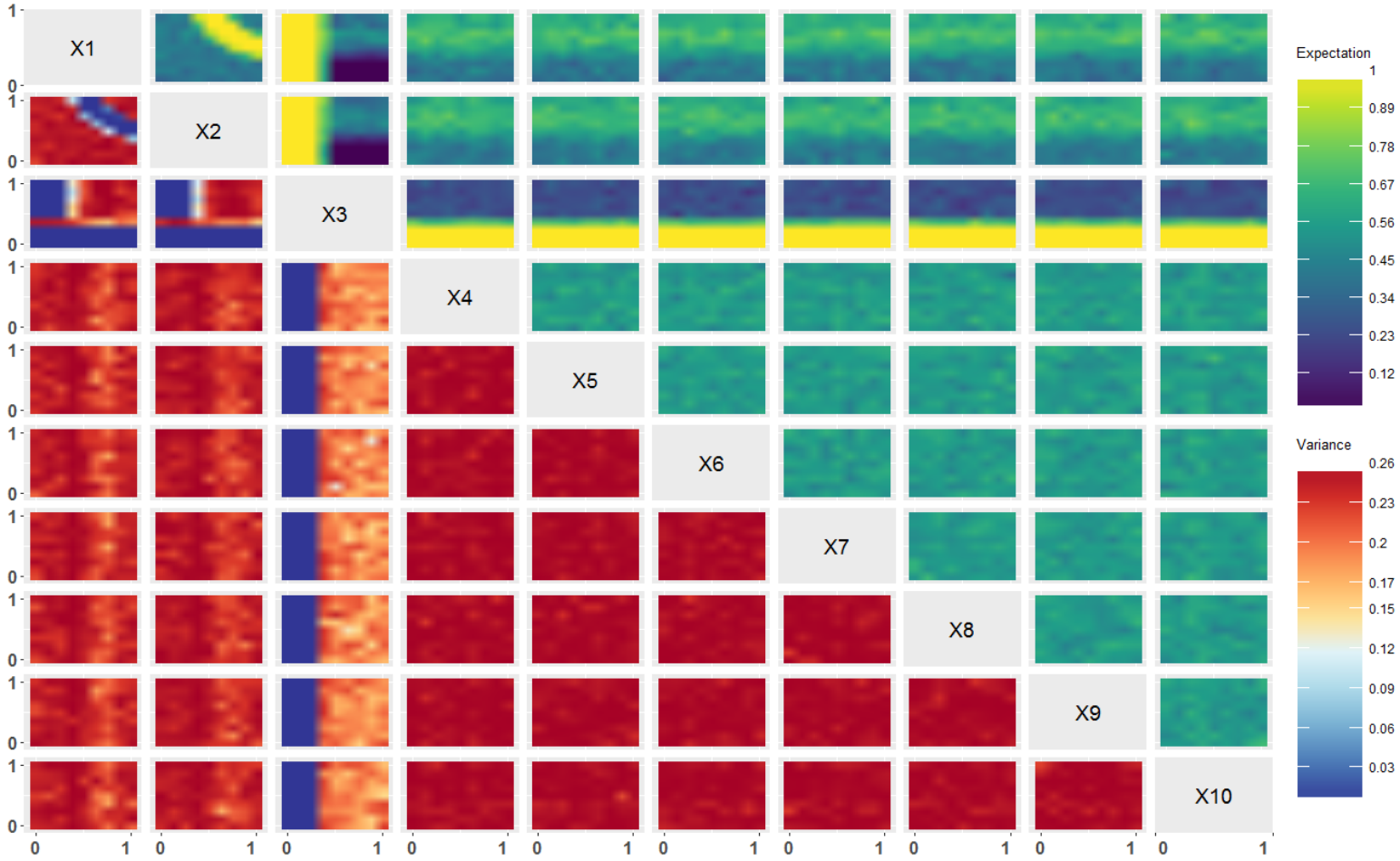

Fig. 2.20 Projection of the parameter space of the function f_3, see equation 2.22. Each subfigure is a projection of the parameter space over two parameters, and the colour indicates the expectation in the upper triangle and the variance in the lower triangle. The axis labels are indicated by the diagonal. The interaction between the parameters x_1 and x_2 is visible.

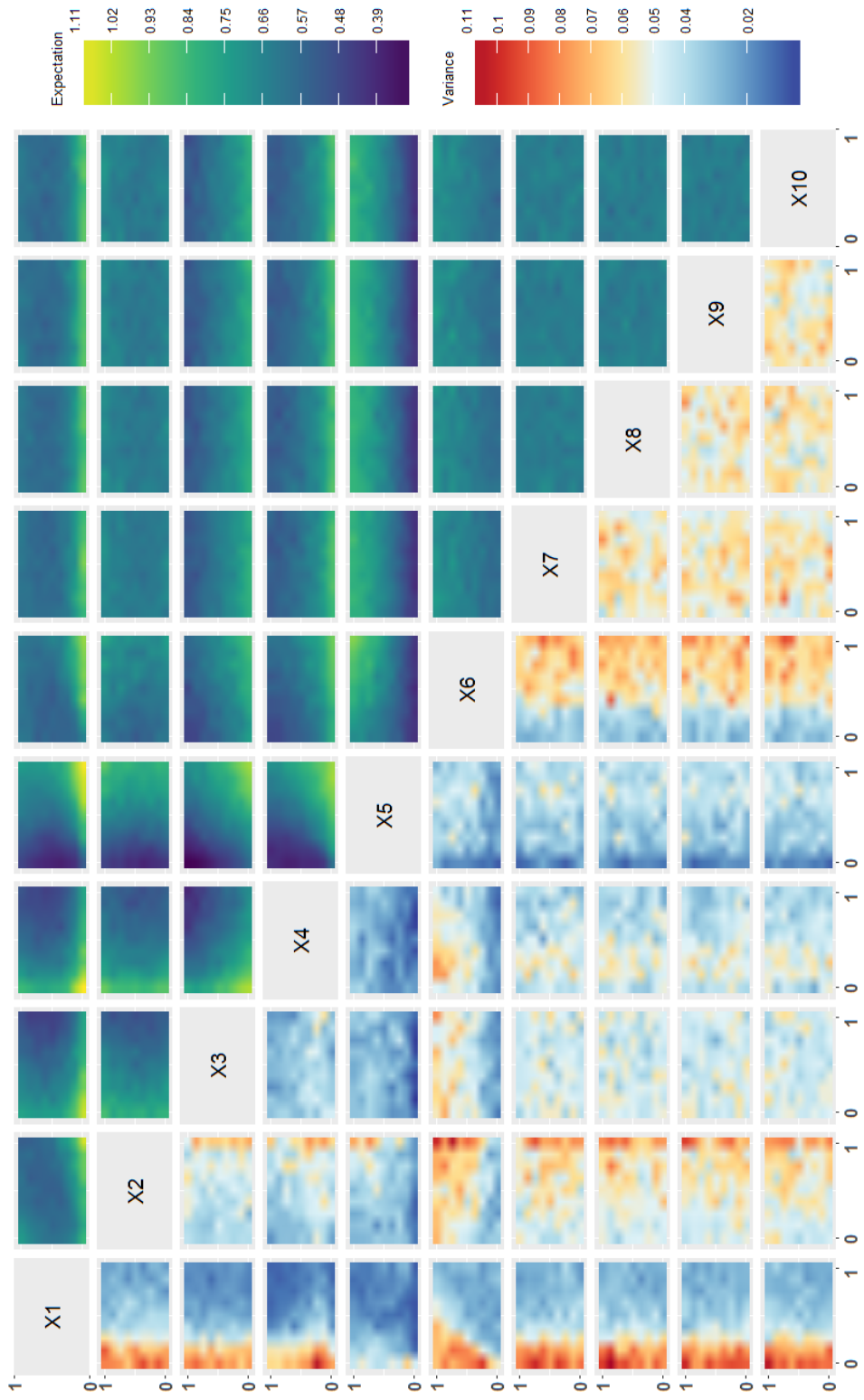

Fig. 2.21 Projection of the parameter space of the function f_5, see equation 2.24. Each subfigure is a projection of the parameter space over two parameters, and the colour indicates the expectation in the upper triangle and the variance in the lower triangle.The axis labels are indicated by the diagonal. Due to its negligible effect the interaction between the parameters x_1 and x_2 is not visible.

Limitation of partial dependence plots

Nevertheless, these multivariate partial dependence plots have been criticized as being inadequate in the face of specific examples. An example was given by Goldstein et al [102] who introduced the function f:

$$f : \begin{cases} [-1 \quad 1]^2 \to \mathbb{R} \\ \mathbf{x} \mapsto -5x_1 + 10x_1 \mathbb{1}_{x_2>0} \end{cases} \tag{2.35}$$

where $\mathbb{1}$ is the Heaviside step function. Goldstein et al showed with simulation that ϕ_1 is nearly constant[4], while it is obvious that X_1 influences the output. We identify in which context this can arise and provide a solution. Let's decompose F[5]:

$$F(\mathbf{x}) = F_1(x_j) + F_2(\mathbf{x_j^c}) + F_3(\mathbf{x}), \tag{2.36}$$

where $F_1(x_j)$ represents the terms in F depending on x_j, ${}_2(\mathbf{x_j^c})$ express the term in F independent of x_j and $F_3(\mathbf{x}) = \left(F(\mathbf{x}) - F_1(x_j) - F_2(\mathbf{x_j^c})\right)$ express the part of F where there is interaction between x_j and j. So we have

$$\phi_j(x_j) = \mathbb{E}_j\left(F(\mathbf{X}|X_j = x_j)\right) = F_1(x_j) + C + \mathbb{E}_j\left(F_3(\mathbf{x})\right), \tag{2.37}$$

as $\mathbb{E}_j\left(F_2(\mathbf{x_j^c})\right) = C$ is constant by definition. Then if

$$\frac{\triangle\, F_1(x_j)}{\triangle\, x_j} = -\frac{\triangle\, \mathbb{E}_j\left(F_3(\mathbf{x})\right)}{\triangle\, x_j}, \tag{2.38}$$

one cannot see the influence of x_j on the output. One can check that the example given in equation 2.35 verifies this condition. To overcome this limitation it is possible to plot $\phi_{ij}(x_i, x_j)$, see Figure 2.20.

2.3.2 Partial interaction plots

To disregard the effect of a single parameter and focus only on interactions we introduce and define the partial interaction plots as:

$$\begin{aligned} \psi_{ij}(x_i, x_j) =& \phi_{ij}(x_i, x_j) - \phi_i(x_i) - \phi_j(x_j) \\ =& \mathbb{E}_{(i,j)}\left(F(\mathbf{X}|X_i = x_i, X_j = x_j)\right) \\ & - \mathbb{E}_i\left(F(\mathbf{X}|X_i = x_i)\right) - \mathbb{E}_j\left(F(\mathbf{X}|X_j = x_j)\right). \end{aligned} \tag{2.39}$$

[4] $\phi_1 = -5x_1 + 10x_1 \int_{[-1\ 1]_.} f(x_1, X_2)\, dX_2 = -5x_1 + 10x_1 \frac{1}{2} = 0$.

[5] This decomposition is not always possible. Indeed, in many cases, the term in x_j cannot be split from the others, in these cases $F_3 = F$, $F_1 = 0$ and $F_2 = 0$.

By decomposing F[6] as

$$F(\mathbf{x}) = F_{i\cup j}(\mathbf{x}) + F_{i\perp j}(\mathbf{x}), \tag{2.40}$$

where $F_{i\cup j}$ denotes the term in F where the parameters i and j interact and $F_{i\perp j}$ where they do not.

Theorem

$$\begin{aligned}\psi_{ij}(x_i,x_j) =& \mathbb{E}_{(i,j)}\left(F_{i\cup j}(\mathbf{X}|X_i=x_i,X_j=x_j)\right) - \mathbb{E}_i\left(F_{i\cup j}(\mathbf{X}|X_i=x_i)\right) - \\ & \mathbb{E}_j\left(F_{i\cup j}(\mathbf{X}|X_j=x_j)\right) + C_{ij},\end{aligned} \tag{2.41}$$

where C_{ij} is a constant. By computing $\psi_{ij}(x_i,x_j)$ the terms of F where i and j do not interact are removed.
Proof: By definition of ψ_{ij} and linearity of the expected value operator:

$$\begin{aligned}\psi_{ij}(x_i,x_j) =& \mathbb{E}_{(i,j)}\left(F_{i\cup j}(\mathbf{X}|X_i=x_i,X_j=x_j)\right) - \mathbb{E}_i\left(F_{i\cup j}(\mathbf{X}|X_i=x_i)\right) \\ & - \mathbb{E}_j\left(F_{i\cup j}(\mathbf{X}|X_j=x_j)\right) + L(x_i,x_j),\end{aligned} \tag{2.42}$$

where

$$\begin{aligned}L(x_i,x_j) =& \mathbb{E}_{(i,j)}\left(F_{i\perp j}(\mathbf{X}|X_i=x_i,X_j=x_j)\right) \\ & - \mathbb{E}_i\left(F_{i\perp j}(\mathbf{X}|X_i=x_i)\right) - \mathbb{E}_j\left(F_{i\perp j}(\mathbf{X}|X_j=x_j)\right).\end{aligned} \tag{2.43}$$

Let's decompose $F_{i\perp j}$:

$$\forall \mathbf{x},\ F_{i\perp j}(\mathbf{x}) = F_{-j}(\mathbf{x}) + F_{-i}(\mathbf{x}), \tag{2.44}$$

with $F_{-i}(\mathbf{x})$ denotes a decomposition of $F_{i\perp j}$ such that $F_{-i}(\mathbf{x})$ does not have term in x_i and $F_{-j}(\mathbf{x})$ does not have term in x_j[7]. Then we have by the linearity of the expected value operator:

$$\begin{aligned}L(x_i,x_j) =& \mathbb{E}_{(i,j)}\left(F_{-i}(\mathbf{X})|X_i=x_i,X_j=x_j\right) - \mathbb{E}_i\left(F_{-i}(\mathbf{X})|X_i=x_i\right) \\ & - \mathbb{E}_j\left(F_{-i}(\mathbf{X}|X_j=x_j)\right) + \mathbb{E}_{(i,j)}\left(F_{-j}(\mathbf{X}|X_i=x_i,X_j=x_j)\right) \\ & - \mathbb{E}_i\left(F_{-j}(\mathbf{X}|X_i=x_i)\right) - \mathbb{E}_j\left(F_{-j}(\mathbf{X}|X_j=x_j)\right).\end{aligned} \tag{2.45}$$

By definition of F_{-j} and F_{-i} we have

$$\begin{aligned}&\mathbb{E}_{(i,j)}\left(F_{-i}(\mathbf{X})|X_i=x_i,X_j=x_j\right) = \mathbb{E}_j\left(F_{-i}(\mathbf{X}|X_j=x_j)\right), \\ &\mathbb{E}_{(i,j)}\left(F_{-j}(\mathbf{X}|X_i=x_i,X_j=x_j)\right) = \mathbb{E}_i\left(F_{-j}(\mathbf{X}|X_i=x_i)\right), \\ &\mathbb{E}_i\left(F_{-i}(\mathbf{X})|X_i=x_i\right) = C_i, \\ &\mathbb{E}_j\left(F_{-j}(\mathbf{X})|X_j=x_j\right) = C_j.\end{aligned} \tag{2.46}$$

[6] Once again, decomposition is not always possible, in this case $F = F_{i\cup j}$ and the theorem holds.
[7] This decomposition is not unique in general.

So by insertion of the equality of equation 2.46 in equation 2.45 we have:

$$\begin{aligned} L(x_i,x_j) &= \mathbb{E}_j\left(F_{-i}(\mathbf{X}|X_j=x_j)\right) - C_i - \mathbb{E}_j\left(F_{-i}(\mathbf{X}|X_j=x_j)\right) \\ &\quad + \mathbb{E}_i\left(F_{-j}(\mathbf{X})|X_i=x_i)\right) - C_j - \mathbb{E}_i\left(F_{-j}(\mathbf{X})|X_i=x_i)\right) \\ &= -(C_i+C_j) \\ &= C_{ij}. \end{aligned} \tag{2.47}$$

It has been proven that:

$$\begin{aligned} \psi_{ij}(x_i,x_j) =& \mathbb{E}_{(i,j)}\left(F_{i\cup j}(\mathbf{X}|X_i=x_i,X_j=x_j)\right) - \mathbb{E}_i\left(F_{i\cup j}(\mathbf{X}|X_i=x_i)\right) - \\ & \mathbb{E}_j\left(F_{i\cup j}(\mathbf{x}|X_j=x_j)\right) + C_{ij}. \end{aligned} \tag{2.48}$$

This theorem is useful to observe the effects of the interaction of the parameters x_i and x_j. As $L(x_i,x_j)=0$ for any pairs (x_i,x_j), $\psi_{ij}(x_i,x_j)$ do not account for the effect of the terms in F which depend only of the parameters x_i and x_j. The case $\psi_{ij}(x_i,x_j)=C_{ij}$, for any x_i and x_j, can be explained by:

- x_i and x_j do not interact. Thus, we have $F_{i\cup j}(x_i,x_j)=C_{ij}$ for any pair x_i,x_j and so $\psi_{ij}(x_i,x_j)=0$ for any pair x_i,x_j. Thus, the partial interaction plot of two non-interacting parameters has a gradient equal to 0.

- $\mathbb{E}_{(i,j)}\left(F_{i\cup j}(\mathbf{X}|X_i=x_i,X_j=x_j)\right) = \mathbb{E}_i\left(F_{i\cup j}(\mathbf{X}|X_i=x_i)\right) + \mathbb{E}_j\left(F_{i\cup j}(\mathbf{x}|X_j=x_j)\right)$. This equality requires very specific functions for a given a specific parameter space.

It is possible to estimate $\psi_{ij}(x_i,x_j\in R)$ by using a similar estimation method as it is done in section 2.3.1 and to plot it to visualise the effect of the interactions. In the next section we give two examples.

2.3.3 Examples of partial interaction plots

In Figure 2.22, we computed the partial plot interaction for the function f_3:

$$f_3(x_1,\ldots,x_{30}) = \begin{cases} 0, & \text{if } (sin(3\pi x_1x_2)<0 \text{ or } x_3<0.4; \\ 1 & \text{otherwise.} \end{cases} \tag{2.49}$$

The interaction term between x_1 and x_2 was not perfectly captured by the tree approaches, see Figure 2.14. However, using partial dependant plot, the interaction between the parameters x_1 and x_2 is directly observable. There is an interaction which is highlighted between the parameters x_1 and x_2 with the parameter x_3. This is due to the fact that f_3 can be rewritten as

$$f_3 = 1 + \mathbb{1}(\sin(3\pi x_1x_2)<0)\mathbb{1}(x_3<0.4) - \mathbb{1}(x_3<0.4) - \mathbb{1}(\sin(3\pi x_1x_2)<0), \tag{2.50}$$

showing that the parameters are interacting over the output. For the other 27 parameters (only the first 10 parameters are posted) the value of ψ_{ij} is nearly constant hinting there is no interaction. For the particularly complex function f_5:

$$\begin{aligned} f_5(\mathbf{x}) =& 0.26 * (x_1^2 + x_2^2) - 0.48 x_1 x_2 + 0.5 e^{-(x_3)} \\ &+ 0.5 e^{(-\frac{x_4}{x_5})} + 0.5 e^{(1 - e^{(\frac{x_1}{x_5 x_6})})}. \end{aligned} \tag{2.51}$$

In addition to nonlinear terms, there are multiple linear and nonlinear interactions. These interactions are:

- x_1 and x_2;
- x_4 and x_5; and
- x_1, x_5 and x_6.

In the initial projection, Figure 2.21, it is difficult to identify which parameters interact. However, all the interactions can be directly visualised and not a single false interaction is detected, see Figure 2.23. Furthermore ψ is useful to indicate how the parameters interact. It can be visualised in the subfigure in the first row and second column that the interaction between x_1 and x_2 is minimised when x_1 is large and x_2 small (and reciprocally). It is possible to identify (in the fifth column) that small values of x_5 increase the negative interaction with the parameter x_1 and x_4. This example shows that the partial interaction plot are able to identify interaction for a complex model.

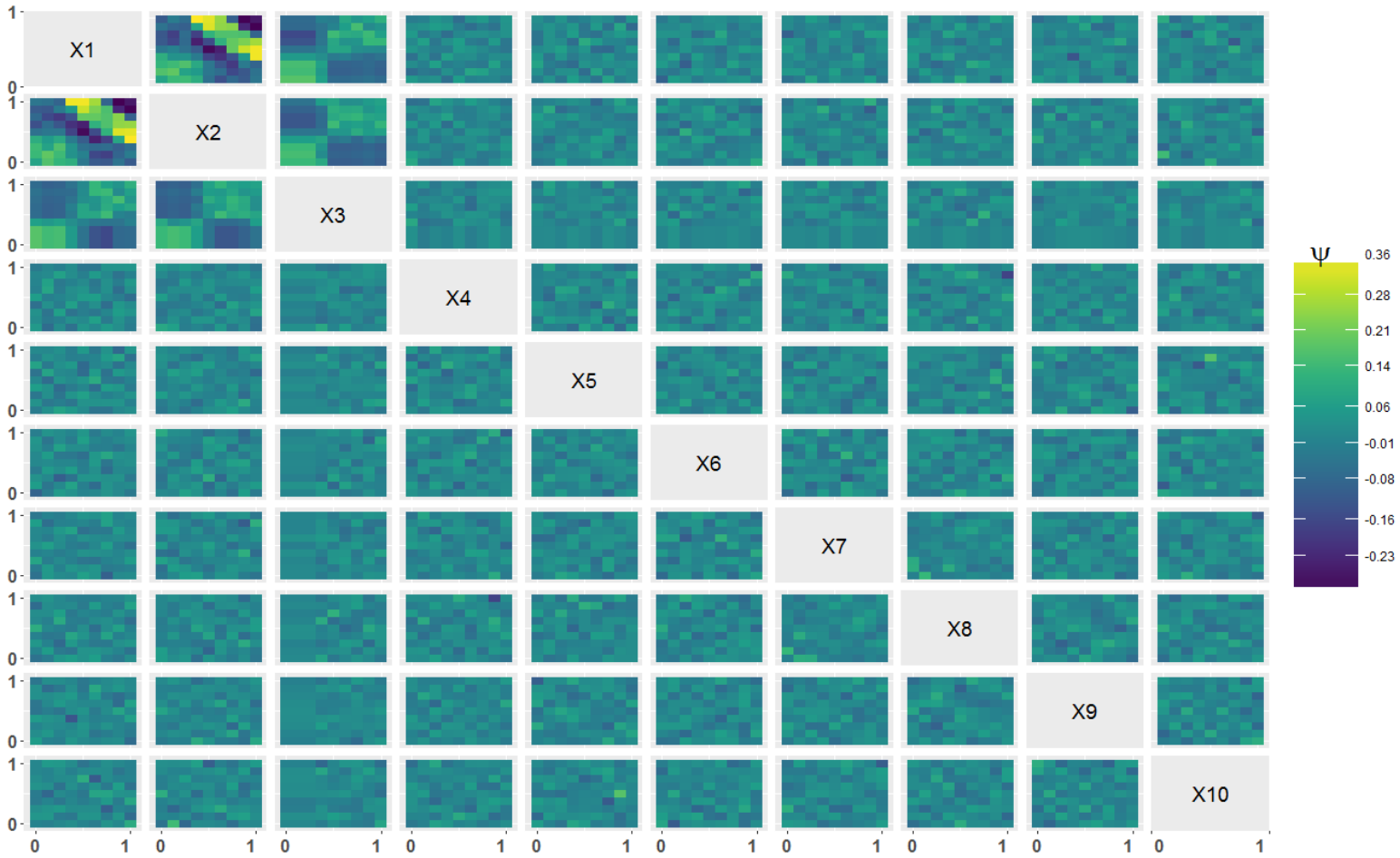

Fig. 2.22 Partial interaction plots of the parameter space of the function f_3, see equation 2.50.The axis labels are indicated by the diagonal. The interaction between the parameters x_1 and x_2 is particularly visible but other interactions (x_3 with x_1 and x_2) are visible. The rest of partial interaction plot shows a noisy background, i.e. they indicate that no interaction are detected.

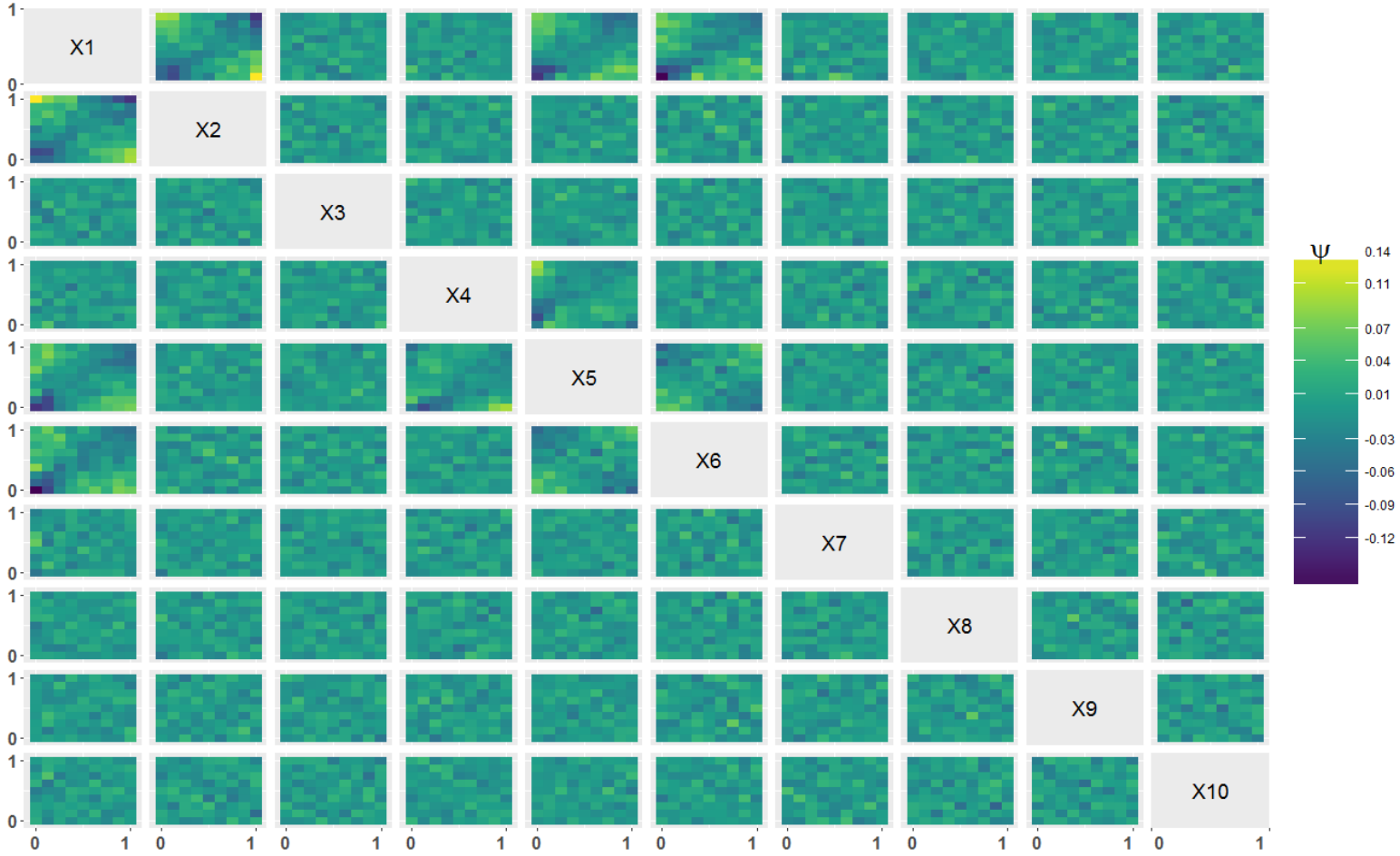

Fig. 2.23 Partial interaction plots of the parameter space of the function f_5, see equation 2.51.The axis labels are indicated by the diagonal. Each subfigure is a projection of the parameter space over two parameters. A subfigure with a gradient of colours indicates a possible interaction.
The known interactions between the parameters are directly visible. The rest of partial interaction plot shows a noisy background, i.e. they indicate that no interaction are detected.

2.3.4 Test for interactions

In this section, we describe an approach which will automatically determine the potential interactions between parameters and create artificial parameters only for those potential parameters with interactions. We recall that the statistical methods used rest on assumptions which are not always valid and thus some interactions could have a high p-values and be not detected by an automatic detection of interactions [119].

We wish to know which combinations of parameter interaction need to be explored. We use a statistical test for interaction. The null hypothesis, H_0, states that the two parameters do not interact in the population. The alternative hypothesis, H_1, states that there is an interaction effect.

$$\begin{cases} H_0, & \mathbb{E}_{(i,j)}\left(F(\mathbf{X}|X_i = x_i, X_j = x_j)\right) = \mathbb{E}_i\left(F(\mathbf{X}|X_i = x_i)\right) + \mathbb{E}_j\left(F(\mathbf{X}|X_j = x_j)\right); \\ H_1 & \mathbb{E}_{(i,j)}\left(F(\mathbf{X}|X_i = x_i, X_j = x_j)\right) \neq \mathbb{E}_i\left(F(\mathbf{X}|X_i = x_i)\right) + \mathbb{E}_j\left(F(\mathbf{X}|X_j = x_j)\right). \end{cases} \tag{2.52}$$

Two-way ANOVA

The two-way Analysis of variance (ANOVA) models all these variables as varying independently and normally around a mean, μ_{kl} with a constant variance, σ such that for the s^{th} simulation $Y_{skl} = \mu_{kl} + \varepsilon_{skl}$ with $\varepsilon_{skl} \overset{i.i.d.}{\sim} \mathcal{N}(0, \sigma^2)$. The assumption of this statistical test are:

- the errors are independent;
- the errors have the same variance; and
- the errors are normally distributed.

Let consider the case where we study the interaction between two parameters i and j. To detect an interaction between two parameters over a continuous output we compare an additive model:

$$\mu_{kl} = \mu + R_k + S_l, \tag{2.53}$$

to a model with linear interaction:

$$\mu_{kl} = \mu + R_k + S_l + \theta R_k S_l, \tag{2.54}$$

where μ_{kl} is the empirical (mean) value of a quantitative output corresponding to the values of the parameter i in its k^{th} region and the parameter j in its l^{th} region. μ is the mean over the whole parameter space, R_k is the additive effect of the i^{th} parameter for values belonging to region k and C_l is the additive effect of j for values belonging to region l. By testing the null hypothesis that $\theta = 0$, we are able to detect some departures from additivity based only on the single parameter θ.

Scheirer–Ray–Hare test

The Scheirer–Ray–Hare test is a non-parametric test [224] which is the extension of the Kruskal-Wallis test and is the non-parametric equivalent of two-way ANOVA with replication. It consists of running a two-way ANOVA on the ranks of the simulations. It is a controversial test [77]. Indeed interactions rely on additivity of effects and interaction terms on the original scale; rank transformations are nonlinear and as a result the rank transformation could completely remove an interaction in the original variables. Thus the power of the test is lower than the regular two-way ANOVA with replication and the latter should be chosen when the assumption of the regular two-way ANOVA test are valid.

Validity of assumptions

The validity of statistical tests relies on assumptions which are often not respected. This can lead to false positive and false negative [112]. A large p-value only suggests that the data are not unusual if all the assumptions used to compute the p-value (including the test hypothesis) were correct. In the meantime, a small p-value can indicate that one of the necessary assumption of the validity of the test is not respected [112]. It is possible to check the validity of these assumptions with further tests such as the Levene's test for homogeneity of variances or the Shapiro-Wilk test for the goodness-of-fit of the simulations set to the normal distribution. Therefore the proposed test is only a test to detect potential interactions and cannot be use to prove the existence of an interaction. However, it can help to further focus on a restricted number of parameters.

Automatic detection of interactions

To experiment the validity of a statistical approach we perform statistical test on the function f_3 and f_5. To recall:

$$f_3 = 1 + \mathbb{1}(\sin(3\pi x_1 x_2) < 0)\mathbb{1}(x_3 < 0.4) - \mathbb{1}(x_3 < 0.4) - \mathbb{1}(\sin(3\pi x_1 x_2) < 0), \quad (2.55)$$

and

$$\begin{aligned} f_5(\mathbf{x}) =& 0.26\ (x_1^2 + x_2^2) - 0.48\ x_1 x_2 + 0.5\ e^{-(x_3)} \\ &+ 0.5\ e^{\left(-\frac{x_4}{x_5}\right)} + 0.5\ e^{(1-e^{\left(\frac{x_1}{x_5 x_6}\right)})}. \end{aligned} \quad (2.56)$$

The Levene's test rejected the homogeneity of variance assumption and thus we disregard the classical two-way ANOVA test and used the Scheirer–Ray–Hare test. Figure 2.24 demonstrates the efficiency of statistical test to detect interaction for the function f_3. In Figure 2.24 the interactions between x_1, x_2 and x_3 are well identified. We remark that few false interactions are identified with a p-value

inferior to 0.1. This is expected as 45 combinations of parameters have been computed. Figure 2.25 shows that the statistical tests identify correctly three linear

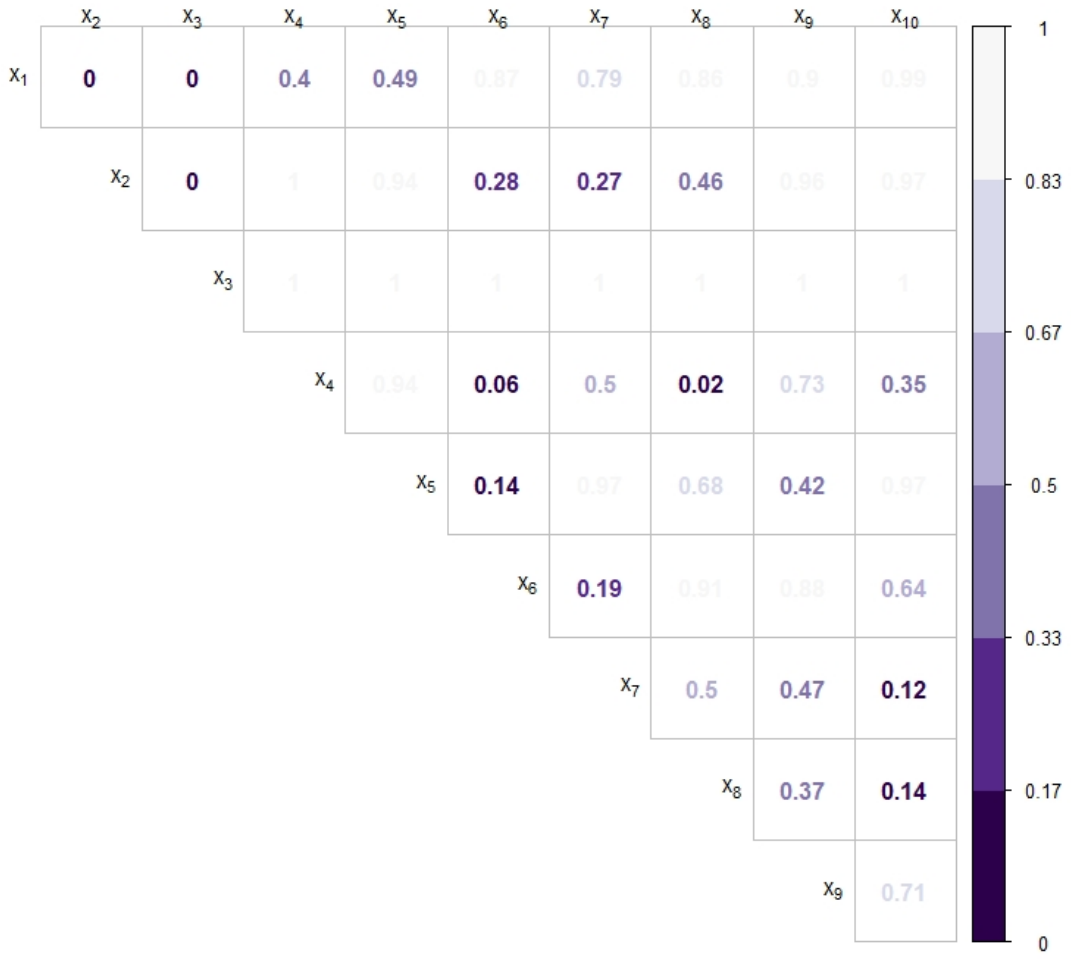

Fig. 2.24 Scheirer–Ray–Hare test to identify parameters with interactions for the function f_3. At a 0.05 threshold the interactions between x_1, x_2 and x_3 are well identified but a false positive is detected between the parameters x_4 and x_8.

and nonlinear interactions of the function f_5. The interactions detected are the linear interaction between x_1 and x_2, the nonlinear interaction between x_1 and x_6 and the nonlinear interaction between x_4 and x_5. However the interactions between the terms x_1 and x_5 and x_5 and x_6 are not detected. These results highlight the limitation of statistical test to detect interactions. In the examples most of the interactions have been found but some have been wrongly rejected and they have been some false positive.

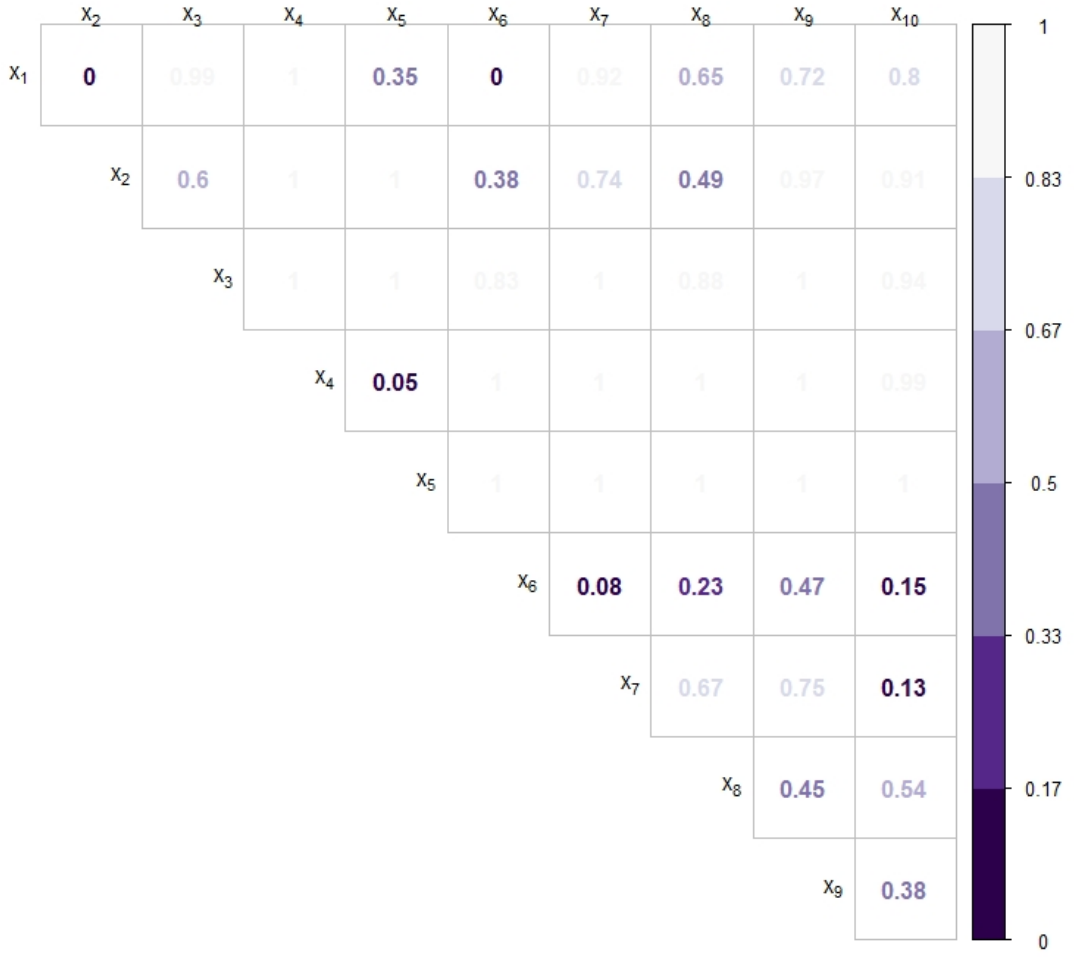

Fig. 2.25 Scheirer–Ray–Hare test to identify parameters with interactions for the function f_5. At a 0.05 threshold the identified interactions are the linear interaction between x_1 and x_2, the nonlinear interaction between x_1 and x_6 and the nonlinear interaction between x_4 and x_5. However the interactions between the terms x_1 and x_5 and x_5 and x_6 are not detected.

2.4 Conclusion

Visual and automatic tests of interactions are complementary. They both offer advantage and inconvenient. A visual approach is more able to detect interactions but depend on human judgement and can be time consuming when there is a high number of parameters. At the opposite statistical tests are fast and provide a p-value which is easy to analyse. However, the validity of statistical tests relies on assumptions which are often not respected and thus can increase the number of false discovery or fail to reject the null hypothesis by lack of power.

Chapter 3

Analyses of the Wendling model

> Mathematics is much more than a language for dealing with the physical world. It is a source of models and abstractions which will enable us to obtain amazing new insights into the way in which nature operates.
>
> Melvin Schwartz, *Principles of Electrodynamics [229]*

This chapter is based on the work published in [83] in collaboration with Dr. Marc Goodfellow and Prof. John Terry.

3.1 Introduction

Neural mass models (NMM) approximate the average behaviour of large populations of neurons and therefore provide an efficient way to simulate electrographic data in order to understand the mechanisms of brain (dys-) function. They have been used to understand a wide variety of physiological and pathophysiological activities of the brain, including the alpha rhythm [17, 165], sleep rhythms [61, 225, 280], brain resonance [243] or dynamics resulting from conditions such as epilepsy [106–108, 281, 283], schizophrenia [87] and dementia [26]. In particular, mechanisms underlying these conditions can be uncovered by inverting NMMs given dynamic data and studying the meaning of model parameters [81, 94, 161, 185]. However, maintaining a sense of biological realism in NMMs results in a high dimensional parameter space. The presence of many parameters renders the estimation of parameters from data, or model inversion, a challenging task because it is difficult to systematically and exhaustively explore large hypervolumes in order to identify subvolumes that are plausible. In order to reduce dimensionality, subsets of parameters can be fixed based on a priori

assumptions. Both the choice of initial values for parameters and the boundaries of the parameter space that are searched are often constrained [99]. Unfortunately, these constraints are often based on previously used values that have sometimes arisen arbitrarily in the literature. For example, the majority of parameters used in the study of [281] are taken directly from a previous study [140]. This study used itself previous parameters values [92, 271]. Ultimately these values were derived from studies made in the 70s [88–91, 165, 166, 290, 299] (see Figure 3.1 for a summarised history of typically cited parameter values for the NMM). In these early derivations of NMMs, parameters that could be experimentally determined were estimated but their uncertainties were not always measured [165].

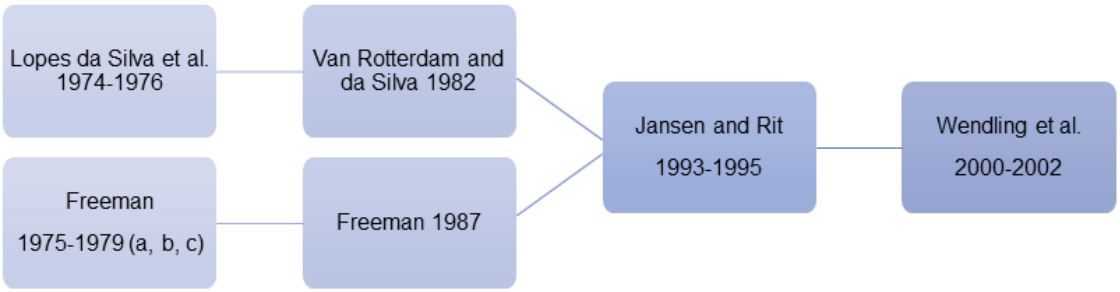

Fig. 3.1 Historical development of the Wendling model. The history of neural mass models typically begins with the work of Lopes da Silva and Freeman in the 1970s, although strictly speaking it can be traced back to Beurle [25]. These classical works from 1970s were extended by van Rotterdam and Freeman during the 1980s, before the classical Jansen and Rit model of 1995. Wendling further extended this model in work at the turn of the millennia extending the number of interneuron populations in the model. Interestingly, many of the parameter choices for the Wendling model in current use can be traced back to these early historic works.

Such parameters at the macroscopic level of a NMM are often presumed to relate directly to properties of individual neurons but aggregated, for example, to mean values [72]. However, large variability has been shown to exist in parameters measured directly from neurons and even parameters that are considered to be quasi-certain in the modelling community, such as synaptic time constants, have been shown to vary significantly in experiments [266]. Furthermore it remains unclear exactly how parameters of NMMs relate to microscopic properties of nervous tissue. Under standard values of NMM parameters, important insight has been gained regarding the generation of spontaneous or evoked electrographic recordings. For example, epileptiform rhythms have been shown to be induced by alterations to the excitatory/inhibitory balance in models [265]. However, fixing default values *a priori* in order to study the generation of particular dynamics does not allow to understand the behaviour of the system at unexplored, potentially plausible parameter values. Thus we cannot discover whether other regions of parameter space permit the same or different conclusions. When specifying prior distributions for model inversion (for example using the Kalman filter or Dynamic

Causal Modelling frameworks [93, 99]) we usually, therefore, do not know to what extent any resulting inference is dependent upon the particular choice of priors or whether unexplored regions of parameter space could also provide reasonable solutions. High dimensionality of parameter space is a particular problem in such settings since inversion algorithms become computationally demanding. It is therefore often prohibitive to explore a large parameter space or conduct inference under alternative choices of priors. The same can also be said for the use of global non-deterministic searches, for example based on evolutionary algorithms [190].

3.2 Methods

3.2.1 Overview

In this section, we remind the reader of the method introduced in chapter 2 and apply it to the Wendling model. The first step consists of choosing a NMM and defining a plausible parameter space, i.e. some constraints on the extreme values that each parameter can take. In this study, we use a variation of the Jansen and Rit model introduced in the context of epilepsy [281], this model, called Wendling model, has 11 parameters. The second step in the methodology consists of transforming the mathematical model into a database. To do this the NMM is simulated a 1,000,000 times using different parameters, which are chosen using a latin hypercube design. This is a space filling design which allows to efficiently explore the whole parameter space given a fixed number of simulations [176]. Each simulation is then classified in terms of some chosen characteristics. Here, we choose to focus on characteristics that are often used to define healthy and epileptiform rhythms, i.e. amplitude, frequency and number of peaks per period. The amplitude was defined as the maximum minus the minimum of the simulation. In cases for which the amplitude was greater than zero, i.e. the simulation was not constant, the frequency of the cycle and the number of peaks per period were calculated. The number of peaks can be used, for example, to characterise pathological dynamics. One of our aims is to characterise qualitative changes in model dynamics over the features above, since such an approach would enable us to find boundaries in parameter space over which dynamics change. Therefore, we seek to “classify” dynamics, rather than, for example, estimate quantitative features. Studying the database with classical statistics such as the joint distribution of the likelihood of seizure dynamics gives new insights into the model, but does not yield a comprehensive analysis.

The final step is to fit the data with a statistical model. Here, we choose to use a tree approach, which cuts the parameter space into rectangular regions of different sizes and is amenable to high dimensional analyses. These regions are created with the aim that each one contains similar dynamics and so trees approximate the parameter space in a simple and interpretable way. Of course,

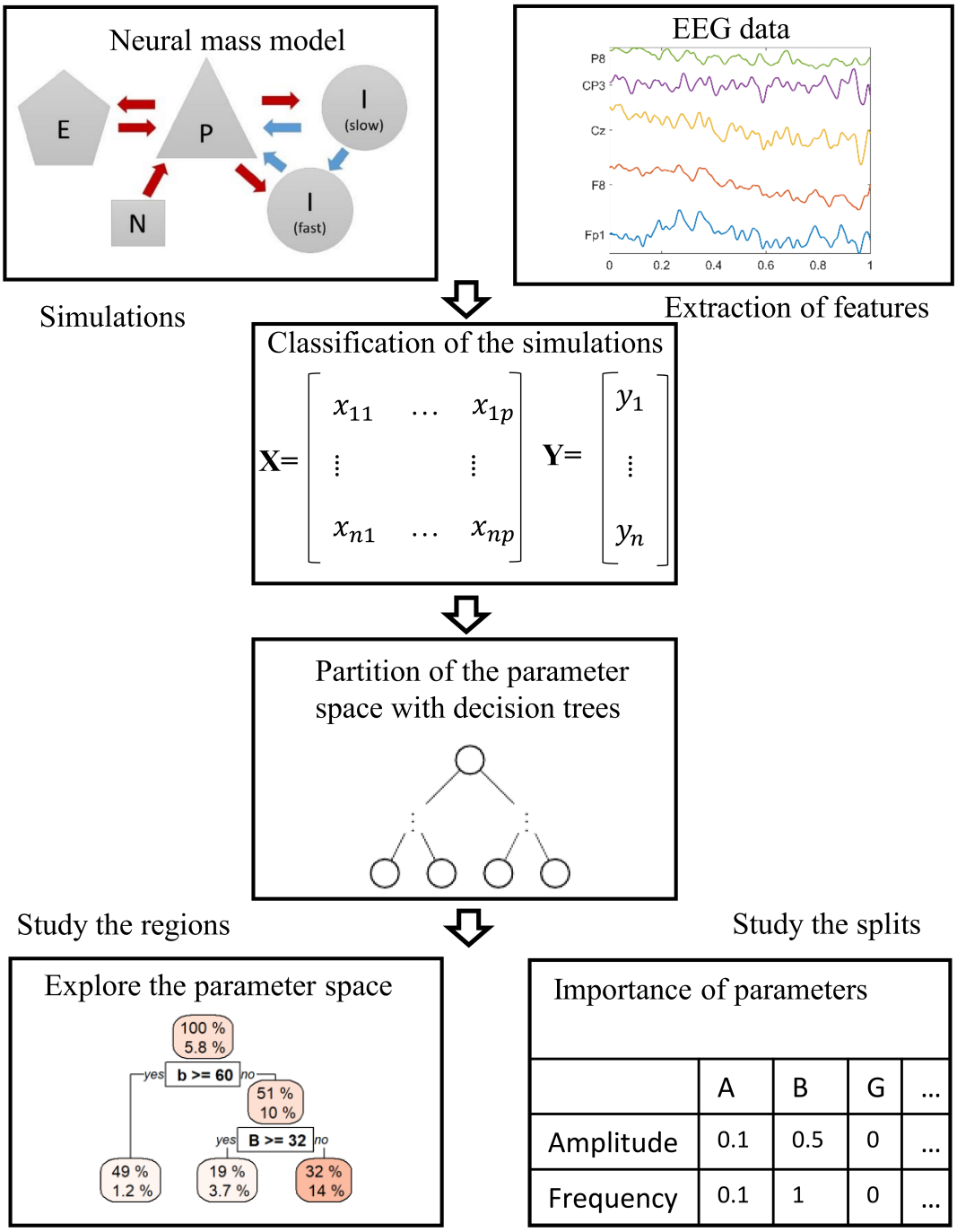

Fig. 3.2 Schematic of the methodology applied to the Wendling model. From top to bottom: The EEG dynamic features of interest are identified and characterised, the Wendling model is chosen as a model able to reproduce these dynamic. The Wendling model is simulated a 1,000,000 times over its parameter space and each simulation is given a classification according to its dynamic features. The parameter space is partitioned using decision tree learning. The partitions are used to characterise the parameter space of the NMM.

we do not expect that the parameter space can be completely mapped to a set of rectangular regions, each containing homogeneous dynamical features. Some regions therefore contain dynamics with different features and the proportion of space in the region filled by particular dynamics is useful information. For example,

one can ask whether certain regions contain a high density of seizure dynamics or exclude regions with certain features from further analyses. The statistical model captures defined characteristics of the mathematical model and summarises them in an efficient way, therefore facilitating the estimation of sensitivity of the dynamics to variations in a particular parameter. Thus critical, or important parameters for a given dynamics can be found.

3.2.2 Wendling model

The extension of the Jansen-Rit model [140] introduced by Wendling et al. [282] considered in this paper has classically been used to study transitions to seizure dynamics. It is a neurophysiological model, i.e. one that has been built to understand interactions in nervous tissue at the macro- or meso-scopic level. It has previously been shown to display a repertoire of important dynamics which occur at ictal and inter ictal states, for example in temporal lobe epilepsy [281, 282]. The model is based on the assumption of the existence of four populations of neurons: pyramidal cells; excitatory interneurons; slow and fast inhibitory interneurons. The activity of each population is governed by the interactions between them, see Figure 3.3.

Each population is characterized by:

1. Its second order linear transfer function. This function transforms the average presynaptic pulse density of afferent action potentials of other populations of neurons (the input) into an average postsynaptic membrane potential (the output). This can be either excitatory, slow inhibitory or fast inhibitory with respective impulse response $h_e(t)$, $h_i(t)$ or $h_g(t)$.

2. A sigmoid function $S(v) = \frac{2e_0}{1+\exp(r(v_0-v))}$ that relates the average postsynaptic potential v of a given population to an average pulse density of action potentials outgoing from the population.

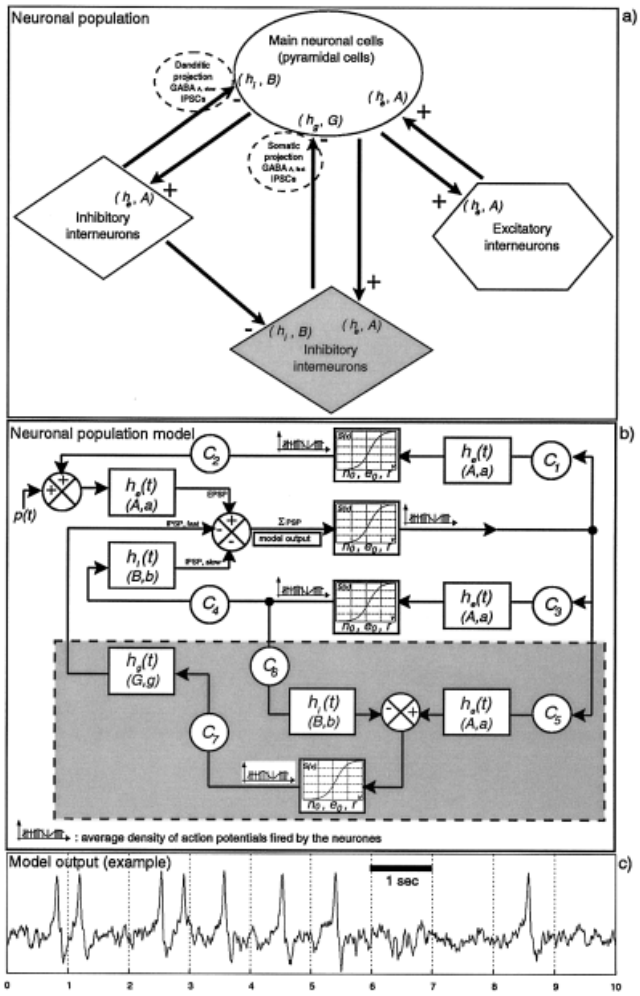

Fig. 3.3 Schematic of the Wendling model. Structurally, the neuronal population is considered to be composed of four neuronal subsets: pyramidal cells, excitatory interneurons, dendritic-projecting interneurons with slow synaptic kinetics (GABAA, slow) and somatic-projecting interneurons (grey rectangle) with faster synaptic kinetics (GABAA, fast). Subset of pyramidal cells project to and receive feedback from subsets of interneurons. (b) The model accounts for the neuronal population organization. In each subset, the average pulse density of afferent action potentials is changed into an average inhibitory or excitatory postsynaptic membrane potential using a linear dynamic transfer function of impulse response $h_e(t)$, $h_i(t)$, or $h_g(t)$, while this potential is converted into an average pulse density of potentials fired by the neurons using a static nonlinear function [asymmetric sigmoid curve, $S(v)$]. The subset of somatic-projecting interneurons (grey rectangle) receive input from both subsets of pyramidal and dendritic interneurons. (c) the model output represents the summated average postsynaptic potentials on pyramidal cells. It reflects an EEG signal. From [281] with authorisation.

The total potential of the pyramidal cell population is given by the aggregated contributions of the three feedback loops of inter-neurons connected to it. This is the output of the model, in analogy with recordings of electroencephalography

(EEG) [187]. These interactions can be summarise in the following set of ordinary differential equations:

$$
\begin{aligned}
\dot{z}_1(t) &= z_6(t) \\
\dot{z}_6(t) &= AaS\{z_2(t) - z_3(t) - z_4(t)\} - 2az_6(t) - a^2 z_1(t) \\
\dot{z}_2(t) &= z_7(t) \\
\dot{z}_7(t) &= Aa(p + C_2 S\{C_1 z_1(t)\}) - 2az_7(t) - a^2 z_2(t) \\
\dot{z}_3(t) &= z_8(t) \\
\dot{z}_8(t) &= BbC_4 S\{C_3 z_1(t)\} - 2bz_8(t) - b^2 z_3(t) \\
\dot{z}_4(t) &= z_9(t) \\
\dot{z}_9(t) &= GgC_7 S\{C_5 z_1(t) - z_5(t)\} - 2gz_9(t) - g^2 z_4(t) \\
\dot{z}_5(t) &= z_{10}(t) \\
\dot{z}_{10}(t) &= BbC_6 S\{C_3 z_1(t)\} - 2bz_{10}(t) - b^2 z_5(t)
\end{aligned}
\tag{3.1}
$$

The biological meaning of the NMM parameters is given in Table 3.1. The linear products of the variables z_1,...,z_5 represent the average postsynaptic potential of the different populations.

Parameter	Interpretation
A	Average excitatory synaptic gain
B	Average slow inhibitory synaptic gain
G	Average fast inhibitory synaptic gain
a	Inverse mean time in the excitatory loop
b	Inverse mean time in the slow inhibitory loop
g	Inverse mean time in the fast inhibitory loop
P	Input to the system from the area of the cortex
C_1	Connectivity pyramidal to excitatory
C_2	Connectivity excitatory to pyramidal
C_3	Connectivity pyramidal to slow inhibitory
C_4	Connectivity slow inhibitory to pyramidal
C_5	Connectivity pyramidal to fast inhibitory
C_6	Connectivity slow inhibitory to fast inhibitory
C_7	Connectivity fast inhibitory to pyramidal
v_0	the postsynaptic potential for
	which a 50% firing rate is achieved
e_0	$1/2$ maximum firing rate of the neural population
r	Steepness of the sigmoidal transformation

Table 3.1 Description of parameters in the Wendling model as introduced in [282].

3.2.3 Neural mass model parameters

As highlighted in the introduction the values of these parameters or their possible ranges are often based on previously used values that have sometimes arisen arbitrarily in the literature. As further experiments are conducted over time, it is possible to gain an improved insight into the range that NMM parameters could take. Examination of the experimental literature reveals that neuronal level mechanisms, which are often assumed to map to NMM parameters, can vary significantly from one species to another, as well as within species [266] (neuroelectro.org). Therefore the plausible range of NMM parameters can be large. The parameters A, B, G, C and P have traditionally been considered to be highly uncertain and dynamics have therefore been studied over substantial ranges of these parameters [100, 140, 281]. In contrast, the synaptic time constants a, b and g have often been considered as relatively certain [140, 281]. However, experimental studies point towards the contrary. For example, there is a large uncertainty of dendritic time constants of the somatic response due to synaptic input for single neurons [2, 114]. Ranges for these values have been shown to be large, from 25 s^{-1} [74] to 140 s^{-1} [146] for pyramidal neurons. Similarly, the synaptic time constant of inhibitory neurons (related to b) could also be considered uncertain, with values ranging from 6.5 s^{-1} to 110 s^{-1} [286]. We use these experimentally determined ranges for values of a and b in our study (see Table 3.2). It is more difficult to find a plausible range for g; values used can be traced back to 1993 [200], in which the authors indicated a large uncertainty. Therefore, we implement a large range for this parameter (350 to 650^{-1}). C was fixed at 135 [140] based on interesting dynamics occurring near this value. Here, we chose to use the initial range of uncertainty in [140] from 0 to 1350. v_0 was considered uncertain in previous studies and has also therefore been examined across a range of values, for example, 2 to 6 mV [140]. Here, we extend the study from 2 to 10. e_0 is often fixed at 2.5 s^{-1} but a range from 0.5 to 7.5 s^{-1} has been recorded [89], and therefore we use this range. Finally, there is very little information about r, the value was found experimentally, but without information regarding uncertainty [88]. We, therefore, studied the range of this parameter from 0.3 to 0.8 mV^{-1}. A summary of ranges of parameter values implemented in our study is given in Table 3.2.

3.2.4 Model simulations

The NMM was simulated 2,000,000 times varying 11 parameters A, B, G, P, a, b, g, C, v_0, e_0 and r using a latin hypercube design to explore the parameter space. The simulations were computed using ODE45 in MATLAB (Runge–Kutta method).

Each time, 20 seconds of EEG activity were simulated, the first 10 seconds were removed to eliminate transients. Simulations were performed in parallel over

4 CPUs each running at 3.5 GHz. It took approximately 4 days to simulate the whole database (i.e. 2,000,000 simulations).

parameter	nominal value	min	max	Reference
A	5 mV	0	10	[29, 140]
B	22 mV	0	50	[29, 140]
G	20 mV	0	50	[29, 140]
P	90 spikes.s^{-1}	0	2000	[100]
a	100 s^{-1}	25	140	[74, 146]
b	50 s^{-1}	6.5	110	[263, 286]
g	500 s^{-1}	350	650	[281]
C	135	0	1350	[107, 140]
v_0	6 mV	2	9	[140]
e_0	2.5 s^{-1}	0.5	7.5	[89]
r	0.56 mV^{-1}	0.3	0.8	[88]

Table 3.2 The range of considered parameter space of the Wendling model. Details of the reference used to define the minimum and maximum value of each parameter is included. Chosen ranges were constrained either by experiments (e.g. a and b) or the widest range described in theoretical studies (e.g. P and C).

3.2.5 Quantifying dynamic transitions in high dimensions

We are interested in understanding the relationship between parameters of the NMM and its dynamics. This understanding can be achieved through an explicit mapping between regions of parameter space and qualitatively different dynamics (e.g. steady states and oscillations). Previous studies have analysed the dynamics of NMMs by characterising features of simulations. Different properties of dynamics have been used for characterisation, such as the power spectrum [281], amplitude or variance [142, 251] and more nuanced features such as the number of spikes within a period of a specific rhythm [29, 190]. These studies have demonstrated that NMMs can recreate key types of epileptiform dynamics such as slow spike-wave rhythms and theta spikes, which are important rhythms for generalised and focal epilepsies, respectively. Based on these previous studies, we consider three key features of simulations that are relevant for delineating different types of dynamics within the NMM: *amplitude*, *frequency* and *number of peaks per cycle*. We use these features to classify regions of parameter space according to the nature of the emergent dynamics. For example, alpha activity corresponds to low-amplitude oscillations with a frequency of around 10Hz. Alternatively, seizure dynamics in this model correspond to low-frequency oscillations (2-8Hz to take into account focal and generalized seizure activity) with additional peaks that correspond to “spikes” or “poly-spikes” in EEG (c.f. Figure 3.4). The simulated times series were classified by firstly removing the first 10 seconds of the time series to remove the effect from initial conditions. If the amplitude of the remaining time series where inferior to a threshold of 10^{-8}, the time series was classified

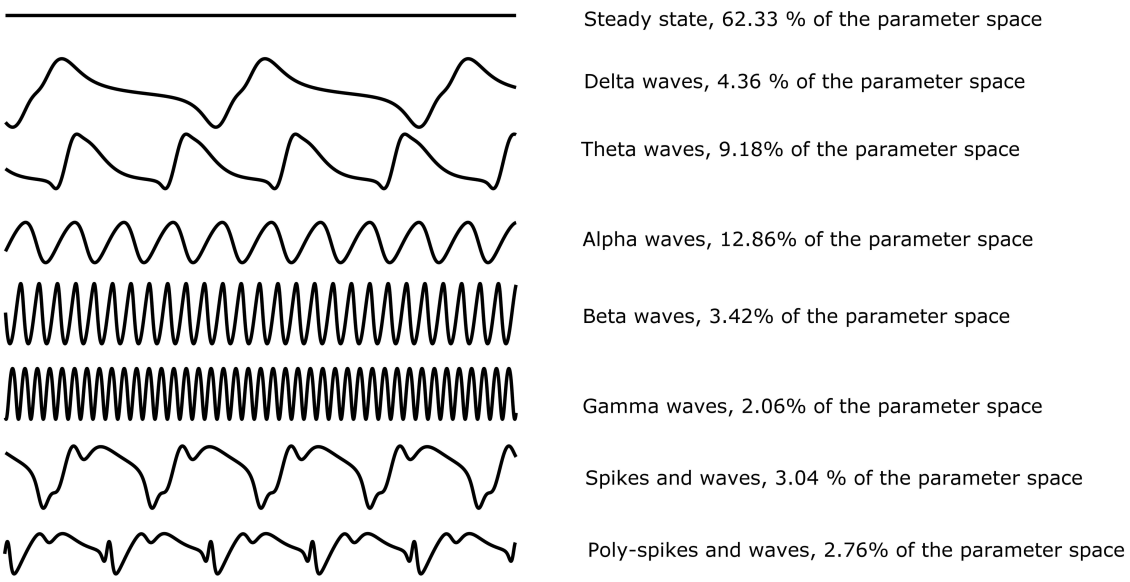

Fig. 3.4 Common dynamic patterns observed in the Wendling model. Non-steady-state solutions are split into two categories: oscillations and poly-spike-wave dynamics. Oscillations are cycles with one peak per period delineated by frequency into the five classical clinical bands: gamma (30-60Hz); beta (13-30Hz); alpha (8-12Hz); theta (4-8Hz); and delta (0-4Hz). Poly-spike-wave dynamics are cycles with one or more spikes per period, riding on an oscillation of between 2 and 8 Hz with a mean of 4 Hz. For the sake of clarity amplitudes don't have uniform y-axis scale.

as steady state. For non steady state simulation, the power spectrum of the time series was computed and the peak of power spectrum which represent the frequency of the system was computed. We would then classify all the time series with 2 peaks per period as spike and wave dynamic, if there were more peaks, the time series is classified as poly-spikes and wave dynamic. In the case of having only one peak per period, the time series is classified as gamma for a frequency from 30 to 60Hz, beta for a frequency from 13 to 30Hz, alpha from 8 to 12Hz, theta from 4 to 8Hz and delta from 0 to 4Hz. Algorithm 1 outlines the process:

Input: A simulated time serie of 20 seconds
Output: classification of the time series
initialisation ;
remove the first 10 seconds of the time series;
if *amplitude inferior to threshold* **then**
    class = Steady state;
else
    Compute power spectrum;
    define frequency of period as the related frequency of the maximum of the power spectrum ;
    if *More than one peak of amplitude per period and frequency between 2 to 8 hz;* **then**
        class = Poly-spike-wave dynamics depending of number of peak per period;
    else
        class = attribute class according its frequency;
    end
end

Algorithm 1: Classification of simulations

3.3 Results

3.3.1 The critical role of parameter, an example with the Wendling model

To demonstrate the importance of the role of usually fixed parameters we computed a series of simulations by fixing all parameters but four; A, B, a and b. The parameters were varied in their biologicaly ranges (specified in table 3.2). A and B are parameters which have been focused on in multiple studies but this is not the case for a and b. Figure 3.5 shows how much the roles of the parameters A and B are dependant of the values of the parameter a and b. in each subfigure the parameters a and b are fixed while A and B change from 0 to 10 and 0 to 50 respectively. For different values of a and b, different transitions occur when changing the values of A and B. For example spike and wave or poly-spikes and wave dynamics (marker of seizure dynamics) occur only for specific values of a and b. Worst the dynamic is influence by A and B in a different ways depending of the values of a and b. For example, when a is high (=140) and b is low (=10) as in the subfigure in the bottom-left corner of Figure 3.5, seizure dynamics only occur for low values of B. On the contrary when b increase (see for exemple the subfigure in the bottom-right corner), seizure dynamics only occur for large values

of B. This results is a warning about studying the parameter space with only two parameters simultaneously.

3.3.2 Analyses of the data set

2,000,000 simulations were computed on the whole parameter space as described in section 3.2.2, using the ranges in Table 3.2. Analysing these simulations, we found that the dynamics of the Wendling model can predominantly be categorised as steady state (62.3% of parameter space). The remaining simulations were classified by frequency and number of peaks (see Figure 3.4 for a description of dynamics). The dynamics 'spike and wave' or 'poly-spike and wave', which are characteristic of seizure dynamics, represent 5.8% of the parameter space. This number can be considered as the likelihood to find seizure dynamics when random parameters are used.

Figure 3.6 provides a 2 dimensional representation of the distribution of steady state and seizure dynamics throughout the whole parameter space. It can be seen that the parameter subspace in which seizure dynamics can be found is large and is not concentrated in small sub-regions. The top right of Figure 3.6 demonstrates that seizure dynamics can be observed across most parameter values; there are few combinations of two parameters for which, regardless of other parameter values, seizure dynamics cannot exist. Examples are the inverse mean time in the excitatory and slow inhibitory loop (a and b), which give rise to dark blue regions in Figure 3.6 (low likelihood of seizure dynamics). Specific combinations of parameters A, B, C, e_0 or r can also preclude seizure dynamics. In contrast, the subfigures for parameters of the fast inhibitory loop (G and g) appear quite homogeneous and therefore do not change the likelihood of seizure dynamics.

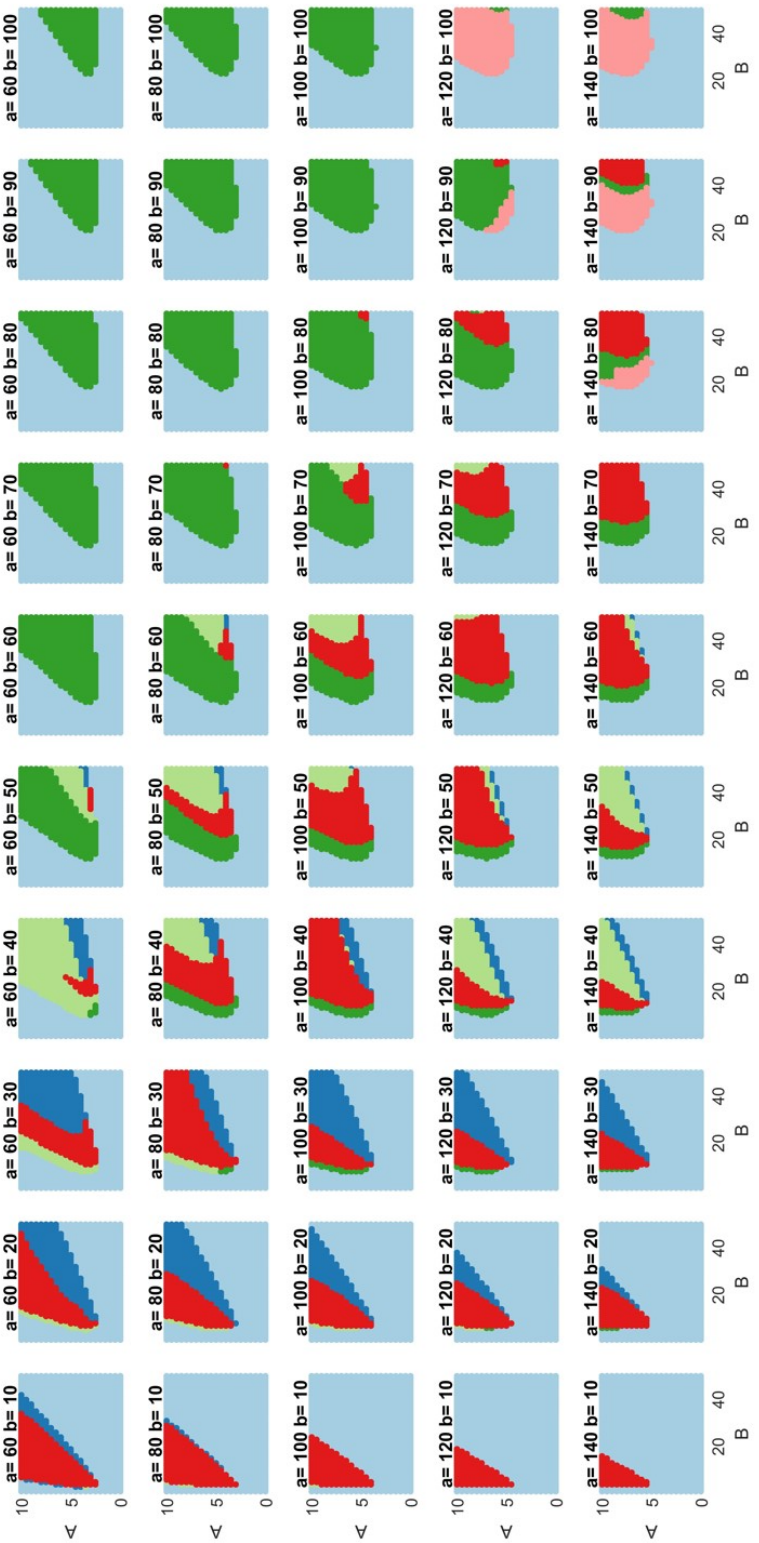

Fig. 3.5 The values of usually fixed parameters can have a huge influence on the dynamic of the model. Parameter values have been fixed to classic values (as in table 3.2) and four parameters are varied A, B, a and b in their biological plausible ranges. The parameters a and b influence the dynamics of the NMMs. For example; one can observe that seizure dynamics appears for small values of B when a is low. However, when a and b are high, seizure dynamics only appears for high values of B.

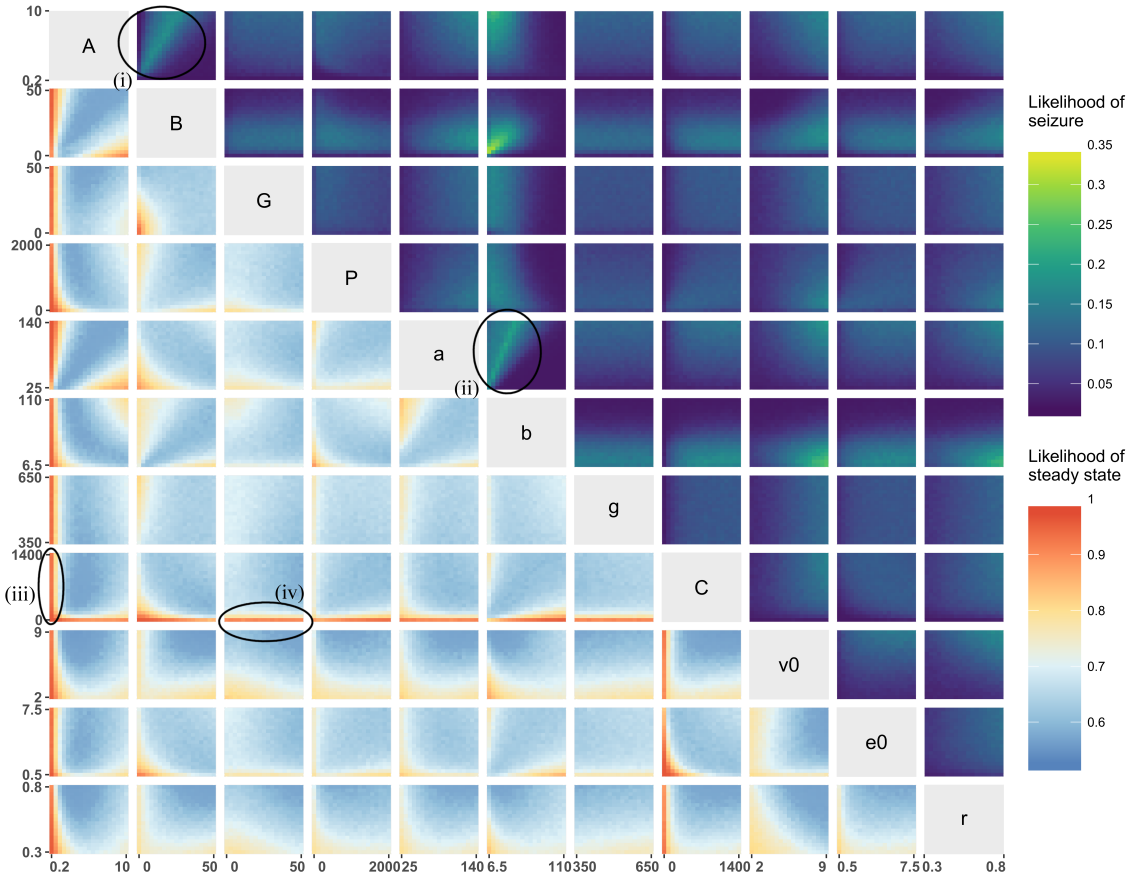

Fig. 3.6 Bivariate joint distribution of the likelihood of steady state (lower triangle) or seizure dynamics (upper triangle). Each subfigure is a projection of the parameter space over two parameters and the colour indicates the likelihood of finding a particular type of dynamics (seizure or steady state) as per the colour bar. The axis labels are indicated by the diagonal. For example, the subfigure in the second column on the first row (encircled and labeled (i)) maps the likelihood of finding seizure dynamics over different values of B (x-axis) and A (y-axis), given variations in all other parameters. In the upper triangle, yellow indicates a high likelihood of observing seizure dynamics, whereas blue indicates a low likelihood of observing seizure dynamics. In the lower triangle, red indicates a high likelihood of observing steady state dynamics, whereas blue indicates a low likelihood of observing steady state dynamics. Each subfigure was computed using equation 2.4 with 20×20 bins over the parameter ranges provided in Table 2. Upper triangle: Specific combinations of parameters can lead to manifolds with a high likelihood of seizure dynamics (see for example the linear relationships between A and B in the encircled subfigure (i) and a and b in the encircled subfigure (ii)). Lower triangle: one can observe that small values of the parameters A or C guarantee a steady state (see for example the encircled subfigures (iii) and (iv)).

However, varying the value of some parameters does reduce the likelihood of observing seizure dynamics: reducing parameters of the excitatory loop (A and a); the connectivity coefficient (C); the maximum firing (e_0); and the inflexion point (v_0) and the slope (r) of the sigmoidal nonlinearity. On the other hand, increasing the inverse mean time in the slow inhibitory loop (b) also reduces the probability of observing seizure dynamics. Intermediate values of the input (P) and the average slow inhibitory gain (B) increase the chance of observing seizure dynamics. Particular combinations of pairs of parameters such as the average synaptic gains (A and B) or the inverse time scales (a and b) can significantly alter the chance of observing seizure dynamics. For example, there is a linear combination of a and b for which the proportion of dynamics in the seizure class is greater than 30%. The lower triangle of Figure 3.6 indicates that steady state dynamics can be observed in a very large proportion of the parameter space. It can be seen that small values of A or C force the system to be at steady state.

Explorations such as undertaken in Figure 3.6 are informative and give a good preliminary indication of the role that each parameter plays in constraining the model dynamics. Nevertheless, in more than two dimensions, visualisation becomes difficult. For example, extending Figure 3.6 to 3 dimensions would require 1,000 2D plots. Therefore, we used tree statistics (see section 2.1.5) to efficiently summarise how a change in a parameter can impact the dynamics of the model. Figure 3.7 presents one such tree that describes the segmentation of parameter space according to the density of seizure dynamics. Recall, that for each branch the tree algorithm scans through the sub-parameter space to identify the optimal separation between the maximum and minimum likelihood of observing the feature of interest (seizure dynamics in this case).

Figure 3.7 is a relatively small tree used to illustrate the method. At the root of this tree, the first parameter used to partition parameter space is the inverse time scale of the slow inhibitory loop, b. $b \geq 60$ reduces the probability of observing seizure dynamics and produces a region that represents 49 % of the parameter space. This region, which represents nearly half of the parameter space, contains only 10% of all parameter combinations that lead to seizure dynamics. Taking $b < 60$ again yields approximately half of the total parameter space (51%), but this region contains 90% of all parameter combinations that lead to seizure dynamics. Since this region is large, and the probability of observing seizures in the whole space is low (5.8%), the *density* of seizures in this region is low at 10%. The next branch cuts through the average slow inhibitory gain at $B = 32$. Above this value, 19% of the parameter space remains and this contains 12% of all parameter combinations that yield seizure dynamics. The remaining 32% of parameter space accounts for 78% of seizure dynamics. Choosing $A \geq 2.1$ further increases the density of seizure dynamics to 17%, incorporating 73% of all parameter sets that lead to seizure dynamics. Further adding the criterion that $v_0 \geq 4.8$ leads to a region with highest density of seizure dynamics (bottom right region in Figure 3.7).

This region represents 15% of the total parameter space and the proportion of seizure dynamics in this region is 22%; thus it accounts for 57% of all parameter combinations that result in seizure dynamics.

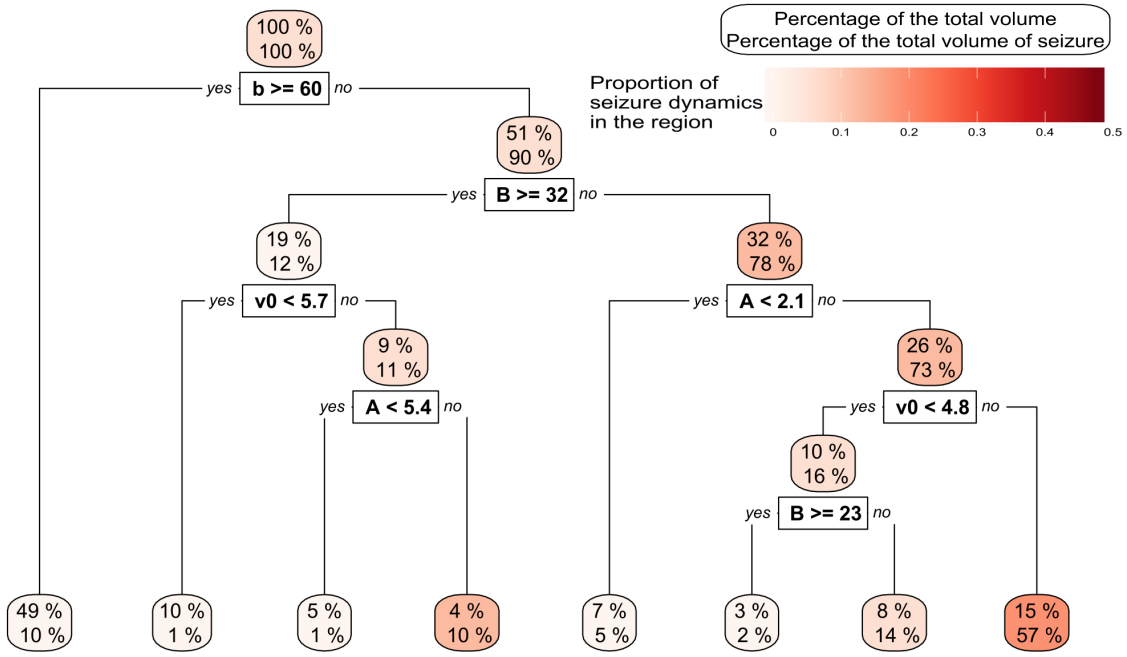

Fig. 3.7 A tree representing how parameter space is split dependent on the presence or absence of seizure dynamics The root region is at the top of the figure and represent 100% of the parameter while the leafs are at the bottom. The upper label of each region indicates the size of the parameter space represented in this region. The lower label indicates the percentage of all parameter combinations that result in seizure dynamics. The colour indicates the density of seizure dynamics in the given region. The parameters A, B, a and b are the most important parameters because they split efficiently the parameter space into subspaces with high or low likelihood of seizure dynamics. Some parameters such as P and C do not appear in this small tree, however, they can appear in a more complex tree (see supplementary material). Values are given to two digits precision.

However, it is possible to create larger trees with more regions giving a finer resolution. There is, of course, a trade-off as larger trees segment the parameter space into more (smaller) hypercubes, making them more cumbersome to analyse (see supplementary materials for more examples). The main conclusion to be drawn from the large tree presented in the supplementary material is that the dependency of dynamics on parameter space is complex: transitions between dynamics can vary between regions. For example, an increase of B or P can either increase or decrease the likelihood of seizure dynamics. However, other parameters exhibit robust transitions; a split at r around 0.52 appears consistently, and e_0 and v_0 tend to slightly increase the seizure likelihood when their values increase. Figure 3.6 seems to show different results from [281]. To recall; in this article, the presence of seizure dynamic would appear only for B superior to 20mV and A superior to 5 (other parameters at standard value as in Table 3.2). At the

opposite in Figure 3.6, the likelihood of seizure when B is superior to 20 is low and higher for small values of B. These show that if a projection of the parameter space in 2 dimensions is helpful to have a quick understanding of the parameter space it does not capture all of its aspects. At contrary in Figure 3.7 with the help of the tree algorithm this manifold is well approximated. Indeed one can see that even for large B (>32) seizure dynamic can appear with the standard values of parameters [281] (fourth leaf from the left). Furthermore, the tree shows that this change appears around $A = 5.4$mV. There are other bigger manifolds in Figure 3.7 for small values of B. These manifold are the one which influence the most the Figure 3.6 and 'hide' results found in [281].

3.3.3 Determining the relative importance of parameters for observing features of interest

To generalise the example of Figure 3.7, we computed the variable importance of model parameters over a random forest of 100 trees. Clearly, the importance of a parameter depends on the characteristics we are interested in. Results regarding the presence of steady states, oscillations with different amplitudes and frequencies, as well as seizure dynamics are provided in Table 3.3. We find that the values of A, B, C and v_0 are important parameters for transitioning between steady state dynamics and the different types of oscillations. Interestingly, the amplitude of oscillations was less dependent on A and instead strongly dependent on C and e_0. This might seem surprising given the importance of A in observing oscillations in the first place. This contrast demonstrates how the relative importance of a parameter is strongly dependent on the observed feature of interest (e.g. frequency vs the amplitude). The input from other regions of the cortex (P) can affect the emergence of oscillations but has a marginal role in tuning the amplitude and the frequency of these oscillations. The connectivity constant (C) is important for governing the amplitude but not the frequency of an oscillation. In fact, few parameters (A, B, a, b and G) are important for determining the frequency of oscillations.

All parameters except g were found to play a role in the generation of transitions between dynamics, but with varying importance. The frequency of an oscillation was found to be predominantly dependant on the inhibitory slow loop parameters (B and b). These parameters were also found to be crucial for producing seizure dynamics. This observation confirms the finding in Fig 3.7 that when these parameters split the space they reduce impurity. Overall the excitatory pair of pyramidal and excitatory interneurons and the slow inhibitory loop are important to create oscillations in the Wendling model. The output of the Wendling model is sensitive to a change of any of these parameters as indicated by the GI measurements (Table 3.3).

	A	B	G	P	a	b	g	C	v_0	e_0	r
steady-state to cycle	1	0.40	0.11	0.15	0.27	0.32	0	0.59	0.48	0.16	0.26
amplitude of oscillation	0.13	0.46	0	0.02	0.13	1	0	0.96	0.11	0.83	0.04
frequency of oscillation	0.14	1	0.09	0.01	0.11	0.86	0.01	0.01	0.01	0.01	0
transition to seizure dynamics	0.25	0.59	0.03	0.09	0.30	1	0	0.22	0.28	0.07	0.15

Table 3.3 The importance of parameters as determined by Gini importance (see 2.1.7) over a random forest of 100 trees. Four characteristics of interest are considered: the switch between steady state and non-steady state, the amplitude of cycles, the frequency of cycles and the switch between any activity (mainly steady state) and seizure dynamics. A value of 1 signifies the parameter with greatest importance for observing the feature of interest (e.g. A is most important for observing transitions from steady-state). A value of 0 implies a parameter has no control over observing a feature of interest.

3.3.4 Extension to parameter ratios

Fig 3.6 demonstrated a potentially important relationship between the parameters A and B and the parameters a and b. We further investigated this by incorporating two artificial parameters $r_{A/B}$ and $r_{a/b}$ which are respectively the ratio of A over B and the ratio a over b. Fig 3.8 shows that smaller values of $r_{a/b}$ lead to a lower likelihood of observing seizure dynamics. A ratio less than 1.6 gives a likelihood of observing seizure dynamics of 0.56% in a very large sub-region that contains 57% of the parameter space. At the opposite extreme, the region on the right of the figure contains 40% of all seizure dynamics in only 5% of the whole parameter space. In this region the proportion of seizures is nearly 50%. It is interesting to note that low values of $r_{a/b}$ reduce the likelihood of seizure dynamics, whereas for $r_{A/B}$, small values ($<$0.19) or large values ($>$1.5) reduce the likelihood of seizure dynamics. A more highly resolved version of this tree can be found in supplementary materials. We recomputed the GI, incorporating these two new parameters over a random forest of 100 trees. The results are in Table 3.4. It is clear that for steady state transitions or frequency of oscillations $r_{A/B}$ is the most important, whereas $r_{a/b}$ is most important for transitions to seizure dynamics. Aside from the amplitude of oscillations, the normalised variable importance of the ratios $r_{A/B}$ and $r_{a/b}$ are larger than for the parameters taken individually.

3.4 Discussion

In this chapter, we introduced a new approach to explore the parameter space of high dimensional NMMs. In contrast to classical studies that considered parameters individually, or in pairs, we used a random forest approach in order to study the entire parameter space simultaneously.

Our approach relies on the creation of a database of dynamic features derived from forward simulations. Other statistical approaches could be used to study the database, but they all suffer from particular deficiencies. For example, artificial neural network models have a vast number of hyperparameters that cannot be interpreted [105]. Support vector machines [63] result in boundaries between regions of parameter space that are not split according to single parameters, and therefore one has to integrate over all parameters to understand the importance of each. We have tested the efficiency of kernel methods such as Gaussian processes [193]. The results have been poor as the efficiency of these methods rest upon the assumption of "smoothness" of data, i.e., proximal parameter sets are assumed to yield similar simulations, which is clearly not the case close to bifurcations. We have attempted to use more complex approaches, combining trees and Gaussian process [18, 109], but simulations have shown that the tree approach was better at taking into account large number of simulation and thus were better to handle complex parameter space as it is the case for the Wendling

	A	B	G	P	a	b	g	C	v_0	e_0	r	$r_{A/B}$	$r_{a/b}$
steady-state to cycle dynamics	0.65	0.24	0.13	0.17	0.16	0.19	0	0.62	0.49	0.17	0.25	1	0.57
amplitude of oscillation	0.10	0.59	0.01	0	0.1	0.89	0	1	0.07	0.89	0.02	0.14	0.15
frequency of oscillation	0.04	0.51	0.04	0	0.11	0.71	0.01	0.01	0	0	0	1	0.41
transition to seizure dynamics	0.11	0.33	0.04	0.12	0.06	0.3	0	0.14	0.31	0.08	0.17	0.8	1

Table 3.4 Importance of parameters as determined by Gini importance (GI, see section 2.1.7) averaged over a random forest of 100 trees. The ratios $r_{A/B}$ and $r_{a/b}$ have been added as additional parameters. Four characteristics of interest are considered: the switch between steady state and non-steady state, the amplitude of cycles, the frequency of cycles and the switch between any activity (mainly steady state) and seizure dynamics. A value of 1 signifies the parameter with greatest importance for observing the feature of interest. A value of 0 implies a parameter has no control over observing a feature of interest.

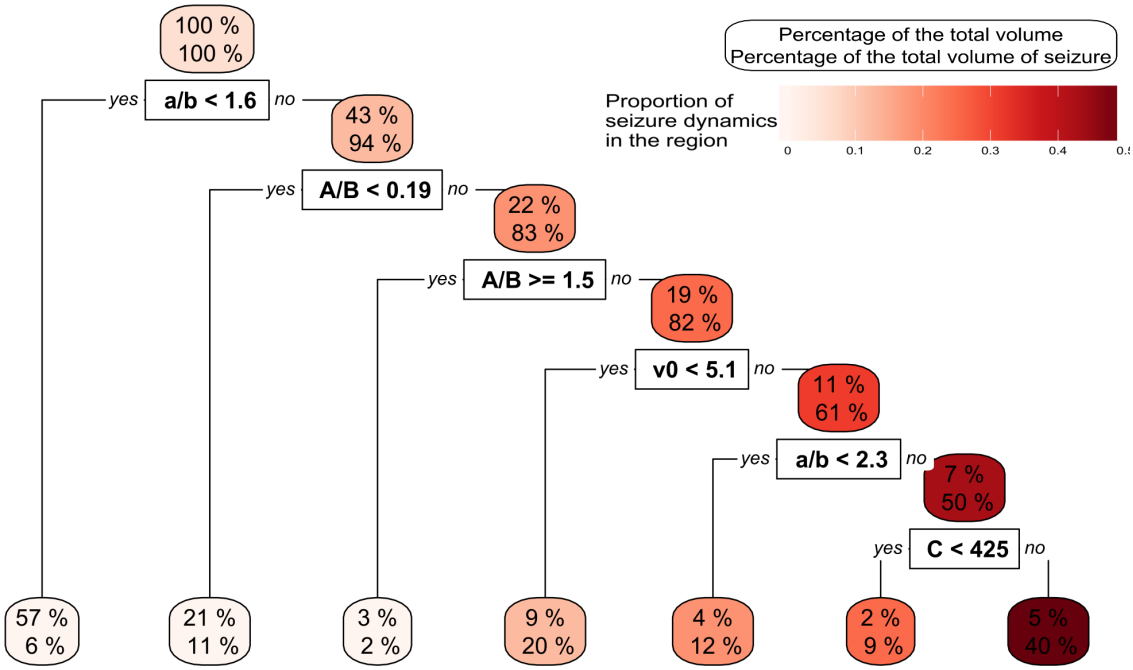

Fig. 3.8 A tree representing how the extended parameter space (incorporating two additional 'ratio parameters' $r_{a/b}$ and $r_{A/B}$) is split dependent on the presence or absence of seizure dynamics. The root region is at the top of the figure and represents the total parameter space, while the leafs are at the bottom. The upper label of each regions indicates the size of the parameter space represented in this region. The lower label indicates the percentage of all parameter combinations that result in seizure dynamics. One can see that the ratios have an important role to split the parameter space. Values are given to two digits precision.

model. In contrast, the approach we employed provides an efficient way to study the influence of model parameters on their dynamics: trees are computationally fast, make no *a priori* assumptions on either the type of model or parameter values and can handle data that are represented on different measurement scales [197]. We thereby demonstrated that random forests are a useful tool to study the dynamics of NMMs.

The implementation of the random forest approach [41] overcomes the issue that each implementation of CART produces a single tree that is locally optimal. A drawback is that the random forest approach introduces some loss of interpretability, but the final solution is more representative of the global optimum. This is particularly important for the GI which measures the relative contribution of parameters to an observed dynamic feature of interest of the model (e.g. a steady-state, oscillation or spike-wave). By this, we mean that effectively, the GI indicates which parameters are critical for segmenting the total parameter space into regions in which a feature of interest is more or less likely to be observed. Further, the GI provides a principled approach for determining whether or not parameters can be fixed, hence reducing the number of parameters to be calibrated from observable data. A consistently low GI across all features of interest means

that the considered parameter plays little role in any dynamic change and can, therefore, be fixed to an arbitrary value within a given physiological range.

For example, in our study of the Wendling model, g has little effect on determining transitions from steady-state to oscillations, or in determining the amplitude and frequency of those oscillations. It can, therefore, be fixed, meaning that the parameter space explored in subsequent calibration is smaller. On the other hand, some parameters have a high GI for specific features of interest and are therefore important for observing that specific feature without playing an important role in altering other aspects of the dynamics. For example, e_0 is critical in determining the amplitude of oscillations but plays a marginal role in the appearance of other features. Therefore if the amplitude is not a particular feature of interest, e_0 could be fixed. When considering networks of dynamical systems, the number of parameters can rapidly become very large, so GI is an important tool for managing this increase in complexity. For example, one could use the framework presented herein to examine whether there are certain network structures in which certain edges can be given fixed weights, thereby reducing the dimension of an optimisation or calibration problem.

The notion of importance is defined using GI due to its robustness and ability to measure the influence of parameters on dynamics [295]. However, the notion behind importance is somewhat nebulous, and it is difficult to directly attribute a small difference in GI to the relative importance of a specific parameter. The pragmatic approach we have adopted is to consider parameters with values of $GI > 0.1$ as playing a role in governing the feature of interest. In contrast, parameters with a GI close to 0 can be disregarded. In the present study, we defined importance specifically in the context of changes in parameters causing changes in asymptotic dynamics. This is relevant to the case in which bifurcations give rise to epileptiform activity. However, there are other possible model scenarios in which changes in dynamics could occur, such as for example, intermittency, bistability and excitability [12]. In these cases, we would seek to characterise importance with respect to changes in unstable invariant sets of the system, for example, boundaries of basins of attraction. Furthermore, importance, as we have defined it in the context of the NMM, does not imply that a parameter is crucial for changes in dynamics at the individual level. For example, it might be necessary to model some seizures using transitions between dynamics that occur only in small regions of parameter space. It is important to highlight that in the random forest approach, other definitions of importance exist, such as the permutation importance or the conditional permutation importance [103]. However, these approaches suffer from lack of robustness [49], hence our focus on GI.

Our analyses of the full parameter space of the Wendling model show that parameters of the slow inhibitory loop (b and B) play the most important role (in term of GI) in the emergence of seizures. The time scale of the slow inhibitory loop (b) is the most important parameter; a small change in its value can transform

steady state dynamics into seizure dynamics robustly, i.e. for the majority of combinations of other parameters in the model. We found the excitatory loop, governed by a and A, together with the offset of the sigmoid function (v_0) to be the second most important components of the system for the emergence of seizure dynamics. These are followed by the other parameters of the sigmoid function (v_0 and r) and the parameter that scales connectivity between the different populations of neurons (C). Interestingly, changes in the fast inhibitory loop (parameters g and G) do not play an important role in the generation of seizure dynamics. We note that a low value of GI in the context of our study does not mean that a parameter is irrelevant to the emergence of other brain dynamics not captured by the choice of features. Furthermore, parameters with low GI may play a role in determining transitions between dynamics in specific subsets of parameter space; GI is purely a global measure. The parameters governing the magnitude of input from other areas (P) or the scaling of intrinsic connectivity (C), for example, were shown herein to have little (global) effect on the emergence of seizure dynamics, but in *a priori* constrained sub-regions have been shown capable of governing transitions in NMMs [107, 108]. Table 3.4 showed a comparison of parameter importance when different features were considered. Parameters of the slow inhibitory loop, b and B, as well as the ratio of time scales $r_{a/b}$, showed relatively high importance across all features. Therefore, it is possible that these parameters are important for transitions between dynamics in general. Verifying this will require exploration of additional features in model dynamics.

We found that the ratio of parameters of the excitatory and inhibitory loops plays an important role in the generation of all the features we considered, with the exception of the amplitude of oscillations. The ratio of time scales ($r_{a/b}$) is the most important factor governing the emergence of seizures, whereas the ratio of gains ($r_{A/B}$) is most important for the onset of cycles and the frequency of these cycles. Reducing $r_{a/b}$ robustly reduces the likelihood of seizures regardless of other parameter values (see e.g. Fig 3.8). $r_{A/B}$ on the other hand, presents an intermediate range of values that have the highest likelihood of seizure dynamics.

Our finding of the importance of $r_{A/B}$ for the emergence of seizure dynamics is in line with previous experimental observations. For example, [59] found that the ratio of Glutaminate to GABA Levels is larger in people with idiopathic generalized epilepsies compared to healthy controls. This also aligns with the action of some antiepileptic drugs, for example, those acting via modulation of neurotransmitters such as GABA [226], the potentiation of which would be reflected in our model by an increase in B, and hence a decrease in $r_{A/B}$. Furthermore, Our finding of the importance of $r_{A/B}$ for the emergence of seizure dynamics confirms previous modelling results [265].

Interestingly, since the highest likelihood of emergent seizure dynamics was found to be for intermediate values of $r_{A/B}$, this would suggest that, depending on the choice of other parameters, *decreasing* the ratio of excitation to inhibition could

also produce a route into seizure dynamics, in line with evidence of the possibility of heightened inhibition at seizure onset [9]. Our finding that the slow inhibitory and excitatory synaptic gains have more influence than the fast inhibitory loop is in line with previous modelling results [29, 124], as are our findings that the parameter r and the ratio $r_{a/b}$ are important for dynamics of the NMM [68, 175, 244].

Few experimental studies have investigated the role that different time constants might play. However, it has been shown that chloride ion homeostasis is perturbed in patients with mesial temporal lobe epilepsy [133], and intracellular chloride ion concentrations have been shown to play a role in the time constants of postsynaptic potentials [130]. This, therefore, presents a possible biophysical interpretation of the importance of $r_{a/b}$. Interestingly, a recent study using dynamic causal modelling applied to a zebrafish model of seizures also demonstrated the potential importance of excitatory and inhibitory synaptic time constants [217].

In our study, we obtained these results using a method in which the influence of all parameters was analysed simultaneously and a complete characterisation of the relative importance of all parameters was possible. In fact, this analysis revealed new combinations of parameters that can potentially govern the emergence of seizure dynamics in the Wendling model, for example v_0. In addition, given our finding that the ratio $r_{a/b}$ is most important for seizure generation it would be interesting to explore the known effect of drugs that could target the inverse mean time ratio $r_{a/b}$.

[281] presented detailed, two-dimensional analyses of the effects that changing system parameters have on emergent dynamics. One of the findings of [281] was that seizure dynamics predominantly occur when $B > 20$. However, our results (Figure 3.7) show that the likelihood of seizures when $B > 20$ appears rather low (but not zero) and is, in fact, higher for small values of B. These results indicate that although a projection of the parameter space in 2 D is helpful to gain a quick understanding of the system, it does not capture the global picture. In our Figure 3.7, with the help of the tree algorithm, we did indeed find that for large B (> 32) seizure dynamics occur for the range of parameters used by [281] (fourth leaf from the left in Figure 3.7). Furthermore, the tree shows that this change appears around $A = 5.4mV$. However, our analysis in Figure 3.7 demonstrates that there are other regions of parameter space, for lower values of b that contain seizure dynamics.

The approach presented herein relies on the construction of a statistical model of dynamics based on simulations. This means that we cannot uncover the dynamic mechanisms that govern the emergence of the features studied, for example, the presence of unstable invariant sets or changes in stability. However, our approach could be combined with traditional methods such as numerical continuation [151]; we would first constraint parameter space by using GI to identify the most important parameters, together with transition boundaries and then perform more detailed analyses therein.

Studies including [12] and [164] describe four alternative mathematical mechanisms underlying the emergence of seizures: bifurcation (a parameter is slowly varied so that the system crosses a bifurcation point), bistability (background and seizure attractors co-exist, with perturbations allowing transitions between the two), transient excitability (the seizure dynamics occurs due to a complex trajectory elicited by a perturbation) and intermittency (background and seizure dynamics are part of the same attractor). In this study, we have focussed on a detailed explanation of the bifurcation mechanism (e.g. how small changes in system parameters can lead to abrupt changes in emergent dynamics). Specifically, we find for the chosen Wendling model that under the bifurcation assumption changes in the slow inhibitory loop or the fact excitatory loop are most likely to underpin the emergence of seizures. It is important to highlight that this finding is specific to the chosen model and further, that it does not exclude the other three possibilities. To explore the possibility of transient excitability and bistability, we would need to extend our statistical model to include system variables (e.g. initial conditions) and properties of perturbations as parameters. We investigated the impact of initial conditions by considering them as parameters and found their GI to be close to zero, indicating that regions of bistability are small in the context of global changes in parameters.

Another possible extension to the results presented herein would be to consider different dynamic models or different characteristic features of their dynamics. For example [216] or [69] focused their attention on the power spectrum of the model in comparison with clinically recorded data. Future work could focus on power spectra as a feature of interest, enabling an appropriate characterisation of the importance of parameters for generating alpha activity in NMMs.

In summary, we presented a framework for the global characterisation of the dynamics of NMMs. Our methods have the potential to advance patient-specific model representations, for example by first determining the relative importance of parameters, and then reducing the parameter space to a subset in which model calibration from data becomes tractable. Such an approach will become increasingly important as the emphasis on networked dynamical systems of the brain increases. Here the number of model parameters grows rapidly, beyond the point for which established approaches such as Kalman filtering [94] or genetic algorithms [190], that work directly with the dynamical system of interest, can be effective.

Chapter 4

Using power spectrum of the EEG to define plausible regions of parameters in the Robinson model

> With four parameters I can fit an elephant, and with five I can make him wiggle his trunk!
>
> John Von Neumann, [76]

4.1 Introduction

Rhythms of the brain are strongly correlated with cognitive processes [11, 278]. However, the underlying neural structures which generate EEG oscillations remains poorly understood. The alpha rhythm of the cortex (8-13 Hz) [23, 192] is perhaps the best known EEG phenomenon as human resting state activity presents a significant peak in this band. Some studies have suggested the thalamus as the primary alpha pacemaker [134] whereas other studies [117] argue that the alpha rhythm would be primarily initiated from cortical areas. Subtle differences in the power spectrum, particularly in the alpha band, are potential biomarkers for different neurological conditions such as Alzheimer's [129], depression [158] and epilepsy [157]. Hence, understanding the mechanisms underlying these differences between healthy and diseased states may advance our understanding of these conditions.

As previously introduced, NMMs approximate the average behaviour of large populations of neurons and therefore provide an efficient way to simulate electrographic data in order to postulate mechanisms of brain (dys-) function. They have been used to understand a wide variety of physiological and pathophysiological activities of the brain, including the fundamental rhythms of the brain [61, 165, 214, 215, 225] or the dynamics resulting from conditions such as

epilepsy [106–108, 283, 293]. In particular, mechanisms underlying these conditions can be uncovered by estimating model parameters from dynamic data [81, 94, 161, 185, 190]. Contrary to previous studies, we focus not on the best fit of the power spectrum but on all plausible fits.

In this chapter we use our approach to estimate a robust computational parameter space, using on the Robinson model [214] as an example case. Previous studies of this NMM have shown it to simulate power spectra similar to that observed in the EEG [219], offer a better understanding of the role of the different circuits in the thalamocortical system [126] and offer insight how different generalized seizures emerge [38]. To facilitate the use of NMM a subvolume of the parameter space has been selected [215]. For each individual the best fit was estimated in [219] by using the Levenberg-Marquardt method [206] which is a gradient descent algorithm which does not guarantee a global minimum. Even if the global minimum is obtained, there are often multiple parameter sets that lead to almost as good fit. Since the data is inherently noisy, any of these minima are in reality a potential best fit. Further, there is a large variation in the power spectrum across individuals within a population [116] rendering the concept of a subspace based on the confidence interval of the mean of the parameter values unreliable. It is important to remember confidence interval of a parameter and the prediction interval of an observation are two different notions. There is a subtle, but important, difference between prediction intervals and confidence intervals. With a confidence interval, the purpose is to obtain an upper and lower limit for the parameter. For a prediction interval, the purpose is to estimate the upper and lower limits on an individual observation. It is relatively frequent to compute a confidence interval for the mean and use it wrongly as if it were a prediction interval for a future observation. The trouble is, confidence intervals for the mean are much narrower than prediction intervals, which can result in a false sense of the accuracy of a given forecast [125, 137, 153][1]. To avoid restricting the parameter space to an unnecessary and potentially misleading subparameter space we argue the necessity to constrain the parameter space not to the ‘best’ fit but to all ‘plausible’ fits. The approach taken in this chapter is similar to the approach proposed by [30] who looked beyond the best fit to find a series of plausible fits. Building on their approach, our method analyses the parameter space to characterise all plausible submanifolds, using the approach introduced in chapter 2 (see [83]). In the methodological part of this chapter, we present the necessary tools to understand the data and the power spectrum, the NMM of Robinson et al. [214] and, provide a formal definition of a plausible simulated power spectrum. In the results section, we first identify the regions of parameter space able to produce a power spectrum similar to the one observed in a human population. Thus we identify a set of parameters that are both biologically and

[1] For a meaningful discussion, one can read the post written by Roos Colman, https://datascienceplus.com/prediction-interval-the-wider-sister-of-confidence-interval/.

computationally plausible, by taking into account the intra-individual variability. In the discussion section, we discuss the main findings of this study, its limitations, and possible directions for further research.

4.2 Methods

4.2.1 Overview

Our approach is to partition the NMM parameter space according to the theoretical power spectrum and its closeness to the power spectrum of the EEG. To do so, we transform the NMM first into a database and then a statistical model, which is a function that maps parameters onto two states: plausible and implausible. This statistical model can then be analysed to understand the relationship between the NMM parameters and a realistic power spectrum (see Figure 4.1 for a general overview).

In this study, we use the model introduced by Robinson et al. [214].

We choose to focus on the broadband power spectrum and consider that a simulation is plausible when its values lie in the band given by the 90% prediction interval of the power spectra of the data. As such a simulation is classified as plausible or implausible.

4.2.2 Subjects EEG data and processing

The dataset contains EEG data with 38 healthy controls between the ages of 16 and 59 years. Healthy control EEG was collected at King's College Hospital EEG department. Controls provided written informed consent, and data collection was approved by King's College Hospital Research Ethics Committee (08/H0808/157). Under United Kingdom law, patient data collected during normal clinical routine and anonymized before research use may be used for research without additional consent; this procedure was reviewed and approved for this project by St.Thomas's Hospital and King's College Hospital's Research and Development departments. A trained clinical EEG technician identified a 20s long state EEG activity from the initial stage of the recordings from each participant. Because signal amplitude may vary between individuals due to different anatomic features (such as the size and shape of the cranium) the data were normalised by dividing the power spectrum in each channel by the total power in the spectrum averaged across all 19 channels. This normalized power preserves relative differences in power between bands. The band of the power spectrum at 5% and 95% of each population is estimated via quantile regression. Whereas the method of least squares results in estimates of the conditional mean of the response variable given certain values of the predictor variables, quantile regression aims to estimate either the conditional median or other quantiles of the response variable. Here, we use a total variation

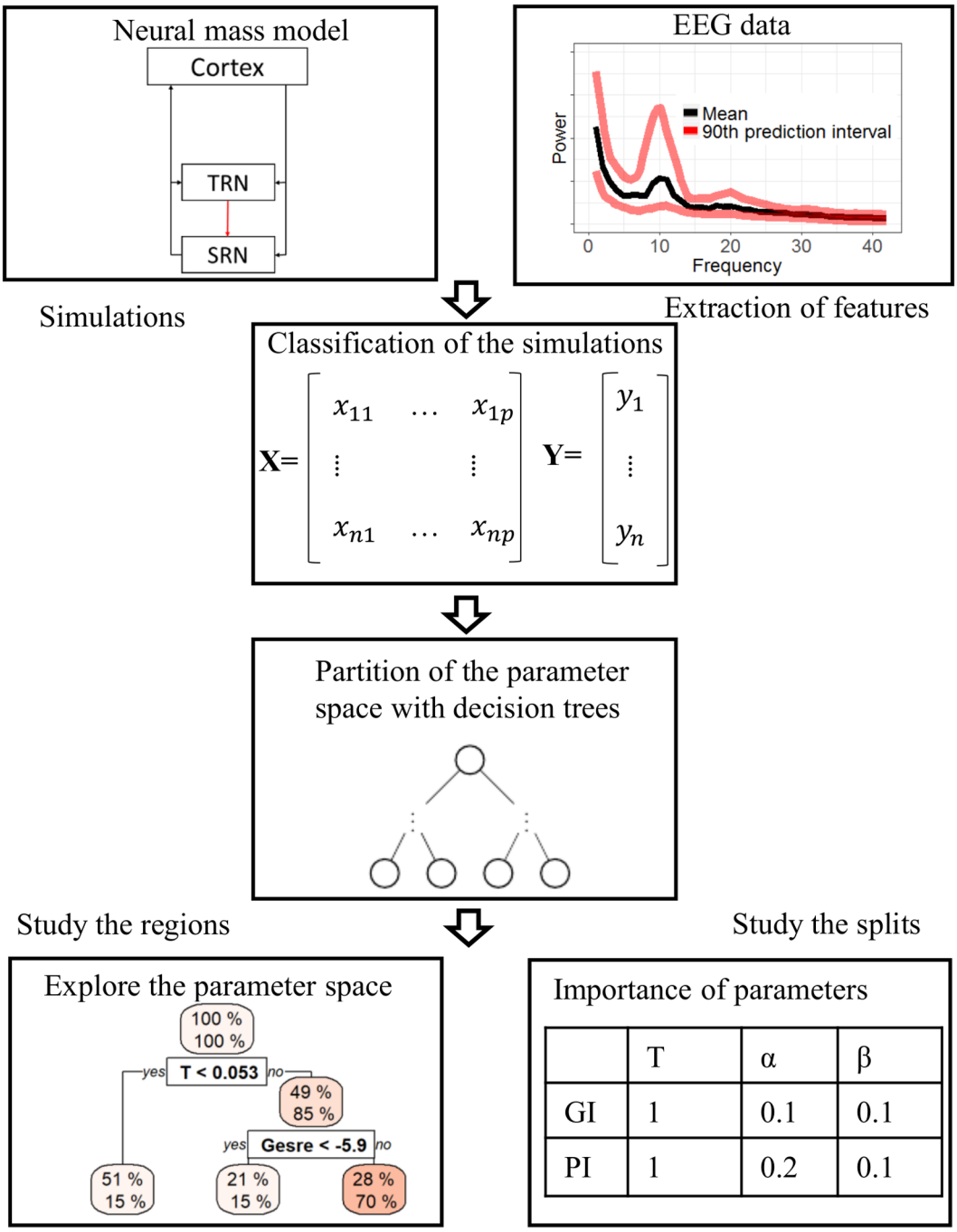

Fig. 4.1 Schematic of the methodology. The dynamic features of interest are identified and characterised as being plausible simulation to reproduce the human EEG power spectrum. The NMM is simulated a large number of times over its parameter space. Next, each simulation is given a classification (plausible or implausible) according to its dynamic features. Then the simulations are partitioned using decision tree learning. The final partitions are used to characterise the parameter space of the NMM.

regularization [148]. This is a non-parametric approach to estimate conditional quantile functions based on g minimising

$$\sum_{i=1}^{n} \rho_\tau (y_i - g(i)) + \lambda J(g). \tag{4.1}$$

The term y_i represents the power at the frequency i, the term

$$\rho_\tau(y_i - g(i)) = (y_i - g(i))\,(\tau - I(y_i - g(i) < 0)) \tag{4.2}$$

generates a fidelity term appropriate for conditional quantile estimation, and the roughness penalty $J(g)$ is taken to be the total variation of the first derivative of g. By visual inspection λ was fixed at 0.4. The R package *quantreg* [149] was used to compute the quantile.

4.2.3 Neural mass model

Large-scale neural activity arises from interactions between several neural populations, notably excitatory and inhibitory cortical neurons and specific subcortical nuclei such as the thalamus, see Figure 4.2 for a schematic.

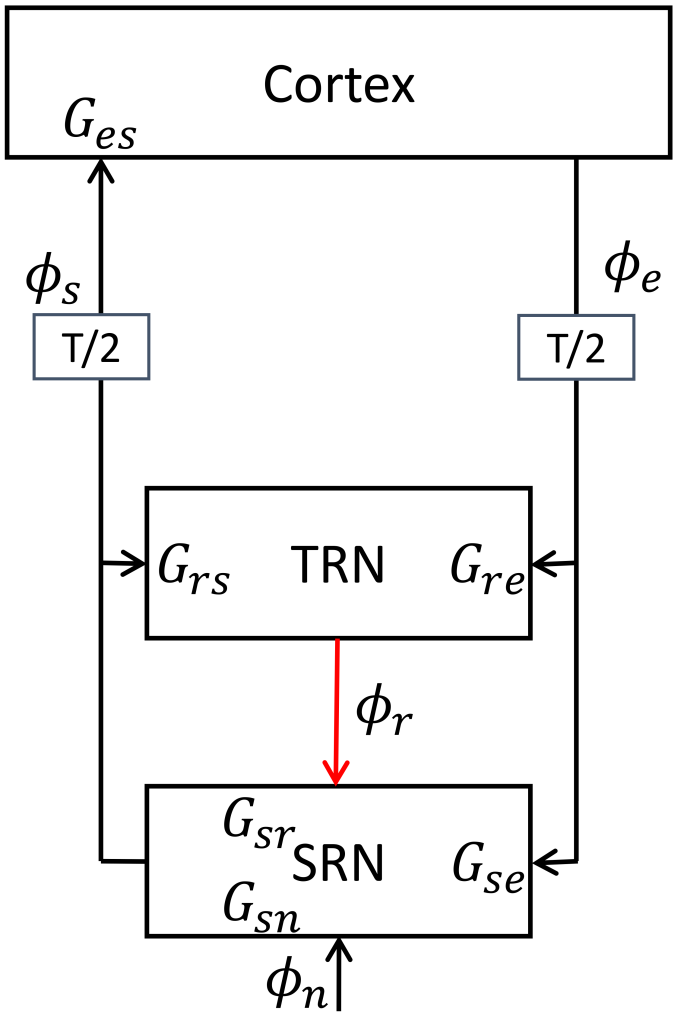

Fig. 4.2 Schematic showing primary pathways between the cortex, specific and secondary relay nuclei (SRN) and the thalamic reticular nucleus (TRN) as presented in [219]. The interconnections are shown with arrows; either black (excitatory) or red (inhibitory). These provide two partially overlapping thalamocortical feedback pathways: one direct and excitatory between the cortex and SRN with total gain $G_{ese} = G_{es}G_{se}$; and one indirect and inhibitory pathway from cortex to TRN to SRN to cortex with total gain $G_{esre} = G_{es}G_{sr}G_{re}$: Intrathalamic feedback between the TRN and SRN is also possible, with gain $G_{srs} = G_{sr}G_{rs}$: Propagation between cortex and thalamus involves delays of $T/2$, and additional small delays are induced by each nucleus due to dendritic filtering. The firing rate in each pathway is $\phi_{a\in e,r,s}$ and ϕ_n is an independent source of signals.

It has been suggested that such interactions are responsible for the alpha waves [32, 165]. The Robinson model [214] has been able to reproduce power spectra nearly identical to the one observed via EEG [219]. In the next section we present the principal characteristics of the model, more details can be found in [215] and reference therein. This model belongs to the class of "lumped" or "mean field" neural models [88, 141, 166, 282]. The corticothalamic model studied here is based on the evolution of two dynamical variables within each of the principal populations of neurons. The variables represent the local mean value of the firing rate density or the mean dendritic potential of a large number of neurons. There are four populations which represent respectively excitatory cortical, inhibitory cortical, specific thalamic nucleus and thalamic reticular nucleus. Excitatory cortical and inhibitory cortical population are assumed to have exactly the same characteristics [203, 212], which is a debatable assumption for true biological neurons [203]. The model can be represented as a set of differential equations [38] and can be simulated using classical numerical approximation such as the Runge-Kutta method [46]:

$$
\begin{aligned}
&\frac{d\phi_e(t)}{dt} = \dot{\phi}_e(t),\\
&\frac{d\dot{\phi}_e(t)}{dt} = \gamma_e^2\left\{S(V_e(t)-\phi_e(t)\right\} - 2\gamma_e\dot{\phi}_e(t),\\
&\frac{dV_e(t)}{dt} = \dot{V}_e(t),\\
&\frac{d\dot{V}_e(t)}{dt} = \alpha\beta\left\{v_{ee}\phi e(t) + v_{ei}S(V_e(t)) + v_{es}S(V_s(t-T/2)) - V_e(t)\right\},\\
&\qquad -(\alpha+\beta)\dot{V}_e(t),\\
&\frac{dV_s(t)}{dt} = \dot{V}_s(t),\\
&\frac{d\dot{V}_s(t)}{dt} = \alpha\beta\left\{v_{se}\phi e(t-T/2) + v_{sn}\phi_n(t) - V_s(t)\right\} - (\alpha+\beta)\dot{V}_s(t),\\
&\frac{dV_r(t)}{dt} = \dot{V}_r(t),\\
&\frac{d\dot{V}_r(t)}{dt} = \alpha\beta\left\{v_{re}\phi e(t-T/2) + v_{rs}S(V_s(t)) - V_r(t)\right\} - (\alpha+\beta)\dot{V}_r(t).
\end{aligned}
\tag{4.3}
$$

Under conditions of spontaneous EEG the external stimuli ϕ_n is so complex that it can be approximated by temporal white noise. The theoretical power spectrum of the excitatory neurons can be then estimated [215] by using a linear approximation:

$$
P_{EN}(\omega) = C\left\|\frac{G_{esn}L(\omega)^2}{(1-G_{srs}L(\omega)^2)(1-G_{ei}L(\omega))}\right\|^2\left\|\frac{\mathrm{Arg}q^2}{\mathrm{Im}q^2}\right\|, \tag{4.4}
$$

with

$$
G_{ab} = \frac{\phi_a^0}{\sigma}\left(1-\frac{\phi_a^0}{Q_{\max}}\right)v_{ab}, \tag{4.5}
$$

where ϕ_a^0 is the steady-state value.

$$q^2(\omega) = \left(1 - \frac{i\omega}{\gamma_e}\right)^2 - \frac{1}{1 - G_{ei}L(\omega)}\left[G_{ee}L(\omega) + \frac{G_{ese}L(\omega)^2 + G_{esre}L(\omega)^3)e^{i\omega T}}{1 - G_{srs}L(\omega)^2}\right], \tag{4.6}$$

$$G_{ese} = G_{es}G_{se}, \tag{4.7}$$

$$G_{esre} = G_{es}G_{sr}G_{re}, \tag{4.8}$$

$$G_{srs} = G_{sr}G_{rs}, \tag{4.9}$$

$$L(\omega) = (1 - i\omega/\alpha)^{-1}(1 - i\omega/\beta)^{-1}. \tag{4.10}$$

4.2.4 Parameter constraints

We set out below the different model-based parameter constraints presented in [215] where the values of the parameters of the different G_{ab}, v_{ab} given the values of the parameters estimated in table 4.8 and some assumptions based on the resting values of firing state ϕ_a of the different population of neurons:
Considering $\widetilde{\phi}_a = \phi_a^0/\phi_0$,

$$G_{es} = \left(\widetilde{\phi}_e/\widetilde{\phi}_s\right)\left(\ln\widetilde{\phi}_e - G_{ee} - G_{ei}\right), \tag{4.11}$$

$$G_{se} = G_{ese}/G_{se}, \tag{4.12}$$

$$G_{re} = \frac{G_{esre}\widetilde{\phi}_r ln\widetilde{\phi}_r}{\left[G_{esre} + G_{srs}\left(\ln\widetilde{\phi}_e - G_{ee} - G_{ei}\right)\right]\widetilde{\phi}_e}, \tag{4.13}$$

$$G_{sr} = G_{esre}/(G_{se}G_{re}), \tag{4.14}$$

$$G_{rs} = G_{srs}/(G_{sr}). \tag{4.15}$$

Given the estimation of the G_{ab} the parameters v_{ab} can then be estimated from

$$v_{ab} \approx G_{ab}\sigma/\phi_a^0, \tag{4.16}$$

and the range of v_{ab} can be estimated by:

$$v_{ab} \in \left[\frac{\min G_{ab}\min\sigma}{\max\phi_a^0}, \frac{\max G_{ab}\max\sigma}{\min\phi_a^0}\right], \tag{4.17}$$

where the maximum and minimum of G_{ab}, σ and ϕ_a^0 are specified in table 4.1.

4.2.5 EMG spectra

The power spectrum observed via EEG data is influenced by two sources; the activity of excitatory neurons and the tonic or burst firing of pericranial muscles known as electromyogram (EMG) [267]. EMG can cause apparent power enhancements in the EEG spectra above approximately 25 Hz and thus its effect needs to be removed. The observed power spectrum can be defined as the linear combinations of the two sources:

$$P_{EEG}(f) = C_1\, P_{EN}(f) + C_2\, P_{EMG}(f), \tag{4.18}$$

where C_1 and C_2 are constant which account for the power normalisation factors. To compensate for EMG artefact in the data, P_{EMG}, we used the theoretical model used by [219]. This non-biophysical based model introduced by [234, 250] which reproduced the power spectrum of EMG observed [269]. It is defined by:

$$P_{EMG}(f) = \frac{(f/f_c)^2}{[1+(f/f_c)^2]^2}, \tag{4.19}$$

with $f_c = 40$.

4.2.6 Formal definition of plausibility

Recall that we consider a simulation to plausible if it belongs to the interval of prediction with a similar shape of EEG data. Two constants C_1 and C_2 have been added to:

- rescale the experimental power spectrum without affecting its shape [219]; and
- remove the effect of P_{EMG} [219].

Effectively, if a linear combination of the two vectors P_{EN} and P_{EMG} belongs to the band delimited by $P_{\min}$ and $P_{\max}$ then the simulation is plausible. Formally, given the vectors P_{EN_i}, P_{EMG_i}, $P_{\min_i}$ and $P_{\max_i}$, $i \in [1,n]$, are there $C_1 > 0$ and $C_2 > 0$ such that:

$$P_{min_i} \leq C_1 P_{EN_i} + C_2 P_{EMG_i} \leq P_{max_i}, \tag{4.20}$$

$$\iff \begin{cases} \frac{P_{min_i} - C_1 P_{EN_i}}{P_{EMG_i}} \leq C_2, i \in [1,n] \\ \frac{P_{max_j} - C_1 P_{EN_j}}{P_{EMG_j}} \geq C_2, j \in [1,n], \end{cases} \tag{4.21}$$

$$\max_{i\in[1,n]} \left(\frac{P_{max_i} - C_1 P_{EN_i}}{P_{EMG_i}}\right) \leq \min_{j\in[1,n]} \frac{P_{max_j} - C_1 P_{EN_j}}{P_{EMG_j}}. \tag{4.22}$$

Let us denote

$$f(C_1) = \max_{i\in[1,n]}\left(\frac{P_{max_i} - C_1 P_{EN_i}}{P_{EMG_i}}\right) - \min_{j\in[1,n]} \frac{P_{max_j} - C_1 P_{EN_j}}{P_{EMG_j}}. \tag{4.23}$$

The expression 4.23 is a piecewise linear function and can be maximised easly. If $arg\,min_{C_1} f(C_1) > 0$ linear combinations of the two vectors P_{EN} and P_{EMG} can belong to the bands between $P_{\min}$ and $P_{\max}$. Furthermore, two constraints were added to bind the model to have a shape similar to the experimental spectrum. The theoretical power spectrum had to have at least one peak of frequency in the delta band and in the alpha band. In Figure 4.3, there is an example of plausible and implausible simulations.

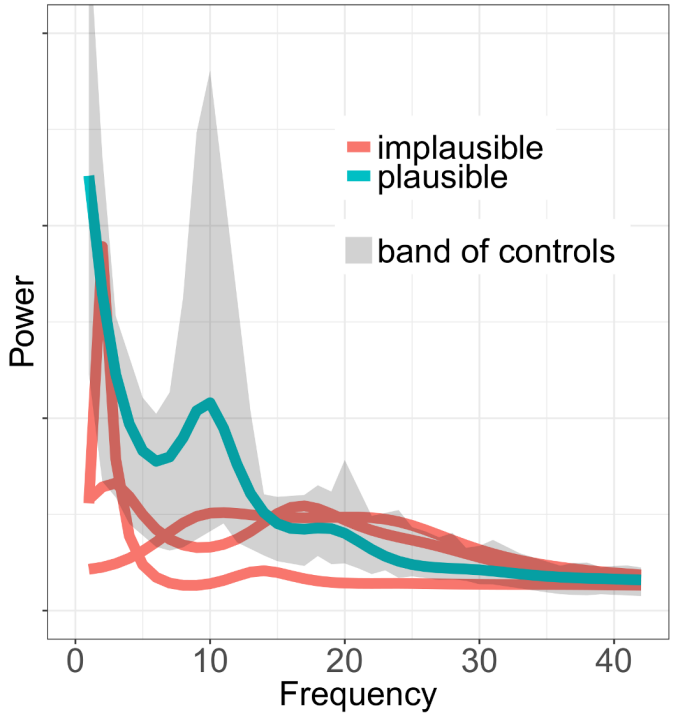

Fig. 4.3 Plausible and implausible simulations. A plausible simulation belongs to the band of control while a non plausible simulation lies partially outside.

4.2.7 Model simulations

The power spectrum was simulated 1,000,000 times varying 9 parameters γ, T, α, β, G_{ei}, G_{ee}, G_{ese}, G_{esre} and G_{srs} using a latin hypercube design [176] to explore the parameter space. The simulations were computed using MATLAB 2017b.

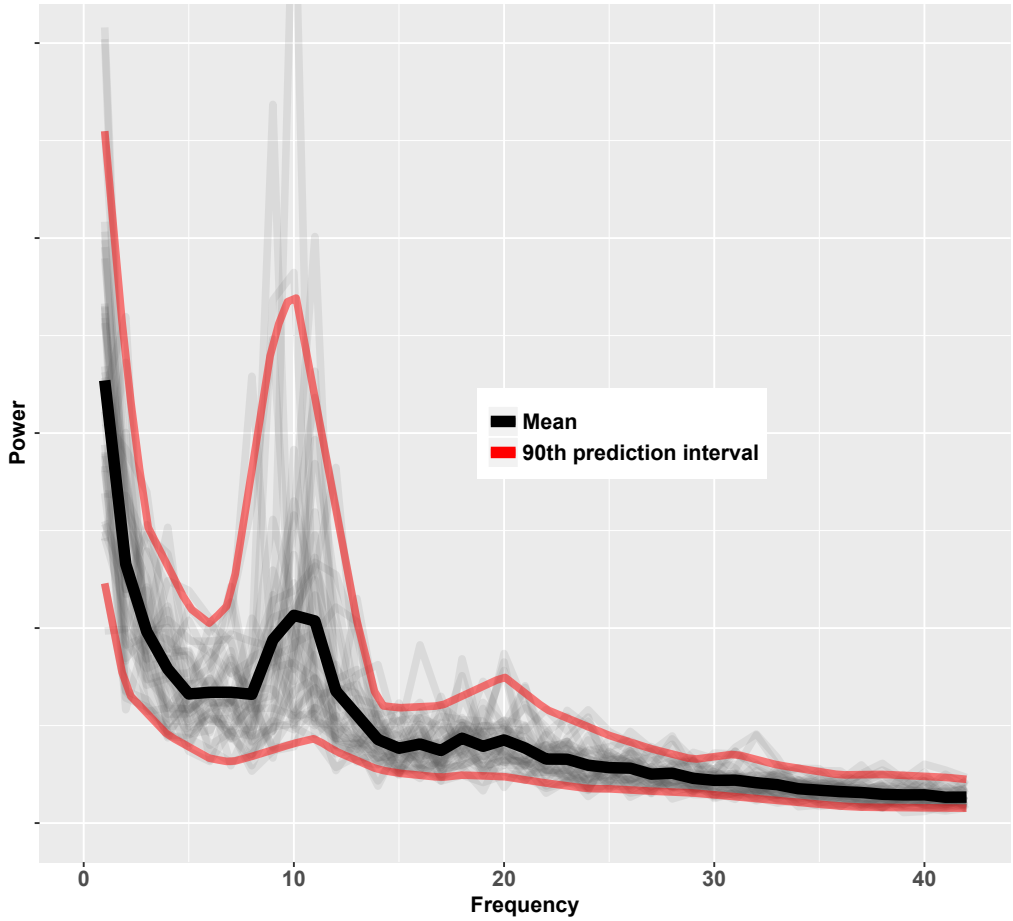

Fig. 4.4 Power spectrum of the subjects. The exterior bands in red indicate the interval of prediction for the values of the power spectrum with a confidence of 90% while the middle lines indicate the mean of the power spectrum. Each individual power spectrum is represented in grey

4.3 Results

4.3.1 Data

Figure 4.4 shows the power spectrum of each subject and the average and the band at 5% and 95% are indicated. The presence of alpha peaks can also be observed.

4.3.2 Partition of the parameter space to identify plausible regions

1,000,000 simulations were computed on the whole parameter space as described in section 4.2.3, using the biological constraint ranges as in Table 4.1. Analysing these simulations, we found that the theoretical power spectrum of the Robinson model is almost always implausible. Genuinely only 4.97% of simulations are plausible. Despite this, the plausible parameter space is much larger than the

parameter space defined in [215] which retains less than $10^{-12}\%$ of the original defined "biological" parameter space.

Figure 4.5 provides a 2-dimensional representation of the distribution of plausibility throughout the whole parameter space. It can be seen that the parameter subspace in which plausible power spectrum can be found (regions which are not in dark blue) is large and is not concentrated in small sub-regions. There are however some regions with a high concentration of plausible power spectrum (yellow colour). This is the case when T is large or γ is small. Figure 4.5 shows there are interactions between parameters. For specific values of two parameters, there is a larger proportion of plausible power spectrum simulations. For example there are complex interactions between α and G_{srs} and a linear interaction between G_{ee} and G_{ei}. On the contrary, the subfigures for the parameter β appears homogeneous, and therefore do not influence the likelihood of plausibility.

We used decision trees (see section 2.1.5) to effectively identify the plausible region of space and summarise how a change in a parameter can impact the dynamics of the model. Figure 4.6 presents one such tree that describes the segmentation of parameter space according to the plausibility. Recall that, for each branch, the tree algorithm scans through the sub-parameter space to identify the optimal separation between the maximum and minimum likelihood of observing the feature of interest (in this case, plausibility).

The different leaves of the tree in Figure 4.6 partition the parameter space in different regions with different densities of plausible simulations. In the regions on the left, the rate of plausibility is small: a negligible number of parameter sets are able to produce plausible simulations. Some regions have a greater ratio of implausibility. The standard values estimated by [215] are situated in the 3$^{\text{rd}}$ regions from the right. In this region of parameter space, the ratio of plausibility is close to 0.34%. Interestingly, there are other regions with a greater ratio of plausibility: in these regions, the ratio of plausibility is 0.39% and 0.44%. We focus on these three regions of high plausibility density. The main differences between these regions of higher density of plausibility and the standard values are for a region the values of G_{ee} and G_{ese}, for another, it is a smaller G_{srs}. Figure 4.7 shows the values of the parameters in these three regions and compares the values to those found in [215]. One can directly observe that in these subregions the values of certain parameters differ. This is the case for G_{ee} and G_{srs}. While region 1 constrains G_{ee} to large values and G_{srs} to small values, region 2 does the opposite; G_{ee} is constrained to small values and G_{srs} to large values. The different regions share common constraints; T, γ and G_{esre} have similar values on the four regions of interest. Some parameters are poorly constrained for the three regions. For example, this is the case for α, β and G_{ei}. Finally, some parameters are only constrained in specific regions. This is the case of α: only constrained in region 2 and G_{ese} only constrained in regions 1 and 3. However, the region identified by

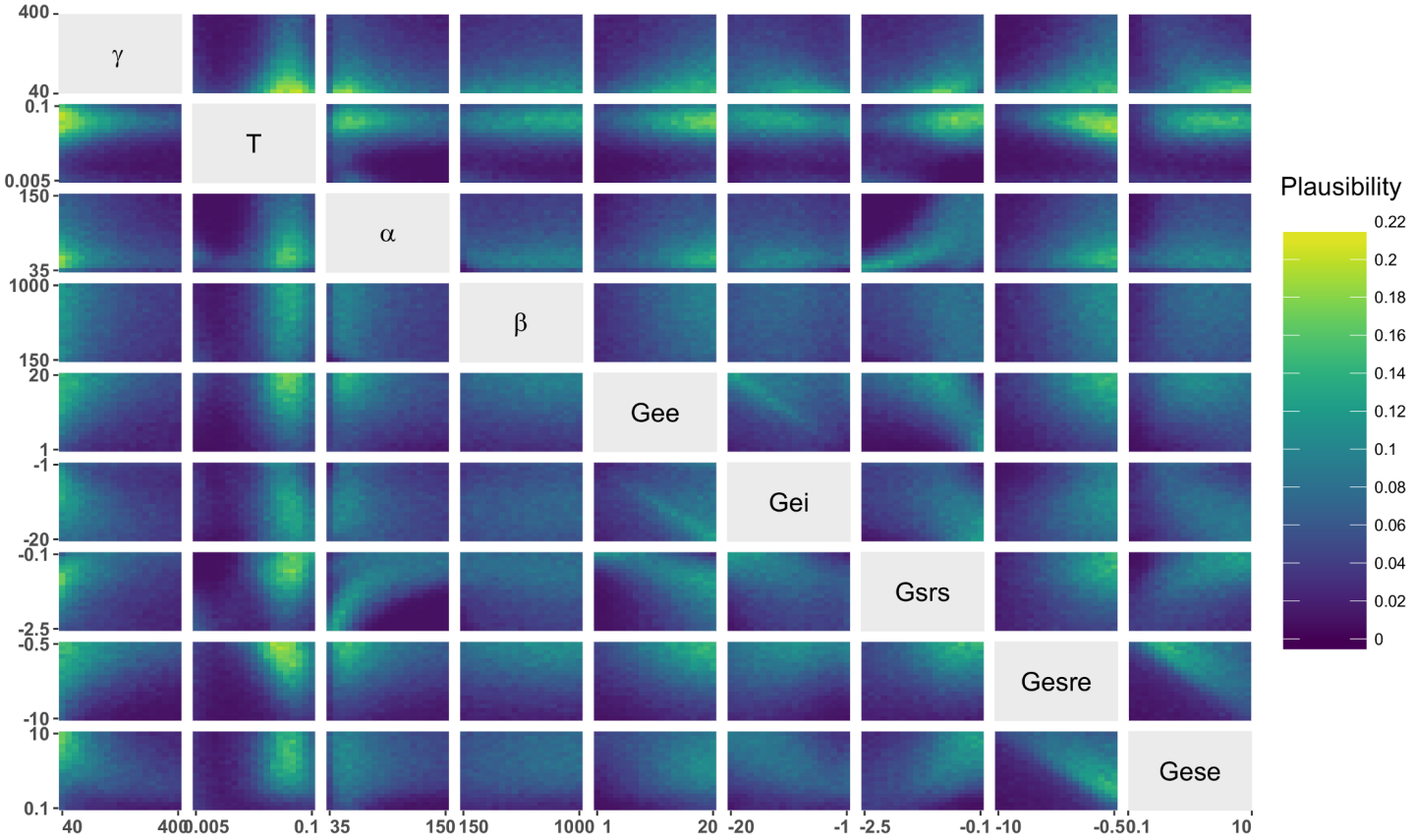

Fig. 4.5 Bivariate joint distribution of the likelihood of plausibility. Each subfigure is a projection of the parameter space over two parameters, and the colour indicates the likelihood of plausibility as per the colour bar.The axis labels are indicated by the diagonal. For example, the subfigure in the second column on the first row maps the likelihood of plausible power spectrum over different values of γ(y-axis) and T(x-axis). According to the colour bar, lighter blue colours indicate a higher likelihood of observing plausible power spectrum. Each subfigure was computed using equation 2.4 with 20 bins over the parameter ranges provided in Table 4.1. Specific combinations of parameters can lead to parameter manifolds with a high likelihood of plausibility. For example, there is a complex relationship between α and G_{srs} where the likelihood of plausibility is large.

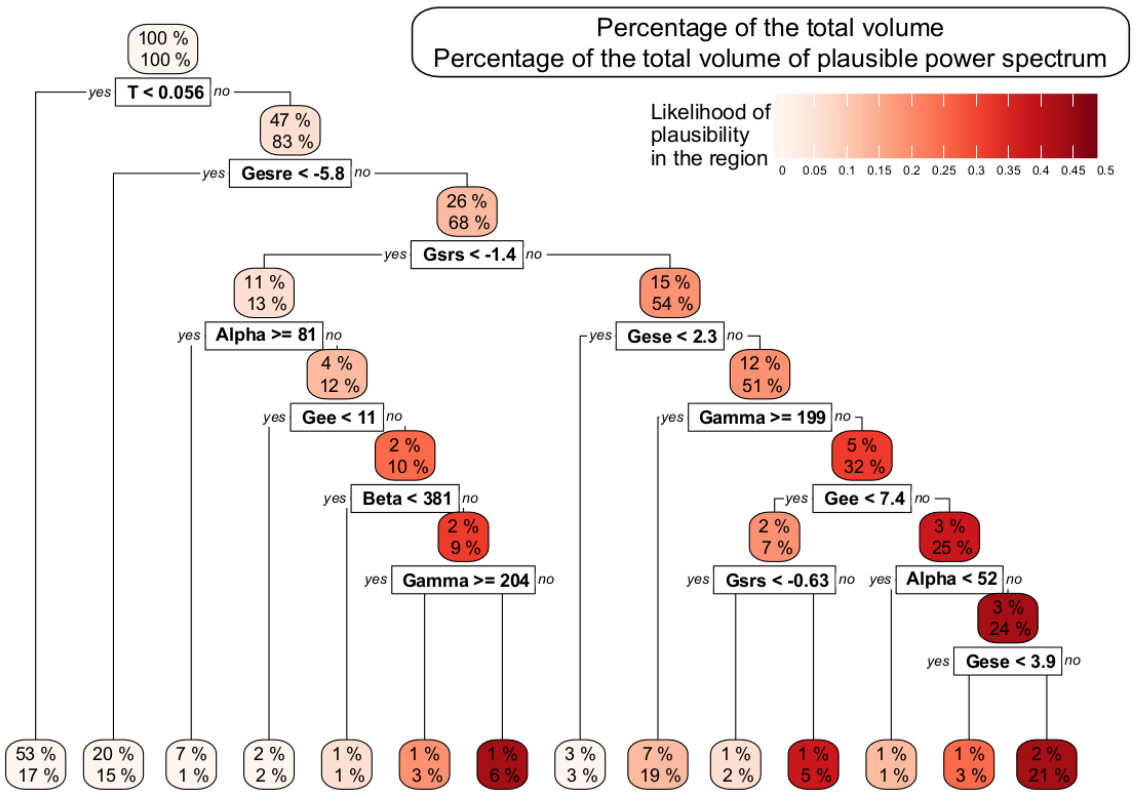

Fig. 4.6 The root region is at the top of the figure and represents the total parameter space, while the leaves are at the bottom. The upper label of each region indicates the size of the parameter space represented in this region. The lower label indicates the percentage of all parameter combinations that result in a plausible power spectrum. In the rest of the chapter, we focus on the three leaves in dark red. Values are given to two digits precision.

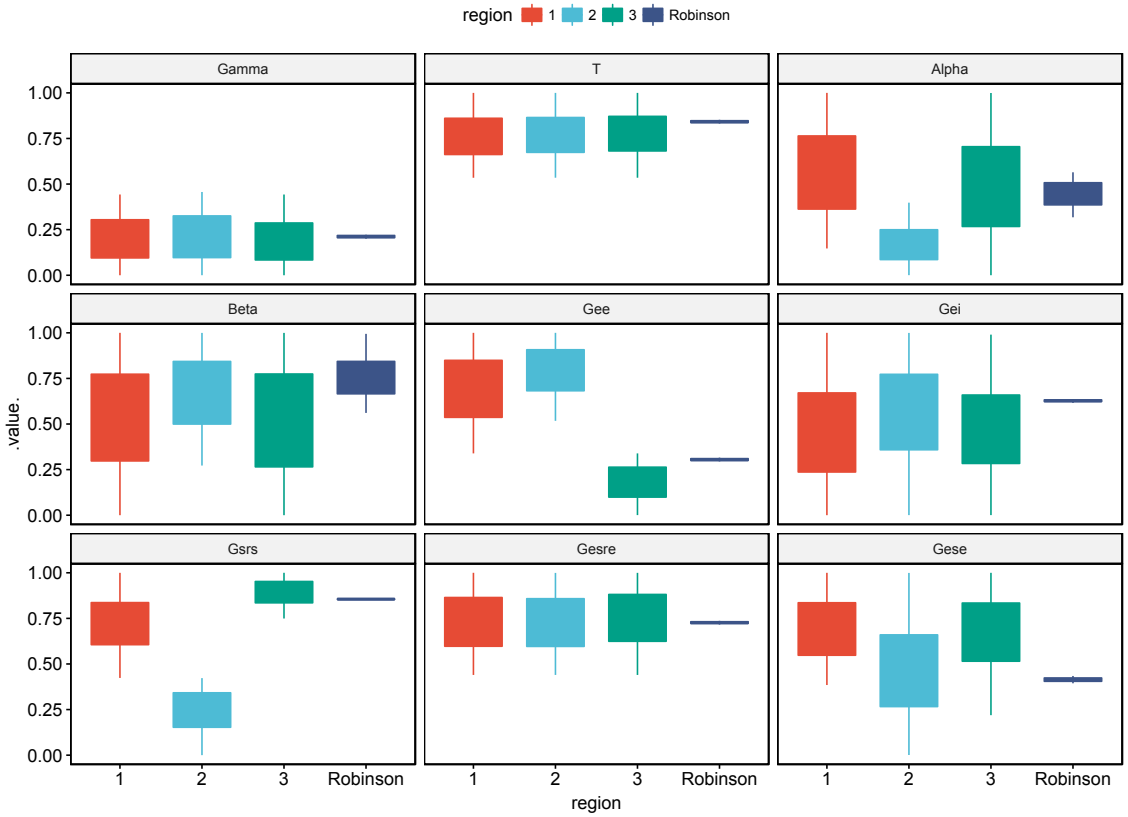

Fig. 4.7 Boxplot of the value of the parameters in the three regions with the highest density of plausibility of the tree in Figure 4.6 and the one presented in Robinson et al. [215]. Some parameter are similarly constrained for each region such as γ and T. The four plausible regions of the parameters space have low values for γ and high values for T. Other parameters follow more complex patterns such as G_{ee} or G_{srs}. G_{ee} and G_{srs} values change a lot for a region to another.
The range of each parameter has been normalised between 0 and 1.

[215] is strongly constrained for all parameters, giving the misleading impression that all parameters are equally important.

4.3.3 Importance of parameters

Whilst identifying regions with high density of plausible simulations is interesting it does not completely answer the question of which parameters it is safe to fix and which ones are the most influential on the plausibility of a simulation and should, therefore, be allowed to vary in a further study. Analysis of the measure of importance over 500 trees, GI and PI, as defined in section 2.1.7, shows that one parameter is much more important than other in term of plausibility: the time delay T. This parameter is consistently the most important parameter in terms of different importance measures. For other parameters, the measures can differ. The three parameters which appears the most of the root of the trees are T, G_{esre} and γ. For these parameters, there is a threshold at which the likelihood of plausibility changes abruptly. As indicated by Figures 4.5 and 4.6 this happens around $T \approx 0.5$, $G_{esre} \approx 6$ or $\gamma \approx 70$. The Gini importance measures indicate that the parameter T is an outlier. The GI of T is twice as high as the second highest GI. This means that it is by far the best parameter to partition effectively the parameter space. The permutation importance reveals that the other parameters can have an important role in plausibility or implausibility of the simulations depending on the values of the other parameters. T is still the most important parameter in this respect but the gain G_{srs} is nearly as important. Figure 4.5 shows that a modification of the values of G_{srs} changes the likelihood of plausibility. We can observe that other parameters have a Gini and permutation index not negligible as the gains G_{ese}, G_{ee}, decay time α and the cortical damping rate γ. There is one last group, G_{ei} and β, with negligible importance. Indeed the values of these parameters do not seem to impact the plausibility of the simulations.

4.3.4 Interaction between parameters

As observed in Figure 4.9. There are multiple interactions between the parameters. Some parameters have a particularly strong interactions such as α and G_{srs}, G_{ee} with G_{ei} and G_{ee} or G_{ese} with G_{esre} and G_{srs} or T with γ, G_{srs}, G_{esre} or G_{ese}. We can identify two broad types of interactions:

- Simple interaction such as γ and T or T and G_{esre}. The effect of the interaction on the likelihood of plausibility can be easily summarised. For example, the effect of low values of γ and large values of T has an effect which is more that additive. At the opposite a large value of T coupled with a small value of G_{esre} has a strong negative influence of the likelihood of plausibility. These interactions are easily taken into account to constrain the parameter space.

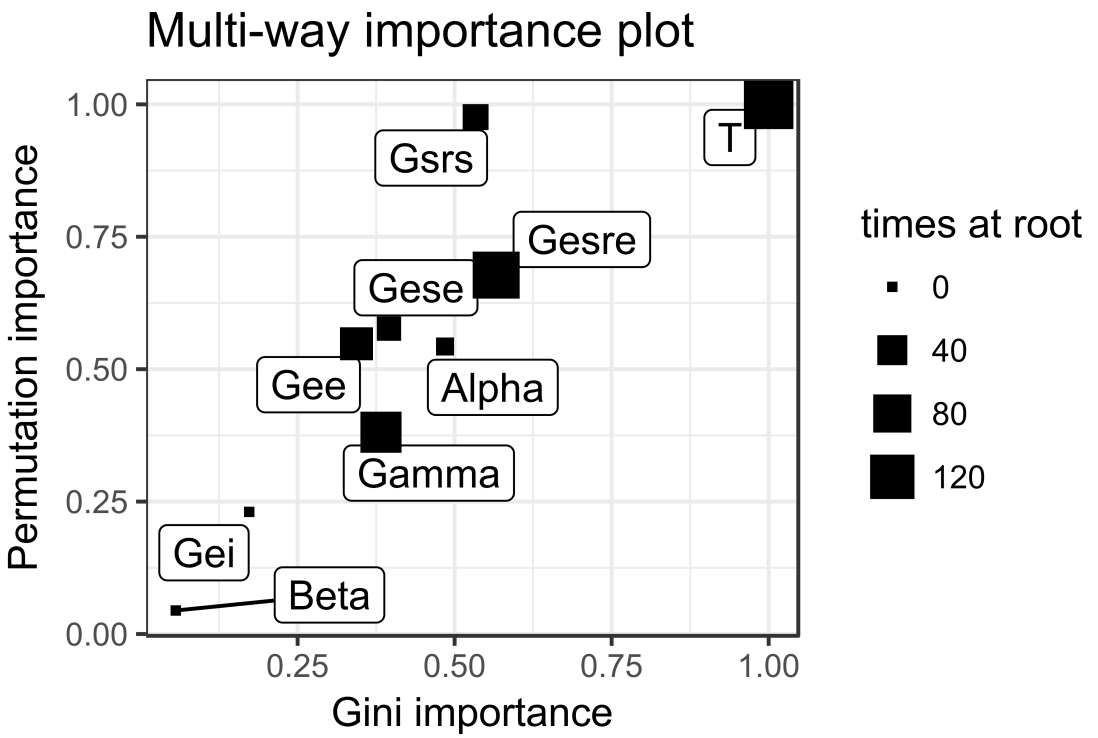

Fig. 4.8 Parameter importance in the Robinson model. The importance of parameters as determined by variable importance measures (see section 2.1.7) averaged over a random forest of 500 trees. The parameter T appears to be a leading parameter to influence the plausibility of a simulation

- Complex interaction; the manifold of the effect of the interaction is hard to describe, this is the case for the interaction between α and G_{srs} or G_{ee} and G_{srs}. These interactions are not easily taken into account to constrain the parameter space.

The large number of interactions, particularly the complex ones, renders difficult to constrain the parameter space with straightforward statistics such as the mean and some confidence intervals.

4.3.5 Identifying a suitable parameter space

These constraints can be used to identify a suitable parameter space for futher study. To identify the ranges of the parameters required for the non-linear version of the model we use the approach presented in [215]. The ranges of the synaptic products v_{ab} is many times larger than the range found in [215]. The reason for this is that unlike [215] which gave a band of $G_{ee} \in [5.6;6]$ and $G_{ei} \in [-8.4;-7.8]$, G_{ee} and G_{ei} are not constraint by the feature “plausibility” and so we have $G_{ee} \in [1;20]$ and $G_{ei} \in [-20;-1]$. As such the ranges of G_{es}, G_{se}, G_{sr}, G_{re} and G_{rs} are large according equations 4.11 to 4.15 and the range of v_{ab} are large according 4.17. Nevertheless these larger intervals take into account the plausibility of the distribution of the power spectrum and not only its average. This can be useful when one wishes to

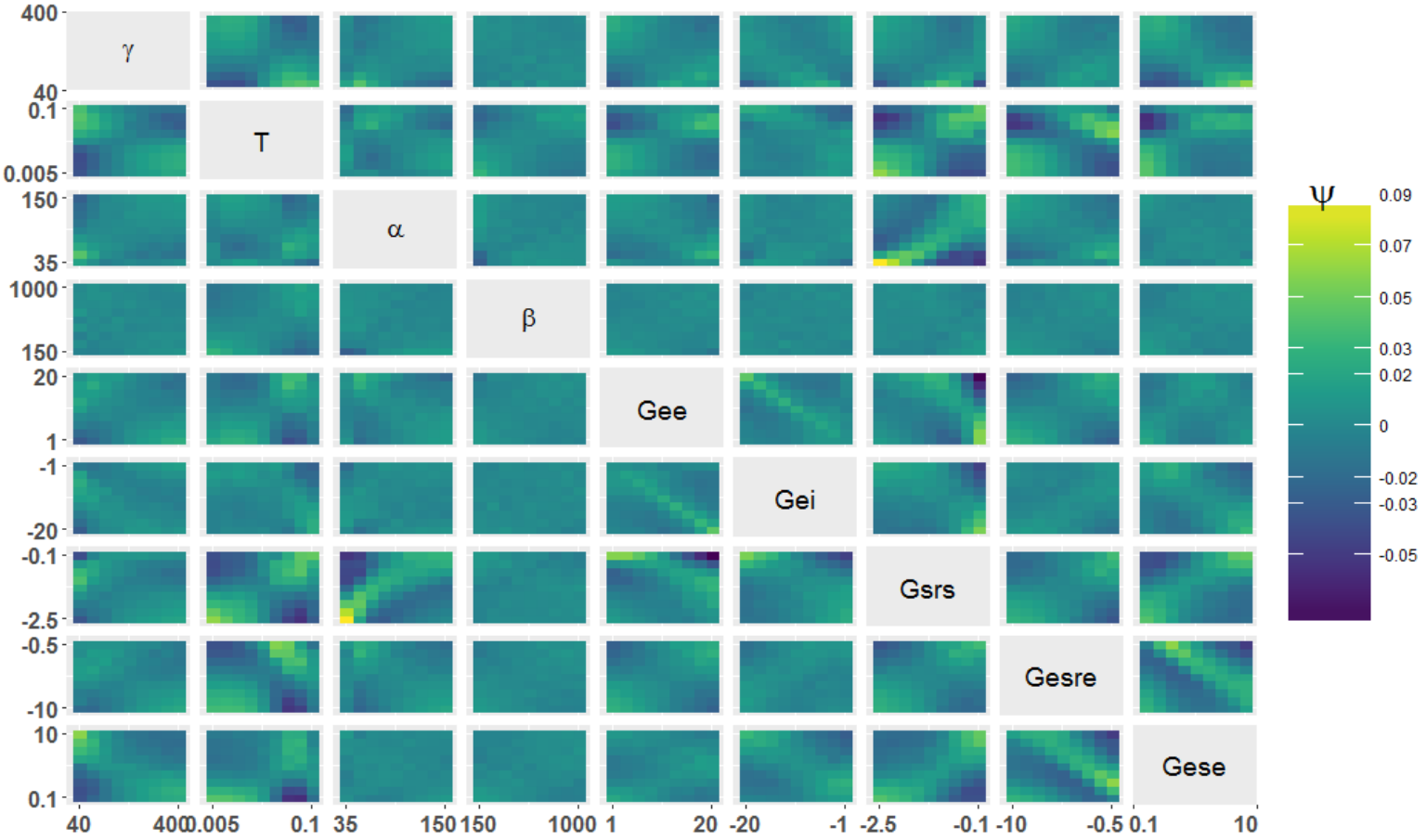

Fig. 4.9 Partial interaction plots of the parameter space of the Robinson model (as defined in section 2.3.2). Each subfigure represents the partial interaction plot over two parameters. Each subfigure was computed using equation 2.39 with 20 bins over the parameter ranges provided in Table 4.1. A subfigure with a large gradient of colours indicates a possible interaction. Multiple interactions between parameters are visible. There is a complex relationship between many parameters. There are strong interactions such as α and G_{srs}, G_{ee} with G_{ei} and G_{ee} or G_{ese} with G_{esre} and G_{srs}. T interacts with all parameters.

study power spectrum at individual level and does not want to take the risk of a bad fit because the initial parameter space was too constrained. Results summarising the biological range, the Robinson range [215] and the plausible range can be found in Table 4.1.

4.4 Discussion

In this chapter, we took a classical NMM of the thalamocortical system [215], and use TDM to characterise the relative importance of model parameters in explaining features of the power spectrum observed in human EEG experiments.

We defined and identified the plausible regions of parameter space. This is useful for future studies using the Robinson NMM as it gives a robust estimation of meaningful parameter regions for which plausible power spectra are possible. The subset of the parameter space determined by [215] belongs to a zone with a high density of plausibility as we might expect. However, the exploration of the parameter space, further showed that the small sub-parameter space selected in [219] did not reflect the fact that other parts of the parameter space are able to fit the power spectrum of people equally well. Indeed, there are other regions of parameters space with a higher density of plausibility. A challenge is that these interactions between parameters are complex and cannot be summarised straightforward statistics such as the mean and some confidence interval as in previous studies [215, 219].

We chose to focus on three regions of the parameter space which include a large proportion of the plausible dynamics while representing a small proportion of the parameter space. For some parameters, the conclusions we reach are the same as in [215], ie, only specific ranges are plausible parameter sets. On the other hand, some parameters are not constrained and any parameters values can lead to plausible simulations. We find the most important parameter by some margin to be the time delay T. Given that T is well constrained, other parameters such as the values of the intrathalamic loop couplings have some influence on the plausibility in conjunction with others parameters. Some parameters do not seem to affect the plausibility of a simulation, whilst for others, the value of a parameter becomes important only given specific combinations of the others.

4.4.1 Best fit versus plausible fit

The partition and the mapping of the parameter space highlight different aspects of the model that were previously ignored. Given the large discrepancy observed in the population, it is, therefore, important to explore a large region of parameter space. As a result, there are large sets of parameters which give a similar power

Quantity	symbol	biological range	[215] range	plausible regions	Unit
Cortical damping rate	γ	40-400	112-120	0-199	s^{-1}
Loop delay	T	0.005-0.1	0.084-0.086	0.056-0.1	s
Decay time	α	35-150	71.5-100	35-150	s^{-1}
Rise time	β	150-1000	625-1000	150-1000	s^{-1}
Maximum firing rate	$Q_{\max}$	220-500	220-500	220-500	s^{-1}
Firing threshold	θ	10-17	10-17	10-17	mV
Threshold spread	σ	3.6-4	3.6-4	3.6-4	mV
Firing rate e	ϕ_e	14-18	14-18	14-18	s^{-1}
Firing rate s	ϕ_s	09-23	09-23	09-23	s^{-1}
Firing rate r	ϕ_r	19-29	19-29	19-29	s^{-1}
Gain ei	$\|G_{ei}\|$	1-20	7.9-8.3	1.0-20	-
Gain ee	G_{ee}	1-20	6.6-7	1.0 - 20	-
Gain ese	G_{ese}	1-20	4-4.4	2.7 - 10	-
Gain esre	$\|G_{esre}\|$	0.01-20	3-3.2	0.1-5.8	-
Gain srs	$\|G_{srs}\|$	0.01-2.5	0.365-0.375	0.1-2.5	-
Synaptic product ee	v_{ee}	0.3-340	1.2-2	0.002-5.7	mV s
Synaptic product ei	$\|v_{ei}\|$	0.04-60	1.4-2.4	0.002 -5.7	mV s
Synaptic product es	v_{es}	0.02-40	0.2-1.0	0.002-5.7	mV s
Synaptic product se	v_{se}	0.03-48	0.2-2.0	0.001-8.9	mV s
Synaptic product sr	$\|v_{sr}\|$	0.02-32	0.2-2.8	0.001-8.9	mV s
Synaptic product sn	v_{sn}	0.0.1-40	0.1-0.5	0.1-0.5	mV s
Synaptic product re	v_{re}	0.07-64	0.03-0.3	0.001-4.2	mV s
Synaptic product rs	v_{rs}	0.02-24	0.007-0.06	0.001-4.2	mV s

Table 4.1 parameter space of the Robinson model according different sources; the biological range, the initial work of Robinson et al. [215] and a plausible region as defined in this chapter.

spectrum. As such the fitting of the model without more accurate a priori on the values of the different parameters could lead to overfitting.

Multiple recent studies focus on the best fit instead of on plausible fits. Approaches to exploit NMM to understand the mechanisms of the brain try to estimate the best fit given the data such as genetic algorithm [62], particle swarm optimization algorithm [233], Kalman filter [95] or dynamical causal modelling [98]. Regarding the physiological interpretation of experimental studies, a natural question is whether the modulation of the system circuits can be inferred directly from the recorded EEG data. Generally, in regard to the high number of parameters and the complex relationship between them this inverse problem is ill-posed. Furthermore, focussing exclusively on the best fit removes the critical idea that the best fit of data does not necessarily give a true parameter set. Indeed two elements need to be taken into account, the noise and the discrepancy of the model, *i.e*, how much, the mathematical model differs from the biological system. We saw that different parameter sets can lead to similar power spectra. As demonstrated in [116], there is the presence of important noise at an individual level in the power spectrum. This means that the average power spectrum cannot be robustly used to represent the power spectrum distribution of an individuals and even less a group of people.

4.4.2 Constraints on the parameter space

The concept of a plausible fit is one that has been previously explored in [30]. Here, our only constraint on the parameters space is the power spectrum. It is possible to further reduce the plausible parameter space by adding constraints. For example [30]; by adding a constraint of “strong biphasic” power rise in the context of modelling the effect of anaesthesia, reduced the number of plausible simulations from 73,454 to 86. We could adopt a similar approach in the case of the Robinson model. In this study, we used biological constraints, power spectrum and firing rates to constrain our parameter space. It could be possible to add temporal constraints to further limit our parameter space. Another constraint could be to do a local sensitivity analysis as in [126] to study the stability of our simulation and verify that modification of key parameters reproduces results observed in experiments. For example, one could seek to observe whether a given parameter set, would a modification of the excitability of excitatory cortical neurons or the inhibition of inhibitory neurons could lead to seizure dynamics or not.

4.4.3 Interactions between parameters

The external constraints on one parameter are assumed to be independent of the constraints on another. This is implied in stating upper and lower bounds for all parameters hence specifying a hypercube in parameter space. However, in reality, these parameters are interrelated in highly complex ways; hence parameters rep-

resenting real human thalamocortical system would map out complex manifolds in the parameter space. Furthermore, the simplifications and assumptions necessary in developing such models mean that the mapping of experimental data to model parameter remains a gross approximation.

4.4.4 Future use of the approach

We saw that the use of non-global methods to study NMMs can lead to overfitting and misleading results. It is thus necessary to use a global approach with realistic, and no overconfident a priori estimate, to study a NMM. This is the only way to achieve robust results when there is a large uncertainty in the parameter values. Mapping a mathematical model in high dimension leads to a new comprehension of the limit and the potential of the NMM.

Chapter 5

Comparison of the plausible parameters of people with and without epilepsy

> There is a saying “all models are wrong, but some are useful”-not understanding that the real problem is that “some are harmful”.
>
> Nassim Nicholas Taleb.
> *The Black Swan [256]*

In this chapter, we focus on the differences between the parameter spaces of people with epilepsy and without epilepsy. We use the same methodology as in chapter 4, i.e. we clean the data with the same process and use the same model. The only major difference is that the focus is made on the comparison between the plausible parameter space of different population groups and not, as in the previous case, plausible versus implausible parameter space.

5.1 Introduction

Slight differences in the power spectrum, particularly in the alpha band, are potential biomarkers for different diseases such as Alzheimer [129], depression [158] or epilepsy [157]. Particularly a lower mean alpha frequency and a larger amplitude was recorded for people with epilepsy but as noted by [116] there are large discrepancies within the populations and it is frequent to find people with epilepsy with a high alpha peak and people without epilepsy with a low alpha peak. [227] showed that is was not possible to identify correctly the alpha peak as a biomarker because of this discrepancy. Nonetheless, differences between the healthy cohort and IGE cohort remains constant at a population level. Understanding the underlying mechanisms behind the differences between

unhealthy and healthy people is still a key question in neuroscience. Studies have pointed to the thalamus as the primary alpha pacemaker [134, 169, 221] while others point out the cortex as the primary alpha pacemaker [45, 162, 270].

To study the mechanisms behind the differences between unhealthy and healthy people we compare the plausible parameter space of different groups of people, controls, IGEs and their relatives.

In the methodological part, we introduce the data used in this chapter. In the results section, we compare which parameters explain the difference of power spectrum (mainly focussed on the alpha band) between people with idiopathic generalized epilepsy (IGE), their first-degree relatives, and healthy controls. In the discussion section, we compare our results with previous studies.

5.2 Methods

EEG data

The dataset contains EEG recordings from people with idiopathic generalized epilepsy (IGE) (30 people), their first-degree relatives (42 people), and healthy controls (38 people) between the ages of 16 and 59 years. The individuals with IGE were drug-naive and recruited through clinics at St Thomas's Hospital. A diagnosis of epilepsy was confirmed in each case by an experienced epilepsy specialist through observation of typical generalized spike-wave (GSW) activity on EEG either spontaneously or following hyperventilation or photic stimulation. For 10 of these people, the diagnosis was confirmed following an initial routine EEG. For the remaining 20, the diagnosis was confirmed following sleep-deprived or longer-term EEG monitoring (including sleep). Similar healthy control EEG was collected at King's College Hospital EEG department. Controls provided written informed consent, and data collection was approved by King's College Hospital Research Ethics Committee (08/H0808/157). Under United Kingdom law, patient data collected during normal clinical routine and anonymized before research use may be used for research without additional consent; this procedure was reviewed and approved for this project by St. Thomas's Hospital and King's College Hospital's Research and Development departments. A trained clinical EEG technician identified a 20s long state EEG activity from the initial stage of the recordings from each participant. Because signal amplitude may vary between individuals due to different anatomic features (such as the size and shape of the cranium) the data were normalized by dividing the power spectrum in each channel by the total power in the spectrum averaged across all channels. This normalised power preserves relative differences in power between bands.

The methods used to process the data and to analyse the parameter space are presented in section 4.2 and chapter 2 respectively.

5.3 Results

5.3.1 Power spectrum

The power spectra of the different groups, illustrated in Figure 5.1, are relatively similar. This figure shows the power spectrum of each subject. The average and the band at 5% and 95% of each group are indicated. We can observe that the beta peak around 20 Hz is present in many individuals group but not always observed. Finally, we can see that in each group some individuals do not follow the global trend. This is particularly the case in the relatives group, where two individuals (blue shaded lines) have a lower alpha peak. The data reflect previous knowledge that there is a large discrepancy in the power spectra among the population as a whole [116].

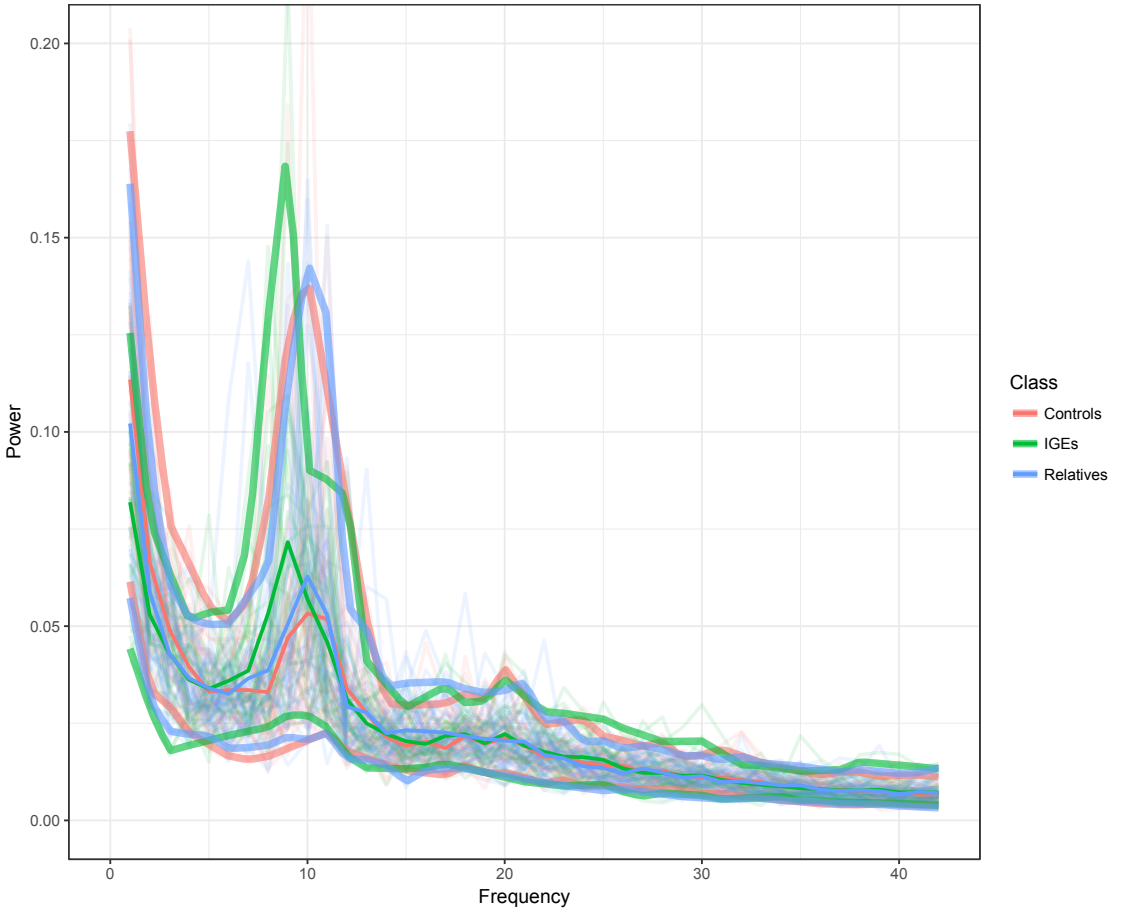

Fig. 5.1 Power spectrum of the subjects. For each group, the exterior bands indicate the interval of confidence for the values of the power spectra with a confidence of 90% while the middle lines indicate the mean of the power spectra.

5.3.2 Alpha peak

On average the alpha peak frequency of IGE cohort is at a lower frequency and with higher power amplitudes than the non-IGE cohorts which is consistent with

previous studies [157]. The band of predictions of the different groups reproduce these trends: the band of the IGEs group is shifted to the low frequencies in the alpha band compared to the two other groups. Visually, there is more power in the alpha band in the IGEs group. The mean of the peak alpha frequency is 9.5Hz for the IGE cohort, 9.97Hz for relatives and 10.13Hz for the control cohort. As seen in Figure 5.2, the intergroup discrepancies are important. There are some trends reflected in the mean; controls mainly have a high alpha peak while IGEs mainly have low alpha peaks and relatives are more balanced with both low and high alpha peaks. We note that the peaks can be found outside the classical alpha band (8-12Hz) with values at 7 and 13. Nevertheless, the large majority of peaks are in the classical alpha band.

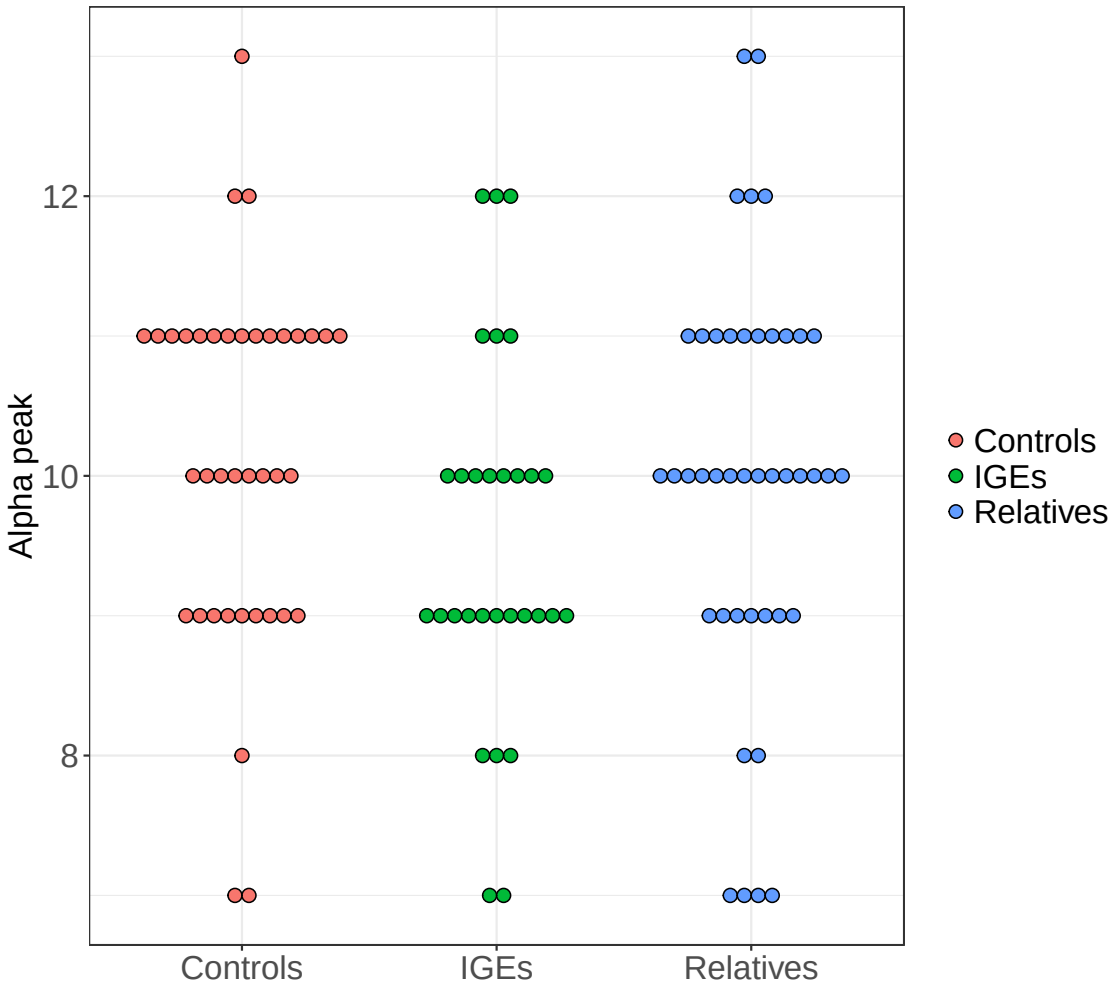

Fig. 5.2 Peak alpha frequency for the different groups. The peak alpha frequency of the control is often at high frequency while the IGEs often has a peak alpha at low frequency.

5.3.3 Difference between the plausible parameter space of IGEs, relatives and controls

Over the simulations, 4.72% of the parameter space was plausible for the controls' cohort, 4.26% for the relatives' cohort and 5.18% for the IGEs' cohort. We used a Venn diagram to depict the connection between the different plausible spaces. The Venn diagram indicates the proportion of sets which are plausible for each group and the sets which are plausible for two or more groups, see Figure 5.3.

As expected, the plausible parameters spaces of the three populations are largely overlapping. 41.2% of the total plausible parameter space, i.e. the set of parameter which gives a plausible power spectrum for at least one of the group, is plausible for the three groups. The control's plausible space and relative's plausible space are the two cohorts overlapping the most; most (86.5%) of the plausible space of the control population is within the relative population's plausible space. Furthermore, controls and relatives cohorts share a large plausible parameter space which is not a plausible space for the IGEs. This shows that the plausible parameter space of the relatives and the controls are similar. On the contrary, IGEs plausible parameter space can be slightly different to the control and relative cohorts' and 18.6% of its plausible space is considered as implausible for the power spectrum observed in both controls and relatives. For controls and relatives, it is respectively at 7.76% and 8.48%. Controls and relatives plausible parameter spaces are similar. The fact that the parameter spaces are highly overlapping does not come as a surprise. The difference in the three plausible parameter spaces is consistent with the difference in the three EEG data cohorts, see Figure 5.1.

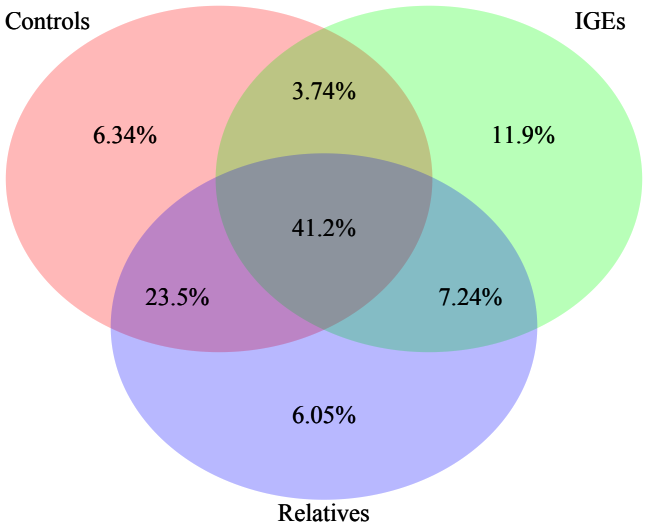

Fig. 5.3 Venn diagram showing the plausible space shared by the three populations. The three plausible parameter spaces overlap, however, the IGE cohort is sensibly different from the other two. The diagram is made with the package of [54].

5.3.4 Importance of parameters

The fact that the relative and control populations are closer to each other than IGE is an interesting finding. In the next section, we determine the parameters which are able to differentiate between the IGE plausible space and the non-IGE plausible space. To compare the plausible parameter space of the IGEs group against the non-IGEs groups we selected the joint plausible parameter space of both groups and use the tree-decision learning group to split the parameter space according to being solely plausible for IGEs or plausible for both groups.

Figure 5.4 computes the different measures of importance. Permutation and Gini importances order the parameters in the same way. One parameter T is highlighted as the most important parameters with more than twice the permutation and Gini importance than the second most important parameter, G_{esre}. Other parameters of importance are α, G_{ee}, G_{ei} and G_{srs}. Then the least important parameters are G_{ese}, γ and finally β.

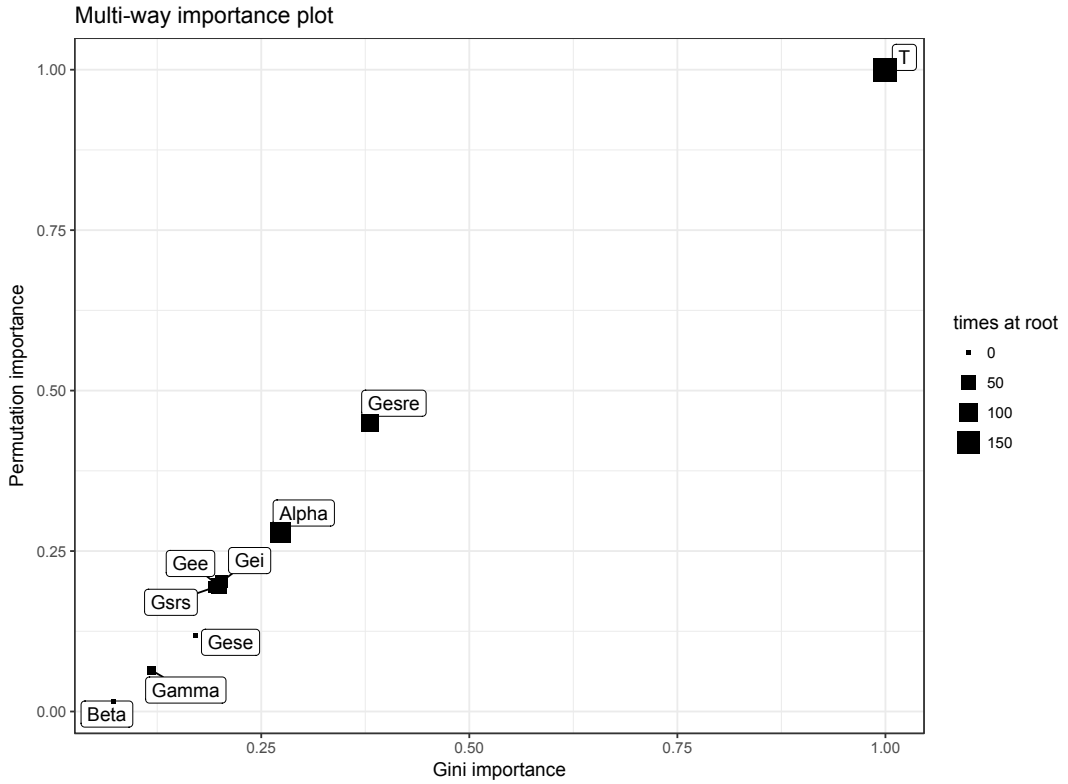

Fig. 5.4 Parameter importance in the Robinson model. The importance of parameters as determined by variable importance measures (see section 2.1.7) averaged over a random forest of 500 trees. The parameter T appears is the leading parameter to influence the plausibility of a simulation for IGE cohort only.

5.3.5 Plausible parameter space for control population

As previously, we used tree statistic measures (see section 2.1.5) to efficiently identify the plausible region of space and summarise how a change in a param-

eter can impact upon the dynamics of the model. Figure 5.5 presents one tree that describes the segmentation of parameter space according to the plausibility. Recall that, for each branch, the tree algorithm scans through the sub-parameter space to identify the optimal separation between the maximum and minimum likelihood of observing the feature of interest (plausibility in this case). The partition of the parameter space shows how the parameters with the most important measures influence the power spectrum, see Figure 5.5. As T is the most important parameter, we will focus particularly on it. In Figure 5.5, the parameter T appears four times. Three times, an increase of T indicates an increase to have a power spectrum corresponding to IGE only and once decreasing T indicates an increase to have a power spectrum corresponding to IGE only. When $T \leq 0.039$ the likelihood to fit only control or relative is small. However, for T between 0.039s and 0.075s, the probability to fit relative and control is higher than simulating an IGE power spectrum. Finally, over 0.075s the probability of only fitting the IGE power spectrum is higher. In summary, the lower frequency alpha peak of IGE group can be explained by two reasons: a small T or a large T. The large T is expected, T is dominating the peak frequency: $1/T$. Without the influence of the other parameters, T=0.105s would correspond to a peak of 9.5Hz. However, when T becomes small it is possible to find plausible parameter sets for the IGE cohort. This is due that for T below 0.04s and rare combinations of the other parameters, the power spectrum simulated has its delta band with a smaller amplitude and an alpha band with a large power and this case can only be found for the IGE cohort data.

We can observe that other parameters can change the probability to be plausible only for the IGE cohort. Smaller values of $|G_{esre}|$ and $|G_{srs}|$ decrease the chance of only fitting the IGE group while large values of α decrease the chance of only fitting the IGE group.

5.4 Discussion

In this study, we explored the plausible parameter space of the Robinson NMM in the case of cohorts of people with and without epilepsy. Our hypothesis was that the plausible parameter space estimated from the power spectrum of background EEG from the people with epilepsy is different from that of their relatives and of a control group. We verified this hypothesis, finding that the parameter T, representing the delay between the thalamus and cortex neural populations, was the most different.

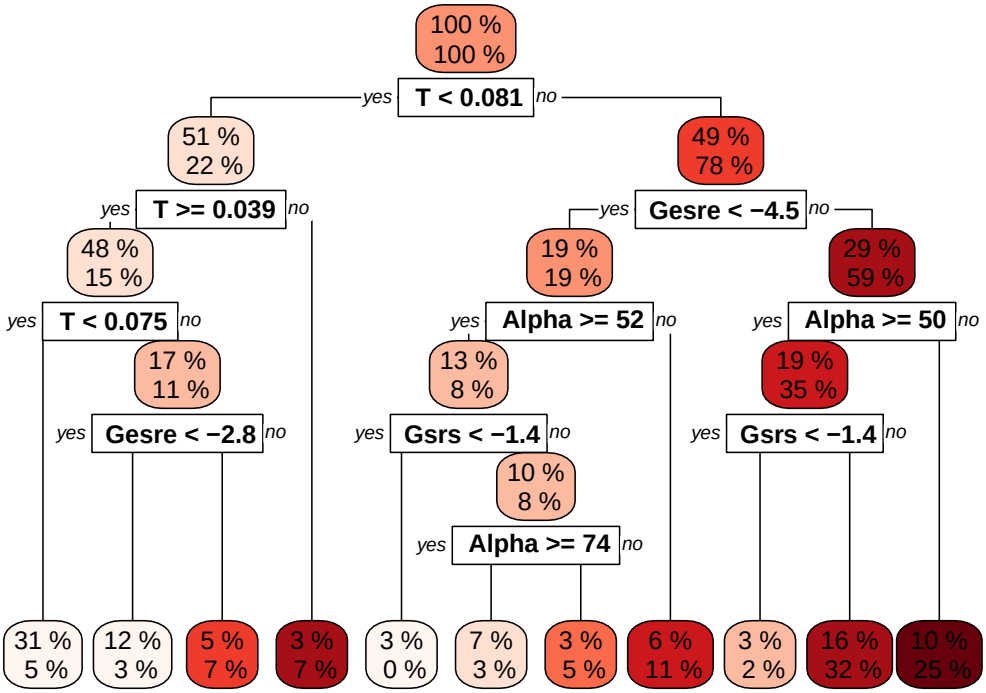

Fig. 5.5 The root region is at the top of the figure and represents the total parameter space, while the leaves are at the bottom. The upper label of each region indicates the size of the parameter space represented in this region. The lower label indicates the percentage of all parameter combinations that result in a plausible power spectrum. Values are given to two digits precision.

5.4.1 Difference between parameter spaces

The fact that for the group IGE, the only plausible regions of parameter space can be identified within two disparate sets of values of T could indicate that different thalamocortical network configurations are able to support the power spectrum characteristic IGE cases. The importance of the parameter T have been identified but the partition values are different. The partition of the parameter space has indicated that for large T there is a non-negligible likelihood of having a plausible simulation while for low values of T the likelihood was negligible. As such, a person with a low value of T (< 0.39s) will have a higher likelihood that his power spectrum will look like an IGE power spectrum while a person with a large $T(> 0.85$s) could have a power spectrum similar to any group (but with an increased probability of belonging to IGE power band only). A T value between 0.39s and 0.85s increases the chance of having a power spectrum between the interaction of the three band interval of prediction or only the relatives and controls. In particular, we observe that other parameters can influence the plausibility, such as the gain G_{esre}, the decay time α and the gain G_{srs}, however, this influence is marginal compared to that of T. These parameters influence the output but less directly than T, however, specific combinations of parameters can have the same effect as a large T. Beyond this, the plausible parameter space identified in the IGE group differs only slightly from the parameter space identified in chapter 4 for healthy controls.

5.4.2 Experimental validation

In light of this strong dominance of T on the plausibility of solutions, we discuss what previous experimental studies identify as important parameter to play a role on the EEG alpha peak. We could find a large number of experimental studies that identify the thalamus [134, 169, 221] or the cortex [45, 162, 270] as the main important part of the brain responsible for the EEG spectrum. However, even if the cortex and thalamus parameters did not have negligible importance measures, they were much smaller than the delay time constant between the thalamus and the cortex, T. The importance measure of the parameters T highlights the role that this parameter plays to determine the appearance of the power spectrum in the Robinson model. This is remarkable because we could not find any experimental articles which would highlight the role of this parameter to influence the EEG power spectrum. Such a difference between what has been experimentally demonstrated: that the cortex or the thalamus play an important role, and what this study shows, lead us to highlight the need of more experimentations to confirm or infirm the importance of the time delay between the thalamus and the cortex.

5.4.3 Assumption of the Robinson model

Chapter 2 of the thesis of Peterson [203] summarises some assumptions made to make the Robinson model and recall that some are known to be false from a biological point of view; for example, excitatory cortical and inhibitory cortical population are assumed to have exactly the same characteristics [203, 212]. Another possible improvement of the Robinson model could be to focus on the way to model the time delay between thalamus and cortex and acquire better experimental approximation. Another fact about the delay between vivo, axonal conduction from cortex to thalamus is much slower than in the reverse direction [249] and so the two different speeds could be modelled by two parameters. There is another connection between the thalamus and the cortex which has not been modelled in the Robinson model; It is a fast (2ms) route which involves activation of the specific nuclei of the thalamus which project mainly to target areas in cortical layer IV as opposed to the target areas in layers I and II of the nonspecific thalamic and brainstem systems [213]. Nevertheless, the addition of new parameters without accurate a priori values would only increase the sensitivity of the model. It is more important than ever to accumulate in vivo data to be able to calibrate meaningful models.

5.4.4 Using decision tree mapping to detect potential misleading model

We have used the DTM approach to identify the abnormal importance of the parameter T demonstrating that whilst the Robinson model is able to accurately reproduce power spectrum from different cohorts of people, our ability to reliably interpret its meaning is questionable. Typical approaches to parameters studies restrict the number of parameters for analysis and consequently the relative importance if a parameter overall can be missed. With complex models, it is often possible to find results similar to experiments. However, care is needed in their interpretation. Here, we find that the Robinson model places significant importance to the value of the time delay, T for which this is limited experimental justification. We argue that combining a systematic study of plausible sets of parameters, alongside detailed understanding of the biological observations is important for making robust observations.

Chapter 6

Conclusion

> Even if a scientific model, like a car, has only a few years to run before it is discarded, it serves its purpose for getting from one place to another.
>
> B. Mankin, R.V. O'Neill, H.H. Shugart and B.W. Rust, *The Importance of Validation in Ecosystem Analysis [174]*

6.1 Summary

Advancing our understanding of the brain will play an important role in better characterising and treating neurological conditions such as epilepsy. Here, the approach used to enhance our understanding is to use NMMs. These models describe the average activity of a large group of neurons. We have seen that classical rhythms of the brain and seizure dynamics can be effectively replicated by the Wendling model and that the Robinson model can reproduce typical EEG power spectra. Such models can be useful to make hypotheses about the gross mechanisms that give rise to the rhythms in EEG.

In this thesis, we introduced a statistical approach to examine how different parameters affect the output of a model and at which parameter values the transitions occur. We applied our approach to different problems using different mathematical models.

In chapter 2, we presented the DTM method to explore and understand the parameter space of a mathematical model. We presented existing tools such as decision tree, random forest and partial plots and introduced a new way to combine them in order to analyse the parameter space. The limitations of these

methods are often due to a lack of data. One of the key advantages of NMMs is the fact that the models can be simulated a large number of times on a simple computer desk in a relatively small amount of time. By creating a large database we can then use machine learning tools to their full potential. In our examples, we showed how DTM was performant on relatively complex models even with a relatively small number of simulations.

The other chapters demonstrated the applications of the DTM approach in different studies related to epilepsy.

In chapter 3, we presented the results achieved with the Wendling model to identify the parameters which are the most important for the transition to seizure dynamic. We reproduced known results, showing that the ratio between the gain and the meantime in the loop of the excitatory and slow inhibitory neurons influence seizure onset. We discovered that previously unstudied parameters can also play a critical role on the dynamics of the neural mass model such as the parameters of the sigmoid function. Furthermore, we showed that the roles of parameters are targeting different characteristics of the dynamics of the Wendling model; some have a huge impact on many characteristics such as the mean time parameter of slow inhibitory interneurons. Other, such as the postsynaptic potential threshold, mainly influence the amplitude of oscillations.

In chapter 4, we applied the TDM method to clinical data. We defined the concept of plausible fit which is more meaningful than the concept of best fit when working with noisy data and a population with intra-variability. We applied this definition to define the plausible parameter space of the Robinson model, fitted to the power spectrum of EEG. Previous analyses have been done on this model but we showed that our global analysis extends these previous results. We showed that the plausible parameter space is much wider than the previous one and that many combinations of parameter sets can lead to similar simulations. Particularly, we observed that the parameter representing the loop delay between the cortex and the thalamus has a leading role in the dynamic of the model.

In chapter 5, we used the same model to compare the plausible parameter space of different groups of people, control, idiopathic generalised epilepsy and their relatives. Controls and relatives share a similar plausible parameter space. However, patients with idiopathic generalised epilepsy have a slightly different plausible parameter space from the two other groups. We observed that the parameter of the loop delay between the cortex and the thalamus was the most important parameter by a significant margin. This parameter has few biological reasons to exist and does not appear in any experiment as being important. As

such new experimentations are needed to validate the importance of the time delay between the thalamus and the cortex.

6.2 Discussion

6.2.1 Mathematical models are highly dependent on their parameters

As we have seen in the chapters 3, 4 and 5, the parameter space of the models studied is much more complex than previously considered. We argued that in only exploring a limited number of parameter simultaneously, there is a danger of missing important information as to the role of certain parameters. By simultaneously studying the whole parameter space, we have shown the complexity of the relationships between the parameter spaces and the dynamics of interest. Some parameters have a global role and changes in their values have an impact on the dynamics of the model. Other parameters have a local role, changes in the values of these parameters change the dynamics only if the other parameters have specific values. Finally, some parameters have a relatively small influence on the dynamics.

6.2.2 Machine learning, a promising tool to analyse the parameters space

The exploration of the parameter space of the models has been made possible thanks to the use of statistical and machine learning approaches. Previous findings have been rediscovered using DTM approach, confirming the validity of the approach. New findings have been discovered, confirming that the approach is complementary to bifurcation analysis or activity map approaches. The use of machine learning offers new insights into understanding and using mathematical models. Furthermore, machine learning approaches make the most of one of the main advantages of mathematical models; the cost of a simulation is cheaper than the cost of experimental observations. This makes it possible to compute a large number of simulations and to create a large database.

6.3 Future research direction

As the mathematical models used in science increase in complexity and detail, the number of parameters is increasing. It will become more important than ever to identify the role of the different parameters on the model's dynamics. We saw that it is critical to explore the parameter space with all the parameters simultaneously. The method proposed offers a fast and efficient way of identifying the parameters

with the most impact on the dynamics and observe how parameters can interact. However, the capacity of the DTM approach to analyse a parameter space can be limited by the sampling and the decision tree methods:

- parameter space can be highly complex in some subregions and simple in other regions, making it necessary to compute more simulations in the highly complex subregions. To increase the number of simulations in regions which seem to be under sampled, one solution could consist of adapting the history matching approach [288];
- we used a decision tree approach to analyse the parameter space but there are other methods which could be used to take into account specific characteristics of the studied mathematical model. For example, for mathematical models which are computationally costly to simulate, there are other machine learning methods such as Gaussian process [78, 287]. Gaussian process can give insightful results even with a small number of simulations. The mapping, however, would be less intuitive than the method presented in this thesis as this approach does not have intuitive visualisation as it is the case for decision trees. Furthermore transitions would not be detected efficiently, either. It can be hoped that new machine learning methods will increase our capacity to explore and analyse the parameter spaces of complex mathematical models; and
- the partition done in this study analyses the output of a mathematical model without taking into account the potential effect of noise on the simulation. To increase the robustness of the partition of the parameter space analyses it could be interesting to integrate a local sensitivity analyse on each simulation to test the stability of its dynamics.

6.4 Final remarks

Mathematical models do not need to reproduce the dynamics of interest exactly, they are only tools to better understand the underlying mechanism of interest. However, to use them to their fullest potential, it is important to fully analyse the parameter spaces of the models of interest. We propose an approach which offers new insights into understanding the relationships between the model's parameter and its dynamics. Our understanding of neural dynamics will continue to improve as more experimental, anatomical and physiological data becomes available. Neural modelling paradigms give us a theoretical framework from which to interpret and explain the plethora of experimental data. The future of neural models, especially when interfacing with experimental neuroscience, is through the validation and veracity of the NMMs. The use of tools is a step in this direction as it helps to invalidate models which produce abnormal results and better understand

models with coherent results. This direction will drive NMMs to keep evolving towards reaching a ‘predictive’ status, where they will become invaluable clinical tools.

References

[1] (2012). Epilepsy. Fact Sheets. Technical report, World Health Organization.

[2] Agmon-Snir, H. and Segev, I. (1993). Signal delay and input synchronization in passive dendritic structures. *Journal of neurophysiology*, 70(5):2066–2085.

[3] Alberts, B., Bray, D., Hopkin, K., Johnson, A., Lewis, J., Raff, M., Roberts, K., and Walter, P. (2014). *Essential Cell Biology*. W. W. Norton & Company.

[4] Alexopoulos, A. V. (2013). Pharmacoresistant epilepsy: Definition and explanation. *Epileptology*, 1(1):38–42.

[5] Amari, S.-i. (1977). Dynamics of pattern formation in lateral-inhibition type neural fields. *Biological Cybernetics*, 27(2):77–87.

[6] Armañanzas, R., Inza, I., Santana, R., Saeys, Y., Flores, J. L., Lozano, J. A., de Peer, Y. V., Blanco, R., Robles, V., Bielza, C., and Larrañaga, P. (2008). A review of estimation of distribution algorithms in bioinformatics. *BioData Mining*, 1(1):6.

[7] Ascoli, G. A., Donohue, D. E., and Halavi, M. (2007). NeuroMorpho.Org: A Central Resource for Neuronal Morphologies. *Journal of Neuroscience*, 27(35):9247–9251.

[8] Aubert, A. and Costalat, R. (2002). A Model of the Coupling between Brain Electrical Activity, Metabolism, and Hemodynamics: Application to the Interpretation of Functional Neuroimaging. *NeuroImage*, 17(3):1162–1181.

[9] Avoli, M., de Curtis, M., Gnatkovsky, V., Gotman, J., Köhling, R., Lévesque, M., Manseau, F., Shiri, Z., and Williams, S. (2016). Specific imbalance of excitatory/inhibitory signaling establishes seizure onset pattern in temporal lobe epilepsy. *Journal of Neurophysiology*, 115(6):3229–3237.

[10] Azevedo, F. A., Carvalho, L. R., Grinberg, L. T., Farfel, J. M., Ferretti, R. E., Leite, R. E., Filho, W. J., Lent, R., and Herculano-Houzel, S. (2009). Equal numbers of neuronal and nonneuronal cells make the human brain an isometrically scaled-up primate brain. *The Journal of Comparative Neurology*, 513(5):532–541.

[11] Başar, E., Başar-Eroglu, C., Karakaş, S., and Schürmann, M. (2001). Gamma, alpha, delta, and theta oscillations govern cognitive processes. *International Journal of Psychophysiology*, 39(2-3):241–248.

[12] Baier, G., Goodfellow, M., Taylor, P. N., Wang, Y., and Garry, D. J. (2012). The importance of modeling epileptic seizure dynamics as spatio-temporal patterns. *Frontiers in Physiology*, 3(July):1–7.

[13] Baker, G. A. (2002). The Psychosocial Burden of Epilepsy. *Epilepsia*, 43:26–30.

[14] Barba, C., Rheims, S., Minotti, L., Guénot, M., Hoffmann, D., Chabardès, S., Isnard, J., Kahane, P., and Ryvlin, P. (2016). Temporal plus epilepsy is a major determinant of temporal lobe surgery failures. *Brain*, 139(2):444–451.

[15] Bear, M., Connors, B., and Paradiso, M. (2014). *NEUROSCIENCE Exploring the Brain*. Wolters Kluwer.

[16] Bear, M. F., Connors, B. W., and Paradiso, M. A. (2007). *Neuroscience: Exploring the Brain*. Philadelphia, PA : Lippincott Williams & Wilkins, c2007., 3rd editio edition.

[17] Becker, R., Knock, S., Ritter, P., and Jirsa, V. (2015). Relating Alpha Power and Phase to Population Firing and Hemodynamic Activity Using a Thalamocortical Neural Mass Model. *PLoS computational biology*, 11(9):e1004352.

[18] Becker, W., Worden, K., and Rowson, J. (2013). Bayesian sensitivity analysis of bifurcating nonlinear models. *Mechanical Systems and Signal Processing*, 34(1-2):57–75.

[19] Beleza, P. and Pinho, J. (2011). Frontal lobe epilepsy. *Journal of Clinical Neuroscience*, 18(5):593–600.

[20] Bender, E. A. (2000). *An Introduction to Mathematical Modeling*. Dover Publications.

[21] Berg, A. T. (2008). Risk of recurrence after a first unprovoked seizure. *Epilepsia*, 49(xx):13–18.

[22] Berg, A. T., Berkovic, S. F., Brodie, M. J., Buchhalter, J., Cross, J. H., Van Emde Boas, W., Engel, J., French, J., Glauser, T. A., Mathern, G. W., Moshé, S. L., Nordli, D., Plouin, P., and Scheffer, I. E. (2010). Revised terminology and concepts for organization of seizures and epilepsies: Report of the ILAE Commission on Classification and Terminology, 2005-2009. *Epilepsia*, 51(4):676–685.

[23] Berger, H. (1929). Uber das Elektrenkephalogramm des Menschen, 2nd report. *J Psychol Neurol (Leipzig)*, 40(1875):160–179.

[24] Betzel, R. F. and Bassett, D. S. (2017). Multi-scale brain networks. *NeuroImage*, 160(August):73–83.

[25] Beurle, R. L. (1956). Properties of a Mass of Cells Capable of Regenerating Pulses. *Philosophical Transactions of the Royal Society B: Biological Sciences*, 240(669):55–94.

[26] Bhattacharya, B. S., Coyle, D., and Maguire, L. P. (2011). A thalamo-cortico-thalamic neural mass model to study alpha rhythms in Alzheimer's disease. *Neural Networks*, 24(6):631–645.

[27] Billingsley, P. (1995). *Probability and measure.* wiley series in probability and mathematical statistics.

[28] Blanchard, P. (2006). *Differential equations*. Thomson Brooks/Cole.

[29] Blenkinsop, A., Valentin, A., Richardson, M. P., and Terry, J. R. (2012). The dynamic evolution of focal-onset epilepsies - combining theoretical and clinical observations. *European Journal of Neuroscience*, 36(2):2188–2200.

[30] Bojak, I. and Liley, D. T. J. (2005). Modeling the effects of anesthesia on the electroencephalogram. *Physical Review E*, 71(4):041902.

[31] Bollen, K. A. (1989). *Structural Equations with Latent Variables*. Wiley-Interscience.

[32] Bollimunta, A., Mo, J., Schroeder, C. E., and Ding, M. (2011). Neuronal Mechanisms and Attentional Modulation of Corticothalamic Alpha Oscillations. *Journal of Neuroscience*, 31(13):4935–4943.

[33] Boon, P., Raedt, R., De, V., Wyckhuys, T., and Vonck, K. (2009). Electrical Stimulation for the Treatment of Epilepsy. *Neurotherapeutics*, 6(2):218–227.

[34] Borgonovo, E. and Plischke, E. (2016). Sensitivity analysis: A review of recent advances. *European Journal of Operational Research*, 248(3):869–887.

[35] Boulesteix, A.-L., Janitza, S., Kruppa, J., and König, I. R. (2012). Overview of random forest methodology and practical guidance with emphasis on computational biology and bioinformatics. *Wiley Interdisciplinary Reviews: Data Mining and Knowledge Discovery*, 2(6):493–507.

[36] Box. . . , G. (1987). *Empirical model-building and response surfaces.* John Wiley & Sons, new york, edition.

[37] Breakspear, M. (2017). Dynamic models of large-scale brain activity. *Nature Neuroscience*, 20(3):340–352.

[38] Breakspear, M., Roberts, J. A., Terry, J. R., Rodrigues, S., Mahant, N., and Robinson, P. A. (2006). A Unifying Explanation of Primary Generalized Seizures Through Nonlinear Brain Modeling and Bifurcation Analysis. *Cerebral Cortex*, 16(9):1296–1313.

[39] Breiman, L. (1996). Bagging Predictors. *Machine Learning*, 24(421):123–140.

[40] Breiman, L. (2000). Some infinity theory for predictor ensembles. Technical report, University of California at Berkeley. Technical Report 577 (August 2000).

[41] Breiman, L. (2001). Random forest. *Machine Learning*, 45(1):5–32.

[42] Breiman, L. (2004). Consistency for a simple model of random forests. Technical report, University of California at Berkeley. Technical Report 670.

[43] Breiman, L., Friedman, J., Stone, C. J., and Olshen, R. (1984). *Classification and Regression Trees*. CRC press, wadsworth edition.

[44] Bressloff, P. C. (2012). Spatiotemporal dynamics of continuum neural fields. *Journal of Physics A: Mathematical and Theoretical*, 45(3):033001.

[45] Buffalo, E. A., Fries, P., Landman, R., Buschman, T. J., and Desimone, R. (2011). Laminar differences in gamma and alpha coherence in the ventral stream. *Proceedings of the National Academy of Sciences*, 108(27):11262–11267.

[46] Butcher, J. C. (1963). Coefficients for the study of Runge-Kutta integration processes. *Journal of the Australian Mathematical Society*, 3(02):185.

[47] Cadwallad, F. J. J. (1972). Commentary on the Nullity of Marriage Act 1971. *The Modern Law Review*, 35(1):57–72.

[48] Calderhead, B. and Girolami, M. (2008). Accelerating Bayesian inference over nonlinear differential equations with Gaussian processes. *Advances in neural . . . .*

[49] Calle, M. L. and Urrea, V. (2011). Letter to the Editor: Stability of Random Forest importance measures. *Briefings in Bioinformatics*, 12(1):86–89.

[50] Campolongo, F., Cariboni, J., and Saltelli, A. (2007). An effective screening design for sensitivity analysis of large models. *Environmental Modelling & Software*, 22(10):1509–1518.

[51] Caruana, R. and Niculescu-Mizil, A. (2006). An empirical comparison of supervised learning algorithms. In *Proceedings of the 23rd international conference on Machine learning - ICML '06*, pages 161–168, New York, New York, USA. ACM Press.

[52] Chaniotis, L. (2016). I was subjected to exorcisms as a child to treat my epilepsy. *Guardian*.

[53] Chen, C., Liaw, A., and Breiman, L. (2004). Using random forest to learn imbalanced data.

[54] Chen, H. and Boutros, P. C. (2011). VennDiagram: a package for the generation of highly-customizable Venn and Euler diagrams in R. *BMC Bioinformatics*, 12(1):35.

[55] Chen, P., Lin, J.-J., Lu, C.-S., Ong, C.-T., Hsieh, P. F., Yang, C.-C., Tai, C.-T., Wu, S.-L., Lu, C.-H., Hsu, Y.-C., Yu, H.-Y., Ro, L.-S., Lu, C.-T., Chu, C.-C., Tsai, J.-J., Su, Y.-H., Lan, S.-H., Sung, S.-F., Lin, S.-Y., Chuang, H.-P., Huang, L.-C., Chen, Y.-J., Tsai, P.-J., Liao, H.-T., Lin, Y.-H., Chen, C.-H., Chung, W.-H., Hung, S.-I., Wu, J.-Y., Chang, C.-F., Chen, L., Chen, Y.-T., and Shen, C.-Y. (2011). Carbamazepine-Induced Toxic Effects and HLA-B*1502 Screening in Taiwan. *New England Journal of Medicine*, 364(12):1126–1133.

[56] Chen, X., Liu, A., Chen, Q., Liu, Y., Zou, L., and McKeown, M. J. (2017). Simultaneous ocular and muscle artifact removal from EEG data by exploiting diverse statistics. *Computers in Biology and Medicine*, 88(February):1–10.

[57] Chilosi, A. M., Brovedani, P., Moscatelli, M., Bonanni, P., and Guerrini, R. (2006). Neuropsychological findings in idiopathic occipital lobe epilepsies. *Epilepsia*, 47(SUPPL. 2):76–78.

[58] Chiosa, V., Seeck, M., and Vulliémoz, S. (2010). Temporal Lobe Epilepsy : From Electro-Clinical Semiology to Surgical Outcome. *Epileptologie*, 27:94–100.

[59] Chowdhury, F. A., O'Gorman, R. L., Nashef, L., Elwes, R. D., Edden, R. A., Murdoch, J. B., Barker, G. J., and Richardson, M. P. (2015). Investigation of glutamine and GABA levels in patients with idiopathic generalized epilepsy using MEGAPRESS. *Journal of Magnetic Resonance Imaging*, 41(3):694–699.

[60] Colombetti, G. (2017). The Embodied and Situated Nature of Moods. *Philosophia (United States)*, 45(4):1437–1451.

[61] Cona, F., Lacanna, M., and Ursino, M. (2014). A thalamo-cortical neural mass model for the simulation of brain rhythms during sleep. *Journal of Computational Neuroscience*, 37(1):125–148.

[62] Cona, F., Zavaglia, M., Massimini, M., Rosanova, M., and Ursino, M. (2011). A neural mass model of interconnected regions simulates rhythm propagation observed via TMS-EEG. *NeuroImage*, 57(3):1045–1058.

[63] Cortes, C. and Vapnik, V. (1995). Support-vector networks. *Machine Learning*, 20(3):273–297.

[64] Cosandier-Rimélé, D., Bartolomei, F., Merlet, I., Chauvel, P., and Wendling, F. (2012). Recording of fast activity at the onset of partial seizures: Depth EEG vs. scalp EEG. *NeuroImage*, 59(4):3474–3487.

[65] Croft, R. and Barry, R. (2000). Removal of ocular artifact from the EEG: a review. *Neurophysiologie Clinique/Clinical Neurophysiology*, 30(1):5–19.

[66] David, B. (2005). *Epileptic*. Jonathan Cape.

[67] David, O. (2015). Neural Mass Models. In *Brain Mapping*, volume 1, pages 563–569. Elsevier.

[68] David, O. and Friston, K. J. (2003). A neural mass model for MEG/EEG: Coupling and neuronal dynamics. *NeuroImage*, 20(3):1743–1755.

[69] David, O., Kilner, J. M., and Friston, K. J. (2006). Mechanisms of evoked and induced responses in MEG/EEG. *NeuroImage*, 31:1580–1591.

[70] de Andrés, I., Garzón, M., and Reinoso-Suárez, F. (2011). Functional anatomy of non-REM sleep. *Frontiers in Neurology*, NOV(November):1–14.

[71] De Tisi, J., Bell, G. S., Peacock, J. L., McEvoy, A. W., Harkness, W. F., Sander, J. W., and Duncan, J. S. (2011). The long-term outcome of adult epilepsy surgery, patterns of seizure remission, and relapse: A cohort study. *The Lancet*, 378(9800):1388–1395.

[72] Deco, G., Jirsa, V. K., Robinson, P. A., Breakspear, M., and Friston, K. (2008). The dynamic brain: From spiking neurons to neural masses and cortical fields. *PLoS Computational Biology*, 4(8).

[73] DeFelipe, J., Alonso-Nanclares, L., and Arellano, J. I. (2002). Microstructure of the neocortex: Comparative aspects. *Journal of Neurocytology*, 31(3/5):299–316.

[74] Derchansky, M., Jahromi, S. S., Mamani, M., Shin, D. S., Sik, a., and Carlen, P. L. (2008). Transition to seizures in the isolated immature mouse hippocampus: a switch from dominant phasic inhibition to dominant phasic excitation. *The Journal of physiology*, 586(2):477–494.

[75] Doyle, A. C. (1921). *The Adventure of the Mazarin Stone*. CreateSpace Independent Publishing Platform.

[76] Dyson, F. (2004). A meeting with Enrico Fermi How one intuitive physicist rescued a team from fruitless research. *Nature*, 427(January):8540.

[77] Dytham, C. (2011). *Choosing and using statistics: a biologist's guide*. John Wiley & Sons.

[78] Ebden, M. (2015). Gaussian Processes: A Quick Introduction. (August).

[79] Edelvik, A., Rydenhag, B., Olsson, I., Flink, R., Kumlien, E., Kallen, K., and Malmgren, K. (2013). Long-term outcomes of epilepsy surgery in Sweden: A national prospective and longitudinal study. *Neurology*, 81(14):1244–1251.

[80] Eykhoff, P. (1974). *System identification; parameter and state estimation*. Wiley.

[81] Falcon, M. I., Jirsa, V., and Solodkin, A. (2016). A new neuroinformatics approach to personalized medicine in neurology. *Current Opinion in Neurology*, 29(4):429–436.

[82] Fernández-Delgado, M., Cernadas, E., Barro, S., Amorim, D., and Amorim Fernández-Delgado, D. (2014). Do we Need Hundreds of Classifiers to Solve Real World Classification Problems? *Journal of Machine Learning Research*, 15:3133–3181.

[83] Ferrat, L. A., Goodfellow, M., and Terry, J. R. (2018). Classifying dynamic transitions in high dimensional neural mass models: A random forest approach. *PLOS Computational Biology*, 14(3):e1006009.

[84] Fisher, R. S., Acevedo, C., Arzimanoglou, A., Bogacz, A., Cross, J. H., Elger, C. E., Engel, J., Forsgren, L., French, J. A., Glynn, M., Hesdorffer, D. C., Lee, B. I., Mathern, G. W., Moshé, S. L., Perucca, E., Scheffer, I. E., Tomson, T., Watanabe, M., and Wiebe, S. (2014). ILAE Official Report: A practical clinical definition of epilepsy. *Epilepsia*, 55(4):475–482.

[85] Fisher, R. S., Boas, W. v. E., Blume, W., Elger, C., Genton, P., Lee, P., and Engel, J. (2005). Epileptic Seizures and Epilepsy: Definitions Proposed by the International League Against Epilepsy (ILAE) and the International Bureau for Epilepsy (IBE). *Epilepsia*, 46(4):470–472.

[86] Fisher, R. S., Cross, J. H., D'Souza, C., French, J. A., Haut, S. R., Higurashi, N., Hirsch, E., Jansen, F. E., Lagae, L., Moshé, S. L., Peltola, J., Roulet Perez, E., Scheffer, I. E., Schulze-Bonhage, A., Somerville, E., Sperling, M., Yacubian, E. M., and Zuberi, S. M. (2017). Instruction manual for the ILAE 2017 operational classification of seizure types. *Epilepsia*, 58(4):531–542.

[87] Fogelson, N., Litvak, V., Peled, A., Fernandez-del Olmo, M., and Friston, K. (2014). The functional anatomy of schizophrenia: A dynamic causal modeling study of predictive coding. *Schizophrenia Research*, 158(1-3):204–212.

[88] Freeman, W. J. (1975). Mass action in the nervous system. *Neuroscience*, 1(5):423.

[89] Freeman, W. J. (1979a). EEG analysis gives model of neuronal template-matching mechanism for sensory search with olfactory bulb. *Biological Cybernetics*, 35(4):221–234.

[90] Freeman, W. J. (1979b). Nonlinear dynamics of paleocortex manifested in the olfactory EEG. *Biological Cybernetics*, 35(1):21–37.

[91] Freeman, W. J. (1979c). Nonlinear gain mediating cortical stimulus-response relations. *Biological Cybernetics*, 33(4):237–247.

[92] Freeman, W. J. (1987). Simulation of chaotic EEG patterns with a dynamic model of the olfactory system. *Biological Cybernetics*, 56(2-3):139–150.

[93] Freestone, D., Kuhlmann, L., Chong, M., Nešić, D., Grayden, D., Aram, P., Postoyan, R., and Cook, M. (2013). Patient-Specific Neural Mass Modeling-Stochastic and Deterministic Methods. In *Recent Advances in Predicting and Preventing Epileptic Seizures*, pages 63–82. WORLD SCIENTIFIC.

[94] Freestone, D. R., Karoly, P. J., NeÅ¡iÄ‡, D., Aram, P., Cook, M. J., and Grayden, D. B. (2014). Estimation of effective connectivity via data-driven neural modeling. *Frontiers in Neuroscience*, 8(November):1–20.

[95] Freestone, D. R., Layton, K. J., Kuhlmann, L., and Cook, M. J. (2017). Statistical Performance Analysis of Data-Driven Neural Models. *International Journal of Neural Systems*, 27(01):1650045.

[96] Friedman, J. H. (2001). Greedy function approximation:a gradient boosting machine. *The Annals of Statistics*, 29(5):1189–1232.

[97] Friedman, J. H. and Popescu, B. E. (2008). Predictive learning via rule ensembles. *The Annals of Applied Statistics*, 2(3):916–954.

[98] Friston, K., Harrison, L., and Penny, W. (2003). Dynamic causal modelling. *NeuroImage*, 19(4):1273–1302.

[99] Friston, K., Kiebel, S., Garrido, M., and David, O. (2007). Dynamic causal models for EEG. *Statistical Parametric Mapping: The Analysis of Functional Brain Images*, pages 561–576.

[100] Geng, S. and Zhou, W. (2017). Influence of extrinsic inputs and synaptic gains on dynamics of Wendling's neural mass model: A bifurcation analysis. *Journal of Integrative Neuroscience*, 15(3):1–21.

[101] Gerber, U. (2003). Metabotropic glutamate receptors in vertebrate retina. *Documenta ophthalmologica. Advances in ophthalmology*, 106(1):83–7.

[102] Goldstein, A., Kapelner, A., Bleich, J., and Pitkin, E. (2015). Peeking Inside the Black Box: Visualizing Statistical Learning With Plots of Individual Conditional Expectation. *Journal of Computational and Graphical Statistics*, 24(1):44–65.

[103] Goldstein, B. A., Polley, E. C., and Briggs, F. B. S. (2011). Random Forests for Genetic Association Studies. *Statistical Applications in Genetics and Molecular Biology*, 10(1):32.

[104] Goltsev, A. V., de Abreu, F. V., Dorogovtsev, S. N., and Mendes, J. F. F. (2010). Stochastic cellular automata model of neural networks. *Physical Review E*, 81(6):061921.

[105] Goodfellow, I., Bengio, Y., and Courville, A. (2016a). Deep Learning. In *Deep Learning*. MIT Press.

[106] Goodfellow, M., Rummel, C., Abela, E., Richardson, M. P., Schindler, K., and Terry, J. R. (2016b). Estimation of brain network ictogenicity predicts outcome from epilepsy surgery. *Scientific reports*, 6(0):29215.

[107] Goodfellow, M., Schindler, K., and Baier, G. (2011). Intermittent spike-wave dynamics in a heterogeneous, spatially extended neural mass model. *NeuroImage*, 55(3):920–932.

[108] Goodfellow, M., Schindler, K., and Baier, G. (2012). Self-organised transients in a neural mass model of epileptogenic tissue dynamics. *NeuroImage*, 59(3):2644–2660.

[109] Gramacy, R. and Lee, H. (2008). Bayesian Treed Gaussian Process Models with an Application to Computer Modeling. *Journal of the American Statistical Asociation*, 103(October):1119–1130.

[110] Gramacy, R. B. and Lee, H. K. H. (2007). Bayesian treed Gaussian process models with an application to computer modeling. page 32.

[111] Grech, R., Cassar, T., Muscat, J., Camilleri, K. P., Fabri, S. G., Zervakis, M., Xanthopoulos, P., Sakkalis, V., and Vanrumste, B. (2008). Review on solving the inverse problem in EEG source analysis. *J Neuroeng Rehabil*, 5:25.

[112] Greenland, S., Senn, S. J., Rothman, K. J., Carlin, J. B., Poole, C., Goodman, S. N., and Altman, D. G. (2016). Statistical tests, P values, confidence intervals, and power: a guide to misinterpretations. *European Journal of Epidemiology*, 31(4):337–350.

[113] Gross, T., Rudolf, L., Levin, S. A., and Dieckmann, U. (2009). Generalized Models Reveal Stabilizing Factors in Food Webs. *Science*, 325(5941):747–750.

[114] Gulledge, A. T., Kampa, B. M., and Stuart, G. J. (2005). Synaptic integration in dendritic trees. *Journal of Neurobiology*, 64(1):75–90.

[115] Gurbani, S., Chayasirisobhon, S., Cahan, L., Choi, S., Enos, B., Hwang, J., Lin, M., and Schweitzer, J. (2016). Neuromodulation Therapy with Vagus Nerve Stimulation for Intractable Epilepsy: A 2-Year Efficacy Analysis Study in Patients under 12 Years of Age. *Epilepsy Research and Treatment*, 2016:1–5.

[116] Haegens, S., Cousijn, H., Wallis, G., Harrison, P. J., and Nobre, A. C. (2014). Inter- and intra-individual variability in alpha peak frequency. *NeuroImage*, 92:46–55.

[117] Halgren, M., Devinsky, O., Doyle, W. K., Bastuji, H., Rey, M., Mak-McCully, R., Chauvel, P., Ulbert, I., Fabo, D., Wittner, L., Heit, G., Eskandar, E., Mandell, A., and Cash, S. S. (2017). The Generation and Propagation of the Human Alpha Rhythm. *bioRxiv*.

[118] Halpern, C. H., Samadani, U., Litt, B., Jaggi, J. L., and Baltuch, G. H. (2008). Deep brain stimulation for epilepsy. *Neurotherapeutics*, 5(1):59–67.

[119] Halsey, L. G., Curran-Everett, D., Vowler, S. L., and Drummond, G. B. (2015). The fickle P value generates irreproducible results. *Nature Methods*, 12(3):179–185.

[120] Hansen, N. (2006). Towards a new evolutionary computation advances in the estimation of distribution algorithms, vol. 192 de. *Studies in Fuzziness and Soft Computing*, pages 75–102.

[121] Harden, C., Tomson, T., Gloss, D., Buchhalter, J., Cross, J. H., Donner, E., French, J. A., Gil-Nagel, A., Hesdorffer, D. C., Smithson, W. H., Spitz, M. C., Walczak, T. S., Sander, J. W., and Ryvlin, P. (2017). Practice guideline summary: Sudden unexpected death in epilepsy incidence rates and risk factors. *Neurology*, 88(17):1674–1680.

[122] Hastie, T., Tibshirani, R., and Friedman, J. (2009). Random Forests. In *Vasa*, pages 1–18.

[123] Hastie, T. and Tibshirani, R. F. (2009). *The Elements of Statistical Learning*, volume 1 of *Springer Series in Statistics*. Springer New York, New York, NY.

[124] Hebbink, J. (2014). *Activity types in a neural mass model*. PhD thesis, University of Twente.

[125] Heskes, T. (1997). Practical confidence and prediction intervals. *Advances in neural information processing systems*, (i):176–182.

[126] Hindriks, R. and van Putten, M. J. (2013). Thalamo-cortical mechanisms underlying changes in amplitude and frequency of human alpha oscillations. *NeuroImage*, 70:150–163.

[127] Hodgkin, A. L. and Huxley, A. F. (1952). A Quantitative Description of Membrane Current and its Application to Conduction and Excitation in Nerves. *J. Physiol.*, 117:500–544.

[128] Homma, T. and Saltelli, A. (1996). Importance measures in global sensitivity analysis of nonlinear models. *Reliability Engineering & System Safety*, 52(1):1–17.

[129] Horvath, A. (2018). EEG and ERP biomarkers of Alzheimer rsquo s disease a critical review. *Frontiers in Bioscience*, 23(1):4587.

[130] Houston, C. M., Bright, D. P., Sivilotti, L. G., Beato, M., and Smart, T. G. (2009). Intracellular Chloride Ions Regulate the Time Course of GABA-Mediated Inhibitory Synaptic Transmission. *Journal of Neuroscience*, 29(33):10416–10423.

[131] Howland, R. H. (2014). Vagus Nerve Stimulation. *Current Behavioral Neuroscience Reports*, 1(2):64–73.

[132] Hrachovy, R. A. and Frost, J. D. (2006). The EEG in selected generalized seizures. *Journal of Clinical Neurophysiology*, 23(4):312–332.

[133] Huberfeld, G., Wittner, L., Clemenceau, S., Baulac, M., Kaila, K., Miles, R., and Rivera, C. (2007). Perturbed Chloride Homeostasis and GABAergic Signaling in Human Temporal Lobe Epilepsy. *Journal of Neuroscience*, 27(37):9866–9873.

[134] Hughes, S. W., Lőrincz, M. L., Blethyn, K., Kékesi, K. A., Juhász, G., Turmaine, M., Parnavelas, J. G., and Crunelli, V. (2011). Thalamic Gap Junctions Control Local Neuronal Synchrony and Influence Macroscopic Oscillation Amplitude during EEG Alpha Rhythms. *Frontiers in psychology*, 2(AUG):193.

[135] Huneau, C., Benquet, P., Dieuset, G., Biraben, A., Martin, B., and Wendling, F. (2013). Shape features of epileptic spikes are a marker of epileptogenesis in mice. *Epilepsia*, 54(12):2219–2227.

[136] Hyafil, L. and Rivest, R. L. (1976). Constructing optimal binary decision trees is NP-complete. *Information Processing Letters*, 5(1):15–17.

[137] Hyndman, R. J. (2013). The difference between prediction intervals and confidence intervals.

[138] Ishwaran, H. (2007). Variable importance in binary regression trees and forests. *Electronic Journal of Statistics*, 1:519–537.

[139] Izhikevich, E. M. (2003). Simple model of spiking neurons. *IEEE Transactions on Neural Networks*, 14(6):1569–1572.

[140] Jansen, B. H. and Rit, V. G. (1995). Electroencephalogram and visual evoked potential generation in a mathematical model of coupled cortical columns. *Biological Cybernetics*, 73(4):357–366.

[141] Jansen, B. H., Zouridakis, G., and Brandt, M. E. (1993). A neurophysiologically-based mathematical model of flash visual evoked potentials. *Biological Cybernetics*, 68:275–283.

[142] Jedynak, M., Pons, A. J., Garcia-Ojalvo, J., and Goodfellow, M. (2017). Temporally correlated fluctuations drive epileptiform dynamics. *NeuroImage*, 146(July 2016):188–196.

[143] Jessen, K. R. and Mirsky, R. (1980). Glial cells in the enteric nervous system contain glial fibrillary acidic protein. *Nature*, 286(5774):736–737.

[144] Jilek-Aall, L. (1999). Morbus sacer in Africa: some religious aspects of epilepsy in traditional cultures. *Epilepsia*, 40(3):382–386.

[145] Jobst, B. C. and Cascino, G. D. (2015). Resective epilepsy surgery for drug-resistant focal epilepsy: A review. *JAMA - Journal of the American Medical Association*, 313(3):285–293.

[146] Kamal, A., Artola, A., Biessels, G. J., Gispen, W. H., and Ramakers, G. M. J. (2003). Increased spike broadening and slow afterhyperpolarization in CA1 pyramidal cells of streptozotocin-induced diabetic rats. *Neuroscience*, 118(2):577–583.

[147] Kloster, R. and Engelskjøn, T. (1999). Sudden unexpected death in epilepsy (SUDEP): a clinical perspective and a search for risk factors. *Journal of neurology, neurosurgery, and psychiatry*, 67(4):439–444.

[148] Koenker, R. (1994). Confidence Intervals for Regression Quantiles. In *Asymptotic Statistics*, number 1978, pages 349–359. Physica, Heidelberg.

[149] Koenker, R. (2017). quantreg: Quantile Regression.

[150] Koutroumanidis, M., Arzimanoglou, A., Caraballo, R., Goyal, S., Kaminska, A., Laoprasert, P., Oguni, H., Rubboli, G., Tatum, W., Thomas, P., Trinka, E., Vignatelli, L., and Moshé, S. L. (2017). The role of EEG in the diagnosis and classification of the epilepsy syndromes: a tool for clinical practice by the ILAE Neurophysiology Task Force (Part 2). *Epileptic Disorders*, 19(4):385–437.

[151] Krauskopf, B., Osinga, H. M., and Galán-Vioque, J. (2007). *Numerical Continuation Methods for Dynamical Systems*. Springer Netherlands, Dordrecht.

[152] Kuhlmann, L., Freestone, D. R., Manton, J. H., Heyse, B., Vereecke, H. E., Lipping, T., Struys, M. M., and Liley, D. T. (2016). Neural mass model-based tracking of anesthetic brain states. *NeuroImage*, 133:438–456.

[153] Kutner, M. H., Nachtsheim, C. J., Neter, J., and Li, W. (2010). *Applied Linear Statistical Models Fifth Edition*. McGraw-Hill/Irwin.

[154] Kwon, O.-Y. and Park, S.-P. (2014). Depression and anxiety in people with epilepsy. *Journal of clinical neurology (Seoul, Korea)*, 10(3):175–88.

[155] Lachaux, J. P., Rudrauf, D., and Kahane, P. (2003). Intracranial EEG and human brain mapping. *Journal of Physiology Paris*, 97(4-6):613–628.

[156] Ladino, L. D., Rizvi, S., and Téllez-Zenteno, J. F. (2016). Epilepsy through the ages: An artistic point of view. *Epilepsy and Behavior*, 57:255–264.

[157] Larsson, P. G. and Kostov, H. (2005). Lower frequency variability in the alpha activity in EEG among patients with epilepsy. *Clinical Neurophysiology*, 116(11):2701–2706.

[158] Lee, P. F., Kan, D. P. X., Croarkin, P., Phang, C. K., and Doruk, D. (2018). Neurophysiological correlates of depressive symptoms in young adults: A quantitative EEG study. *Journal of Clinical Neuroscience*, 47:315–322.

[159] Leisch, F. and Dimitriadou, E. (2010). mlbench: Machine Learning Benchmark Problems.

[160] Liley, D., Cadusch, P., and Dafilis, M. (2002). A spatially continuous mean field theory of electrocortical activity. *Network: Computation in Neural Systems*, 13(1):67–113.

[161] Liu, X., Gao, J., Wang, G., and Chen, Z.-W. (2017). Controllability Analysis of the Neural Mass Model with Dynamic Parameters. *Neural Computation*, 29(2):485–501.

[162] Lopes da Silva, F., Amitai, Y., and Connors, B. (1991). Intrinsic oscillations of neocortex generated by layer 5 pyramidal neurons. *Science*, 251(4992):432–435.

[163] Lopes da Silva, F., Blanes, W., Kalitzin, S., Parra, J., Suffczynski, P., and Velis, D. (2003). Dynamical diseases of brain systems: different routes to epileptic seizures. *IEEE Transactions on Biomedical Engineering*, 50(5):540–548.

[164] Lopes da Silva, F., Blanes, W., Kalitzin, S. N., Parra, J., Suffczynski, P., and Velis, D. N. (2003). Epilepsies as Dynamical Diseases of Brain Systems: Basic Models of the Transition Between Normal and Epileptic Activity. *Epilepsia*, 44(s12):72–83.

[165] Lopes da Silva, F. H., Hoeks, A., Smits, H., and Zetterberg, L. H. (1974). Model of brain rhythmic activity - The alpha-rhythm of the thalamus. *Kybernetik*, 15(1):27–37.

[166] Lopes da Silva, F. H., van Rotterdam, A., Barts, P., van Heusden, E., and Burr, W. (1976). Models of Neuronal Populations: The Basic Mechanisms of Rhythmicity. *Progress in Brain Research*, 45(C):281–308.

[167] Lorente de Nó, R. (1938). Architectonics and structure of the cerebral cortex. *Physiology of the nervous system*, pages 291–330.

[168] Lorenz, E. N. (1963). Deterministic Nonperiodic Flow. *Journal of the Atmospheric Sciences*, 20(2):130–141.

[169] Lőrincz, M. L., Kékesi, K. A., Juhász, G., Crunelli, V., and Hughes, S. W. (2009). Temporal Framing of Thalamic Relay-Mode Firing by Phasic Inhibition during the Alpha Rhythm. *Neuron*, 63(5):683–696.

[170] Lu, M. and Ishwaran, H. (2017). A Machine Learning Alternative to P-values.

[171] Lüders, H. O., Najm, I., Nair, D., Widdess-Walsh, P., and Bingman, W. (2006). The epileptogenic zone: General principles. *Epileptic Disorders*, 8(SUPPL. 2):1–9.

[172] Lytton, W. W. (2008). Computer modelling of epilepsy. *Nature reviews. Neuroscience*, 9(8):626–637.

[173] Mahjoory, K., Nikulin, V. V., Botrel, L., Linkenkaer-Hansen, K., Fato, M. M., and Haufe, S. (2017). Consistency of EEG source localization and connectivity estimates. *NeuroImage*, 152(February):590–601.

[174] Mankin, J. B., O'Neill, R. V., Shugart, H. H., and Rust, B. W. (1975). The importance of validation in ecosystems analysis.

[175] Marreiros, A. C., Daunizeau, J., Kiebel, S. J., and Friston, K. J. (2008). Population dynamics: Variance and the sigmoid activation function. *NeuroImage*, 42(1):147–157.

[176] McKay, M. D., Beckman, R. J., and Conover, W. J. (1979). Comparison of Three Methods for Selecting Values of Input Variables in the Analysis of Output from a Computer Code. *Technometrics*, 21(2):239–245.

[177] Melnik, R. (2015). Universality of Mathematical Models in Understanding Nature, Society, and Man-Made World. In *Mathematical and Computational Modeling*, chapter 1, pages 1–16. John Wiley & Sons, Inc, Hoboken, NJ.

[178] Milborrow, S. (2017). rpart.plot: Plot 'rpart' Models: An Enhanced Version of 'plot.rpart' version 2.1.2.

[179] Miller, K. D. (2003). Understanding layer 4 of the cortical circuit: a model based on cat V1. *Cerebral cortex (New York, N.Y. : 1991)*, 13(1):73–82.

[180] Milton, J. G. (2010). Epilepsy as a dynamic disease: A tutorial of the past with an eye to the future. *Epilepsy and Behavior*, 18(1-2):33–44.

[181] Mohammad, Y., Al-Hussain, F., Hussain, S., and Al Raddadi, K. K. (2016). Traditional treatment of epilepsy. *Neurology*, 87(10):1064–1064.

[182] Mohammed, H. S., Kaufman, C. B., Limbrick, D. D., Steger-May, K., Grubb, R. L., Rothman, S. M., Weisenberg, J. L. Z., Munro, R., and Smyth, M. D. (2012). Impact of epilepsy surgery on seizure control and quality of life: A 26-year follow-up study. *Epilepsia*, 53(4):712–720.

[183] Molaee-Ardekani, B., Benquet, P., Bartolomei, F., and Wendling, F. (2010). Computational modeling of high-frequency oscillations at the onset of neocortical partial seizures: From 'altered structure' to 'dysfunction'. *NeuroImage*, 52(3):1109–1122.

[184] Moran, R., Kiebel, S., Stephan, K., Reilly, R., Daunizeau, J., and Friston, K. (2007). A neural mass model of spectral responses in electrophysiology. *NeuroImage*, 37(3):706–720.

[185] Moran, R., Pinotsis, D. a., and Friston, K. (2013). Neural masses and fields in dynamic causal modeling. *Frontiers in computational neuroscience*, 7(May):57.

[186] Mountcastle, V. B. (1957). Modality and topographic properties of single neurons of cat's somatic sensory cortex. *Journal of neurophysiology*, 20(4):408–34.

[187] Murakami, S. and Okada, Y. (2006). Contributions of principal neocortical neurons to magnetoencephalography and electroencephalography signals. *The Journal of Physiology*, 575(3):925–936.

[188] Nadkarni, S. and Devinsky, O. (2005). Psychotropic Effects of Antiepileptic Drugs. *Epilepsy Currents*, 5(5):176–181.

[189] Najm, I., Jehi, L., Palmini, A., Gonzalez-Martinez, J., Paglioli, E., and Bingaman, W. (2013). Temporal patterns and mechanisms of epilepsy surgery failure. *Epilepsia*, 54(5):772–782.

[190] Nevado-Holgado, A. J., Marten, F., Richardson, M. P., and Terry, J. R. (2012). Characterising the dynamics of EEG waveforms as the path through parameter space of a neural mass model: Application to epilepsy seizure evolution. *NeuroImage*, 59(3):2374–2392.

[191] Ngugi, A. K., Bottomley, C., Kleinschmidt, I., Sander, J. W., and Newton, C. R. (2010). Estimation of the burden of active and life-time epilepsy: A meta-analytic approach. *Epilepsia*, 51(5):883–890.

[192] Niedermeyer, E. (1997). Alpha rhythms as physiological and abnormal phenomena. *International Journal of Psychophysiology*, 26(1-3):31–49.

[193] Oakley, J. E. and O'Hagan, A. (2004). Probabilistic sensitivity analysis of complex models: A Bayesian approach. *Journal of the Royal Statistical Society. Series B: Statistical Methodology*, 66(3):751–769.

[194] Obeid, T., Abulaban, A., Al-Ghatani, F., Al-Malki, A. R., and Al-Ghamdi, A. (2012). Possession by 'Jinn' as a cause of epilepsy (Saraa): A study from Saudi Arabia. *Seizure*, 21(4):245–249.

[195] Olejniczak, P. (2006). Neurophysiologic basis of EEG. *Journal of Clinical Neurophysiology*, 23(3):186–189.

[196] Olesen, J., Gustavsson, A., Svensson, M., Wittchen, H. U., and Jönsson, B. (2012). The economic cost of brain disorders in Europe. *European Journal of Neurology*, 19(1):155–162.

[197] Pal, M. and Mather, P. M. (2003). An assessment of the effectiveness of decision tree methods for land cover classification. *Remote Sensing of Environment*, 86(4):554–565.

[198] Panayiotopoulos, C. P. (2010). *A Clinical Guide to Epileptic Syndromes and their Treatment*, volume 14. Springer London, London.

[199] Pearce, J. M. S. (2002). Bromide, the first effective antiepileptic agent. *Journal of neurology, neurosurgery, and psychiatry*, 72(3):412.

[200] Pearce, R. A. (1993). Physiological evidence for two distinct GABAA responses in rat hippocampus. *Neuron*, 10(2):189–200.

[201] Pelikan, M., Goldberg, D. E., and Cantu-Paz, E. (1999). *BOA: The Bayesian Optimization Algorithm*. Morgan Kaufmann.

[202] Pesenson, M. M. Z. (2013). Introduction: Multiscale Analysis - Modeling, Data, Networks, and Nonlinear Dynamics. In *Multiscale Analysis and Nonlinear Dynamics*, pages 1–17. Wiley-VCH Verlag GmbH & Co. KGaA, Weinheim, Germany.

[203] Peterson, A. D. (2015). *The Neurodynamics of Epilepsy: A Bifurcation Analysis of the Effects of Conductance-based Synapses on the Transition to Seizure in a Neural Field Model*. PhD thesis, University of Melbourne.

[204] Pianosi, F., Beven, K., Freer, J., Hall, J. W., Rougier, J., Stephenson, D. B., and Wagener, T. (2016). Sensitivity analysis of environmental models: A systematic review with practical workflow. *Environmental Modelling & Software*, 79:214–232.

[205] Pisapia, J. and Baltuch, G. (2016). Vagus nerve stimulation. In *Neuromodulation in Psychiatry*, pages 325–334. John Wiley & Sons, Ltd, Chichester, UK.

[206] Press, W., Teukolsky, S., Vetterling, W., and Flannery, B. (1992). *Numerical Recipes in C - The Art of Scientific Computing*. Cambridge University Press.

[207] Prilipko, L., Saxena, S., and Boer, H. (2005). *Atlas : epilepsy care in the world*, volume 129. World Health Organization.

[208] Quinlan, J. R. (1990). Learning logical definitions from relations. *Machine Learning*, 5(3):239–266.

[209] R Core Team (2008). *Computational Many-Particle Physics*, volume 739 of *Lecture Notes in Physics*. Springer Berlin Heidelberg, Berlin, Heidelberg.

[210] Razavi, S. and Gupta, H. V. (2016a). A new framework for comprehensive, robust, and efficient global sensitivity analysis: 1. Theory. *Water Resources Research*, 52(1):423–439.

[211] Razavi, S. and Gupta, H. V. (2016b). A new framework for comprehensive, robust, and efficient global sensitivity analysis: 2. Application. *Water Resources Research*, 52(1):440–455.

[212] Rennie, C. J., Robinson, P. A., and Wright, J. J. (1999). Effects of local feedback on dispersion of electrical waves in the cerebral cortex. *Physical Review E*, 59(3):3320–3329.

[213] Robinson, D. L. (1983). An Analysis of Human Eeg Responses in the Alpha Range of Frequencies. *International Journal of Neuroscience*, 22(1-2):81–98.

[214] Robinson, P., Rennie, C., and Wright, J. (1997). Propagation and stability of waves of electrical activity in the cerebral cortex. *Physical Review E*, 56(1):826–840.

[215] Robinson, P. A., Rennie, C. J., Rowe, D. L., and O'Connor, C. (2004a). Estimation of multiscale neurophysiologic parameters by electroencephalographic means. *Human Brain Mapping*, 23(1):53–72.

[216] Robinson, P. A., Rennie, C. J., Rowe, D. L., and O'Connor, C. (2004b). Estimation of multiscale neurophysiologic parameters by electroencephalographic means. *Human Brain Mapping*, 23(1):53–72.

[217] Rosch, R. E., Hunter, P., Baldeweg, T., Friston, K., and Meyer, M. (2017). Imaging and dynamic causal modelling reveal brain-wide changes in effective connectivity and synaptic dynamics during epileptic seizures. *bioRxiv*.

[218] Rossi, S., Hallett, M., Rossini, P. M., and Pascual-Leone, A. (2012). Safety, ethical considerations, and application guidelines for the use of transcranial magnetic stimulation in clinical practice and research. *Clinical Neurophysiology*, 120(12):323–330.

[219] Rowe, D. L., Robinson, P. A., and Rennie, C. J. (2004). Estimation of neurophysiological parameters from the waking EEG using a biophysical model of brain dynamics. *Journal of Theoretical Biology*, 231(3):413–433.

[220] Rubinov, M. and Sporns, O. (2010). Complex network measures of brain connectivity: uses and interpretations. *NeuroImage*, 52(3):1059–69.

[221] Saalmann, Y. B., Pinsk, M. A., Wang, L., Li, X., and Kastner, S. (2012). The Pulvinar Regulates Information Transmission Between Cortical Areas Based on Attention Demands. *Science*, 337(6095):753–756.

[222] Saltelli, A., Annoni, P., Azzini, I., Campolongo, F., Ratto, M., and Tarantola, S. (2010). Variance based sensitivity analysis of model output. Design and estimator for the total sensitivity index. *Computer Physics Communications*, 181(2):259–270.

[223] San-juan, D., Morales-Quezada, L., Orozco Garduño, A. J., Alonso-Vanegas, M., González-Aragón, M. F., Espinoza López, D. A., Vázquez Gregorio, R., Anschel, D. J., and Fregni, F. (2015). Transcranial Direct Current Stimulation in Epilepsy. *Brain Stimulation*, 8(3):455–464.

[224] Scheirer, C. J., Ray, W. S., and Hare, N. (1976). The analysis of ranked data derived from completely randomized factorial designs. *Biometrics*, pages 429–434.

[225] Schellenberger Costa, M., Weigenand, A., Ngo, H. V. V., Marshall, L., Born, J., Martinetz, T., and Claussen, J. C. (2016). A Thalamocortical Neural Mass Model of the EEG during NREM Sleep and Its Response to Auditory Stimulation. *PLoS Computational Biology*, 12(9):1–20.

[226] Schmidt, D. and Schachter, S. C. (2014). Drug treatment of epilepsy in adults. *The BMJ*, 348:g254.

[227] Schmidt, H., Woldman, W., Goodfellow, M., Chowdhury, F. A., Koutroumanidis, M., Jewell, S., Richardson, M. P., and Terry, J. R. (2016). A computational biomarker of idiopathic generalized epilepsy from resting state EEG. *Epilepsia*, 57(10):e200–e204.

[228] Schomer, D. and Lopes da Silva, F. (2012). *Niedermeyer's Electroencephalography: Basic Principles, Clinical Applications, and Related Fields*. Oxford University Press, sixth edit edition.

[229] Schwartz, M. and Schmidt, G. (1973). Principles of Electrodynamics. *American Journal of Physics*, 41(7):938–939.

[230] Scornet, E., Biau, G., and Vert, J.-P. (2015). Consistency of random forests. *The Annals of Statistics*, 43(4):1716–1741.

[231] Shah, A. and Mittal, S. (2014). Invasive electroencephalography monitoring: Indications and presurgical planning. *Annals of Indian Academy of Neurology*, 17(5):89.

[232] Shakirullah, Ali, N., Khan, A., and Nabi, M. (2014). The Prevalence, Incidence and Etiology of Epilepsy. *International Journal of Clinical and Experimental Neurology*, 2(2):29–39.

[233] Shan, B., Wang, J., Deng, B., Wei, X., Yu, H., Zhang, Z., and Li, H. (2016). Particle swarm optimization algorithm based parameters estimation and control of epileptiform spikes in a neural mass model. *Chaos: An Interdisciplinary Journal of Nonlinear Science*, 26(7):073118.

[234] Shwedyk, E., Balasubramanian, R., and Scott, R. N. (1977). A Nonstationary Model for the Electromyogram. *IEEE Transactions on Biomedical Engineering*, BME-24(5):417–424.

[235] Singh, A., Sabharwal, P., and Shepherd, T. (2017). Neuroimaging in Epilepsy. In *Epilepsy Board Review*, volume 05, pages 273–291. Springer New York, New York, NY.

[236] Singh, A. and Trevick, S. (2016). The Epidemiology of Global Epilepsy. *Neurologic Clinics*, 34(4):837–847.

[237] Slingerland, R. and Lee, K. (2011). Princeton University Press. In *Mathematical Modeling of Earth's Dynamical Systems*, chapter Modeling a, pages 1–22. Princeton University Press.

[238] Smith, M. L., Olds, J., Snyder, T., Elliott, I., Lach, L., and Whiting, S. (2014). A follow-up study of cognitive function in young adults who had resective epilepsy surgery in childhood. *Epilepsy & Behavior*, 32(October):79–83.

[239] Sobol, I. (2001). Global sensitivity indices for nonlinear mathematical models and their Monte Carlo estimates. *Mathematics and Computers in Simulation*, 55(1-3):271–280.

[240] Sossin, W. S., Sweet-Cordero, a., and Scheller, R. H. (1990). Dale's hypothesis revisited: different neuropeptides derived from a common prohormone are targeted to different processes. *Proceedings of the National Academy of Sciences of the United States of America*, 87(June):4845–4848.

[241] Sotero, R. C., Bortel, A., Martínez-Cancino, R., Neupane, S., O'Connor, P., Carbonell, F., and Shmuel, A. (2010). Anatomically-constrained effective connectivity among layers in a cortical column modeled and estimated from local field potentials. *Journal of Integrative Neuroscience*, 09(04):355–379.

[242] Sperling, M. R. (2004). The consequences of uncontrolled epilepsy. *CNS spectrums*, 9(2):98–101, 106–9.

[243] Spiegler, A. (2011). *Dynamics of biologically informed neural mass models of the brain*. PhD thesis, Universitatsverlag Ilmenau.

[244] Spiegler, A., Kiebel, S. J., Atay, F. M., and Knösche, T. R. (2010). Bifurcation analysis of neural mass models: Impact of extrinsic inputs and dendritic time constants. *NeuroImage*, 52(3):1041–1058.

[245] Sporns, O., Tononi, G., and Kötter, R. (2005). The Human Connectome: A Structural Description of the Human Brain. *PLoS Computational Biology*, 1(4):e42.

[246] Sprengers, M., Vonck, K., Carrette, E., Marson, A. G., and Boon, P. (2017). Deep brain and cortical stimulation for epilepsy. In Boon, P., editor, *Cochrane Database of Systematic Reviews*, number 6. John Wiley & Sons, Ltd, Chichester, UK.

[247] Staley, K. J. and Dudek, F. E. (2006). Interictal Spikes and Epileptogenesis. *Epilepsy Currents*, 6(6):199–202.

[248] Stefanescu, R. A., Shivakeshavan, R., and Talathi, S. S. (2012). Computational models of epilepsy. *Seizure*, 21(10):748–759.

[249] Steriade, M., Jones, E., and Llinas, R. (1990). *Thalamic oscillations and signaling*. John Wiley \& Sons.

[250] Stulen, F. B. and De Luca, C. J. (1981). Frequency Parameters of the Myoelectric Signal as a Measure of Muscle Conduction Velocity. *IEEE Transactions on Biomedical Engineering*, BME-28(7):515–523.

[251] Suffczynski, P., Kalitzin, S., and Lopes Da Silva, F. H. (2004). Dynamics of non-convulsive epileptic phenomena modeled by a bistable neuronal network. *Neuroscience*, 126(2):467–484.

[252] Suffczynski, P., Kalitzin, S., Pfurtscheller, G., and Lopes da Silva, F. (2001). Computational model of thalamo-cortical networks: dynamical control of alpha rhythms in relation to focal attention. *International Journal of Psychophysiology*, 43(1):25–40.

[253] Suffczynski, P., Lopes da Silva, F., Parra, J., Velis, D., and Kalitzin, S. (2005). Epileptic transitions: model predictions and experimental validation. *Journal of Clinical Neurophysiology*, 22(5):288–299.

[254] Suffczynski, P. and Wendling, F. (2006). Some insights into computational models of (patho) physiological brain activity. *Proceedings of the IEEE*, 94(4):784–804.

[255] Suszkiw, J. B. (2012). Synaptic Transmission. In *Cell Physiology Source Book*, pages 563–578. Elsevier.

[256] Taleb, N. N. (2007). *The black swan: The impact of the highly improbable*. Penguin Books paperback.

[257] Tang, G., Rabie, A., and Hägg, U. (2004). Indian Hedgehog: A Mechanotransduction Mediator in Condylar Cartilage. *Journal of Dental Research*, 83(5):434–438.

[258] Therneau, T., Atkinson, B., and Ripley, B. (2017). rpart: Recursive Partitioning and Regression Trees. R package version 4.1-11.

[259] Therneau, T. M., Atkinson, E. J., and Mayo Foundation (2018). An introduction to recursive partitioning using the rpart routines. Technical report, Mayo Foundation.

[260] Thierens, D. (2010). The linkage tree genetic algorithm. In *International Conference on Parallel Problem Solving from Nature*, pages 264–273. Springer.

[261] Thom, M. (2014). Review: Hippocampal sclerosis in epilepsy: A neuropathology review. *Neuropathology and Applied Neurobiology*, 40(5):520–543.

[262] Thomas, G. and Jobst, B. (2015). Critical review of the responsive neurostimulator system for epilepsy. *Medical Devices: Evidence and Research*, 8:405.

[263] Thomson, A. and Deuchars, J. (1997). Synaptic interactions in neocortical local circuits: dual intracellular recordings in vitro. *Cerebral Cortex*, 7(6):510–522.

[264] Tokmakian, R., Challenor, P., and Andrianakis, Y. (2012). On the use of emulators with extreme and highly nonlinear geophysical simulators. *Journal of Atmospheric and Oceanic Technology*, 29(11):1704–1715.

[265] Touboul, J., Wendling, F., Chauvel, P., and Faugeras, O. (2011). Neural Mass Activity, Bifurcations, and Epilepsy. *Neural Computation*, 23:3232–3286.

[266] Tripathy, S. J., Savitskaya, J., Burton, S. D., Urban, N. N., and Gerkin, R. C. (2014). NeuroElectro: a window to the world's neuron electrophysiology data. *Frontiers in neuroinformatics*, 8(April):40.

[267] Urigüen, J. A. and Garcia-Zapirain, B. (2015). EEG artifact removal-state-of-the-art and guidelines. *Journal of Neural Engineering*, 12(3):31001.

[268] Ursino, M., Cona, F., and Zavaglia, M. (2010). The generation of rhythms within a cortical region: Analysis of a neural mass model. *NeuroImage*, 52(3):1080–1094.

[269] Van Boxtel, A. (2001). Optimal signal bandwidth for the recording of surface EMG activity of facial, jaw, oral, and neck muscles. *Psychophysiology*, 38(1):22–34.

[270] Van Kerkoerle, T., Self, M. W., Dagnino, B., Gariel-Mathis, M.-A., Poort, J., van der Togt, C., and Roelfsema, P. R. (2014). Alpha and gamma oscillations characterize feedback and feedforward processing in monkey visual cortex. *Proceedings of the National Academy of Sciences*, 111(40):14332–14341.

[271] van Rotterdam, A., Lopes da Silva, F. H., van den Ende, J., Viergever, M. A., and Hermans, A. J. (1982). A model of the spatial-temporal characteristics of the alpha rhythm. *Bulletin of Mathematical Biology*, 44(2):283–305.

[272] Ventriglia, F. (1978). Propagation of excitation in a model of neural system. *Biological Cybernetics*, 30(2):75–79.

[273] Vezzani, A., Friedman, A., and Dingledine, R. J. (2013). The role of inflammation in epileptogenesis. *Neuropharmacology*, 69(October 2009):16–24.

[274] Viana, F. A. C. (2013). Things You Wanted to Know About the Latin Hypercube Design and Were Afraid to Ask. *10th World Congress on Structural and Multidisciplinary Optimization*, pages 1–9.

[275] Viana, F. A. C. (2016). A Tutorial on Latin Hypercube Design of Experiments. *Quality and Reliability Engineering International*, 32(5):1975–1985.

[276] von Neumann, J. and Oskar, M. (1944). *Theory of games and economic behavior*. Princeton University Press.

[277] Vos, T. and Murray, C. J. L. (2016). Global, regional, and national incidence, prevalence, and years lived with disability for 310 diseases and injuries, 1990–2015: a systematic analysis for the Global Burden of Disease Study 2015. *The Lancet*, 388(10053):1545–1602.

[278] Ward, L. M. (2003). Synchronous neural oscillations and cognitive processes. *Trends in Cognitive Sciences*, 7(12):553–559.

[279] Wassermann, E. M. (1998). Risk and safety of repetitive transcranial magnetic stimulation: report and suggested guidelines from the International Workshop on the Safety of Repetitive Transcranial Magnetic Stimulation, June 5–7, 1996. *Electroencephalography and Clinical Neurophysiology/Evoked Potentials Section*, 108(1):1–16.

[280] Weigenand, A., Schellenberger Costa, M., Ngo, H.-V. V., Claussen, J. C., and Martinetz, T. (2014). Characterization of K-Complexes and Slow Wave Activity in a Neural Mass Model. *PLoS Computational Biology*, 10(11):e1003923.

[281] Wendling, F., Bartolomei, F., Bellanger, J. J., and Chauvel, P. (2002). Epileptic fast activity can be explained by a model of impaired GABAergic dendritic inhibition. *European Journal of Neuroscience*, 15:1499–1508.

[282] Wendling, F., Bellanger, J. J., Bartolomei, F., and Chauvel, P. (2000). Relevance of nonlinear lumped-parameter models in the analysis of depth-EEG epileptic signals. *Biological cybernetics*, 83(4):367–378.

[283] Wendling, F., Benquet, P., Bartolomei, F., and Jirsa, V. (2015). Computational models of epileptiform activity. *Journal of Neuroscience Methods*, pages 1–19.

[284] Wiebe, S. (2000). Epidemiology of Temporal Lobe Epilepsy. *The Canadian Journal of Neurological Sciences*, 27(01):S6–S10.

[285] Wiebe, S. (2012). Epilepsy: Outcome patterns in epilepsy surgery—the long-term view. *Nature Reviews Neurology*, 8(3):123–124.

[286] Wierenga, C. J., Müllner, F. E., Rinke, I., Keck, T., Stein, V., and Bonhoeffer, T. (2010). Molecular and electrophysiological characterization of GFP-expressing ca1 interneurons in GAD65-GFP mice. *PLoS ONE*, 5(12):1–11.

[287] Williams, C. K. I. and Rasmussen, C. E. (2006). Gaussian processes for machine learning.

[288] Williamson, D., Goldstein, M., Allison, L., Blaker, A., Challenor, P., Jackson, L., and Yamazaki, K. (2013). History matching for exploring and reducing climate model parameter space using observations and a large perturbed physics ensemble. *Climate Dynamics*, 41(7-8):1703–1729.

[289] Willie, J. T., Laxpati, N. G., Drane, D. L., Gowda, A., Appin, C., Hao, C., Brat, D. J., Helmers, S. L., Saindane, A., Nour, S. G., and Gross, R. E. (2014). Real-Time Magnetic Resonance-Guided Stereotactic Laser Amygdalohippocampotomy for Mesial Temporal Lobe Epilepsy. *Neurosurgery*, 74(6):569–585.

[290] Wilson, H. R. and Cowan, J. D. (1972). Excitatory and inhibitory interaction sin localized populations of model neurons. *Biophysical Journal*, 12:1–24.

[291] Wilson, H. R. and Cowan, J. D. (1973). A mathematical theory of the functional dynamics of cortical and thalamic nervous tissue. *Kybernetik*, 13(2):55–80.

[292] Wilson, J. V. K. and Reynolds, E. H. (1990). Translation and analysis of a cuneiform text forming part of a Babylonian treatise on epilepsy. *Medical History*, 34(02):185–198.

[293] Woldman, W. and Terry, J. R. (2015). Multilevel Computational Modelling in Epilepsy: Classical Studies and Recent Advances. In *Validating Neuro-Computational Models of Neurological and Psychiatric Disorders SE - 7*, volume 14, pages 161–188. Springer, Cham.

[294] Wolpert, D. H. and Macready, W. G. (1997). No Free Lunch Theorems for Optimization. *IEEE Transactions on Evolutionary Computation*, 1:67–82.

[295] Wu, X., Kumar, V., Ross Quinlan, J., Ghosh, J., Yang, Q., Motoda, H., McLachlan, G. J., Ng, A., Liu, B., Yu, P. S., Zhou, Z.-H., Steinbach, M., Hand, D. J., and Steinberg, D. (2008). Top 10 algorithms in data mining. *Knowledge and Information Systems*, 14(1):1–37.

[296] Yasiry, Z. and Shorvon, S. D. (2012). How phenobarbital revolutionized epilepsy therapy: the story of phenobarbital therapy in epilepsy in the last 100 years. *Epilepsia*, 53 Suppl 8:26–39.

[297] Ye, K. Q. (1998). Orthogonal Column Latin Hypercubes and Their Application in Computer Experiments. *Journal of the American Statistical Association*, 93(444):1430–1439.

[298] Zavaglia, M., Astolfi, L., Babiloni, F., and Ursino, M. (2006). A neural mass model for the simulation of cortical activity estimated from high resolution EEG during cognitive or motor tasks. *Journal of Neuroscience Methods*, 157(2):317–329.

[299] Zetterberg, L. H., Kristiansson, L., and Mossberg, K. (1978). Performance of a model for a local neuron population. *Biological Cybernetics*, 26:15–26.

[300] Zhdanov, M. S. (2015). Forward and Inverse Problems in Science and Engineering. In *Inverse Theory and Applications in Geophysics*, pages 3–31. Elsevier.